Environmental Remediation Applications of Ionic Liquids

Developing Ionic Liquid Technologies for Aqueous and Gaseous Waste Management

Dominic Burns
BSc Medicinal Chemistry

Primary supervisor: Prof John Holbrey
Secondary supervisor: Prof Małgorzata Swadzba-Kwasny
Industrial supervisor: Dr Hye-Kyung Timken

School of Chemistry & Chemical Engineering
A thesis submitted to Queen's University Belfast for the degree of Doctor of Philosophy

Contents

Acknowledgements

I would like to thank John for being a mentor in everything from chemistry to Linux and LaTeX, entertaining my countless tangents on energetics and inspiring me to re-write the classic joke - whats black, white and red all over? My thesis after John's corrected it. Gosia for always being exceeding fair, helping me with extra funding during my COVID extension and suggesting I got to the Gordon research conference even though California is just as far from Maine as Ireland. Hye-Kung Timken, for endless encouragement and taking care of me during my time in California. Evan Hatakeyama and Huping Luo for guidance during my research and helping me to feel welcome half way round the world.

I also want to thank my friends Anne, Emily, Mark, Sam and Beth for endless craic, coffee breakdowns and tolerating my general mess - sorry for nearly deleting your entire PhD Mark.

I would also like to thank everyone else that has helped me along the way including Deborah, Yoan, Nimal, Donal, Angela, Connor, Ben and George. Everyone at Chevron; Dave Carter, Ryan Carter, Mark Fernandez, Raja Jadhav, Cesar Ovalles, Dani Cuspard, Toni Miao, Hung Khuu,

I am thankful for the funding for this project which came from an EPSRC CASE award that was supported by Chevron. Dr Aisling McGuigan and Dr Syed Nasir Shah also need credit for doing the preliminary scoping studies that identified Cyphos® 101 as a liquid ion exchanger and laid the foundations for this project.

I would also like to acknowledge that Tuesday is the worst day of the week.

Abstract

This work focuses on the use of ionic liquids in two areas of industrial pollution management, aqueous sulfate removal and carbon dioxide capture from flue gas.

Chapter two investigated the potential use of hydrophobic ionic liquid chlorides as liquid anion exchangers where sea water was used to model a competitive source of aqueous sulfate. Five ionic liquids (Cyphos® 101, Aliquat® 336, $[HN_{888}]Cl$, $[P_{1888}]Cl$ and $[N_{2OH888}]Cl$) that contain functional groups common to anion exchange resins where shown to form aqueous biphasic systems with water with varying levels of water saturation from 8 to 26.6 wt%. These systems were characterised by FT-IR and capillary NMR experiments to show that the absorbed water was hydrogen bonded to the chloride anion with varying degrees of strength. Cyphos® 101 was shown to be the least effective at extracting aqueous sulfate while the other four all performed broadly similar across a range of sulfate extractions from 5 - 100 mM, extracting *ca.* 55% from the most concentrated solutions. The ionic liquids were shown to extract aqueous sulfate via an ion-exchange process that was strongly inhibited by the presence of aqueous chloride but enhanced via the addition of acid. Finally $[HN_{888}]Cl$ was shown to be reusable across four cycles through successive neutralisation and protonation.

Chapter three aimed to build on the previous chapter whereby weakly binding bis or tris (thio)urea anion receptors were added to water saturated Cyphos® 101 and Aliquat® 336. The aim was to enhance the sulfate extraction via synergised anion recognition and ion-exchange. The receptors were all found to be highly soluble in the hydrated ionic liquids where they initially bind to the chloride anions. Binding studies in polar DMSO solvent revealed that five of the six receptors showed a moderate preference for chloride over sulfate. This selectivity appears to reverse in the ionic liquid solvents as the addition of every receptor improved the sulfate extraction by as much as 14.6% when an equimolar amount of receptor:sulfate was used.

Chapter four moves away from aqueous sulfate removal and focuses on the development of a chemisorbant ionic liquid process for CO_2 removal from flue gas. Initially, a small series of ionic liquids were tested for CO_2 absorption under dry and humid conditions. [DBUH][Im] was shown as a potential candidate for a high temperature absorption-desorption cycle under humid conditions with absorption and

desorption temperatures of 95 and 160 °C respectively. Under these conditions a working capacity of *ca.* 50 $g \cdot kg^{-1}$ (0.25 $mol \cdot mol^{-1}$) was demonstrated across six cycles. TGA-MS, FT-IR and NMR analysis was used to show that in the presence of water, CO_2 was absorbed in the form of bicarbonate with a maximum observed capacity of 150 $g \cdot kg^{-1}$ (0.75 $mol \cdot mol^{-1}$). Desorption from this point then causes two bicarbonate anions to decompose into CO_2, H_2O and divalent carbonate. Successive absorption-desorption cycles after this point then swing between carbonate and bicarbonate species. The use of high temperatures and humid conditions solves two of the biggest problems in ionic liquid carbon capture by significantly reducing the viscosity of [DBUH][Im] and increasing the kinetics of absorption/desorption. Finally, a chemisorbant flue gas capture process was designed based on this work.

Nomenclature

Acronyms

ABS	Aqueous biphasic system
AHA	Aprotic heterocyclic anion
AMD	Acid mine drainage
CESR	Cost-effective sulfate removal
CMC	Critical micelle concentration
DFT	Density functional theory
DI	Deionised
ED-XRF	Energy dispersive X-ray fluorescence
ENIL	Encapsulated ionic liquids
ESI	Electrospray ionisation
FT-IR	Fourier transform Infrared
G	Guest molecule
GYP-CIX	Gypsum continuous ion-exchange
H	Host molecule (receptor)
H-bonds	Hydrogen bonds
HBA	Hydrogen bond acceptor
HBD	Hydrogen bond donor
HG	Host-guest complex
HRMS	High resolution mass spectrometry

IL	Ionic liquid
ITC	Isothermal calorimetry
IX	Ion-exchange
MS	Mass spectrometry
NF	Nano-filtration
NMR	Nuclear magnetic resonance
PIL	Protic ionic liquid
PSA	Pressure-swing absorption
PVR	Phase-volume ratio
RM	Reverse micelle
RO	Reverse osmosis
SC-XRD	Single crystal X-ray diffraction
SILM	Supported ionic liquid membrane
SRB	Sulfate reducing bacteria
TGA	Thermogravimetric analysis
TSA	Temperature-swing absorption
TSIL	Task specific ionic liquid
UF	Ultra-filtration
UV	Ultra-violet

Chemical abbreviations

1,2-DCE	1,2-Dichloroethane
2-CNPyr	2-Cyanopyrrole
2-FPhO	2-Fluorophenol
2-SCH$_3$BnIm	2-Methylthiobenzimidazole
3-CH$_3$-5-CF$_3$-Pyra	3-Methyl-5-trifluoromethylpyrazole

3-Triz	1,2,3-Triazole
4-MeIm	4-Methylimidazole
4-Triz	1,2,4-Triazole
6-BrBnIm	6-Bromobenzimidazole
A^{n-}	Anion
Aliquat® 336	Trioctylmethylammonium chloride, $[N_{1888}]Cl$
$[BMIm]^+$	1-Butyl-3-methylimidazolium
BnIm	Benzimidazole
C4P	Calix[4]pyrrole
$[C_xC_yIm]^+$	Dialkylimidazolium
CF_3-Pyra	3-Trifluoromethylpyrazole
Cyphos® 101	Trihexytetradecylphosphonium chloride, $[P_{66614}]Cl$
DCM	Dichloromethane
DMAEA	2-(Dimethylamino)ethylamine
DMAPA	3-(Dimethylamino)propylamine
DMF	Dimethylformamide
DMSO	Dimethylsulfoxide
DBU	1,8-Diazabicyclo[5.4.0]undec-7-ene
EO	Ethylene oxide
Im	Imidazole
Inda	Indazole
L	Ligand or receptor
M^{n+}	Metal cation
MEA	Monoethanolamine
Met	Methionine

MTBDH	7-Methyl-1,5,7-triazabicyclo(4.4.0)dec-5-ene
$[NTf_2]^-$	Bis(trifluoromethane)sulfonimide
Pro	Proline
TBA	Tetrabutylammonium
TBMA	Tributylmethylammonium
THF	Tetrahydrofuran
TMG	Tetramethylguanidine

Mathematical constants

$a - d$	Fitting parameterss used in data analysis
a_e	Micelle surface area per molecule
A	Absorption
c	Molar concentration
C	Initial concentration
D	Distribution ratio
EE	Extraction efficency
ΔG	Gibb's free energy change
$[G]$	Guest concentration
$[G]_o$	Initial guest concentration
h	Plank's constant
ΔH	Enthalpy change
$[H]$	Host concentration
$[H]_o$	Initial host concentration
$[HG]$	Host-guest concentration
i	van't Hoff index
I	Intensity

K_a	Acid dissociation constant
ΔK_a	Difference between two K_a values
K_b	Binding constant
pK_b	Stability constant
l	Path length
l_o	Tail length
MW	Molecular weight
n	Moles
P	Pressure
P_c	Critical pressure
P_r	Reduced pressure
PP	Packing parameter
q	Amount absorbed
r	Phase-volume ratio, volume of the organic phase divided by the aqueous phase
R	Ideal gas constant
ΔS	Entropy change
t	Time
T	Absolute temperature
T_c	Critical temperature
T_r	Reduced temperature
u	Van der Waals terms relating to the intermolecular interactions
v	Van der Waals terms relating to the volume occupied by one mole of molecules
v_o	Tail volume

V	Volume
w	Mass fraction
Z	Lee-Kesler correction factor
α	Head-group repulsion
δ_{obs}	Observed chemical shift
δ_{H}	Chemical shift of the host
δ_{HG}	Chemical shift of the host-guest complex
ε	Molar extinction coefficient
$\Delta\mu^{o}$	Chemical potential change
ν	Frequency
Π	Osmotic pressure
ρ	Density
σ	Interfacial free energy
χ	Mole fraction

Publications arisen from this Work

Energy Efficient Post-Combustion CO_2 Capturing Process using Ionic Liquid Absorbent
Patent developed and filed by Chevron, *Attorney Docket No. 70205.0674USP1 (T-11879)*

1. Introduction

This is an Engineering & Physical Sciences Research Council (ESPRC) industrial Centre for Advanced Sustainable Energy (CASE) project in collaboration with the Chevron Corporation that started in October 2019. Initially the project was to explore liquid-liquid extraction technologies utilising ionic liquids to treat saline process water with the initial objective of selective sulfate removal from sea water. Preliminary work done between QUILL (Queens University Ionic Liquids Laboratory) and Chevron screened a small series of common ionic liquids and identified $[P_{66614}]Cl$ (trade name Cyphos® 101) as a possible liquid ion exchanger, capable of partially removing sulfate from water via an ion-exchange mechanism. During the summer of 2022, there was the opportunity to work at the Chevron research and development facility in Richmond, California. At this point the scope of the project was widened to include research into chemisorbant ionic liquids for flue gas carbon dioxide capture.

1.1 Ionic Liquids

Ionic liquids (ILs) are a class of salts, defined as having melting points below 100 °C. Common inorganic salts have high melting points due to being composed of small ions with relatively high charge density, providing a high lattice enthalpy due to strong coulombic attraction. Through delocalisation of these charges and asymmetry in the ions, physically separating the charges through packing constraints, the coulombic attraction can be reduced and the melting point lowered. This yields a family of liquids, composed of ions, with extremely high ionic strength and negligible vapour pressure.

ILs were originally labelled ‘designer solvents’ due to the large number of potential IL-forming ion pairs that can be predicted (10^6) [1]. This hype is finally giving way to realistic applications of ILs as their limitations are beginning to be understood. There are a number of excellent reviews summarising the history and current state of the field. A recent review by Prof. Tom Welton is the best place to start for anyone new to the field [2].

Their unique properties can act both as invaluable tools for solving problems of

the modern world, and a torture for the lab practitioner. Coulombic attraction pulls the ions close together, increasing their density and surface tension [3], providing a highly polar environment which can be used to enhance organic reactions and catalysis [4]. This also reduces their vapour pressure and flammability, excellent for the safety of workers but potentially disastrous from uncontrolled environmental release. The coulombic attraction pulling the asymmetrical ions close together and restricted diffusion can cause some ILs to be horribly viscous so measuring them by volume is only for the brave or foolish as stated by Welton and coworkers [5]. They are also not as 'green' as the literature may suggest, while $[BF_4]^-$ and $[PF_6]^-$ are rarely used nowadays, the synthetically complex bis(trifluoromethanesulfonyl)imide ($[NTf_2]^-$) is still widely employed in research. Although, being composed of ions, ILs are particularly well suited for use as electrolytes where non-coordinating fluorinated anions are highly attractive for electrochemical applications in batteries and super capacitors. These properties are very general and exceptions can be found for all of them; including ILs that can be distilled [6].

The properties of specific ILs will be discussed further in later sections but for emphasis, some real world applications in which they have already been deployed will be acknowledged here. Figure 1.1 shows some of the biggest industrial applications of ILs in the last three decades, Roland Kalb also has also published a recent book chapter on the industrialisation of ILs [7]. ILs are also on the verge of several new major applications such as cellulose dissolution [8, 9], carbon capture [10], biomass processing [11], energy storage [12] and natural fibre welding [13].

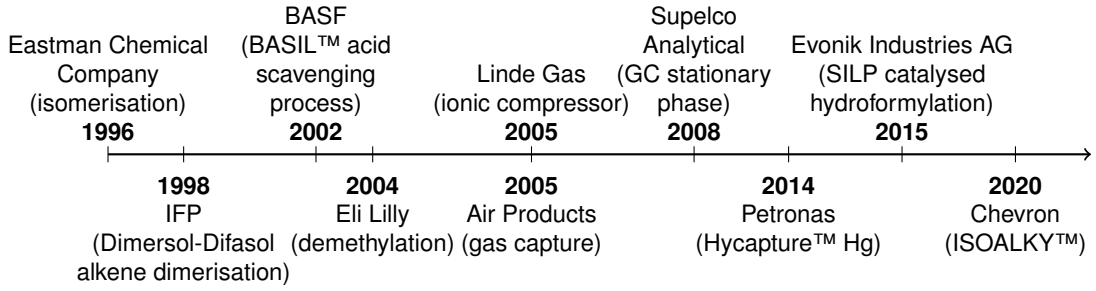

Figure 1.1: Timeline of some example industrial processes utilising ILs, reproduced from reference [14].

1.2 Sulfate removal

Sulfate is a divalent oxyanion that can accept up to twelve hydrogen bonds through it's four tetrahedrally orientated oxygens as shown in figure 1.2 [15]. This makes it extremely hydrophilic as shown by its large Gibbs free energy of hydration (ΔG_{hyd} = -1080 kJmol^{-1} [16]). As sulfate is the conjugate base of sulfuric acid, its speciation

is therefore pH dependant as shown in figure 1.3, where in neutral waters it is present as the $[SO_4]^{2-}$ ion. The acid dissociation constants K_{a1} and K_{a2} for sulfuric acid are -6.62 and 1.99 respectively.

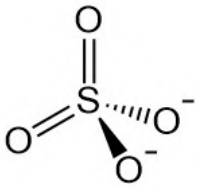

Figure 1.2: Structure of the sulfate ion.

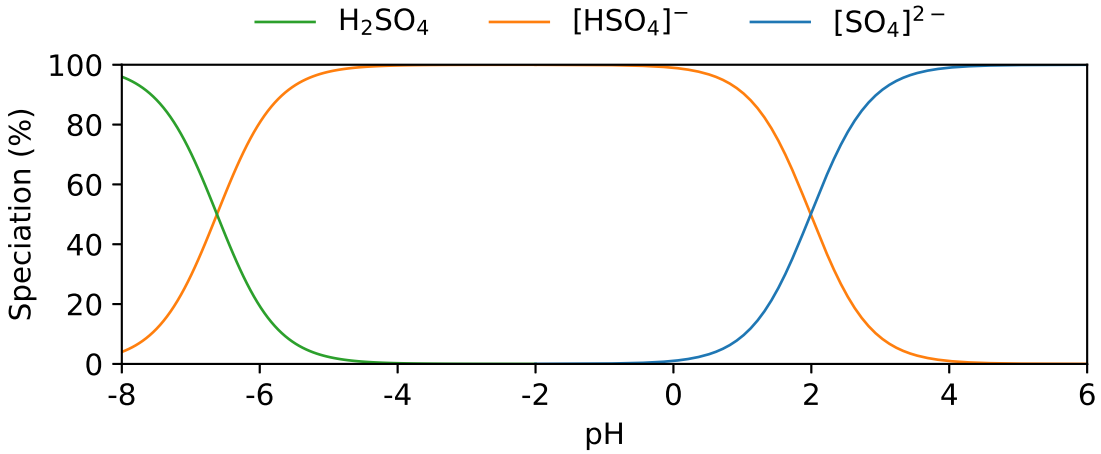

Figure 1.3: pH dependant speciation of the sulfate ion.

World-wide, about 200 million tonnes of sulfuric acid are consumed each year [17] making it the largest volume inorganic chemical manufactured in the world [18]. Much progress has been made to develop new methods for specific removal of sulfate from water as it poses specific chemical issues to several fields such as nuclear waste remediation where its low solubility in borosilicate glass hinders the vitrification process [19] and secondary oil recovery where the presence of barium in formation water causes scaling of the pipes [20]. Aqueous sulfate also poses an environmental problem where unnatural sources of sulfate such as acid mine drainage (AMD) [21], fertiliser leaching and agricultural and industrial wastewater run-offs where it can have toxic effects on aquatic plants and animals including fish, invertebrates and amphibians [22]. The concentrations of sulfate, and ions relevant to its removal typically found in these sources are shown in table 1.1. Most countries now have restrictions on the ion concentration of waste waters before it can be disposed of which limit sulfate concentrations between 250 and 2000 ppm. The world health organization does not suggest any health based guidelines but

report that sulfate has a lower taste threshold of 250 ppm and that higher than 600 ppm can have a adverse effects on humans [23, 24].

Table 1.1: Example concentrations in $mg \cdot L^{-1}$ of ions relevant to sulfate removal of 'standard' sea water, formation water and acid mine drainage (AMD).

Water	SO_4^{2-}	Cl^-	Na^+	K^+	Ca^{2+}	Mg^{2+}	Ba^{2+}	Reference
Sea	2,712	19,352	10,784	399	412	1,284	-	[25]
Formation	153	37,410	14,682	295	5,361	1,732	391	[26]
AMD	9,790	27	170	132	480	2,000	-	[27]

1.2.1 Current methods

In this section the main currently used industrial water treatment methods will be discussed in terms of sulfate removal ability as well as some novel approaches that current research groups are developing to tackle this problem. Passive processes such as constructed wetlands for AMD remediation will not be discussed as in these cases the treatment can take years as the water is not intended to be used for any further purposes.

Water treatment processes have been used for millennia now and like most aged processes, many advancements have been made since it was first 'purified' by boiling or sand and gravel filtration methods. This is now a vast field with many different approaches all meeting specific needs depending on the initial purity of the water and the final purity required. The main goal is to remove only the required impurities, therefore spending the least amount of energy. For example it would require far more energy to distil the worlds drinking water than to use a reverse osmosis process, although membrane fouling and pre-treatment need to be considered among other factors. A plethora of reviews on current sulfate removal technologies have already been published and cover the specific challenges that different industries face with aqueous sulfate treatment [21, 28–32].

Precipitation

These are amongst the earliest and most commonly used methods used to reduce sulfate levels in water due to their simplicity and use of inexpensive reagents however they are also amongst the most wasteful due to the large amounts of solid waste that is generated. The earliest methods of sulfate removal involve the addition of lime ($CaCO_3$) to cause the precipitation of gypsum ($CaSO_4 \cdot 2\,H_2O$) as per

equation 1.1 while also raising the pH to precipitate metal hydroxides.

$$CaCO_3 + [SO_4]^{2-}_{(aq)} \longrightarrow CaSO_4 \cdot 2\,H_2O\downarrow + [CO_3]^{2-}_{(aq)} \tag{1.1}$$

This treatment can reduce sulfate levels down to approximately 2000 ppm, the saturation point of calcium sulfate, but for many purposes this is still too high. The cost-effective sulfate removal (CESR) [33] and SAVMIN^{TM} processes were both developed at the end of the 90's to reduce sulfate levels in mine and mineral waters below required discharge limits. Both processes consist of four steps involving metal hydroxide precipitation, gypsum precipitation through lime addition, further sulfate reduction by ettringite ($Ca_6Al_2(SO_4)_3(OH)_{12} \cdot 26\,H_2O$) precipitation via addition of aluminium hydroxide and finally pH reduction by carbonation. These processes can reduce sulfate levels to below 200 ppm but the ettringite precipitation step is inhibited by magnesium as it competes with calcium for aluminium to form a hydrotalcite-type compound [34].

Barium salts such as $BaCl_2$ and $BaCO_3$ can be used to precipitate out insoluble barium sulfate (barite) as per equation 1.2, however this is impractical for large scale use due to the high costs. These stem from the energy intensive regeneration of the barium salts where the the barite is heated with carbon to 1100℃ in an oxygen free atmosphere to produce BaS as per equation 1.3 [35, 36]. The BaS is then treated with HCl to yield $BaCl_2$ or dissolved in water and treated with CO_2 to produce $BaCO_3$. These $BaCl_2$ and $BaCO_3$ salts are also incredibly toxic, ingestion will interfere with potassium pumps in the body leading to irreversible damage [37–39]. Barium precipitation has also been used for quantitative analysis of aqueous sulfate solutions by gravimetric analysis [40], however, this is less common now due to advancements in analytical techniques such as inductively coupled plasma and ion chromatography.

$$BaCl_2 + [SO_4]^{2-}_{(aq)} \longrightarrow BaSO_4\downarrow + 2\,Cl^-_{(aq)} \tag{1.2}$$

$$BaSO_4 + 2\,C \xrightarrow{1100℃} BaS + 2\,CO_2 \tag{1.3}$$

Membrane exclusion

Filtration methods have come a long way since the invention of the hippocratic sleeve. There are now a wide range of filtration technologies that are well established. Figure 1.4 is a generalisation of some of the most common filtration systems for water [41, 42]. Processes utilising membranes with smaller pore sizes or higher impurity concentrations in the feed usually require higher operational pressures. Due to filtration being an exclusion based separation technique, excluded

particles will eventually clog the pores inside the membrane leading to membrane fouling which increases operational costs as the membranes will eventually need replaced. As well as the filtrate stream, a reject stream which contains higher concentrations of impurities than the feed is also produced which then must be treated and disposed.

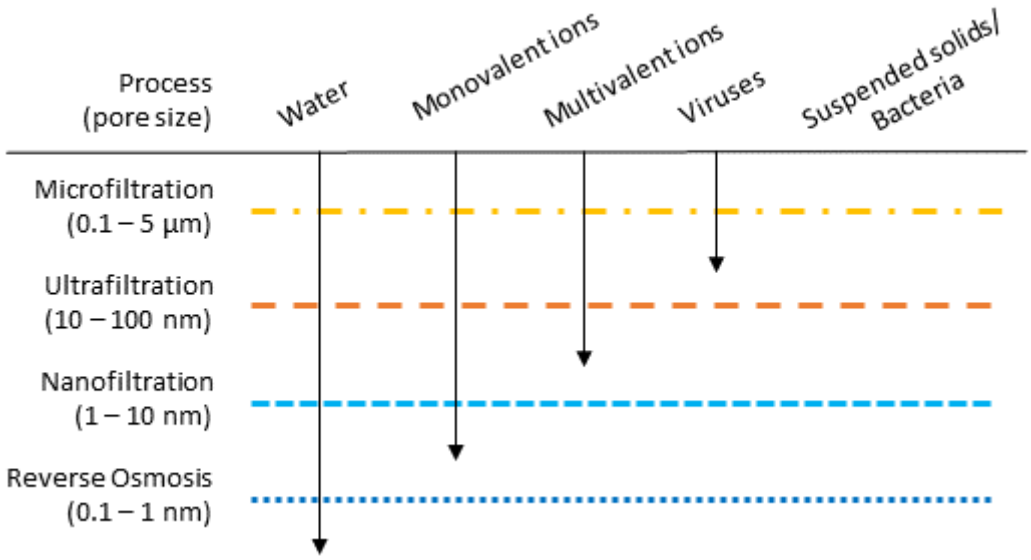

Figure 1.4: Comparison of different filtrations methods and examples of some impurities that can be excluded from their filtrate, based on data from ref [42].

Ultra-filtration (UF), nano-filtration (NF) and reverse osmosis (RO) all rely on three main exclusion mechanisms; steric exclusion where the impurity is too large to enter the pores, dielectric exclusion where the ion with its hydration shell is too large to enter the pores and Donnan exclusion where a charged membrane will repel similarly charged ions [43, 44]. The exclusion mechanism that any ion experiences will therefore be a factor of its size, Gibbs free energy of hydration (ΔG_{hyd}) and the membrane respectively.

Reverse osmosis (RO) is used globally to turn sea water into drinking water [45]. As of 2022, the worlds largest RO plant is in Saudi Arabia and produces 600,000 cubic meters of desalinated water per day [46]. Due to the difference in ionic concentrations on each side of the membrane, a large osmotic pressure builds up, pulling water back to the feed side of the membrane, this back pressure can be as high 27 bar for sea water. An external force must be applied to the feed to overcome this osmotic pressure and produce a useful filtrate flow rate, this can be as high as 80 bar in some cases, contributing to high operational costs. Dow have even developed membranes for high pressure reverse osmosis where applied pressures can reach 120 bar [47]. The main drawbacks of the RO process are the replacement of expensive membranes and the high operational costs which do not scale well for more concentrated solutions as the osmotic pressure is directly

proportional to the ionic strength of the solution as per van't Hoff's equation 1.4. Where Π is the osmotic pressure, *i* is the is the dimensionless van 't Hoff index, *c* is the molar concentration of solute, *R* is the ideal gas constant, and *T* is the absolute temperature.

$$\Pi = icRT \tag{1.4}$$

A few processes have also been developed on the concept of electrodialysis (ED) where a voltage is applied across a solution to induce the movement of cations to the cathode and anions to the anode [48]. In these methods, charged membranes rely on Donnan exclusion to be impermeable to either cations or anions and separate the water into diluted and concentrated streams.

Biological reduction

Sulfate reducing bacteria (SRB) have been been well studied for decades now, they are anaerobic microorganisms and so reside mainly in anoxic environments such as oil fields, the deep subsurface [49] and even the worlds oldest isolated ground water [50]. Bioreactor process such as the THIOPAQ^{TM} process, can remove sulfate in one step by reduction to hydrogen sulfide which can spontaneously precipitate out as metal sulfides if the appropriate metals are present or else this step will produce hydrogen sulfide as shown in equation 1.5. This hydrogen sulfide must then be further treated, usually by reduction to elemental sulfur by aerobic bacteria in a separate step shown in equation 1.6.

$$4\,CH_3OH + 3\,{SO_4}^{2-} \longrightarrow 4\,{HCO_3}^{-} + 3\,HS^{-} + H^{+} + 4\,H_2O \tag{1.5}$$

$$2\,HS^{-} + O_2 + 2\,H^{+} \longrightarrow 2\,S^{0} + 2\,H_2O \tag{1.6}$$

This process requires a electron donor such as hydrogen gas or methanol but many other sources can be used as well [28]. This method of sulfate removal has many advantages such as operating at ambient pressures and temperatures and being able to treat waters with extremely high sulfate concentrations of 30,000 ppm. On the other hand, this process is slow and also produces a lot of sludge waste due to the use of whole cells as well as requiring stoichiometric amounts of an electron donor. The active site of these bacteria is an excellent sulfate receptor and discussed in greater detail in section 1.3.2.

Ion-exchange

Anion exchange resins are typically a polymer such as polystyrene that has been functionalised with cationic ammonium groups as shown in figure 1.5 and are typically loaded with 'sacrificial' anions such as chloride or hydroxide [51]. A feed

solution is then passed through the resin in a packed column and anions from the feed will displace the sacrificial anions the with ion-exchange (IX) efficiency being determined by the difference in relative affinity between the mobile and stationary phases [52]. IX resins are commonly used with water but other solvents such as ethanol can also be used to adjust the relative affinity for the mobile phase. The IX resins will eventually displace all the counter ions on its exchange sites and need to be regenerated by passing through a concentrated regenerant solution, displacing the contaminant ions for more sacrificial ions. It it worth noting that when sulfate (ΔG_{Hyd} = -1080 kJ·mol^{-1}) is exchanged for two equivalents of chloride anions (ΔG_{Hyd} = -340 kJ·mol^{-1} [16]) there is a thermodynamic loss of 400 kJmol^{-1} as sulfate is more than three times more hydrophilic than chloride.

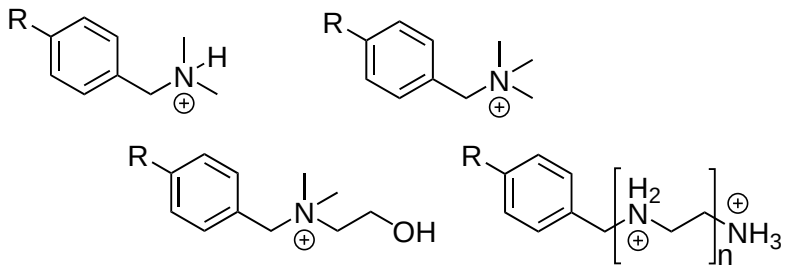

Figure 1.5: General structures of common anion exchange resin types: (top left) weak basic, (top right) Strong basic type I, (bottom left) Strong basic type II, (bottom right) Polyamine.

This technology has been employed industrially by Chemeffco with the Gypsum Continuous Ion Exchange (GYP-CIX) process which was then later developed into the Sulf-IX^{TM} process by BioteQ Environmental Technologies, Inc [53]. The feed first passes through a strong acid cation exchange resin which exchanges calcium ions for two equivalents of protons. This acidic solution then passes through a weak base anion exchange resin, this type of resin does not actually have any exchange ions but rather has amine functional groups which will be protonated by the acid and then in turn bind the sulfate anion. This presence of competing cations, specifically magnesium can reduce the overall efficiency of the process by competing with calcium in the first step and so pre-treatment of lime precipitation is usually required. It was reported by BioteQ that this process can reduce sulfate levels to below 500 ppm [54].

There is ongoing effort to develop IX resins from biomass, agricultural wastes and even saw dust [55] as replacements for current plastic polymers. For example, Marshall and Wartelle successfully functionalised soybean hulls with 0.71 mmol·g^{-1} of quaternary ammonium groups which was then able to remove highly hydrophilic oxyanions from water [56]. Cao *et al.* also took a similar approach, functionalising rice straw with quaternary ammonium which had a maximum sulfate adsorption

capacity of 74.76mg·g^{-1} [57].

1.2.2 Ionic liquids as liquid ion exchangers

Anion exchange is a common step in the synthesis of many ionic liquids and so it follows that this ability to exchange ions could be utilised to remove unwanted anions from an aqueous stream. This has also made them appealing components in liquid-liquid extracting phases which has been widely explored for the extraction of metal ions from acidic leachates where the metals are commonly extracted as anionic coordination complexes [58, 59]. The various mechanisms of metal extraction into an IL are described by Janssen *et al.* in an in depth review [60]. This same approach has not yet been explored for non-metallic anions as they are generally seen as less profitable compared to metals which can then be converted into high value products.

The use of hydrophobic ILs for aqueous extraction was first aimed towards the recovery of valuable metal ions from sources such as acid leachates. Dai *et al.* were the first to suggest this and show that ILs could be used for the extraction of metal ions where strontium was found to migrate into a [BMIm][PF_6] (-Butyl-3-methylimidazolium hexafluorophosphate) phase with an unusually high partition coefficient for an organic phase that was enhanced greatly by the addition of a crown ether ligand [61]. Dietz *et al.* then further showed that if the IL cation was hydrophilic enough, it would result in a much larger partition coefficient due to a combination of complexation and IX of the cationic species [62, 63]. A large number of other ILs have also been shown to be useful metal extracting phases [64], in these cases the metal complexation was achieved either through the cation [65] or anion [66]. In some cases where an extractant has been used, ILs can display identical properties to molecular solvents [67]. Aliquat® 336 ([N_{1888}]Cl) is currently commercially used for the liquid-liquid extraction of metals via an IX process where the metals are extracted from acidic media as their anionic chloride complexes [68, 69]. Cyphos® 101 ([P_{66614}]Cl) is another IL that has been developed more recently and is being used for similar processes while being more thermally stable and hydrophobic than Aliquat® 336, structures of which are shown in figure 1.6. Here there is the advantage of the lone chloride being hydrophilic and the metal chloride complexes being relatively hydrophobic due to a small charge spread over a relatively large volume, thus providing a driving force for the IX process in both directions.

While there has been much interest in the way of developing new ILs for high value economical processes, very little work has been done to see if these ILs could be used as alternatives to IX resins for wastewater treatment or removal of

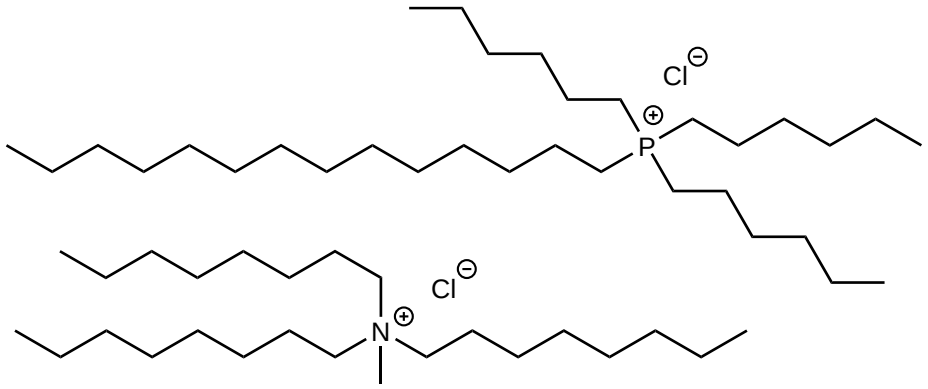

Figure 1.6: Chemical structures of (top) Cyphos® 101 and (bottom) Aliquat® 336, ignoring the branching and variation in chain length that exists in the commercial products.

unwanted anions from aqueous streams. A handful of papers do exist testing the use of Aliquat® 336 and Cyphos® 101 dispersed in kerosene, toluene or xylene for the extraction of hydroxide [70], perrhenate [71] and uranate [72] respectively.

The common functional groups in commercially available IX resins were shown previously in figure 1.5. Comparing the structures, it is clear that the methyl group in Aliquat® 336 may mimic the functionality found in a strongly basic type I resin. Removal of the methyl group and subsequent protonation with HCl will then yield a protic IL that can mimic a weakly basic resin. Interestingly, this protic IL is used commercially and is available under the trade name Alamine 336 where it is sold as the free trialkylamine base with a mixture of C_8 - C_{10} chains [73]. It is used for the extraction of metal ions from acidic (HCl) leachate solutions where the amine will inevitably become protonated and form the IL [74–76]. Aliquat® 336 is really just the modern day replacement for Alamine 336 due to its improved stability and phase transfer properties [77]. A strongly basic type II resin could also be mimicked via the addition of a 2-hydroxyethyl group to trioctylamine which has been reported before as a surfactant [78, 79]. And finally, phosphonium analogues of Aliquat® 336 could differentiate between ammonium and phosphonium functionality as well as possible improvements in chemical or physical properties. Structures of these proposed IL cations are shown in figure 1.7. Polyamine resins are also commercially available although much less ubiquitously. They have been reported to be the most selective for multivalent ions due to the close proximity of the formal charges. However, this may lead to leaching or problems in an analogous liquid ion exchanger as adding multiple charged groups will increase the hydrophilicity of the cation.

IX resins are usually loaded with either hydroxide, chloride or nitrate (ΔG_{Hyd} = -400, -340 and -300 $kJ \cdot mol^{-1}$ respectively) [80, 81] as sacrificial anions depending on the use case. The choice of sacrificial anions is more limited when it comes to

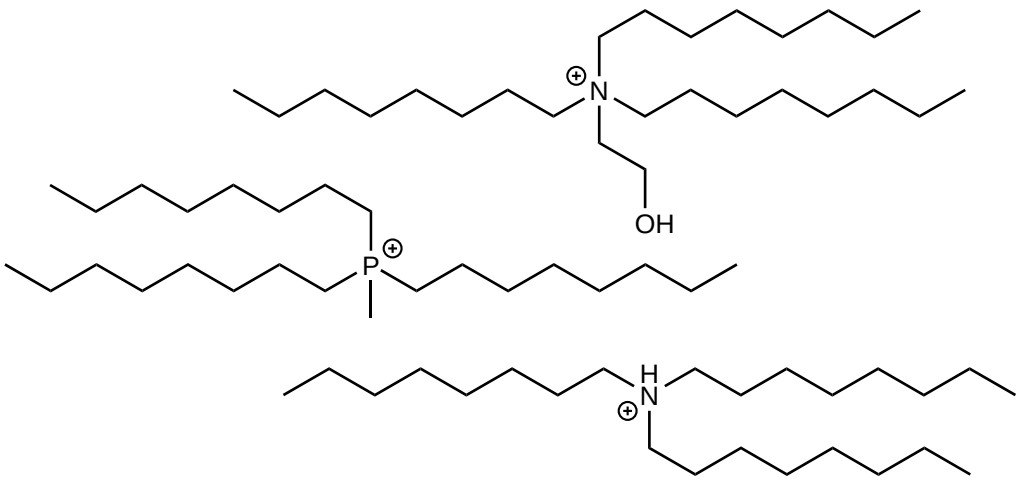

Figure 1.7: Proposed IL cations that correspond to the functionality found in commercial IX resins; (top) $[N_{2OH888}]^+$ for strongly basic type II, (middle) $[P_{1888}]^+$ is a phosphonium analogue of Aliquat® 336 and (bottom) $[HN_{888}]^+$ for weakly basic resins.

developing ILs as liquid anion exchangers. Hydroxide ILs tend to be very corrosive, waxy solids that are hard to handle and, when paired with tetraalkylphosphonium cations, can form ylides [82] or carbenes when paired with imidazolium cations [83]. The nitrate salts on the other hand provide the weakest driving force for the IX process and can also have undesirable energetic properties [84–86].

The presence of a hydrophilic anion such as chloride in these ILs (Aliquat® 336 and Cyphos® 101) increases the solubility of water in the IL ($\chi_{H_2O} > 0.8$) and so when used for aqueous extraction they can be thought of as aqueous biphasic systems (ABSs) (also know as aqueous two-phase systems), similar to those of polymers like polyethylene glycol [87]. Aqueous biphasic systems were first reported in 1896 by Martinus Beijerinck in a paper titled 'About a peculiarity of the soluble starch' [88]. Since then their use has mainly been in the area of large biomolecule separation and purification however they have found uses in the separation of heavy metals [89] and even carbon nanotubes [90]. It was noted that these systems had high mass transport kinetics enabling faster equilibration times than expected and this was thought to be connected to the extremely low interfacial tensions observed in these systems [91]. Recently Kaplanow *et al.* showed for the first time that in these systems it is the large interfacial area created upon mixing that accounts for the fast protein partitioning rather than fast diffusion within the phases [92]. Most of this work however, has been done with polymer ABSs which have a low ionic strength in comparison to extraction systems with Aliquat® 336 and Cyphos® 101. Despite their low ionic strength, Dilip *et al.* have demonstrated the use of Polyethylene glycol resins that form a solid-liquid ABS system to extract perchlorate and mercury(II) from water through modulation of kosmotropic

and chaotropic salts [93].

Recently a paper demonstrated a very simple ABS could also form with the roles of the ions switched. Mixtures of water, LiCl and Li[NTF_2] form a biphasic mixture in which the upper layer is rich in hydrophilic chloride and the bottom layer rich with more hydrophobic [NTf_2]$^-$ anion [94]. This seems surprising given the aqueous solubility's of the salts expressed in mass fractions are 0.45 and 0.8 respectively [95], showing that both salts are hydrophilic, so why do they phase split? Celso *et al.* who showed that in a system comprised of a neutral solvent and two salts with a common ion (ie Li^+), if the ion sizes are sufficiently different (ie Cl^- and [NTf_2]$^-$), this will spontaneously induce as phase separation as it becomes thermodynamically favourable to satisfy the electroneutrality and packing constraints of the ions separately rather than mixed [96]. Gutowski *et al.* have also shown that even simple hydrophilic ILs such as [BMIm][Cl] can form ABS through the use of kosmotropic salts [97], while Freire *et al.* have shown that the addition of water miscible, chaotropic salts such as [BMIm][Cl] or [P_{4444}][Cl] to polyethylene glycol-water mixtures can induce the formation of an ABS [98].

1.2.3 Liquid structure of ionic liquids

It was originally unclear whether ILs had a homogenous and disordered structure like conventional molecular liquids or concentrated salt solutions or an organised liquid phase like molten salts with an alternating cation-anion structure [99]. In the last decade advances in computational and experimental techniques have allowed for a deeper insight into the structure of liquids, even the structure of water and the effect of dissolved ions is still being refined to this day [100, 101]. Several comprehensive reviews on the structure of ILs were published in 2015 [102–104] while a more recent review looks specifically at the extent of ion dissociation in ILs [105].

In the 80's and 90's liquid crystal phases were discovered for pyridinium [106], ammonium [107], phosphonium [108] and long chain imidazolium [109] salts. These developments suggested that some degree of mesomorphic structure also existed within similar ionic liquids. Bradley *et al.* first used small angle X-ray scattering to study long chain (> C_{12}) imidazolium ILs and found evidence of enantiotropic smectic A mesophases, or in simple term, layered sheets similar to a lipid bilayer with alternating polar-non-polar sheets as shown in figure 1.8 [110].

Using molecular dynamic simulations in 2006, Canongia Lopes and Pádua suggested that the alkyl chains only needed to be C_4 in length before they begin to aggregate into non-polar domains, while the charged species form a dynamic three-dimensional ionic network throughout the bulk as shown in figure 1.9 [111].

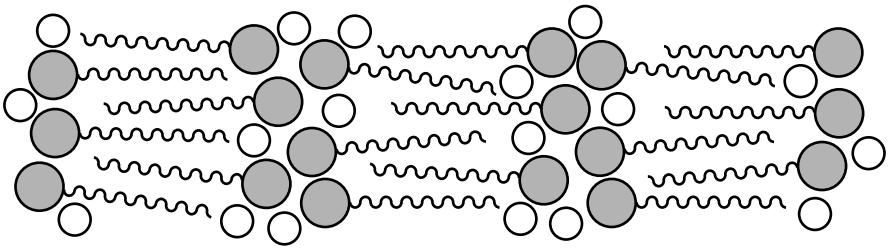

Figure 1.8: Cartoon representation of the enantiotropic smectic A mesophases reported for $[C_{18}C_1Im]Cl$ from reference [110]. Cationic headgroups shown in grey with anions shown in white.

Hardacre *et al.* also examined these same intermediate chain length ILs using small angle neutron scattering which showed that while there was no long range ordering in the liquid, they observed a 'low-Q length correlation indicative of a locally structured ionic lattice'. [112]. In 2013, Kiantz *et al.* measured the diffusion coefficients of various neutral and charged solutes in several ILs and found large deviations from the values predicted by the Stokes-Einstein equation [113]. Araque *et al.* used molecular dynamics to explain these deviations and build a model as shown in figure 1.10 [114]. They showed that neutral solutes will be pushed to the non-polar/hydrophobic/fatty domains via the hydrophobic effect and that these domains are 'soft' (lower local density and viscosity) and so will provide lower local friction therefore allowing higher mobility. Conversely, charged solutes will be attracted to the polar/hydrophilic/charged network domains which are 'stiff' (higher local density and viscosity) and their mobility is reduced to a concerted motion with the surrounding ions of the IL which is hard to escape [115]. This is the current consensus for amphiphilic ILs, alternating cation-anion structure in polar regions with the non-polar alkyl tails aggregating into non-polar domains.

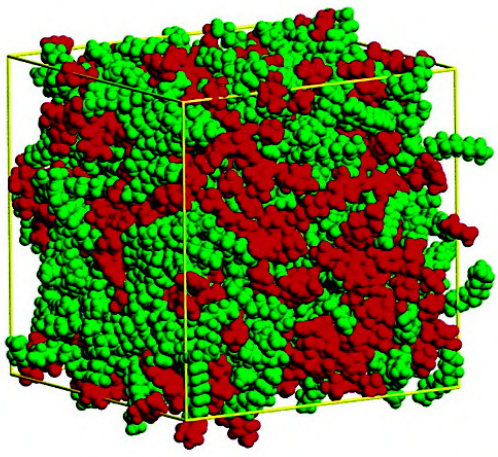

Figure 1.9: Canongia Lopes and Pádua's computed structure for $[C_{12}C_1Im][PF_6]$. Red is the polar headgroup and anion, green is the non-polar alkyl chains [111]

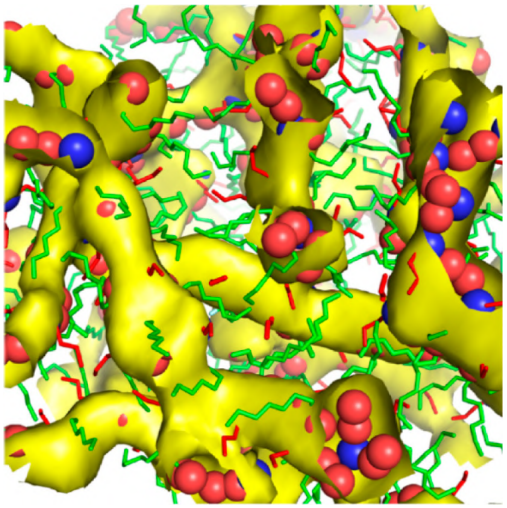

Figure 1.10: Computed structure for butylammonium pentadecafluorooctanoate reported by Araque *et al.*. Yellow represents the charge alternating polar network[114].

An earlier competing idea at the time proposed the structure of ILs to be similar to that of (reverse) micelles with spheres of anions and cationic head-groups either surrounding or surrounded by alkyl chains, simple diagrams of these are shown in figure 1.11 [116–118] These models were simplistic, and while they were based on the grounded knowledge of surfactant self-assembly into liquid crystals, they imply the existence of micellar cubic lyotropic mesophases with less efficient packing than the structures described above. Moreover, cubic micellar and continuous mesophases of lyotropic surfactants have even greater order and viscosity than ILs which are not normally liquid crystalline.

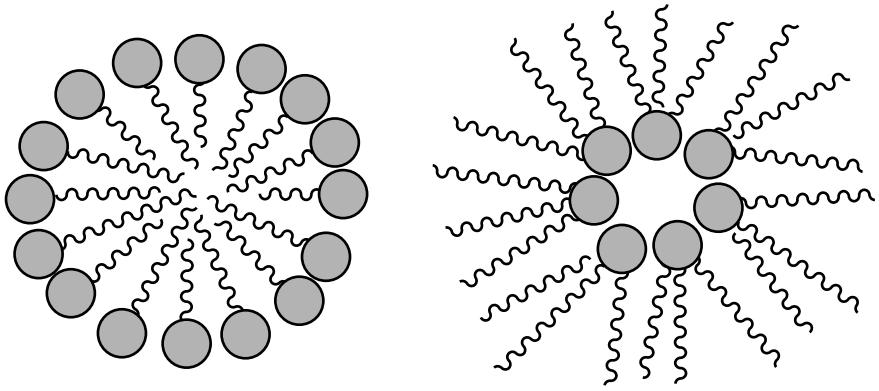

Figure 1.11: Cartoon representation of a (left) micelle and (right) reverse micelle showing the polar headgroups (anionic or cationic) in grey.

The phenomena of surfactant self-assembly has been well studied for decades, in 1973 Tanford first proposed the hydrophobic effect to describe why they form, how they grow and why they cannot grow past a limit [119]. He proposed opposing

forces to calculate the standard free energy change of aggregation as follows:

$$\left(\frac{\Delta\mu^o}{kT}\right) = \left(\frac{\Delta\mu^o}{kT}\right)_{Transfer} + \left(\frac{\sigma a_e}{kT}\right)_{Interface} + \left(\frac{\alpha}{kTa}\right)_{Head} \tag{1.7}$$

Here the transfer term is strongly dependant on the tail length as it represents the favourable transfer of the tails from their unfavourable contact with water to the hydrophobic core and is the only negative contribution to the free energy. The interface term accounts for the residual tail-water contact that exists at the surface of the micelle core represented by the product of the interfacial free energy, σ, and the surface area per molecule a_e. The head term accounts for the steric and electrostatic repulsive force between the head groups with the headgroup parameter α. Israelachvili, Mitchell, and Ninham then proposed the packing parameter: [120]

$$PP = \frac{v_o}{a_e l_o} \tag{1.8}$$

Where Vo/lo represents the ratio of the tail volume to tail length and a_e represents the surface area of the hydrophobic core per molecule ie. how tightly packed the headgroups are, shown pictorially in figure 1.12. For one and two carbon chains, V_o/l_o is a constant at 21 and 42 Å respectively, so the morphology is only dictated by the surface area a_e. If $0 \leq P \leq 1/3$ there is a bias towards the formation of spherical micelles, $1/3 \leq P \leq 1/2$ favours rod-like micelles and $1/2 \leq P \leq 1$ for a bilayer (similar to the structure shown in 1.8), with the geometrical constraint that the radius or half-bilayer thickness cannot be greater than l_o. Rationally this makes sense as surface curvature of each morphology reduces as the surfactant becomes more uniform along its length.

Nearly thirty years later Nagaraian explained some anomalous results by showing that under ideal conditions, the tail length is really what defines the morphology of the aggregate [121]. Surfactants with longer alkyl chains are known experimentally to have lower critical micellar concentrations (CMC) and aggregation numbers due to the greater negative contribution by the transfer term in the free energy of aggregation [122]. He used this to deduce that for ionic surfactants, the cross-sectional area per molecule at the micellar interface is dependant on the ionic strength of the solution, thus in solutions were the ionic surfactant is the only solute present at the CMC, the surface area occupied by each monomer is dependant on the chain length as per:

$$a_e \propto \sqrt{\frac{1}{l_o}} \tag{1.9}$$

This effectively means that having a longer chain creates a greater driving force for self-assembly but also reduces the packing efficiency.

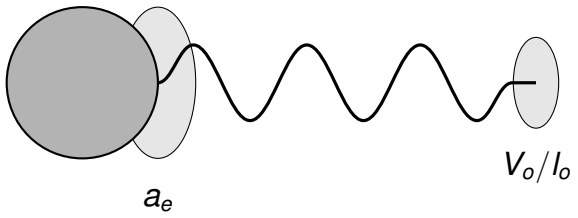

Figure 1.12: Cartoon representation of the molecular packing parameter considerations for each monomer in a molecular assembly, where V_o/l_o represents the ratio of the tail volume to tail length and a_e represents the surface area of the hydrophobic core per molecule from ref [120].

Most of the scientific focus was on the formation of micelles in water rather than the less common reverse micelles that exist in hydrophobic solvents, a recently published review details the current understanding and some potential applications for reverse micelles [123]. Reverse micelles differ in several ways with the main difference being the ionic headgroups and counterions are attracted to each other providing the driving force for the assembly rather than the exclusion of alkyl groups from bulk water. However, because the ions are now in such close proximity, electrostatic repulsion plays a key role as well as the interfacial tension as the core can be thought of as a water droplet of high ionic strength. Here, co-surfactants (usually short to medium chain length alcohols) can help to reduce the interfacial tension, interpolating between the surfactant molecules to reduce repulsion forces and lower the interfacial tension. In 1978 Eicke and Christen proposed that water may be a necessary component in the formation of reverse micelles but due to experimental limitations, no one at the time could sufficiently dry reverse micelles to show they could form in anhydrous conditions [124]. There are now several examples of 'dry' reverse micelles in the literature however they are still not well understood. [125]. More than 40 years after the work of Eicke and Christen, Rusanov would build on this to show that water indeed reduces the CMC of reverse micelle systems by expanding the volume of the core, reducing the curvature and electrostatic repulsion between headgroups thereby stabilising the assembly [126].

In conclusion it is the unfavourable interactions between the hydrophobic tails and the water that lead to the hydrophobic effect and the driving force for the self-assembly of micelles. For reverse micelles the favourable electrostatic attraction between the charged headgroups and counterions as well as the incorporation of water into the core to stabilise this pocket of high charge density is the driving force for the self-assembly of reverse micelles For both assemblies, the morphology of the resulting structure is mostly dependant on the ratio of the tail area V_o/l_o to the headgroup area a_e.

Aliquat® 336 has been known to form reverse micelles in non-polar solvents for

decades with a host of applications, mainly purification of large biomolecules similar to the ABSs described above, being reported in the literature. Jolivalt *et al.* have shown that in a solution of isooctane with co-surfactant isotridecanol can extract α-chymotrypsin from aqueous solutions, interestingly they also mention the co-extraction of water and alcohols into the extracting phase [127]. Dövyap *et al.* later showed that a similar system could also extract amino acids [128], while Oliveira and Bertazzoli showed that Aliquat® 336 could form micelles in 0.1 M K_2SO_4 with a CMC of $4x10^{-5}$ M [129]. Duad and Cattrall examined the extraction of Zn^{II} with methyltrioctylammonium and methyltridecylammonium chloride (two major components of Aliquat® 336) and showed that these do not form reverse micelles but weak dimers in chloroform and isobutylmethylketone by vapour phase osmometry [130].

In 2018 Williams *et al.* reported a 'surprisingly simple' yet effective reverse micelle forming extractant for sulfate, shown in figure 1.13 [131]. The authors used a branched isoparaffinic solvent (isopar L) without co-surfactant and confirmed the existence of large reverse micelles using small angle X-ray scattering. An exceptionally large distribution ratio of 5,300 was measured for sulfate, from an aqueous solution containing 0.1 mM Na_2SO_4 and 10 mM NaCl. This is an unprecedented reversal of selectivity, with a reported selectively factor of 4,300 for $[SO_4]^{2-}$ over Cl^-. The authors postulated that the divalent charge of sulfate was better able to stabilise the core of the reverse micelles and that the water in the core allows the extraction process to circumvent the large hydration enthalpy as the extracted ion does not need to shed it's hydration sphere. The guanidinium core of this extractant is also able to complex with the sulfate through hydrogen bonding as will be discussed in the next section.

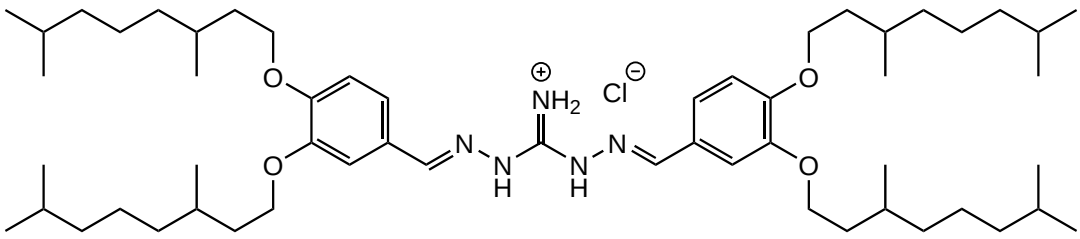

Figure 1.13: Guanidinium receptor that has remarkable selectivity for sulfate over chloride by forming reverse micelles.

1.3 Anion coordination

The first report of an anion receptor was by Park and Simmons in 1968 [132–134]. They were investigating the conformational properties of macrobicyclic amines and

showed that there was a different conformational preference when the amines were protonated by HF and HCl. With HCl they showed that a chloride ion is encapsulated inside the receptor and held by hydrogen-bonds (H-bonds). This work was not fully recognised at the time and it took another decade for the concept of anion coordination to be proposed by Lehn [135]. Lehn was further investigating the chemistry of aza-crown ether ligands when he recognised that these molecules also encapsulated anions through hydrogen bonds (H-bonds), one of these complexes is as shown in figure 1.14. The field is now widely recognised and has been extensively reviewed [80, 136–144]. A Bowman-James's 2005 paper is seminal in the field as it lays out the history and draws parallels to the field of metal coordination [145].

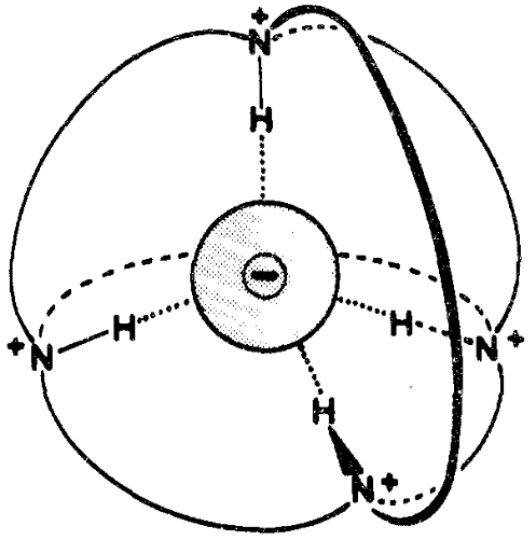

Figure 1.14: A chloride ion encapsulated by a spheroidal N-protonated macrotricyclic cryptand. One of the first formal recognitions of an anion complex [135].

Anion coordination is very similar to transition metal coordination as shown in figure 1.15, the main difference is the kind of coordination bond. Whereas metals are Lewis acidic and accept a pair of electrons from a Lewis base, anions are Lewis and Brønsted basic and donate an electron pair into the antibonding orbital of a Brønsted acidic hydrogen. This sharing of a hydrogen between two electronegative atoms is a weak interaction that can be estimated by the pK_a slide rule developed by Gilli *et al.* [146]. The strength of metal-ligand dative bond is usually around 100 - 500 kJ·mol^{-1}, while H-bonds tend to be much weaker, in the range of 5 - 50 kJ·mol^{-1}. The terminology used also differs slightly; where ligands bind to metals, anions bind to receptors.

As with traditional metal ligation, many of the same principles apply for anion complexes such as the chelate and macrocycle effects but specific orbitals interactions such as π back-bonding do not. In fact, because of the relative weakness of

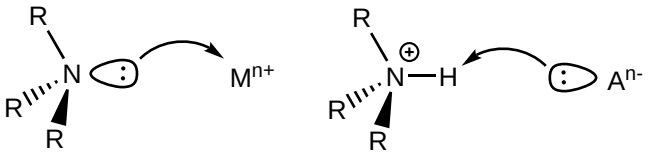

Figure 1.15: schematic showing the difference between (left) a metal dative bond and (right) an anion hydrogen bond.

H-bonds, it is crucial for strong receptors to have optimal binding geometry and a maximal number of H-bonds. Similar to enzymology, many receptors have an 'active site' where the guest is bound and around which other groups may be added such as alkyl chains to increase hydrophobicity or chromophores for sensing. It has been suggested that this area of anion coordination could find applications such as transmembrane transport [147], sensing [148, 149], separation and extraction applications such as nuclear waste treatment [19], anion driven supramolecular assemblies [150] and even anion driven organocatalysis [151].

Direct sulfate coordination for selective removal has not been employed industrially to date due to the difficulty of the challenge and wide range of other options available as discussed in section 1.2.

1.3.1 Hydrogen bond donors

Gilli *et al.* related the strength of a hydrogen bond to the ΔpK_a between the respective donor and conjugate acid of the acceptor [146]. For an acid dissociation reaction as shown in equation 1.10, the acid dissociation constant, K_a of a proton is the degree of dissociation of that proton in a given solvent as per equation 1.11 and the pK_a is the negative logarithm of the K_a as per equation 1.12. A smaller pK_a relates to a more acidic proton.

$$HA \rightleftharpoons H^+ + A^- \tag{1.10}$$

$$K_a = \frac{[H^+][A^-]}{[HA]} \tag{1.11}$$

$$pK_a = -\log(K_a) \tag{1.12}$$

If the ΔpK_a is very low then the proton is shared evenly between the two species, forming a strong low-barrier hydrogen bond [152–154]. They also proposed charge and resonance assisted H-bonds, here the delocalisation or charge balancing helps to stabilise and strengthen the H-bond. With sulfate being so weakly basic, sulfate complex H-bonds will always be relatively weak. Rozenberg *et al.* have calculated the hydrogen bond strength of sulfuric acid and water, here each hydrogen bond is $\approx$ 25 kJmol^{-1} with the strongest being between two sulfate molecules at

31.6 kJmol^{-1} [155].

All pK_a values in this section are reported with a subscript that denotes the solvent in which it applies and most are taken from the Bordwell pK_a table [156]. Although the conversion has not been used in this review, Rossini *et al.* have developed and empirical method for converting the pK_a of a substrate from one solvent to another [157]. To generalise, O−H bonds are more acidic in water by about 7 - 8 pK_a units while amine N−H bonds are usually similar, differing by $\pm$0.5 units. Thioureas, squaramides and imides are also more acidic in water by about 3.5 - 6 units.

Nitrogen based functional groups are by far the most common for anion receptor chemistry. The simplest of them, a neutral amine group is a very weak donor as the protons are not acidic as reflected by their large $pK_{a\,(DMSO)} > 37$. Upon gaining a proton to form the ammonium ion as shown in figure 1.16, the $pK_{a\,(water)}$ drops to *ca.* 10, making it a much better donor. The positive charge on the ammonium ion also attracts the negative charge of an incoming anion forming a stronger, charge stabilised H-bond. As stated earlier, tetraalkylammonium functional groups are commonly used in anion exchange resins but in these cases the anion is only attracted by electrostatics as there are no acidic hydrogens to form H-bonds. Aromatic amines such as aniline are also commonly employed as the electron withdrawing phenyl ring increases the acidity of the hydrogen sites to $pK_{a\,(DMSO)} = 30.6$. More commonly, aromatic diamines such as *o*-phenylenediamine, naphthalene-1,8-diamine or *m*-xylyldiamine are used as central spacers or scaffolds for anion receptors as will be discussed in section 1.3.2. The aromatic ring also enables resonance stabilised H-bonds, allowing tighter binding than their pK_a's would suggest.

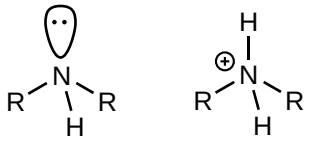

Figure 1.16: Structures of a (left) secondary amine and (right) tertiary ammonium ion.

Amide groups as shown in figure 1.17 are commonly employed in the synthesis of anion receptors. Not only do they offer a good hydrogen bonding site but also because they are easily accessible synthetically and can connect structural components. They can have a broad range of pK_a values depending on the R group attached to the α-carbon or nitrogen. If both substituents are methyl groups, the $pK_{a\,(DMSO)}$ is 25.9, however, if both are electron withdrawing phenyl rings then this drop to 18.8, allowing the formation of stronger H-bonds. Amides are also commonly found in biological anion binding, eg. the sulfate binding protein *salmonella*

typhimurium, which will also be discussed in section 1.3.2, binds sulfate through five amide groups along its polymer backbone.

Squaramides also shown in figure 1.17 have also been widely investigated despite their expensive dialkoxysquarate or squarate dichloride starting material due to their remarkable hydrogen bonding ability. They can donate two electron pairs from the carbonyl groups while donating two hydrogens through the two amine groups, this allow for simultaneous binding of a cation and anion. The lone pairs on the nitrogens are not nucleophilic as they conjugate into the π system of the ring which further acidifies the hydrogens. Their acidity has not been quantified extensively but with electron withdrawing substituents, the $pK_{a\,(DMSO)}$ has been reported to vary from 8.5 to 16.5 [158]. The two hydrogens point slightly inwards when in the *syn-syn* conformation which allows them to be 10 - 50 times stronger halide receptors than corresponding thioureas [159]. The formation of these N−H H-bonds and the donation of the oxygen lone pairs to a Lewis acid, all contribute to greater aromaticity of the four member ring which stabilises the resulting complex [160]. Thiosquaramides have also been synthesised and reported to have greater acidity and aromaticity to their oxygen analogues, however they have not received much attention from the anion coordination community due to deprotonation as they are significantly more acidic than their oxo counterparts [161].

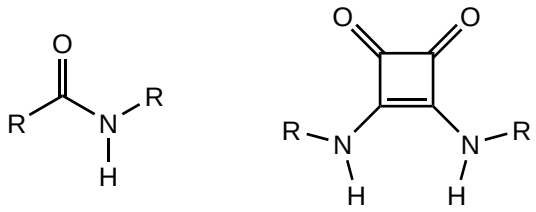

Figure 1.17: Structures of doubly substituted (left) amide and (right) squaramide.

Ureas and thioureas as shown in figure 1.18 are the most common motifs in anion coordination chemistry and are among the most commonly used. They are easily accessible synthetically, and are used like amides to link structure components via the simple reaction of a primary amine with an iso(thio)cyanate. They are also strong bidentate hydrogen bond donors, especially to oxyanions because of their two parallel N−H groups. While urea has a relatively high $pK_{a\,(DMSO)}$ of 26.9, thiourea is much more acidic due to the larger sulfur atom being better able to stabilise the negative charge, its $pK_{a\,(DMSO)}$ being 21. The addition of alkyl or phenyl groups further acidify these groups and it is common to see them linked by phenyl rings as will be seen in the next section. Similar to squaramides, (thio)ureas preferentially protonate on the oxygen or sulfur as it is more nucleophilic than the lone pairs on the nitrogen which are delocalised through resonance. Thioureas are also nucleophilic enough to be alkylated into isothiouronium salts, these moieties have

been used in anion recognition but have not been widely explored due to their base catalysed hydrolysis into thiols [162]. Neutral guanidines are extremely basic and so are usually found as the protonated guanidinium cations. Guanidinium groups, while less used due to their more challenging synthesis, are still of interest because of their appropriate $pK_{a\ (water)}$ of 13.6, and the positive charge providing electrostatic attraction which further enables strong binding. Selenoureas also exist, however due to their toxicity and are synthetically expensive so they have not been widely studied [163–165].

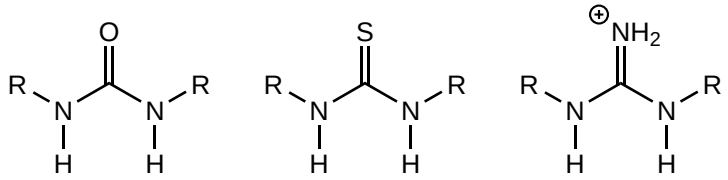

Figure 1.18: Structures of doubly substituted (left) urea, (middle) thiourea and (right) guanidinium.

The last nitrogen containing functional groups to be discussed are heterocycles such as those shown in figure 1.19. The most popular of which are pyrrole and indoles (α,β-fused phenylpyrroles), which are found in sulfate binding protein and anion-binding calixpyrroles, a class of conical receptor and an intermediate in the synthesis of porphyrins. The relatively low $pK_{a\ (DMSO)}$ of 23 and 21 of pyrroles and indoles respectively mark them as prime candidates for hydrogen bonding with conjugate base anions of strong acids. Similarly, imidazole, triazoles and tetrazoles have been been used as the replacement of each ring C with N further increases the acidity of the N – H sites.

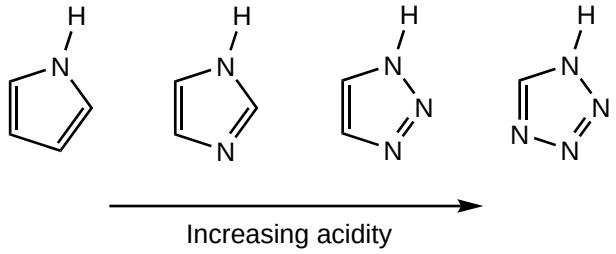

Figure 1.19: Structures of (from left to right) pyrrole, imidazole, 1,2,3-triazole and tetrazole.

Hydroxyl groups have received a lot of attention [166] and have $pK_{a\ (water)}$ values around 16, so they are good hydrogen bond donors. However, they are hard to place into favourable conformations for binding as they are terminal substituents, unlike amines that can be incorporated into the backbone of a receptor. This also gives them another degree of freedom as the C – O bond can rotate freely, and so

the O−H bond orientation will be constantly changing. They are also prone to deprotonation, as the O−H···A^- bond forms, electron density builds on the oxygen, making it more nucleophilic and more likely to form a second H-bond with a neighbouring proton in the solution. Phenols with their even lower $pK_{a\ (water)}$ of roughly 10 have also been used in some cases although less common and even catechols have been used although they usually only form one H-bond with an anion as the other hydroxy forms an intramolecular H-bond to stabilise the first bond.

While it is widely recognised that C−H groups are weaker hydrogen bond donors than the corresponding N−H groups, some researchers have activated C−H bonds through use of highly electron withdrawing groups [167]. These ligands tend to be reasonable hydrogen donors but this not a viable method of approach for industry due to their complex nature and under performance. One notable mention is that of imidazolium containing receptors, as the C_2 position in the ring is especially acidic, as shown in ILs previously, it can deprotonate to form a carbene [168]. Anions as weakly basic as acetate have been shown to have transient carbene concentrations in imidazolium ILs [169].

1.3.2 Sulfate receptors

In this section an overview of the novel and notable advancements in the evolution of sulfate binding receptors will be discussed although binding of other anions will be mentioned where appropriate. Where applicable, as in crystal or solution state complex formulae, it is common practice to reduce the receptor name to L to show the stoichiometry.

The binding of a receptor can be defined by equation 1.13, where H is the host (receptor), G is the guest and HG is the host-guest complex. The strength of binding can be quantified by the equilibrium constant K_b (also known as the binding or association constant), which is the ratio of the host-guest complex concentration to the product of the host and guest concentrations as shown in equation 1.14. In this chapter, binding constants will be reported as stability constants, or pK_b values which is the log of K_b as per equation 1.15, a larger value relates to stronger binding. For receptors that bind in a 1:2, 2:1 or greater stoichiometries, binding constants can be determined for each binding step.

$$H + G \rightleftharpoons HG \tag{1.13}$$

$$K_b = \frac{[HG]}{[H][G]} \tag{1.14}$$

$$pK_b = \log(K_b) \tag{1.15}$$

Binding constants are more commonly denoted as K_a, however, this may cause some confusion with acid dissociation constants discussed previously and so will be referred to as K_b in this work. Similarly to pK_a's, the pK_b's in this section will be shown with a subscript to denote the solvent in which they were measured. For most receptors, sulfate binding will be at a minimum in the highly competitive environment of water whereas DMSO provides a slightly less competitive environment and acetonitrile even less so, enabling stronger binding. Once the binding constant is known, the Gibbs free energy of binding can then also be calculated as per equation 1.16, which can then also give information on the thermodynamics of the system using equation 1.17 to derive the van't Hoff equation 1.18 where R is the ideal gas constant and T is the temperature in Kelvin.

$$\Delta G = -RT \ln K_b \tag{1.16}$$

$$\Delta G = \Delta H - T\Delta S \tag{1.17}$$

$$\ln K_b = -\frac{\Delta H}{R} \cdot \frac{1}{T} + \frac{\Delta S}{R} \tag{1.18}$$

Quantifying the strength and stoichiometry of an interaction between two molecules in solution can be exceptionally difficult and there are now a number of practical guides to help with these studies [170, 171]. The basics are as follows; firstly to determine the stoichiometry, a Job plot (aka method of continuous variation) is used. In these studies, the concentration of the host-guest complex ([HG]) is measured against varying molar ratios of the host ([H]) and guest ([G]) where the sum of the molar concentrations is held constant ([H] + [G] = constant). This should lead to a single peak, where [HG] is at a maximum at the stoichiometry that corresponds to the most favourable for that host and guest. To determine the binding strength, a binding study is conducted where [H] is kept constant, while [G] is gradually increased and again [HG] is measured. The rate at which [HG] increases as a function of [G] can be analysed using a non-linear regression by programs such as Bindfit [172] and Suprafit [173] or the older WinEQNMR2 [174]. It is worth noting that most researchers now skip over the Job plot step as the newer data analysis programs will analyse the data for all reasonable stoichiometries to determine the best fit [175]. While this is an effective way for researchers to reduce the practical work load, it places extra emphasis on the binding study which is notoriously sensitive and difficult to conduct.

The two most common practical methods used for binding studies are NMR and UV-vis spectroscopy [171]. While ^{13}C and ^{19}F NMR spectroscopy are sometimes used, ^{1}H NMR is by far the most common nowadays due to the quick acquisition time and the information it yields about the specific interactions at each hydrogen

site. Modern NMR instruments can now obtain good quality spectra with concentrations as low as 10^{-4} M, allowing for determination of pK_b values up to 6, although 4 or 5 is commonly referred to as the practical limit. If the rate of association and disassociation is slower than the NMR timescale then the ratio of [H] to [HG] can be determined by integration of the reducing host peaks and the growing host-guest complex peaks. Much more commonly, the rate is faster that the NMR timescale and so the observed peak (δ_{obs}) will be the weighted average of the proton in both species and is described by equation 1.19.

$$\delta_{obs} = \delta_H + (\delta_{HG} - \delta_H)\left(\frac{[HG]}{[H]_0}\right) \tag{1.19}$$

The problem is that it is usually very difficult to accurately determine the equilibrium concentrations [H], [G] and [HG]. Thankfully, [HG] can be calculated using only $[H]_0$, $[G]_0$ and K_b and the following quadratic equation 1.20 which has only one relevant solution.

$$[HG] = \frac{1}{2}\left\{\left([G]_0 + [H]_0 + \frac{1}{K_b}\right) - \sqrt{\left([G]_0 + [H]_0 + \frac{1}{K_b}\right)^2 - 4[H]_0[G_0]}\right\} \tag{1.20}$$

This allows for the determination of K_b via an iterative approach where known values of $[H]_0$ and $[G]_0$ are used in equation 1.20 along with estimates of K_b, the resulting [HG] value is then used in equation 1.19 and the calculated and measured δ_{obs} values can be compared until the best fit is found.

For UV-vis spectroscopy, the receptor must be UV active which usually requires the inclusion of a chromophore group such as a nitrophenyl or porphyrin ring. With a strong chromophore, host concentrations of 10^{-7} M can be analysed, allowing for determination of pK_b's up to 9, although receptors this strong are rare. In UV-vis the concentrations of each species is directly related to the absorption at each wavelength as per the Beer-Lambert law.

$$A = \varepsilon l c \tag{1.21}$$

Where A is the absorption, ε is the molar absorptivity, l is the sample length and c is the concentration. This therefore requires a significant change in the hosts molar absorptivity upon complexion and formation of the complex. It is also desirable for the guest to have no overlapping peaks, although this is usually the case with small cationic and anionic guests.

For both methods it is absolutely crucial that the host and guest are both soluble in the same solvent, for many sulfate receptors DMSO is the only practicable option

and this poses a significant problem. The traditional method for binding studies is titration where a host solution is made at say 1 mM, and a guest solution is made at 20 mM which also contains 1 mM host. This way the host solution can be analysed, an aliquat of guest solution is then added which increases [G] while keeping [H] constant, and the resulting solution analysed again. It is desirable to have at least 15-20 data points (addition-analysis cycles) in the range between minimum and maximum response for 1:1 binding, and more data points for more complex equilibria. DMSO is extremely hygroscopic, at only 30% relative humidity at 22℃, it will absorb 1 mg of water per cm^2 surface area per hour, [176]. over the course of 20 additions, the concentration of water in the solvent will gradually increase and since the titration measures a gradual response from the sample, the effect of the water will be effectively camouflaged into the data. This systematic error accumulation could potentially be avoided by preparation of all the necessary samples at one time, however this requires much more host, guest and solvent and can introduce random error between samples. Most published binding studies ignore this and state a solvent composition of DMSO-0.5% water without any explanation if this water was added or just the assumed water from ambient absorption. This should be kept in mind when viewing results from DMSO binding studies performed via a titration method, unless performed in labs that operate at 0% humidity.

Isothermal titration calorimetry (ITC) is now the gold standard for measuring binding constants as it directly measures the tiny change in sample temperature while adding the guest to the host. This is a direct measurement of the enthalpy change as a function of stoichiometry which can then be used to calculate the entropy and Gibbs free energy of binding. There are several barriers to ITC however, one problem is that one ITC machine can cost upwards of £100,000 and so is unaffordable to many chemists, it is also a highly specialised piece of equipment so many research departments will not prioritise it over a more versatile instrument such as a UV or NMR spectrometer.

For sulfate extraction studies the results are often presented as a percentage of sulfate removal, however, distribution ratios ($D_{sulfate}$) are also used by some groups where:

$$D_{sulfate} = \frac{[SO_4]^{2-}_{\text{total organic}}}{[SO_4]^{2-}_{\text{total aqueous}}} \tag{1.22}$$

Extractions are considered to be technologically useful when $D_{sulfate}$ is greater than 1 as stagewise extraction is generally considered viable. It is worth noting that the distribution ratio is only equivalent to the partition coefficient if the extracted species does not have any secondary equilibria. This is generally considered the case for sulfate in neutral or alkaline waters as there will be negligible acid base equilibria being so far from sulfuric acid's pK_{a1} of 1.99. Both coefficients also assume that

thermodynamic equilibrium has been reached at an infinite dilution whereas real world extractions usually occur at high concentrations.

Nature is often a good place to begin when looking for inspiration. In the early 1990's F. Quiocho *et al.* first elucidated the atomic basis for the selectivity of sulfate and phosphate binding proteins isolated from the periplasmic space of gram-negative bacteria *Salmonella Typhimurium* [177]. These receptors are involved in active transport of the ions and so must be highly specific for each. In the sulfate binding protein, dehydrated sulfate is held tightly in a cleft where it is bound by seven hydrogen bonds from neutral donor groups as shown in figure 1.20. The

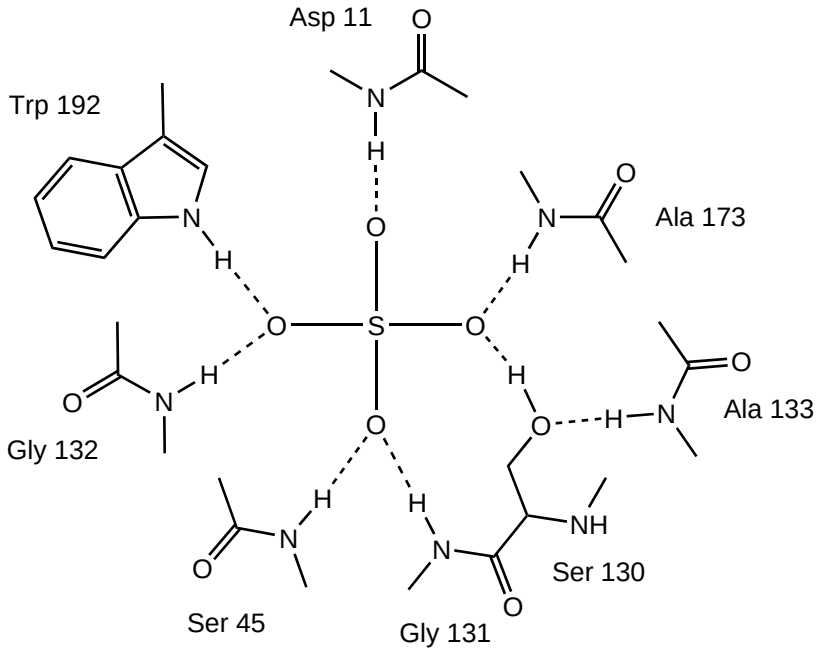

Figure 1.20: Hydrogen bond donor groups involved in sulfate binding from wild type *Salmonella Typhimurium* binding protein. Reproduced from ref. [177].

donor groups are one indole ring from tryptophan 192 and a hydroxyl from serine 130 which is in turn receiving a hydrogen bond from the neighbouring alanine 133. The final five hydrogen bonds are from the amide groups in the peptide chain from aspartic acid 11, serine 45, glycine 131 and 132 and alanine 173. The wild type protein is reported to have a dissociation constant of 0.17 µM (pK_a = 6.8) [178].

Shortly after, in 1995 Nishizawa *et al.* were the first to report on a series of synthetic thiourea receptors using a *m*-xylyldiamine spacer that had high affinity for dihydrogen phosphate [179, 180]. They showed that thiourea groups promoted the binding more so than urea groups and that this could be enhanced by the addition of electron withdrawing phenyl groups rather than alkyl chains. Subsequently, they reported that the *bis*(phenylthiourea) receptor shown in figure 1.21 could overcome the hydration enthalpy of sulfate and partially extract it into 1,2-dichloroethane, the first receptor that could do so [181]. The binding constant $pK_{b\ (1,2\text{-DCE})}$ was reported

to be 6.41, 1,000 times greater than corresponding binding constants for chloride and acetate. It was also unclear in this case how charge balance was maintained ie. whether sodium ions were co-extracted or whether the tetraphenylborate supporting electrolyte anion was exchanged, the latter is suspected to be the case.

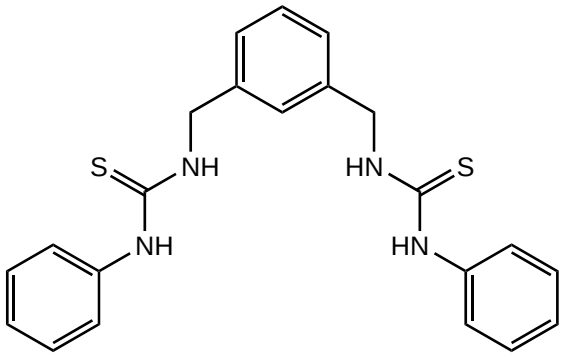

Figure 1.21: Structure of the early receptor reported to extract sulfate into 1,2-dichloroethane from ref. [181].

Brooks *et al.* then changed the middle spacer unit and tested a series of receptors based on *o*-phenylenediamine, some of which are shown in figure 1.22 and showed they had greater $pK_{b\,(DMSO)}$ values with acetate than *m*-xylyldiamine receptors [182]. Crucially they also showed that due to the lack of methylene spacers in these receptors, the large sulfur atom in the thioureas causes distortion in the receptors, preventing them from binding in the same plane and reducing their binding constants compared to the corresponding urea receptors [183]. Li *et al.* then used a small sample of these receptors to grow crystals of the sulfate and phosphate complexes and used SC-XRD to show these receptors bind in a similar fashion to that of metals and the 2,2'-bipyridine ligand [184]. Three receptors can bind to one central phosphate totalling twelve H-bonds whereas only two receptors bind to each sulfate for a total of eight H-bonds. The success of crystal growth depended heavily on the counter ion species present with the most success being found with alkylammonium cations or K^+[18]crown-6. Expanding upon this, UV-vis and ^{1}H NMR titrations showed that a 1:1 receptor:sulfate complex was preferred in solution and that the thiourea receptor was also observed to deprotonate in the presence of basic anions due to its higher acidity. Nearly a decade after the original paper, Moore *et al.* then showed that a series of these simple bis(urea) receptors could act as transmembrane transporters, able to facilitate the transport of chloride, carbonate and carboxylate anions across cell walls [185].

Jia *et al.* then expanded the receptor motif to include three (thio)urea units, making the linear trisurea receptors shown in figure 1.23 that can bind in a similar way to the terpyridine ligand [186]. Crystal structures revealed the receptors could bind phosphate in a 2:1, ligand:anion fashion and although no crystal structure

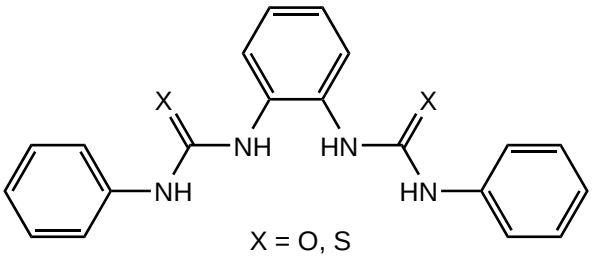

Figure 1.22: Structures of the simplest *o*-phenylenediamine based bis(thio)urea receptors from ref. [183].

could be obtained for sulfate, this conformation was also determined to be optimal by DFT calculations. Further analysis then showed that a 1:1 receptor-sulfate complex exists in solution with $pK_{b\ (75/25,\ DMSO/water)}$ of 4.73 for the trisurea receptor, determined by NMR titration. The authors also reported 'reversible binding and release of sulfate was also achieved by the modulation of Et_3N and $HClO_4$'. Zhang *et al.* also showed that systematically replacing the urea groups with thiourea weakened the strength of binding with sulfate. One central thiourea reduced the $pK_{b\ (75/25,\ DMSO/water)}$ to 3.54, while replacing all three reduced it further to 3.17 [187], reinforcing the previous work of Brooks *et al.* [183].

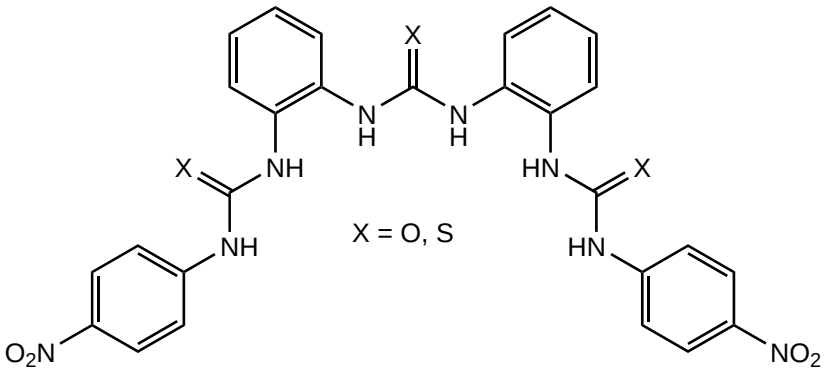

Figure 1.23: Structure of the linear trisurea receptors that binds to sulfate and phosphate in a 2:1 host:guest ratio from ref. [186].

Since Jia *et al.* [186] showed that three linear ureas were better than two, the *o*-phenylenediamine spacer was substituted with tris(2-aminoethyl)amine (tren) to yield tripodal receptors, the general structure of which is shown in figure 1.24. This family of receptors was actually first reported in 1995 by Raposo *et al.* [188] but research on these receptors did not continue until the late 2000's. Since then, they have been explored by many different groups but only those studies relating to sulfate extraction and transport will be mentioned here. In 2008 Wu *et al.* developed a tris(3-pyridylurea) receptor and showed co-crystallisation of this receptor with metal sulfate salts from a 50/50 water/methanol solution. The crystal complexes had compositions of $[M(H_2O)_6][L_2SO_4]$ where M = Zn or Mn and the sulfate is bound

by twelve hydrogens but unusually, some hydrogens appear to be shared between the sulfur's oxygens. Custelcean has also published a short review on tren based (thio)urea receptors for tetrahedral oxyanions, comparing their crystal structures and binding studies [189]. A potential application of nuclear waste remediation was discussed as it was shown that Wu *et al.*'s original tris(3-pyridylurea) receptor could selectively precipitate out a $Na_2SO_4(L)_2(H_2O)_4$ species from an aqueous sodium hydroxide solution, although the process took four days [190].

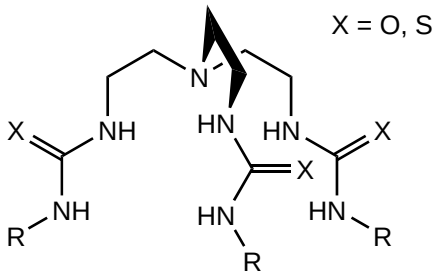

Figure 1.24: Basic structure of the tripodal tren based family of ligands.

Busschaert *et al.* investigated a series of ten tren based (thio)urea receptors with various fluorinated phenyl rings in the R positions as lipophilic transmembrane transporters [191]. Binding studies indicated a general trend in the binding constants $pK_{b\,(DMSO)}$ of $[SO_4]^{2-}$ > $[H_2PO_4]^-$ > Cl^- >$[HCO_3]^-$ » $[NO_3]^-$, where every receptor had a $pK_{b\,(DMSO)}$ > 4 for sulfate. They also noted that the more acidic receptors had lower binding constants which is unexpected but was attributed to increased competition from the solvent molecules. Only the receptor with pentafluorophenyl-thiourea functionality showed $Cl^-/{SO_4}^{2-}$ antiport activity indicating that the hydrophobic receptor could effectively screen the charge of the sulfate from the lipid bilayer, transporting chloride out of the cell and sulfate into the cell.

The Ghosh group also studied the same pentafluorophenyl-thiourea receptor [192] as well as two 4-cyanophenyl-(thio)urea receptors [193]. They used ITC to determine the $pK_{b\,(DMSO)}$ of the pentafluorophenyl receptor to be 4.67 while the thiourea-4-cyanophenyl receptor was only tested with $[HSO_4]^-$ and the $pK_{b\,(DMSO)}$ found to be 2.83, suggesting that sulfate protonation causes weaker binding by a reduction in H-bond acceptor ability. Extraction studies into chloroform were also performed for the fluorinated receptor, with tetrabutylammonium (TBA) chloride or carbonate added to the organic phase to help solubilise the receptors and to act as exchangeable ions. The pentafluorophenyl-thiourea receptor showed no sulfate extraction when the TBA chloride salt was used, however, when the divalent carbonate was used, almost quantitative extraction of sulfate was observed. The authors attribute this to the larger binding constants for sulfate over carbonate

($pK_{b\ (DMSO)}$ = 4.67 vs 4.07) and the large free energy of hydration of the carbonate anion, ΔG_{hyd} = -1315 $kJmol^{-1}$ compared to -1080 $kJmol^{-1}$ for sulfate [16].

Since three ureas were better than two, a hexa-urea dodecadentate receptor, shown in figure 1.25, was the next logical step for Jia *et al.* [194]. This receptor consisted of a tren base with three *o*-phenylenediamine bis(urea) arms. The authors report a crystal structure of the 1:1, receptor:sulfate complex where the sulfate is totally encapsulated by a tetrahedral cage bound by twelve H-bonds, Upon further addition of sulfate past one equivalent, ^{1}H NMR analysis shows the possible formation of a 1:2, ligand:sulfate complex. $pK_{b\ (DMSO)}$ could not accurately be determined but was measured to be larger than 4 by NMR titration. The authors also showed that this receptor could extract sulfate from an aqueous phase into a chloroform phase using sacrificial chloride ions to maintain charge balance, with extraction efficiencies above 95% with an equimolar amount of sulfate and receptor in the system. In 2022, the same group reported on a small series of these hexa-urea receptors and showed that they could be reused by washing with HCl and demonstrated eight reuse cycles with extraction efficiencies above 88% [195].

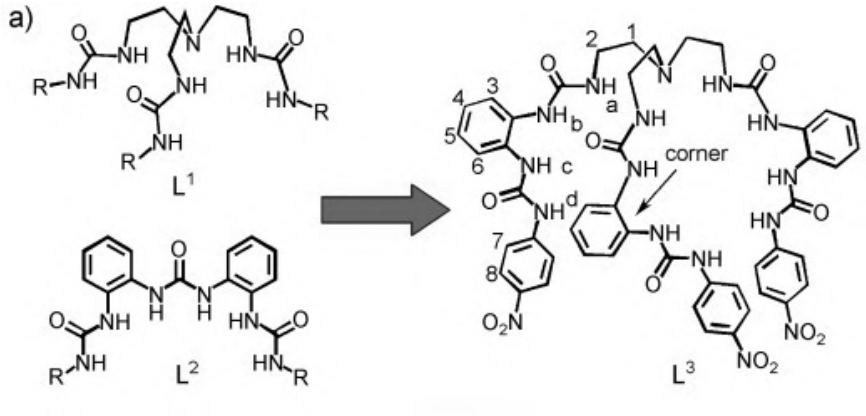

Figure 1.25: Rational behind the synthetic design of the hexaurea receptor [194].

In 2020 Qin *et al.* reported a macrocyclic tris-squaramide receptor (shown in figure 1.26) and investigated its extraction and transport properties [196]. ^{1}H NMR binding studies showed $pK_{b\ (CDCl3)}$ values greater than 4 for both sulfate and nitrate. In initial sulfate transport studies, aqueous $[TBA]_2[SO_4]$ was contacted with chloroform solutions of the receptors and it was found that one equivalent of sulfate was extracted in the form of $[SO_4(L)][TBA]_2$, $[TBA]^+$ being co-extracted. No sulfate was extracted when the aqueous phase contained only Na_2SO_4. In competitive solutions with the $[TBA]^+$ cation present, it was shown that the receptor preferentially extracts nitrate in a 10:1 $[NO]^-/[SO_4]^{2-}$ ratio at pH 7.4, but this lowers to 10:3 when the pH is reduced to 3.2 due to possible protonation of the pyridine moieties reducing the selectivity. Finally, they demonstrated a Cram U-tube set up with the bottom of the U being occupied by a chloroform membrane, while one side contains

aqueous Na_2SO_4 and the other side contains aqueous $BaNO_3$. Again, no sulfate transport was observed until TBA[NO_3] was added to the chloroform phase which then allowed the transport of sulfate across the U-tube. Sulfate transport was even observed from a highly competitive nuclear waste simulant solution although the rate was much slower.

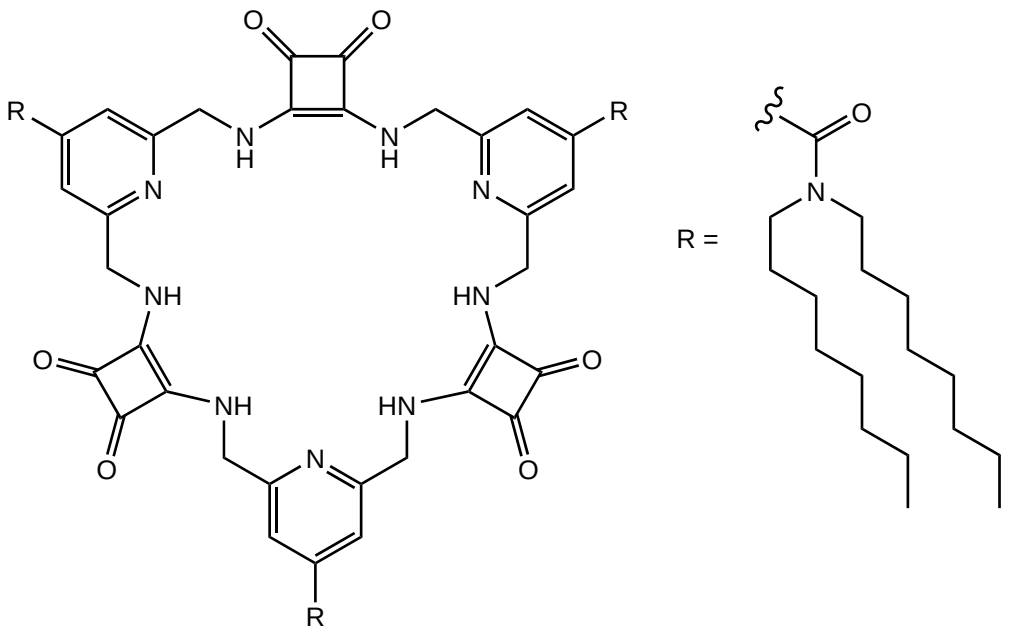

Figure 1.26: Structure of the macrocyclic squaramide receptors shown to transport sulfate across a U-tube from ref [196].

Calix[4]pyrrole (C4P) receptors have been known for many decades, in fact the first reported synthesis of *meso*-octamethyl-C4P, as shown in figure 1.27 was described by Baeyer in 1886 [197]. These molecules can sometimes be referred to as porphyrinogens because if there are *meso*-hydrogens present then the ring can easily be oxidised into a planar porphyrin. Fowler *et al.* first combined two fluorinated calix[n]pyrrole (n = 4 or 5) receptors with Aliquat 336N (N indicates that the chloride anion has been replaced with nitrate), the idea being to promote synergised ion-exchange, sulfate recognition combined with ion-exchange to maintain charge balance (this work was done before most of the work with the tren receptors using exchangeable ions) [198]. They showed that this significantly improved the sulfate extraction into chloroform and toluene. $D_{sulfate}$ values were able to be pushed just above 1 using 0.1 M Aliquat 336N combined with β-fluorinated C4P. Moyer *et al.* then expanded upon this and tested a larger series of decorated C4Ps and noted that halogenation of the receptor, counter-intuitively reduces the sulfate extraction [199]. They note *'Such effects suggest that interactions other than simple H-bond strength are operative in this system. One possibility that bears further investigation is that the quaternary ammonium cation may be playing a role in the*

context of the supramolecular structure of the organic-phase complex.'

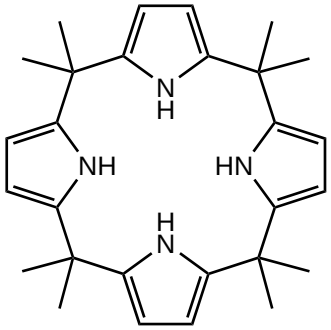

Figure 1.27: Structure of the *meso*-octamethylcalix[4]pyrrole receptor.

Soon after, they discovered that the synergised ion-exchange is markedly reduced when the quaternary ammonium ion does not bear a methyl group [200]. The crystal structure as shown in figure 1.28 clearly shows the insertion of the methyl group from the tributylmethylammonium (TBMA) cation into the cavity of the receptor, revealing a supramolecular structure of $[SO_4(L)(TBMA)]$. This had already been observed several times in the literature [201–203] and C4P had also been shown to act as an ion pair receptor for halogens and the Cs^+ ion in the same way [204] but was not yet recognised as being beneficial to the extraction of anions. This discovery led to a much more in depth study on the thermodynamics of the synergised ion-exchange where ion-exchange and ion-pairing occurs as a discrete first step, followed by the C4P binding [205]. One of the limitations of this receptor is its low solubility in many organic solvents, an easy method of overcoming this was to replace the acetone in the synthesis with 2-octanone to yield a tetrahexyltetramethyl receptor that is much more soluble in organic solvents [206]. Interestingly, the presence of longer alkyl chains increased the TBMA-chloride ion-pair binding from $pK_{b\ (CDCl3)}$ = 4.14 to 5.05 whereas replacement of the two methyl groups with a closed cyclohexyl ring reduces the binding [207]. This simple receptor has since been expanded into a whole family of 'strapped' C4Ps [208], bipyrrole strapped receptors have been shown to be 10 times better at extracting sulfate into chloroform than *m*-octamethyl C4P [209].

As discussed with the tren based family of receptors, sulfate receptors can be used to isolate anions via crystallisation. Crystal structure prediction is notoriously difficult which makes the design of precipitation agents very challenging. Custelcean *et al.* found a simple glyoxalbis(amidiniumhydrazone) receptor that spontaneously precipitates from aqueous sulfate solutions as a $[(SO_4)(H_2O)_5(L)]$ species with a solubility of 7.2 x 10^{-4} M [210]. Again this strategy involves phase separation of the sulfate with some of its hydration sphere, partially circumventing its free energy of hydration. The receptor is reported to be extremely easy to make as shown

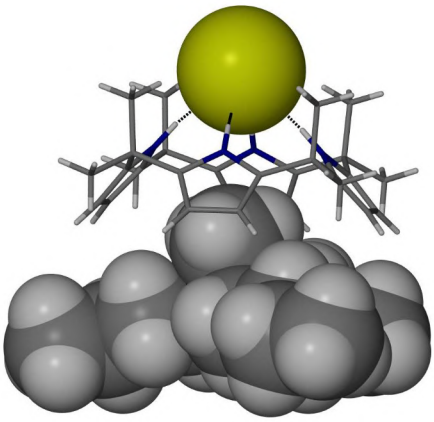

Figure 1.28: Crystal structure of methyltributylammonium chloride with *meso*-octamethylcalix[4]pyrrole, showing interpolation of the ammonium methyl group and H-bonding to the chloride anion [205].

in figure 1.29, and could be synthesised *in situ*, in the sulfate solution that is to be purified.

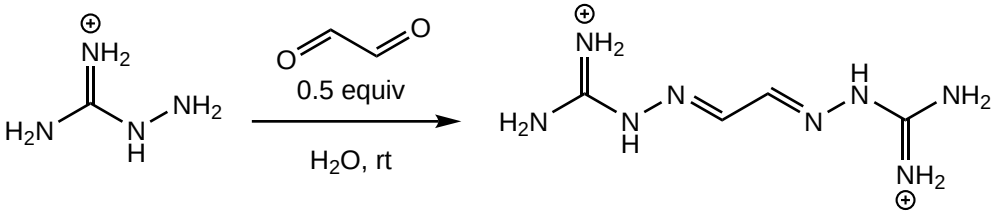

Figure 1.29: Synthesis of the glyoxalbis(amidiniumhydrazone) cation receptor that will selectively precipitate out sulfate from aqueous solutions from ref. [210].

One major problem that is not often addressed with using receptors for extraction is the process of back extraction, removing the sulfate from the receptor so it can be reused. Many receptors that can achieve sulfate removal are reported to be easily regenerated by barium precipitation [194, 196]. But in that case, why use the receptor at all? Why not just perform barium precipitation on the original feed source? Especially since regeneration from $BaSO_4$ is very energy intensive as previously discussed. Recently, Einkauf *et al.* published work on a diiminoguanidinium photoresponsive receptor shown in figure 1.30 [211]. Here the receptor is in the 'off' position when the imine double bonds are Z,Z as the pyridyl ring forms internal H-bonds to the guanidinium and so are not available for anion binding. Binding studies of the receptor in this state revealed a binding constant of $K_{b\,(DMSO)} = 1.85$. Once irradiated with UV light, the receptor converts to the E,E isomer where anion binding is turned 'on', and $K_{b\,(DMSO)}$ increases to 7.25, a 10^5 magnitude increase in binding. The receptor can then be switched off again by thermal relaxation which happens slowly at room temp or rapidly at 50 °C. One main drawback however is the receptor can never be fully turned 'off' with roughly $\chi = 0.3$ (χ= mole frac-

tion) of the receptor being E,E at ambient conditions. The authors also showed that in DMSO, precisely two equivalents of sulfate would induce precipitation of a $[(SO_4)_2(L)]^{3-}$ species and this could be redissolved and precipitated by repeated UV-heat cycles.

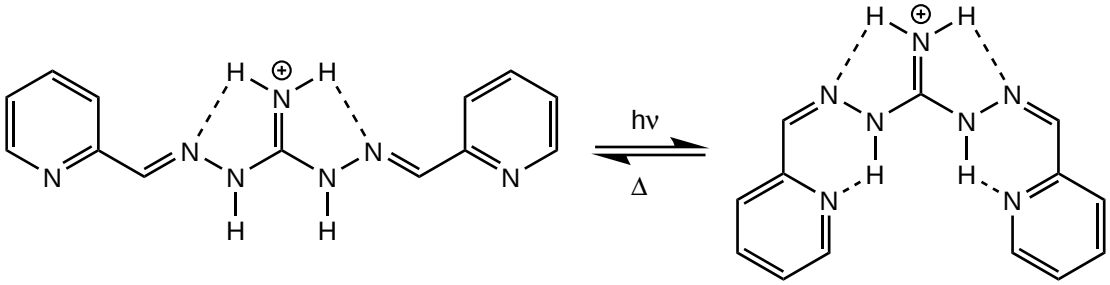

Figure 1.30: E,E and Z,Z conformations of the photoresponsive receptor from ref. [211]

1.4 Sulfate Conclusions

Sulfate represents a difficult challenge to selectively remove from aqueous streams due to its large free energy of hydration, especially in the presence of competing anions. This is a challenge faced by many industries and areas of chemistry so further research could prove invaluable.

Currently employed methods of sulfate removal have their own strengths and weaknesses, depending on the specific situation. Precipitation methods while cheap to operate, produce vast amounts of waste and are generally considered outdated. Membrane exclusion can produce very high flow through rates of purified water but are burdened with membrane fouling and high operational costs. Ion-exchange columns do have high reusability but they are also expensive, require prior filtration and have limited selectivity. Clearly there is room for improvement.

Anion coordination is still a new and growing field but considerable advancements have now demonstrated the potential use cases of anion coordination chemistry in many areas of research. Studies by numerous groups have shown that anion receptors can overcome the large free energy of hydration to extract sulfate into an organic phase with very high selectivities and efficiencies. The strength of binding is now so strong in some cases that once the sulfate has been extracted, barium precipitation is required to reuse the extractant phase, although, new methods such as pH or photoresponsive receptors are showing some promise. As seen with the reverse micelle forming extractant, the glyoxalbis(amidiniumhydrazone) receptor and the tren-tris(3-pyridylurea) receptor, phase separation of sulfate with all or part of its hydration shell is one viable approach to separation while circum-

venting the large free energy of hydration. There is still a gap, however, between receptors that are applicable for small scale sensing of sulfate and receptors capable of economically viable bulk sulfate removal from target water streams.

1.5 Carbon Capture Using Ionic Liquids

1.5.1 Introduction

A number of review papers outlining the current state of ionic liquids (ILs) as materials for carbon capture already exist for this topic and go into great detail compiling the data, outlining trends and general shortcomings [212–217]. While this review will only focus on neat ILs for CO_2 capture from flue gas, some researchers are exploring the effects of supporting the ILs in membranes (SILMs), encapsulating the ILs in porous media (ENILs), using mixed ILs or the addition of additives such as amines among other approaches. There are also a number of published technoeconomic analysis reviews, however, only one analyses a chemisorbant IL with good CO_2 capacity where the authors estimated a cost of \$81.32 $t^{-1}_{CO_2}$ using $[P_{2228}]$[2-CNPyr], shown in figure 1.31 [218].

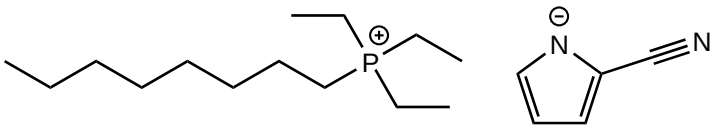

Figure 1.31: Structure of the $[P_{2228}]$[2-CNPyr] IL.

All liquids will have some ability to physisorb CO_2 to a greater or lesser extent, that is to allow CO_2 into the bulk of the liquid, without the formation of a formal chemical bond and is dictated by non-specific interactions such as van der Waals forces. Chemisorption of CO_2 is to bind CO_2 with the formation of a new chemical bond, chemisorption therefore binds CO_2 much stronger, requiring more energy intensive regeneration conditions but also allowing for much higher CO_2 capacities. Selectivity is not necessarily better for chemisorption or physisorption but depends on the specific absorbent, gas composition and absorption conditions.

Chemisorbant CO_2 capture is more ubiquitously known, and taught earlier than many people may realise. Joseph Black discovered the first test for CO_2 in the mid 1700's by bubbling the gas through a solution of limewater ($Ca(OH)_2$) and observing that the solution turned cloudy via the precipitation of $CaCO_3$ as shown in equation 1.23.

$$Ca(OH)_2 + CO_2 \longrightarrow CaCO_3\downarrow + H_2O \tag{1.23}$$

While the low solubility of the calcium salts is great for detection of CO_2, it is a significant drawback for carbon capture as the hydroxide cannot easily be regenerated from the carbonate salt. In these solutions, the hydroxide ion is acting as a strong nucleophile to attack the weakly electrophilic central carbon. The use of a nucleophile to absorb the CO_2 is the basis of all CO_2 chemisorption processes.

The metal cations are just bystanders in the initial nucleophilic attack step but are critical to precipitation as multivalent metal carbonates are well known to have low solubility in water.

To circumvent the precipitation, the use of alternative nucleophile sources have been explored such as neat or aqueous amines. The use of amines for gas scrubbing was first patented in 1930 [219] however, it wasn't deployed until the early 1980's [220]. Stowe and Hwang have shown that different amines have different CO_2 capture mechanisms with complex equilibria involving multiple species and pathways present in solution [221]. Primary and sterically unhindered secondary amines are known to bind CO_2 as a carbamate, although the pathway to this carbamate is still disputed. One plausible mechanism is shown in figure 1.32, where the capture proceeds via a short-lived zwitterion and another amine is required for deprotonation, limiting CO_2 capacity to 0.5 mol·mol^{-1}. On the other hand, sterically hindered secondary amines and tertiary amines capture CO_2 as bicarbonate where a termolecular pathway is thought to dominate due to the slower reaction kinetics. An example of this termolecular transition state is shown in figure 1.33. This pathway only involves one amine and so the theoretical capacity is increased to 1 mol·mol^{-1} and requires the presence of an equimolar amount of water.

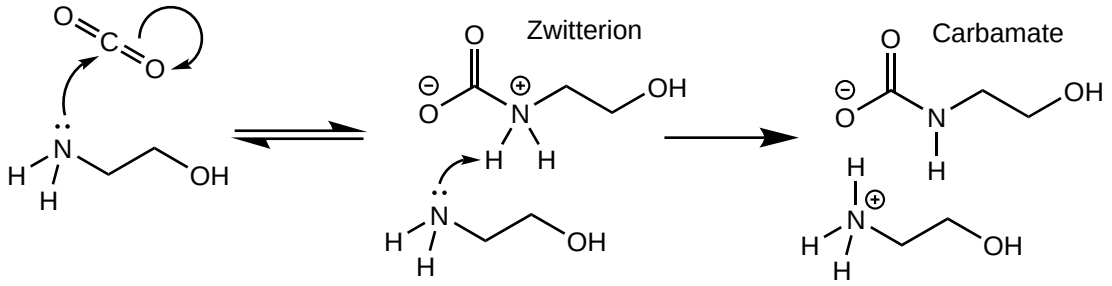

Figure 1.32: Mechanism of CO_2 capture by monoethanolamine via a short lived zwitterion that quickly deprotonates to form a carbamate. This is representative of most primary amines [221].

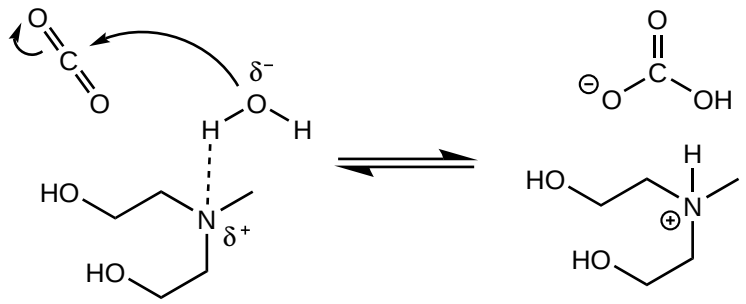

Figure 1.33: Termolecular CO_2 capture mechanism by methyldiethanolamine resulting in the formation of bicarbonate. This is representative of most tertiary amines or sterically hindered amines ie. 2-amino-2-methylpropanol [221].

Current industrial CO_2 capture from flue gas is done with the use of aqueous amine scrubbers such as aqueous monoethanolamine (MEA) or piperazine solutions [222]. These solutions are highly efficient at capturing CO_2 with fast absorption kinetics and the optimal operational parameters around 30 wt% MEA and near-ambient absorption conditions able to achieve 0.33 $mol_{(CO_2)} \cdot mol^{-1}{}_{(MEA)}$ or ≈ 73 $g_{CO_2} \cdot kg^{-1}{}_{MEA}$ [223]. Desorption requires high temperatures of *ca* 120℃ to regenerate the MEA solution [224]. These materials have significant drawbacks which has caused many researchers and industries to be reluctant to embrace them. Firstly, due to their relatively low molecular weight they evaporate during the regeneration stage which contaminates the concentrated CO_2 stream. Corrosion of carbon steel pipes over time also needs to be considered which is why more concentrated amine solutions are rarely explored [225]. Finally, oxidative and thermal degradation during the stripping process is the biggest problem, greatly reducing the lifetime of the sorbent solutions [220]. The main counterpoint to all of this is simply that the amines are cheap and can be replaced easily, although their disposal is rarely considered. All of these drawbacks lead to higher operational costs of ≈ 100 $\$ \cdot t^{-1}{}_{(CO_2)}$ [226, 227].

In 2006 Abu-Zahra *et al.* evaluated the technical [223] and economic [227] costs of using aqueous MEA solutions for CO_2 capture from power plants. A decade later Patricia Luis outlined the consequences of the scale up required to make MEA a global solution for CO_2 capture [228]. Here, the author states that *'The use of MEA and other amines in CO_2 capture is a point of concern and a global application does not seem to be the best strategy'*. For any material to be industrially viable it would need to far outperform these amine scrubbers in terms of CO_2 uptake, and operational energy consumption. ILs have been identified as promising materials for this area for several reasons including non-volatility leading to negligible loss of material and no contamination of the concentrated CO_2 stream, the possibility of lower operational costs due to lower temperature and pressure requirements for stripping and higher $mol \cdot mol^{-1}$ CO_2 capacity

The main challenge as will be discussed later is the stability and inertness of CO_2, which is why it is the end product of combustion. To chemically capture a very stable species, a very reactive species must be used and with high reactivity inevitably comes a reduced selectivity. This makes carbon capture from flue gas stream a difficult challenge as common compositions can be approximately 70% N_2, 20% water and 10% CO_2 while also containing traces of O_2, CO, SO_x and NO_x which can poison chemisorbant scrubbers [229].

Physisorption is an alternative option for CO_2 capture where the absorbed CO_2 is not chemically bound to the scrubber, instead it is absorbed through non-specific interactions. This lack of a formal bond allows for the use of much lower regen-

eration conditions and reduces the effects of poisoning from SO_x and NO_x. The downside is that the lack of specific interactions also reduces the total CO_2 capacity of the material significantly compared to chemisorbants.

Chemisorption generally enables much higher uptake capacities to be achieved compared to physisorption which is advantageous for large scale deployment as less IL would need to be circulated for every tonne of CO_2 captured, reducing capital and operational costs. Uptake capacities of 0.5 - 1 $mol \cdot mol^{-1}$ are commonly described for ILs in the literature, and any increase above the maximum theoretical capacity is usually attributed to additional physisorption of CO_2 into the IL. Due to the much stronger interactions from chemisorption, ($\Delta H \approx$ - 50 $kJ \cdot mol^{-1}$, [230]) harsher regeneration conditions are often, but not always, required to break $IL-CO_2$ bonds and recover captured CO_2.

To add a small note about units, the units of $mol_{CO_2} \cdot mol_{sorbent}^{-1}$ do not always give an accurate reflection of the real world performance as the molecular weight of the sorbent material can vary greatly (61.08 $g \cdot mol^{-1}$ for MEA vs 322.47 $g \cdot mol^{-1}$ for $[P_{2228}][2\text{-CNPyr}]$). The ratio of masses such as $g_{CO_2} \cdot kg_{sorbent}^{-1}$ may give the reader a better understand of the real world performance of each sorbent but again, it does not reflect the performance of diluted systems ie. 30 wt% aqueous amine sorbents where the 70 wt% of water is not included in the calculation of sorbent weight.

1.5.2 Chemisorption with ionic liquids

The Brennecke group first noted the unusually high physisorption solubility of CO_2 in $[BMIm][PF_6]$ when trying to use supercritical CO_2 for liquid-liquid extraction of non-volatiles from ILs. They reported a capacity of 1.5 $mol \cdot mol^{-1}$ at a high pressure of 80 bar [231], while these are not applicable conditions for carbon capture, this work sparked significant interest in the use of ILs for decarbonisation. Further research into the mechanism of CO_2 physisorption showed that the disordered structure of imidazolium cations provides a large amount of free volume when paired with large non-coordinating anions [232, 233]. Additionally, the heavily fluorinated anions that were fashionable at that time promoted physisorption through $F^{\delta-} \cdots C^{\delta+}O_2$ interactions [234]

The first report of a chemisorption capture mechanism by an IL was by the Davis's group where they implemented the functionality of well known amine absorbents. This was done by appending a primary amine group to an imidazolium cation as shown in figure 1.34. It was reported that at ambient pressure, this IL would absorb nearly 0.5 $mol \cdot mol^{-1}$ of CO_2 via the same mechanism shown in previously in figure 1.32, far more than similar ILs that lacked amine groups, and close to the theoretical maximum for an ammonium carbamate salt [235]. This led Davis

to coin the term task-specific ionic liquids (TSILs) [236], one of many acronyms to derive from the Davis lab.

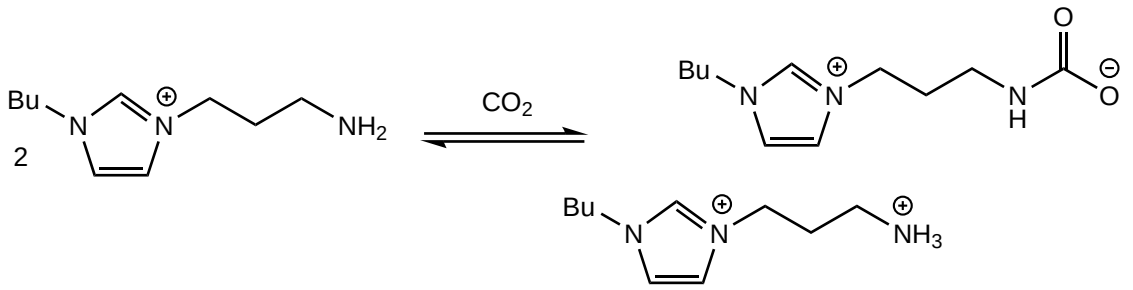

Figure 1.34: CO_2 capture by an amine functionalised imidazolium cation as first reported by the Davis group, and displaying the 0.5 mol·mol^{-1} theoretical CO_2 capacity [235].

The Brennecke group also went on to investigate chemisorption approaches using anions derived from amino acids where the carboxylate was deprotonated to form the anion, leaving the amine available for CO_2 capture [237, 238]. These were the first ILs that could uptake equimolar CO_2 at ambient conditions and were guided by *ab inito* calculations of where best to tether the amine. Calculations suggested that amines on the cation will favour the zwitterion formation shown in figure 1.32 and therefore a maximum capacity of 0.5 mol·mol^{-1}. Tethering the amine to the anion however, prevents the second deprotonation step as this would result in the formation of an unstable dianion due to the close proximity of the negative charges. What happens instead is an intramolecular proton transfer that yields a neutral carbamic acid moiety. This enables a theoretical capacity of up to 1 mol·mol^{-1}.

All of these amino acid ILs were reported to be highly viscous, characteristic of the $[P_{66614}]^+$ cation that was used. The authors reported that binding of CO_2 further increased the viscosity due to the formation of hydrogen-bonded networks resulting in glassy or gel-like materials [239]. The high viscosity is also partially due to the lack of a non-reactive co-solvent to screen the charges on the ions [5], the authors reported that low concentrations of water $\approx$ 1 wt% significantly reduced the viscosity but also resulted in a partial reduction of the CO_2 capacity. Reducing the viscosity of IL absorbents is critical to their success as it significantly inhibits the mass transfer of gas in and out of the material, this increased the residence time in absorption and desorption steps while also significantly increasing the pumping costs of circulating the IL between each step. Of the amino acid derived ILs, the proline ($[Pro]^-$) derived IL shown in figure 1.35, displayed the least increase in viscosity upon CO_2 absorption due to its cyclic structure making it the only amino acid with a secondary amine group, therefore reducing the potential for hydrogen bonding. At 40 ℃, $[P_{66614}][Pro]$ has a reported viscosity of 300 cP, which increased

to 460 cP upon saturation with CO_2. As a point of reference, fully loaded, 45 wt% piperazine solutions are have a reported viscosity of 21 cP at 40 °C [240].

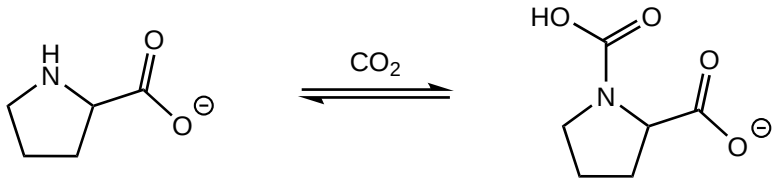

Figure 1.35: Equimolar CO_2 capture mechanism by the amino acid derived IL, $[P_{66614}][Pro]$. The $[P_{66614}]^+$ cation has been omitted for clarity [237].

While exploring the synthesis of 1,3-dialkylimidazolium salts, Holbrey *et al.* synthesised 1,3-dimethylimidazolium-2-carboxylate via the reaction between 1-methylimidazole and dimethyl carbonate [241]. The proposed mechanism was carboxylation of 1,3-dimethylimidazolium by the basic methyl carbonate anion, forming methanol as a by-product. In 2010, the Dai's group began investigating ILs for CO_2 capture and decided to use non-nucleophilic superbases to promote the carbene formation in imidazolium ILs [242]. This enables equimolar CO_2 absorption as shown in figure 1.36. The use of low viscosity ILs such as $[BMIm][NTf_2]$ [243] with the addition of liquid superbases like 1,8-diazabicyclo-[5.4.0]undec-7-ene (DBU) enabled relatively fast uptake kinetics for an IL and the authors even suggested mild regeneration conditions of 80 °C. Even though this system could uptake equimolar CO_2 due to the size of the IL and DBU, this only corresponds to a *ca.* 7 wt% uptake and is prohibitively expensive for scale up due to the use of the $[NTf_2]^-$ anion [244]. Gurau *et al.* have shown that a similar carbene absorption mechanism can been achieved by using weakly basic ILs such as in imidazolium acetates [245].

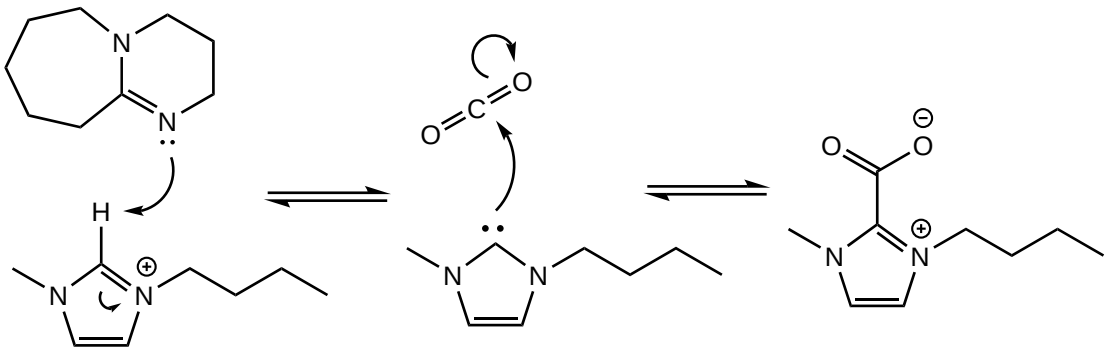

Figure 1.36: Equimolar CO_2 capture mechanism of $[BMIm][NTf_2]$ when carbene formation is induced by the addition of DBU superbase [242].

Holbrey *et al.*'s reported carbene formation also inspired the Brennecke group as they postulated that *'isoelectronic N-heterocyclic anions might be capable of the same chemistry'* [246]. They used molecular electronic structure calculations to

predict the reaction enthalpies of CO_2 and functionalised aprotic heterocyclic anions (AHAs) which guided them towards several cyano and trifluoromethyl pyrrolide anions. To simplify the process, they used a tetraalkylphosphonium cation to ensure the resulting salts were low melting ILs and to give a fair comparison of the anions. The synthesised ILs proved to be very effective chemisorbants with up to 0.9 mol·mol^{-1} CO_2 uptake under 1 bar of pressure with $[P_{66614}]$[2-CNPyr] found to have the best performance. Although these ILs were viscous, characteristic of the $[P_{66614}]^+$ cation, there is virtually no change in viscosity upon CO_2 absorption due to the lack of potential for hydrogen bonding with the anions. They later went on to synthesise a series of substituted AHAs and showed that the reaction enthalpy of the forward CO_2 absorption process has a sigmoidal relationship with the uptake of CO_2 at 0.15 bar and 22℃ (post-combustion relevant conditions) as shown in figure 1.37 [247].

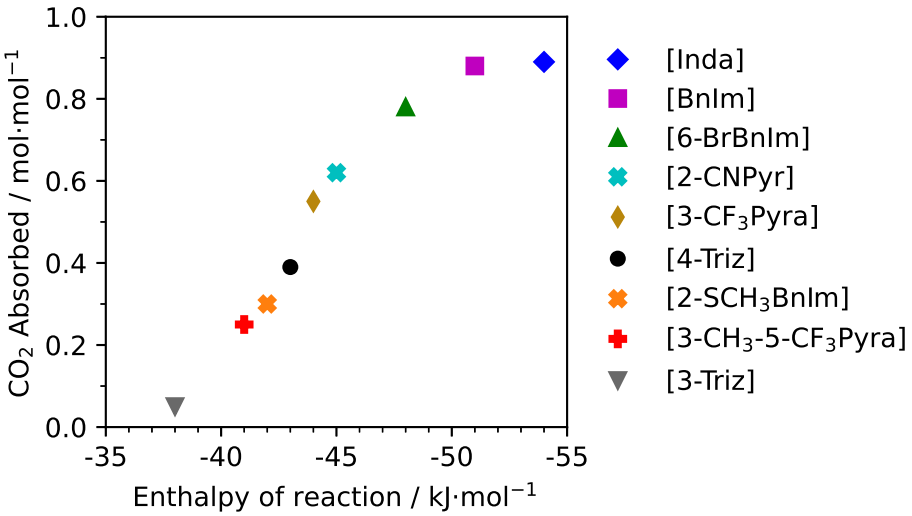

Figure 1.37: Absorption of CO_2 in $[P_{66614}]$[AHA]'s at a partial pressure of 0.15 bar vs the reaction enthalpy derived from the absorption isotherms. Reproduced from ref [247]. From top to bottom: [Inda] = indazolide, [BnImm] = benzimidazolide, [6-BrBnIm] = 6-bromobenzimidazolide, [2-CnPyr] = 2-cyanopyrrolide, [CF_3-Pyra] = 3-trifluoromethylpyrazolie, [4-Triz] = 1,2,4-triazolide, [2-SCH_3BnIm] = 2-methylthiobenzimidazolide, [3-CH_3-5-CF_3-Pyra] = 3-methyl-5-trifluoromethylpyrazolide, [3-Triz] = 1,2,3-triazolide.

Wang *et al.* were also working on ILs with similar AHAs independently. Rather than pairing the anions with phosphonium cations, they made a novel series of protic ionic liquids (PILs) from superbases and AHAs which are weak acids, some of which are shown in figure 1.38 [248, 249]. These ILs were able to absorb equimolar amounts of CO_2 and could be regenerated at 80℃ but the biggest advantage was their low viscosities. For example, the viscosity of [MTBDH][Im] (PIL from 7-

methyl-1,5,7-triazabicyclo(4.4.0)dec-5-ene and imidazole) was reported to be 32 cP at ambient conditions (vs 21 cP for CO_2 absorbed piperazine solutions [240]).

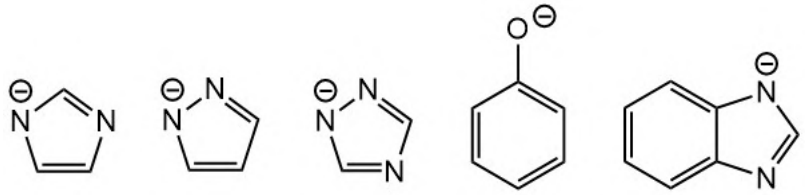

Figure 1.38: A range of popular anions derived from weak acids, first reported by the Dai group [248, 249]. From left to right; imidazolide ($[Im]^-$), pyrazolide($[Pyra]^-$), 1,2,4-triazolide($[4\text{-}Triz]^-$), phenolate($[PhO]^-$) and benzimidazolide($[BnIm]^-$).

This strategy of using superbases and weak acids to form strongly nucleophilic PILs was adopted by numerous researchers for carbon capture but also for SO_2 scrubbing, catalysis and biomass processing [250]. 1,8-Diazabicyclo(5.4.0)undec-7-ene (DBU) and 1,1,3,3-tetramethylguanidinium (TMG) are popular superbases for this strategy as they are both relatively inexpensive, have low molecular weights and are roughly 'globular' in shape. Shang *et al.* were the first to publish work on $[TMGH]^+$ PILs where they tested the phenolate, imidazolide and trifluoroacetate salts for SO_2 capture [251]. Lei *et al.* then took the [TMGH][Im] PIL and tested it for CO_2 capture, its low viscosity of 5.4 cP at 40 °C enables fast uptake kinetics while its low molecular weight and equimolar CO_2 absorption gives an impressive capacity of 192 $g{\cdot}kg^{-1}$ [252]. They also reported excellent cycling stability with absorption and regeneration at 35 °C and 65 °C respectively. This work was later confirmed by Li *et al.* who also studied the pyrrolate and phenolate salts [253]. Importantly, they showed that in the presence of water and CO_2, bicarbonate is formed which deceases the capacity over multiple cycles as it cannot be regenerated at 60 °C. Higher regeneration temperatures were not tested although DFT calculations suggested energy barriers of 16.7 and 20.5 $kcal{\cdot}mol^{-1}$ for regeneration from the carbamate and bicarbonate species respectively.

Of the two superbases, DBU is favoured due to the strong complexion between the $[TMGH]^+$ cation and carboxylate salts which can increase viscosity or induce crystallisation [254]. In 2016 Wang *et al.* reported on [DBUH][Im] for the synthesis of furanones utilising CO_2 [255], this then lead Zhu *et al.* to investigate a series of ILs based on functionalised imidazole anions [256]. They found that any modification of the anion resulted in lower $mol{\cdot}mol^{-1}$ capacity, however, the base [DBUH][Im] could nearly uptake equimolar CO_2, *ca.* 180 $g{\cdot}kg^{-1}$ under ambient conditions. Zhu *et al.* later went on to test a 1,2,4-triazolide ($[4\text{-}Triz]^-$) PIL that could approach 1.5 $mol{\cdot}mol^{-1}$, they proposed the capture mechanism shown in figure 1.39 [257]. Gao *et al.* also studied the $[DBUH]^+$ cation with a range of substituted phenolic, heterocyclic and carboxylic acid based anions [258]. However, their results contra-

dict those of Zhu *et al.*, reporting CO_2 capacity of 1.19 mol·mol^{-1} in [DBUH][Im] and only 0.55 mol·mol^{-1} in [DBUH][4-Triz].

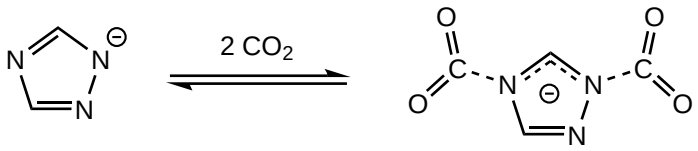

Figure 1.39: Proposed CO_2 capture mechanism of the 1,2,4-triazolide anion by Zhu *et al.* [257].

Vijayraghavan *et al.* were the first to use diamines and carboxylic acids to form PILs, enabling a free amine group to remain available for CO_2 capture [259]. This strategy improved on traditional aqueous amine solutions in two ways; the ionic charges reduce the volatility of the amines while the absence of water reduces the formation of bicarbonate, enabling lower regeneration temperatures, thereby reducing thermal degradation and energy costs. The absorption/desorption kinetics were slow but the the authors reported a temperature-swing absorption (TSA) cycle with only 5 °C difference (20 to 25 °C) between the absorption and desorption with up to *ca.* 136 g·kg^{-1} uptake, corresponding to 0.4 mol·mol^{-1}. Oncsik *et al.* then substituted the the carboxylic acids with pyrazole, imidazole and 1,2,4-triazole [260]. The pK_a's would suggest that the amines are not basic enough to deprotonate the heterocycles, however ^{1}H NMR spectra does show full proton transfer. This strategy nearly doubled the CO_2 uptake to 252 g·kg^{-1}, where it was suggested that the anion is the primary chemisorption site rather than the free amine as shown in figure 1.40. Excellent cycling stability was demonstrated over three cycles with desorption at 50 °C, although slow kinetics resulted in one hour for absorption and two hours for desorption. Zhao *et al.* also investigated these diamine PILs using a series of fluorinated phenolate anions to increase hydrophobicity, physisorption, reduce viscosity and tune the nucleophilicity of the anions [261]. The authors reported high capacities of up to 176 g·kg^{-1} which correlated with the pK_a of the anions conjugate acid. While not addressed, there is a possibility of forming HF via an S_NAr side reaction due to the presence of electron withdrawing fluorine ring substituents and moderate nucleophiles [262].

Using tetraalkylphosphonium cations to screen anions was popular due to the large suppression of the melting point, ensuring the resulting salts were ILs and allowed for a fair comparison of chemisorbant anions. In 2014, Gohndrone *et al.* of the Brennecke group showed that these cations were not as inert as previously thought [263]. They showed that at lower temperatures of *ca.* 20 °C, the expected carbamate formation is dominant, but at elevated temperatures of *ca.* 60 °C, an ylide pathway begins to dominate the CO_2 capture mechanism. In these cases, the

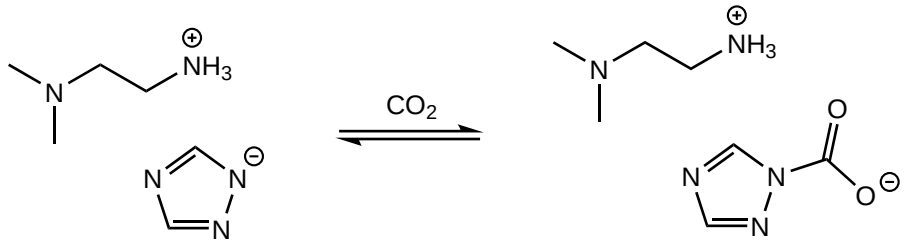

Figure 1.40: Proposed CO_2 capture mechanism of the diamine protic ionic liquid 2-(dimethylamino)ethylammonium 1,2,4- triazolide ([DMAEAH][4-Triz]) by Oncsik *et al.* [260]

basic anions are able to deprotonate acidic α-CH_2 groups adjacent to the P-sites of the cation as depicted in figure 1.41. This mechanism for chemisorption of CO_2 may be responsible for several contradictions in the literature, particularly with the phenolate anion [82]. [TMGH][PhO] was reported to have no CO_2 uptake by Li *et al.* [253], while Taylor *et al.* also reported that $[P_{66614}]$[PhO] initially absorbed CO_2, but this was then expelled while still in the absorption phase. Conversely, Wang *et al.*, Huang *et al.* and Zhang *et al.* report up to 0.5 mol·mol^{-1} CO_2 uptake [264–266]. An alternative option is to use ammonium cations, in which the α-CH_2 groups are less acidic and so are more chemically stable under basic conditions. This chemical stability come at the cost of lower thermal stability, quaternary amines usually degrade around 200°C which may limit regeneration conditions, whereas analogous phosphonium cations are usually stable to around 300°C [267].

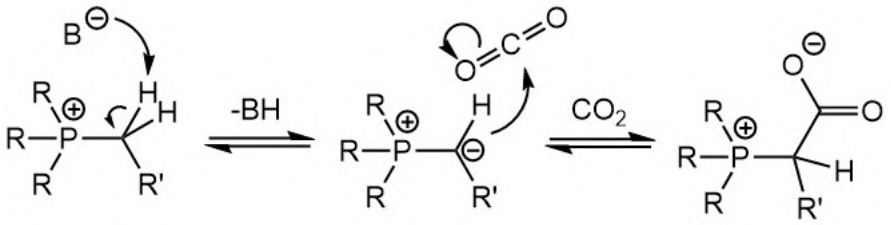

Figure 1.41: General reaction pathway for ylide formation via deprotonation of the α-CH_2 and subsequent binding of CO_2.

1.5.3 Effect of flue gas composition

Flue gas mainly consists of nitrogen and composition can vary depending on the emission source. The CO_2 concentration is usually 10-15% however gas turbine flue gas can be as low as 3% CO_2 and cement kiln off-gas can be as high as 33% [268]. There are many other competitive and non-competitive impurities that may also be present such as mercury and HCl [269]. In addition, the gas can be hot, pressurised and contain fly ash or other particulates. Some example flue gas compositions are shown in table 1.2.

Table 1.2: Example compositions of several flue gas streams, all values are given in vol% [268, 270].

Industry	N_2	CO_2	H_2O	O_2	Traces
Coal	75.2	14.4	6.1	3.4	High SOx and NOx, particulates
Oil	74.2	11.9	9.6	3.3	High SOx and NOx
Gas	71.4	8.4	16.7	2.5	Low SOx and NOx
Cement	59.4	32.3	4.8	2.7	Moderate SOx and NOx

The amount of water in a flue gas stream can vary significantly depending on the plant design. For example the gas stream may be saturated if CO_2 capture is to take place after a wet desulfurization unit. As shown in the previous section, physical CO_2 absorption is more efficient at lower temperatures, so cooling the flue gas can have a two-fold benefit of increasing CO_2 removal while also condensing some of the water. Depending on the CO_2 absorption process, water may also have differing effects on the capture efficiency.

For example moisture in the flue gas has no effect on the capacity of aqueous amines, however if a zeolite absorbent is being used, water will out-compete CO_2, reducing the capacity to zero [271]. Drying a gas stream can be extremely expensive depending on the temperature, amount of water and the required level of 'dryness'. This make it hard to estimate how much it will cost to dry a specific gas stream, and therefore, how much better an absorber must perform under dry conditions to make the process economical. Peh *et al.* have reported a technoeconomic analysis on the use of a metal organic framework for wet (3 vol%) flue gas carbon capture where they compared the cost of drying vs not drying the gas stream [272]. In their study, the most economical option was to completely dry the feed, in total costing \$91 $t^{-1}_{CO_2}$, with the drying step accounting for half of the total costs. Panja *et al.* have also conducted a technoeconomic analysis for the coal plant at Hunters Station, Utah [273]. The authors propose the use of aqueous amines, specifiably Mitsubishi Heavy Industries' KM-CR Process® with KS-1™ solvent and report capture costs of only \$50 $t^{-1}_{CO_2}$, despite the flue gas containing 8 vol% water. Ironically, due to the water solvent and high regeneration temperatures of the amines, the hot CO_2 rich feed is saturated with water which must then be at least partially removed for either sequestration or chemical conversion.

There are many reports on hydrophobic ILs, but the word hydrophobic in these cases refers specifically to the miscibility of the ILs with water, it does not imply a exclusion of water from the ionic liquid phase. Freire *et al.* have shown that even the most hydrophobic ILs absorb a small amount of water [274–276], for example, the mole fraction solubility of water in [BMIm][NTf_2] is 0.26 at 25 ℃. It is well known to

any researchers of ILs that they are hygroscopic [277], Watanabe *et al.* have used this property to show that ILs can be very effective desiccants [278]. As discussed previously in section 1.2.3, this is because water can effectively screen the charges on the ions, reducing the steric repulsive forces between the ions which reduces their viscosity. It is therefore safe to assume that water from a flue gas stream will be absorbed by an IL scrubber.

ILs derived from the amino acids proline (Pro) and methionine (Met), $[P_{66614}][Pro]$ and $[P_{66614}][Met]$ where tested for CO_2 absorption in the presence of water by Goodrich *et al.* [238]. They showed that the addition of *ca.* 5 wt% water significantly reduced the viscosity of the ILs however, it also reduced the total CO_2 capacity, proportional to the amount of water in the IL. It was later shown that this decreased capacity was accompanied by partial protonation of the anion which then resulted in a mixed carbamate/bicarbonate capture mechanism [279]. Contrary to this, the addition of 2 wt% of water to $[P_{66614}][4\text{-Cl}-\text{PhO}]$ was shown to increase the CO_2 capacity from 0.5 to 0.89 $mol \cdot mol^{-1}$ [264]. In this case the authors also suggested that the presence of water was enabling the formation of bicarbonate but that this was more favourable for phenolates than carboxylates due to the increased basicity. $[P_{66614}][2\text{-CNPyr}]$ also showed an increase in CO_2 absorption in the presence of water where a significant increase in uptake was observed at low CO_2 partial pressures [247]. This was later shown to also be due to the formation of bicarbonate which was observed by NMR [280]. Additionally, the absorption of CO_2 by $[P_{66614}][2\text{-CNPyr}]$ was found to be fully reusable in the presence of water, with regeneration conditions (that were not optimised) of 60 °C and 3 days. Li *et al.* have also shown an increase in CO_2 capacity with the superbase derived PIL [TMGH][Im], with a maximum capacity at 7 wt% water [253]. Again the strongly basic nature of the imidazolide anion seems to favour bicarbonate formation, however in this case, 60 °C was not sufficient to regenerate the IL as the capacity was shown to half after just 4 cycles. The authors did not investigate regeneration at higher temperatures.

It appears that that for weakly basic anions such as carboxylates, the presence of water reduces the CO_2 capacity through competitive hydrogen bonding to the carboxylate, reducing its availability for carbonate formation with CO_2. For moderate to strongly basic anions such as $[2\text{-CNPyr}]^-$ or $[Im]^-$, the presence of water favours absorption of CO_2 via the formation of bicarbonate. The decomposition of bicarbonate requires a proton to release the absorbed CO_2, in these cases it appears that the more acidic 2-cyanopyrrole enables the IL to be regenerated at lower temperatures than the presence of imidazole in [TMGH][Im]. Of course this simplified explanation neglects the presence of the cations as $[TMGH]^+$ may coordinate to the bicarbonate and stabilise it more than the $[P_{66614}]^+$ cation. A reaction

scheme showing the reversible reaction pathway between imidazolate, CO_2 and water is shown in figure 1.42.

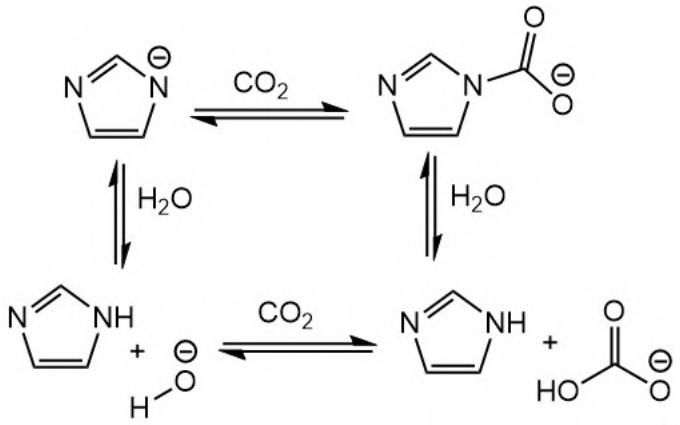

Figure 1.42: Reaction pathways for the reaction of imidazolide with CO_2 and water resulting in bicarbonate formation.

The Hardacre group has recently investigated the effects of SO_2 and NO contaminants on $[P_{66614}][BnIm]$. Initially they tested the effects of water on a range of tetraalkylphosphonium ILs and found that the 1,2,4-triazolide or benzimidazolide ILs were still able to absorb a significant degree of CO_2 (0.88 and 0.89 mol·mol^{-1}) with $\approx$ 10 wt% water [281, 282]. They then tested the ILs with a gas composition of 14% CO_2 and 0.2% SO_2 in argon and showed that SO_2 significantly reduces the reusability of the ILs as the SO_2 binds much stronger to the benzimidazolide anion [229]. They then went on to test the effects of NO on the benzimidazolide IL with a gas stream containing 14% CO_2 and 0.2% NO in argon, in this case the IL is much more stable across ten cycles although there is a small drop in performance over the last few cycles indicating that eventually the binding of N_2O_2 will inhibit the chemisorption [283]. This appears to occur through a stepwise addition of NO where the first addition is slightly disfavourable, followed by a very favourable second addition of NO. The gas phase absorption energies (ΔG) of benzimidazolide with CO_2, NO (2 equivalents) or SO_2 were calculated using DFT and found to be -9.60, - 33.15 and - 69.50 kJ·mol^1 respectively. The reactions between the benzimidazolide anion and either SO_2 or NO is shown in figure 1.43.

The use of ionic liquids for SO_2 scrubbing was first published in 2004 [284] and has since gained a lot of interest from researchers [285]. Due to SO_2 being more electrophilic than CO_2, the enthalpies of absorption are often greater, causing most chemisorbants to be selective for SO_2 over CO_2. One noteworthy gap in the literature is the effect of SO_2, NO_x and water together on CO_2 absorption. It is well known that SO_x and NO_x readily dissolve in water to form mineral acids which could presumably have differing effects than the anhydrous gaseous oxides. Tian *et al.*

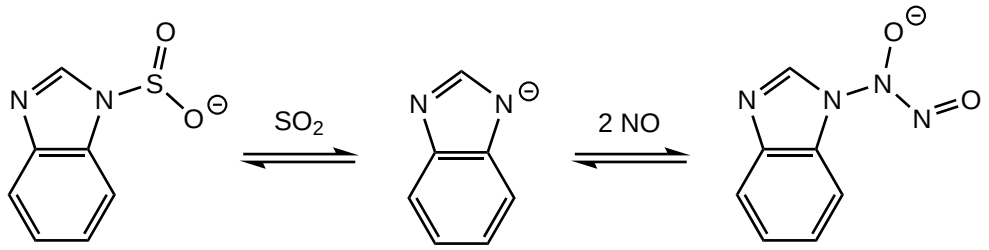

Figure 1.43: Reaction of the benzimidazolide anion with either (left) SO_2 or (right) two equivalents of NO [283].

have demonstrated this for an SO_2 scrubbing IL where sulfurous acid is formed which is then deprotonated, capturing SO_2 in the form of bisulfite [286].

1.5.4 Methods

The literature in this field has reported many different approaches to measuring the CO_2 solubility in ILs. The methodologies broadly break down into two distinct categories; open systems and closed systems. It is important to remember that the method used to test CO_2 sorption will have a large effect on kinetics and so care must be taken when comparing the rates of sorption tested with different methodologies.

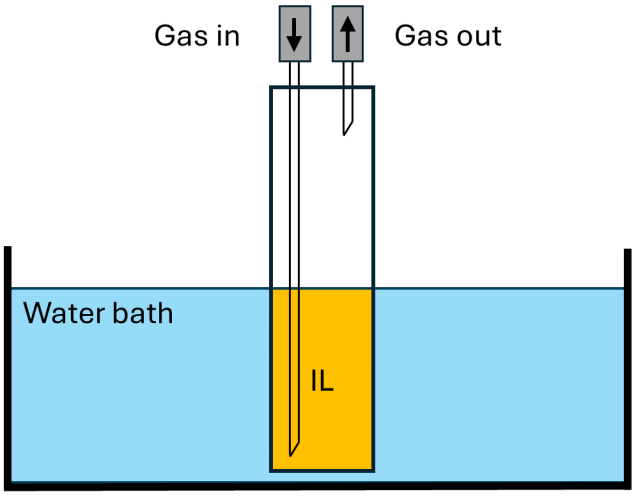

Figure 1.44: Schematic of a simple open system setup for measuring gas solubility in ionic liquids.

Open systems are the ‘easier’ and significantly more affordable of the two approaches and usually involves bubbling the CO_2 containing stream through the IL and then measuring the increase in weight of the sample. This allows for the temperature to be easily controlled although it limits the pressure to just 1 atm. This has been done in a variety of different ways, but the most common is to simply bubble gas through the IL and measure the weight of the sample continuously, every

minute or just after a long period of time [249, 259, 260, 264]. An example setup for this approach is shown in figure 1.44. Some researchers have even just left their sample open in a container with dry ice for however long it takes the sample to stop increasing in weight CO_2 [287].

Closed systems (aka. isochoric systems) on the other hand are experimentally more complicated but this method is used by many groups as it is much more precise than an open system [237, 265, 288], a simplified setup is shown in figure 1.45. This approach normally uses two separate vessels of known volumes that are held at the same temperature. Initially, a known amount of IL is loaded into the equilibrium cell and the whole system is put under vacuum. Then a gas reservoir is filled with the gas that is to be tested, and from this initial pressure in the gas reservoir, the moles of gas in the system can be calculated. The connecting value is then opened allowing the gas to enter the equilibrium vessel where the IL will immediately begin to absorb the gas and lower the pressure, eventually stabilising at an equilibrium pressure. From this final pressure, the final moles of gas in the system can be calculated thus giving the moles of gas absorbed by the material.

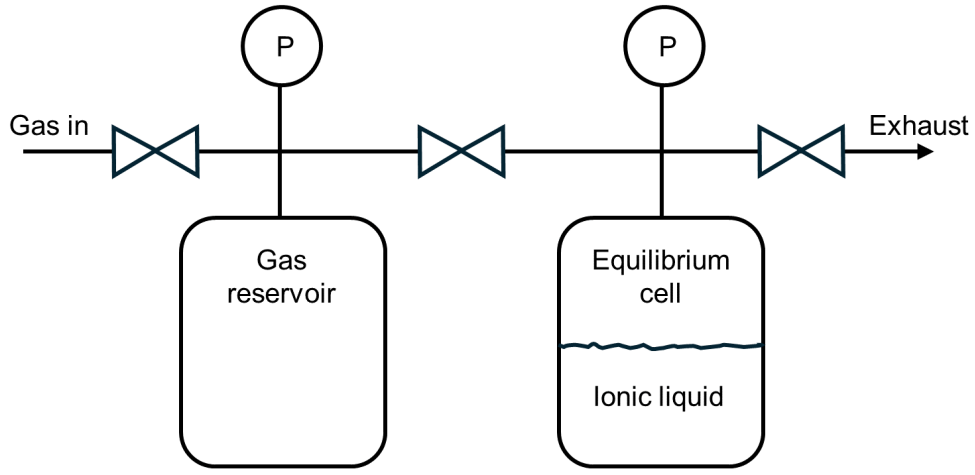

Figure 1.45: Schematic showing a simplified closed system setup for determining gas solubility in ionic liquids. P = pressure transducer.

Closed systems approaches can also take several other forms. One common method, mass flow measurement, involves setting a target pressure and quantifying the amount of gas required to maintain that pressure within the system [289]. Gravimetric measurements, however, are widely regarded as the most accurate, as they directly measure the increase in sample weight resulting from gas absorption [290]. Unlike other closed system methods, gravimetric measurements are unaffected by factors such as gas non-ideality or variations in sample volume, which can introduce minor errors in alternative approaches.

The closed system approach also has some drawbacks as the time taken to

reach equilibrium can take days to weeks for viscous ILs with slow uptake kinetics. Additionally, without the use of *in-situ* gas measurements, gas mixtures can not be analysed as the pressure sensors cannot differentiate between separate gas species. Young *et al.* have recently developed a new headspace gas chromatography technique that overcomes both of these limitations [291]. In this method, sample vials are loaded with an absorbent species, evacuated, and then filled with a gas mixture. The sample vials can then be removed from the apparatus and set aside so many samples can be equilibrating simultaneously. Once the samples have been assumed to be equilibrated, the headspace can then be analysed by gas chromatography to measure the amount of gas that was not absorbed, as well as its composition.

There is some variation as to which equation of state can be used for these calculations. The simplest approach is to assume the gas is ideal and use the ideal gas law shown in equation 1.24.

$$PV = nRT \tag{1.24}$$

Here, P is the pressure, V is the volume, n is the moles of gas in the system, R is the ideal gas constant and T is the absolute temperature. However, it is well known that the ideal gas law only describes a perfect gas as it assumes no interactions and dimensionless molecules. To adjust for this the van der Waals equation, shown in equation 1.25 includes the terms i which relates to the intermolecular interactions and v, the volume occupied by one mole of molecules.

$$(P + u\frac{n^2}{V^2})(V - nv) = nRT \tag{1.25}$$

This equation is an improvement on the perfect gas law above the critical temperature but is also has limitations, especially when working below the critical temperature and close to the critical pressure. Finally there is the Lee-Kesler equation which employs a correction factor Z, also known as the compressibility factor, to correct for deviations around the critical region [292].

$$PV = ZnRT \tag{1.26}$$

The compressibility factor, Z is a function of the reduced pressure, reduced temperature and acentric factor of the gas in question, where the reduced pressure and temperature are simply the ratios of the measured values to the critical values ie. $P_r = P/P_c$. When $Z = 1$ the gas is said to be behaving ideally and the value of Z is furthest from 1 when $P_r = 1$ and $T_r = 1$ (at the critical point). The Lee-Kesler approach is the most popular among researchers today when calculating the CO_2

absorption. However, while the critical temperature of CO_2 is T_c = 31.0 ℃, because the pressures in question are so far from the critical pressure of P_c = 73.8 bar, the values of Z will only range between 0.97 and 1.00 in the range of 0 - 2 bar and 30 - 80 ℃.

1.5.5 Carbon Capture Conclusions

With the need for carbon capture and sequestration being ever more apparent, there is an increasing need for greener technologies than the currently favoured amines. Ionic liquids have been shown to be viable absorbents for carbon dioxide capture from flue gas, however, whether they can be used in a way that is more economical than the currently used aqueous amines is still unclear.

Their biggest clear advantage is their lack of vapour pressure which negates any contamination of the resulting lean and rich CO_2 streams. Additionally, some ILs have demonstrated exceptionally high CO_2 capacities, both in terms of per mol and per weight basis. Some ILs are even reported to have viable temperature swing absorption cycles with a difference of only 5 ℃ between absorption and desorption.

Despite these achievements, they have still not been adopted for several reasons. Many of the reported ILs are prohibitively expensive for deployment at large scale with supply chains potentially not able to meet the demand for many of the starting materials. Their viscosity, both before and after CO_2 absorption is also a concern as it causes a two-fold penalty, first on the absorption kinetics which then requires longer residence times in absorbing units, and secondly on pumping costs which can significantly increase operational expenditure. Finally the effects of competing species in a flue gas stream have been shown to have a negative impact on many ILs where the effects of water, SO_x and NO_x require harsher regeneration conditions than in the ‘ideal’ simulant gas streams.

2. Ionic Liquid Chlorides as Liquid Anion Exchangers

2.1 Introduction

In this chapter a series of ionic liquid tetraalkylammonium and tetraalkylphosphonium chloride salts have been investigated as potential liquid anion exchangers. The series of ionic liquids shown in figure 2.1 were designed to contain functional groups commonly found in solid anion exchange resins. Two ILs that are already commercially available are Cyphos® 101, a long chain tetraalkylphosphonium chloride salt and Aliquat® 336, a methyltrialkylammonium chloride salt where the methyl group may mimic the functionality found in a strongly basic type I resin. Additionally, although much less widely used, Alamine 336 is the trioctylamine free base precursor to Aliquat® 336, protonation with HCl could therefore yield a mimic of a weakly basic resin. Alkylation of trioctylamine with ethylene oxide (EO) or a halohydrin would then yield the corresponding alkanolamine that could mimic a strongly basic type II resin. Finally, methylation of trioctylphosphine could yield a phosphonium analogue of Aliquat® 336.

Sulfate was chosen as a target anion for extraction for two reasons; firstly because of the current demand for more methods of sulfate removal, especially by liquid-liquid extraction. Secondly, due to sulfate's extreme hydrophilicity, it is one of the most challenging anions to extract from water (alongside phosphate, $[PO_4]^{3-}$ and carbonate, $[CO_3]^{2-}$), making it an excellent model anion to benchmark the activity of anion exchangers.

Synthesis of both $[HN_{888}]Cl$ and $[P_{1888}]Cl$ was straightforward, with both ILs being produced in near quantitative yields. $[HN_{888}]Cl$ was synthesised via the direct addition of HCl to trioctylamine while $[P_{1888}]Cl$ was synthesised via methylation of trioctylphosphine with dimethylcarbonate under microwave irradiation, followed by addition of HCl to decompose the methylcarbonate anion and yield the chloride salt. The synthesis of $[N_{2OH888}]Cl$ was much more challenging, initially following the work of Li *et al.* [79], alkylation of $[HN_{888}]Cl$ with EO in dry isopropylalcohol was tried however no reaction was observed due to the absence of wa-

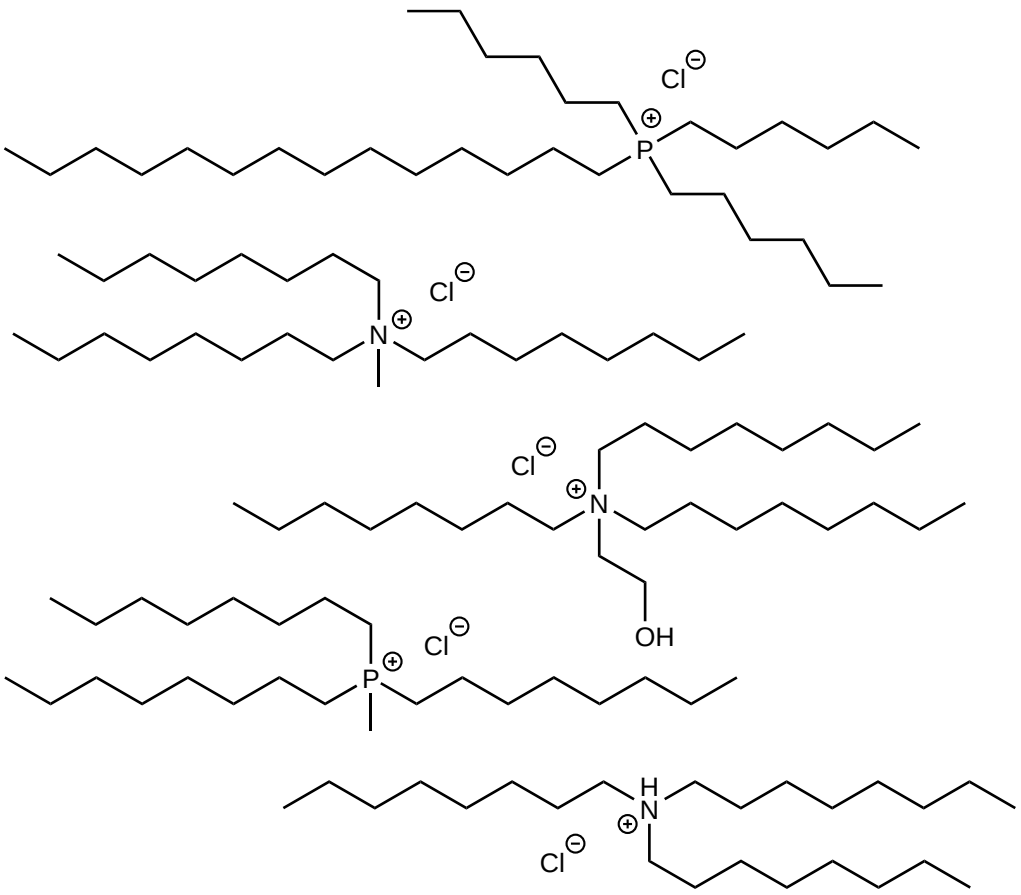

Figure 2.1: Structures of the ILs used in this work. From top to bottom; Cyphos® 101, Aliquat® 336, $[N_{2OH888}]Cl$, $[P_{1888}]Cl$ and $[HN_{888}]Cl$. Ignoring branching and chain length variation that exists in Cyphos® 101 and Aliquat® 336.

ter. When repeated with the addition of water, the reaction proceeded, however over-alkylation occurred. approximately one quarter of the product was the desired $[N_{2OH888}]Cl$, while one half was alkylated with two equivalents of EO, yielding $Oct_3N^+-CH_2-CH_2-O-CH_2-CH_2-OH$ and the other quarter with three equivalents of EO. This product was labelled $[N_{PEG888}]Cl$ and also tested. $[N_{2OH888}]Cl$ was finally afforded via the reaction between trioctylamine and 2-bromoethanol in toluene followed by ion exchange using a chloride loaded IX resin. Although the separation of product from residual Trioctylamine was challenging, it was possible via successive recrystallisations in dry diethyl ether. Purification by column chromatography was also possible by eluting starting material with ethyl acetate, slowly switching to acetonitrile and finally 5 vol% acetic acid in acetonitrile to elute the product.

NMR analysis of Cyphos® 101 and Aliquat® 336 revealed a small amount of branching of the alkyl chains as shown in appendix figures 6.1 - 6.5. For simplicity, these commercial products are treated as pure mixtures of $[P_{66614}]Cl$ and $[N_{1888}]Cl$ respectively. For calculations involving their molecular weight, values of 519.31 and

404.16 g·mol^{-1} were used.

All of the ILs are shown to form aqueous biphasic systems with water, the water content of the IL rich phases was measured and the phases analysed by FT-IR and ^{1}H NMR spectroscopy. The ability for the ILs to act as liquid anion exchangers was quantified by their ability to extract aqueous sulfate from increasing concentrations of Na_2SO_4 solutions. The effects of phase-volume ratio, competitive aqueous chloride and the presence of acid was also measured for Cyphos® 101 and Aliquat® 336. Finally potential methods of re-use were tested and the results compared to conventional precipitation and IX resin methods.

2.2 Characterization of water saturated ILs

2.2.1 Physical properties

When fully dried, four of the five ILs are waxy solid at room temperature (Cyphos® 101 being the exception), however they were all observed to melt below 100℃, qualifying them as ILs. These salts are also hygroscopic and will liquefy spontaneously when left open to humid air as only a small amount of water is required for liquefaction although much more can be absorbed. From preliminary work done with those ionic liquids it was clear that water was very soluble in the ionic liquid phase due to the presence of the chloride anion, while the ionic liquid itself was not very soluble in water due to the large hydrophobic cations. When in contact with an aqueous phase, these systems can also be thought of as aqueous biphasic systems with an upper IL rich phase and a lower IL lean phase. To investigate this, the mutual solubilities of deionised (DI) water and each IL were tested and are shown in table 2.1.

Table 2.1: Mutual solubility between water and the hydrophobic ILs at room temperature. IL in water was measured by total organic carbon and water in IL was measured gravimetrically and by integration of the ^{1}H NMR water peak.

Ionic Liquid	IL in water	Water in IL		
	g·kg$^{-1}{}_{TOC}$	wt·%$_{Weight}$	wt·%$_{NMR}$	χ_{H_2O}
Cyphos® 101	0.272	14.1±0.6	11.4	0.826
Aliquat® 336	1.384	24.9±2.3	23.0	0.871
$[P_{1888}]Cl$	1.326	26.6±1.3	27.4	0.894
$[HN_{888}]Cl$	0.731	8.0±0.2	6.5	0.653
$[N_{2(OH)888}]Cl$	1.686	17.1±1.7	16.7	0.833

Values for water in the ILs is from the weight loss upon prolonged heating above the melting point of the ILs under reduced pressure and is all within 3% of the

values obtained from integration of the water peak in the neat ^{1}H NMR spectra. Values for the mole fraction of water were calculated using the gravimetric mass loss results. The values for IL in the water was measured by total organic carbon analysis. The order of water solubility in the ILs follows the order:

$$[P_{1888}]Cl > \text{Aliquat}^{®}\ 336 > > [N_{2(OH)888}]Cl > \text{Cyphos}^{®}\ 101 > > [HN_{888}]Cl \quad (2.1)$$

While the solubility of IL in water follows the order:

$$[N_{2(OH)888}]Cl > \text{Aliquat}^{®}\ 336 \approx [P_{1888}]Cl > [HN_{888}]Cl > \text{Cyphos}^{®}\ 101 \quad (2.2)$$

Interestingly, $[HN_{888}]Cl$ absorbs the least amount of water, possibly due to the equilibrium kinetics of the acidic proton causing a low transient concentration of neutral trioctylamine while slightly acidifying the water in the IL phase. Cyphos 101 and $[N_{2OH888}]Cl$ both absorb an intermediate amount of water while Aliquat® 336 and $[P_{1888}]Cl$ both absorb significantly more water than the others. The presence of a methyl group appears to significantly increase the solubility of water in these ILs while the phosphonium ILs absorb more water due to the larger cationic centre being more accessible to the water due to longer C – P bonds and a slightly increased degree of hydrogen bonding from the more acidic α-protons. For the ILs in water, it is suspected that the resulting stability of the reverse micelles (RMs) increases the solubility such that $[N_{2(OH)888}]Cl$ forms the strongest RMs due to the space filling of the hydroxyethyl group and Cyphos 101 has no propensity to form RMs due to its 'globular' structure. In terms of mole fractions, the solubility of the ILs in water is below $\chi_{IL} = 0.001$ in all cases. It is also expected that the mutual solubilities would be significantly reduced when in contact with salt water solutions due to Hofmeister salting out effects [97, 293].

The data for Cyphos® 101 is in good agreement with literature values, where the solubility of water in the IL have been reported to range from $\chi_{H_2O} = 0.817$ to 0.829 [294–298] at 25 °C while the ILs solubility in water is reported to be $\chi_{IL} = 0.000017$ determined via ion chromatography [297]. Previously reported values for Aliquat® 336 range from $\chi_{H_2O} = 0.822$ to 0.851 [296, 299, 300] between 20 and 30 °C, slightly lower than the value reported here and may suggest some batch variability. Values for the solubility of Aliquat® 336 in water range massively, two online resources list this to be 6 and 10 $g{\cdot}L^{-1}$ [77, 301] while only one published value exists stating 1.3 $g{\cdot}kg^{-1}$ [299] from cloud point titration, this last value agrees well with this data, suggesting poor accuracy of the reported online values. No relevant literature data was found for $[P_{1888}]Cl$, $[N_{2OH888}]Cl$ or $[HN_{888}]Cl$, even when searching for Alamine 336.

The density and viscosity of each water saturated IL is import for understanding the mass transport limitations determining the rate of ion exchange and the energy required to pump it through pipes in a real world application. It was noticed that the uptake in water greatly reduced the viscosity of $[P_{66614}]Cl$ and liquefied the other ILs which are hygroscopic solids when dry at room temperature as stated earlier. The density and viscosity of each water saturated IL phase is shown in table 2.2 along with the values for *n*-octane and water for comparison. The order of dynamic viscosity of the water saturated ILs follows the order:

$$\text{Aliquat}^{®}\ 336 > > [N_{2(OH)888}]Cl > [HN_{888}]Cl > \text{Cyphos}^{®}\ 101 > [P_{1888}]Cl \quad (2.3)$$

While the density of the water saturated ILs follows the order:

$$[N_{2(OH)888}]Cl > [P_{1888}]Cl > \text{Cyphos}^{®}\ 101 \approx \text{Aliquat}^{®}\ 336 > [HN_{888}]Cl \quad (2.4)$$

Table 2.2: Physical properties of hydrophobic IL-Cls at 20℃ with *n*-octane and water given as comparisons.

Ionic Liquid	Dynamic viscosity (mPa·s)	Density ($g \cdot cm^{-3}$)
Cyphos® 101[a]	3275.5	0.8868
Cyphos® 101[b]	155.1	0.9066
Aliquat® 336[b]	354.5	0.9036
$[P_{1888}]Cl$[b]	94.1	0.9294
$[HN_{888}]Cl$[b]	193.3	0.8927
$[N_{2(OH)888}]Cl$[b]	266.4	0.9427
n-Octane[302][a]	0.552	0.7025
Water[303, 304]	1.002	0.9982

[a] Dry
[b] Water saturated

Comparison of the amount of water absorbed by each IL and the resulting density or viscosity of each IL shows no obvious correlation, ie. if an IL absorbs a lot of water, it will not necessarily have a low viscosity or high density. This is well demonstrated by Aliquat® 336 which absorbs 6.75 molar equivalents of water, but still has a relatively high viscosity or $[N_{2OH888}]Cl$ which absorbs only 1.88 molar equivalents of water but has a relatively high density.

There is also a large discrepancy in the values reported for the viscosity of water saturated Cyphos® 101 ranging from 95.8 to 830 mPa·s [295, 296, 305] while only one density value is reported at 0.9016 $g \cdot cm^{-3}$ [295]. Values for Aliquat® 336 are slightly more consistent ranging from 79.05 to 150 mPa·s [296, 300], 200 mPa·s less than the value reported here, and only one reported density of 0.91 $g \cdot cm^{-3}$ [300]. Again, no relevant literature data was found for $[P_{1888}]Cl$, $[N_{2OH888}]Cl$

or [HN_{888}]Cl. Jacquemin *et al.* have investigated the solubility of water in a series of short alkyl chain ILs and its effect on the density and viscosity [306]. Although their hydrophobic ILs absorbed only *ca.* 2 wt% water, this caused a dramatic decrease in viscosity and a reduction in density (as the dry ILs were more dense than water). Philippi *et al.* have suggested that there are two contributing factors to the viscosity of ILs; compaction of the IL through coulombic attraction resulting in a higher density and the formation of a charged network [5]. In the hydrophobic IL chlorides investigated here, water may therefore be reducing the bulk viscosity by charge separation but may also be helping to structure the charged network in the same way that it aids in the formation of reverse micelles [126].

From the above data, the concentration of each IL in its water saturated form can be calculated using the following equation to allow for comparisons of the ILs based on volume.

$$c = \frac{\rho \cdot w}{MW} \tag{2.5}$$

Where c is the concentration of the IL in mol·L^{-1}, ρ is the density of the water saturated IL in g·L^{-1}, w is the mass fraction of IL and MW is the molecular weight of the IL. The concentrations of the ILs are shown in table 2.3, were it can be seen that Cyphos® 101 is the least concentrated while [HN_{888}]Cl is the most concentrated due a combination of having the lowest molecular weight and lowest saturated water content.

Table 2.3: Molar concentration of the IL components in fully water saturated ILs.

Ionic Liquid	Concentration / M
Cyphos® 101	1.50
Aliquat® 336	1.68
[P_{1888}]Cl	1.62
[HN_{888}]Cl	2.11
[$N_{2(OH)888}$]Cl	1.80

The emulsification properties of these ILs was also observed but not investigated. They all produced strong emulsions when shaken with water, however, emulsions of the phosphonium ILs were much stronger than those of their nitrogen counterparts. An emulsion of [P_{1888}]Cl and water was shelf stable for more than five months and required prolonged centrifugation to completely phase separate. This propensity to form emulsions may also partly explain the wide range of water solubilities and physical properties reported for Cyphos® 101 and Aliquat® 336.

2.2.2 Spectroscopic analysis

The water environment with water-saturated ILs was investigated using a combination of neat ^{1}H NMR and FT-IR spectroscopy The neat ^{1}H NMR spectra of each IL are shown in figure 2.2 and show clearly that water in the IL has a different shift from the reference D_2O capillary at 4.79 ppm. Cyphos® 101 has the most shielded water peak at 4.15 ppm presumably due to the large alkyl chains most effectively disrupting the hydrogen bonding of the bulk water. $[N_{2OH888}]Cl$ is the second most shielded with it's internal water at 4.30 ppm appearing much broader than the other ILs due to proton exchange with the primary hydroxy group. Aliquat® 336 and $[P_{1888}]Cl$ both have very similar water peaks at 4.44 and 4.49 ppm respectively, the slight difference arising due to the difference in the acidity of the α-protons and greater electrostatic attraction to larger P centre as it's more accessible through longer $C-P$ bonds. Finally, $[HN_{888}]Cl$ is the only IL to have an internal water environment that is more deshielded than neat D_2O, with a very broad peak centred at 5.34. An enhanced image of the $[HN_{888}]Cl$ water peak is shown in appendix figure 6.7.

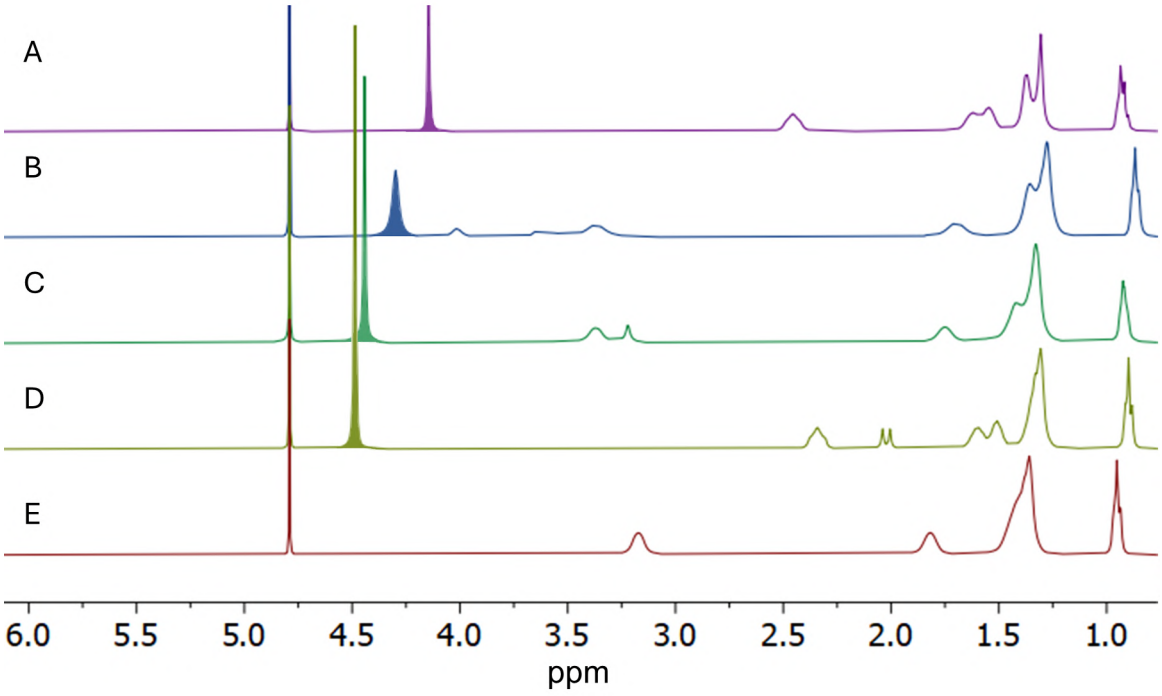

Figure 2.2: Neat ^{1}H NMR of each water saturated ionic liquid with D_2O capillaries. A = Cyphos® 101, B = $[N_{2OH888}]Cl$, C = Aliquat® 336, D = $[P_{1888}]Cl$ and E = $[HN_{888}]Cl$. From top to bottom, the saturated water peaks are observed at 4.15, 4.30, 4.44, 4.49 and 5.37 ppm, all referenced to the D_2O capillary peak at 4.79 and shaded to stand out.

The FT-IR spectra of the water saturated ILs are shown in figure 2.3. All of the

ILs show four peaks at 2853, 2872, 2923 and 2955 cm^{-1} from the alkyl C–H stretch and two close bending peaks at 1458 and 1465 cm^{-1} and another at 1377 cm^{-1}. Cyphos® 101 and $[P_{1888}]Cl$ both show a small peak at 1411 cm^{-1} corresponding to the phosphonium C–P bending while Aliquat 336 and $[N_{2OH888}]Cl$ both have a shoulder at 1486 cm^{-1} corresponding to the ammonium C–N bending. This same C–N bending shoulder in $[HN_{888}]Cl$ is not evident, however the broad peak at 2550 cm^{-1} can be assigned to the quaternary N–H stretch peak. All of the samples show two water peaks, a bending peak at 1629 cm^{-1} that is relatively unchanged between each sample, and a stretching band from *ca.* 3000 to 3600 cm^{-1}. four of the samples show a similar 'shark fin' stretching band that peaks at *ca.* 3400 cm^{-1}, the outlier being $[N_{2OH888}]Cl$ that has a pronounced shoulder at *ca.* 3200 cm^{-1}. Rajapriya *et al.* have investigated the hydration states of some bio-compatible ILs and used peak deconvolution to resolve this stretching band into two peaks, at *ca.* 3200 cm^{-1} and 3400 cm^{-1} that were associated with strongly and weakly hydrogen-bonded water molecule to the anion respectively [307]. The prominence of the peak at *ca.* 3400 cm^{-1} in every samples suggest that water is weakly coordinated to the chloride anion of the IL and is relatively unaffected by the cation expect for $[N_{2OH888}]Cl$ where strong hydrogen bonding is observed due to the large shoulder at 3200 $cmcm^{-1}$.

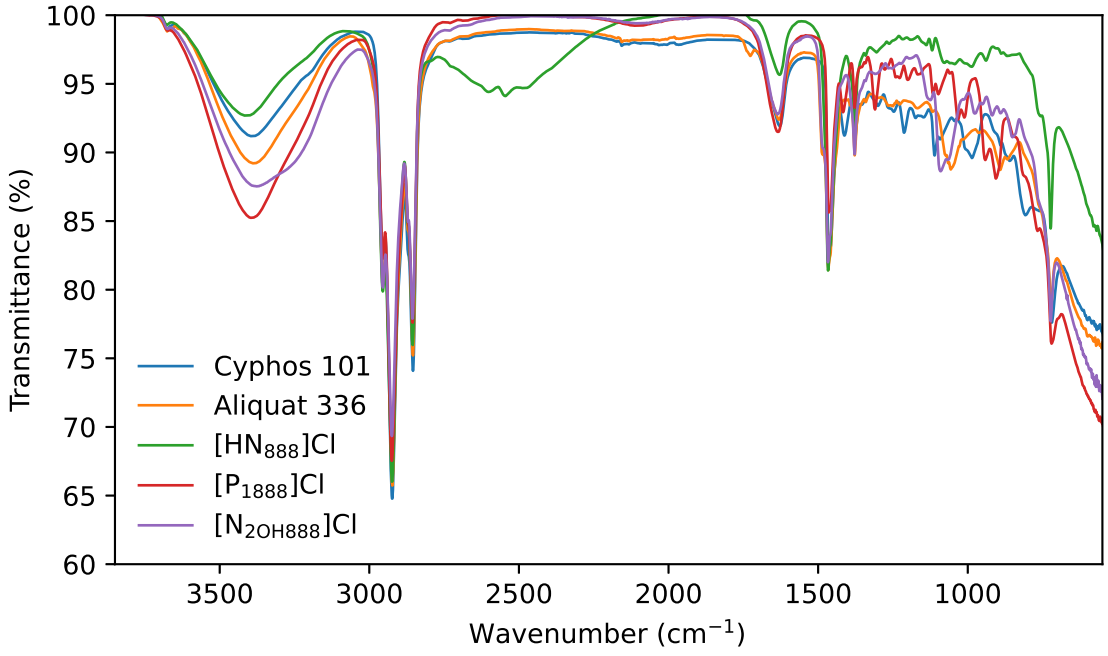

Figure 2.3: FT-IR spectra of each water saturated ionic liquid chloride.

2.3 Sulfate Extractions

2.3.1 Sulfate concentration

The IX ability of the ILs was determined indirectly by contacting the water saturated ILs with aqueous sodium sulfate concentrations from 5 - 100 mM, the resulting aqueous sulfur and chlorine content was then analysed by Energy dispersive X-ray fluorescence (ED-XRF). The sulfur:chlorine content of the IL phases could not be measured directly due to the concentration of chloride in ILs overlapping with any sulfur peak in the XRF spectrum. The XRF spectra of Cyphos® 101 is shown in appendix figure 6.8 and shows that a small sulfur peak would be masked by the large phosphorus and chlorine peaks. A strongly basic type II IX resin Amberlite™IRA-410 also tested as a comparison, where the total number of exchangeable ions available in the resin was equivalent to the Cyphos® 101 sample tested (The least concentrated IL at 1.50 M). The degree of sulfate extraction after contacting with an aqueous phase containing initial sulfate concentrations between 5 and 100 mM is shown in figure 2.4.

It can be seen that at low concentrations, there is an initial high degree of sulfate extraction from the aqueous phase of >90% for all samples. However, as the initial sulfate concentration is increased, the sulfate extraction reduces to 33% for Cyphos® 101, and *ca.* 55-60% for all other ILs. The data in figure 2.4 can be fitted, at least in the range of 5 - 100 mM, by the equation 2.6 which was used to generate smooth lines for the plot. No physical meaning is atributed to the the constancts *a*, *b*, *c* or *d*, this is simply an empirical equaiton used to fit the data.

$$EE = ae^{bC} + ce^{dC} \tag{2.6}$$

Here, *EE* is the extraction efficiency and *C* is the initial aqueous sulfate concentration while *a*, *b*, *c* and *d* are constants, values for the fitting can be found in appendix table 6.1.

This shows that Cyphos® 101 is the least active as a liquid ion exchanger, presumably from a combination of it being the least concentrated in its extracting phase and the four long alkyl chains sterically inhibiting the electrostatic attraction between the cationic centre and extracted sulfate. All four of the other ILs (Aliquat® 336, $[HN_{888}]Cl$, $[N_{2(OH)888}]Cl$ and $[P_{1888}]Cl$), performed in a broadly similar fashion despite having a wide range of IL concentrations and functionalities. Amberlite™IRA-410 outperformed all of the ILs in this scenario as expected as it is well known that resins show a selectivity for multivalent ions from solutions of low ionic strength [308, 309]. This resin is functionalised with two methyls and a

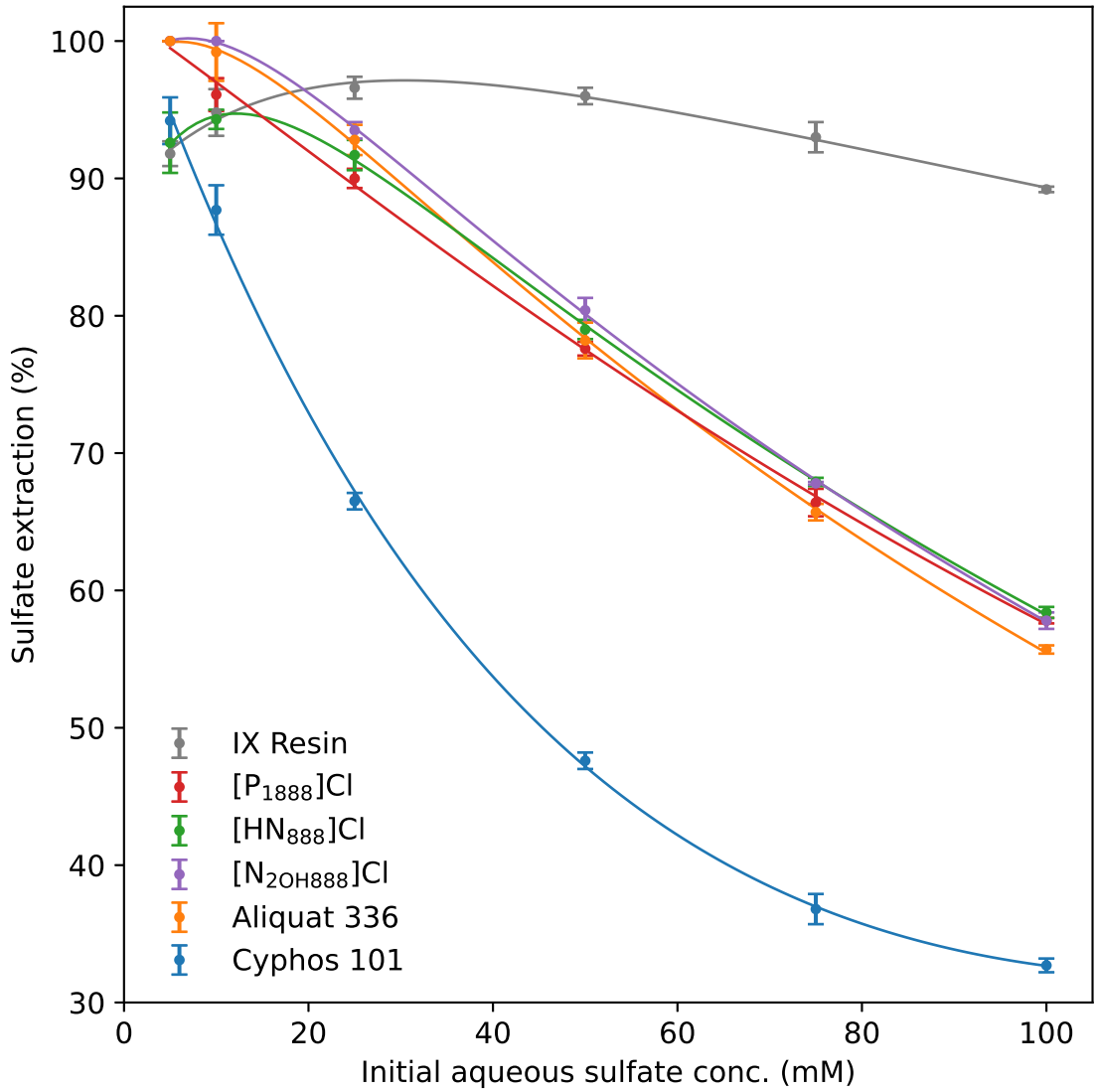

Figure 2.4: Sulfate extraction from varying concentrations of aqueous sulfate by each IL using a phase volume ratio of 0.5 with a solid IX resin, Amberlite™IRA-410 being used as a comparison.

2-hydroxyethyl on its quaternary ammonium groups which allows for strong electrostatic attraction between the anions and the cationic sites while also providing a weakly acidic hydrogen for the formation of H-bonds. It is also reported to contain *ca.* 45 wt% of water when hydrated, however, resins swelling and shrinking is known to occur during any exchange process as the ions dictate the degree of hydration of the resin. It appears then that maximising the degree of electrostatic attraction between the sulfate and the cationic site is the biggest driving force for the IX process with shorter alkyl chains and larger phosphonium cations showing a beneficial effect. Secondary factors such as available protons for H-bonding and saturated water for ion hydration also appear to be favourable. All factors that increase hydrophilicity. . . Perhaps serendipitously, it appears that these factors are

balanced so that Aliquat® 336, [HN_{888}]Cl, [$N_{2(OH)888}$]Cl and [P_{1888}]Cl all exchange nearly equal amounts of chloride for sulfate.

The IX ratio was determined by comparing the reduction in the aqueous sulfur peak to the appearing aqueous chlorine peak Figure 2.5 shows the variation in IX ratio for each material across the range of solutions tested. It shows that the IX ratio for chloride to sulfate reduces as the sodium sulfate concentration increases. If the only equilibria occurring is the chloride-sulfate IX, then this would remain constant at 2 across the range of concentrations. All of the tested material displayed IX ratios larger than 2 from solutions with low ionic strength, suggesting a complete ion-exchange mechanism plus additional migration of chloride into the aqueous phase as the IL is partially soluble in water. However, The IX resin and the phosphonium ILs (Cyphos® 101 and [P_{1888}]Cl) both show IX ratios below 2 at higher sodium sulfate concentrations, indicating some degree of ion-pair extraction where sodium and sulfate both migrate into the IL phase. It is important to note here that sodium content in the aqueous phase was not directly measured but implied by the observed IX ratio. For [P_{1888}]Cl this drops to 1.89 at 100 mM, showing only a small degree of ion-pair extraction while Cyphos® 101 shows an IX ratio of 1.69. The IX resin shows a large degree of ion-pair extraction with an IX ratio of 1.51, meaning three chlorides are exchanged for two sulfates and one sodium ion which may help to help screen the charged surface of the IX resin via formation of a double layer [308].

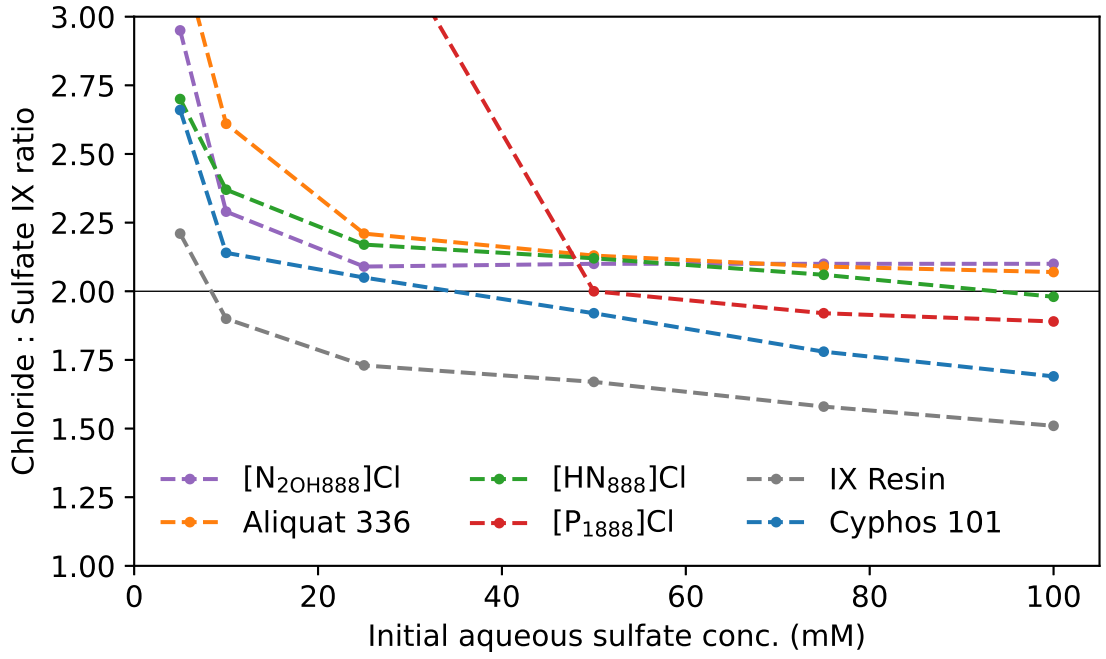

Figure 2.5: Plot of the chloride:sulfate ion-exchange ratio across the range of tested sodium sulfate solutions.

As the volume of extracting phase was kept constant in this study, the moles of IL used for each series is different and therefore the ILs cannot be easily compared on a molecular basis. Cyphos® 101 and Amberlite™IRA-410 is the only comparison that can be made on a molecular basis as the amount of IX resin was calculated to be consistent with the amount of chloride in 3 mL of the IL. For IX resins, it is commonplace to plot the final aqueous sulfate concentration against the final resin concentration (sometimes referred to as the equilibrium resin capacity) to generate a removal isotherm, this is shown in appendix figure 6.9. In this scenario, the IX resin is not included as a final resin concentration would need to be calculated based on an inaccurate estimate of the resin volume from the wet bed volume. To normalise the ILs based on their concentration, the final concentration of sulfate in the IL phase can be divided by the concentration of IL (ie. comparing the millimoles of sulfate extracted per mole of IL) and is shown in figure 2.6.

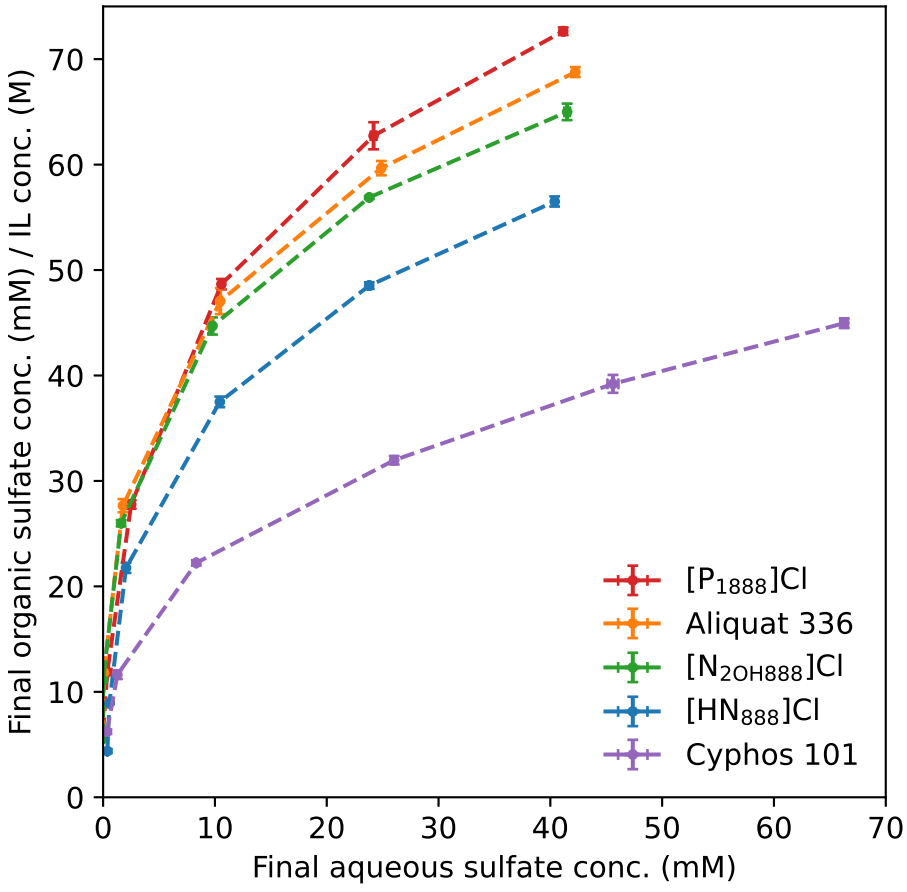

Figure 2.6: Plot of the equilibrium concentration of sulfate between the aqueous and organic phases with the organic phase concentration being normalised by dividing by the concentration of each IL.

For every IL, there is a sharp increase in the final organic (IL) sulfate content observed at low aqueous sulfate concentrations Increasing the aqueous sulfate

concentration further then shows diminishing sulfate extraction by the IL phase. A clear trend is revealed where the chloride for sulfate IX ability of each IL follows the order:

$$[P_{1888}]Cl > \text{Aliquat}^{®}\ 336 > [N_{2(OH)888}]Cl > [HN_{888}]Cl > \text{Cyphos}^{®}\ 101 \qquad (2.7)$$

This shows that ion pairing is greatest for $[P_{1888}]_2[SO_4]$ where after contact with the 100 mM sulfate solution, $[P_{1888}]Cl$ becomes *ca.* $Na_{0.01}[P_{1888}]Cl_{0.87}[SO_4]_{0.07}$. $[P_{1888}]Cl$ appears to be the best performing IL due to it's large cationic centre, acidic α-protons and short methyl group allowing for strong electrostatic attraction between the anion and cations.

2.3.2 Phase volume ratio

To find the optimum phase-volume ratio (PVR), sulfate extractions were performed with different volumes of Aliquat® 336 and Cyphos® 101. For simplicity, only Aliquat® 336 and Cyphos® 101 will be carried forward for further study due to being commercial products. Additionally, Aliquat® 336 was shown to have a similar sulfate extraction profile to the other ILs in figure 2.4. Aqueous sodium sulfate at a concentration of 27.1 mM was used as this represents the concentration of sulfate in standard sea water and equates to 2,600 ppm of sulfate. The results are shown in figure 2.7.

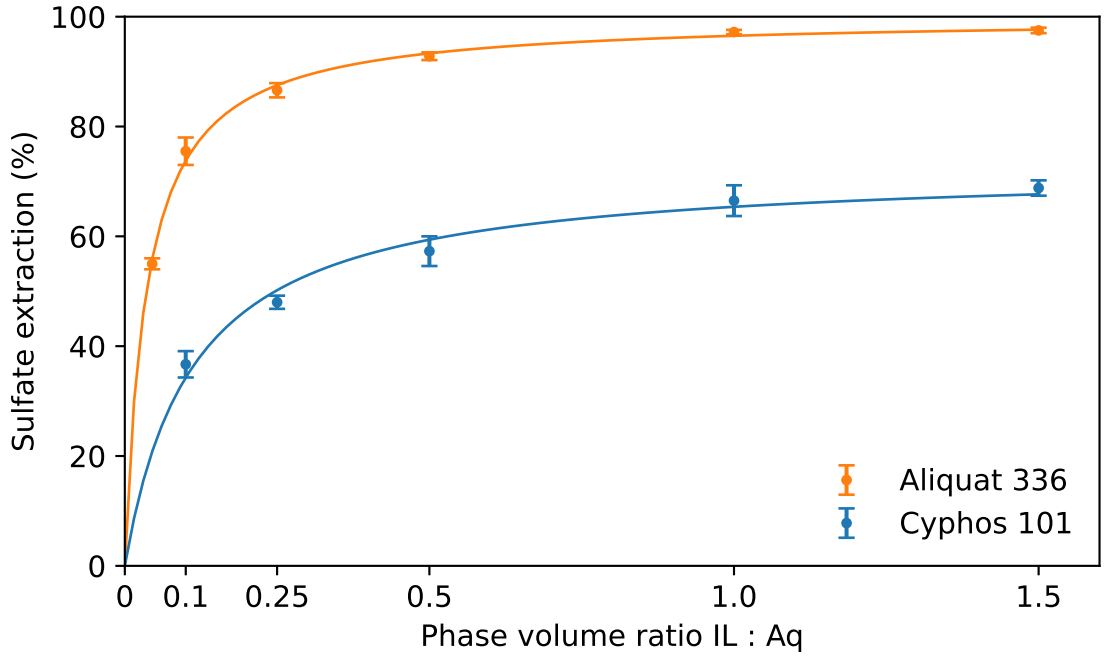

Figure 2.7: Sulfate extraction from a 27.1 mM Na_2SO_4 solution varying the phase volume ratio of IL:Aq.

For both ILs, there is an initial large degree of sulfate extraction at low phase-volume ratios that plateaus at higher ratios. In all cases, Aliquat® 336 shows approximately double the sulfate extraction of Cyphos® 101 in agreement with the previous study. The results clearly show that increasing the phase volume ratio is beneficial for the remove of sulfate however for both ILs, there is little improvement above a phase volume ratio of 0.5.

The data can be modelled remarkably well using the Michaelis-Menten equation shown in equation 2.8 which was used to generate smooth lines for the plot.

$$EE = \frac{ar}{b + r} \tag{2.8}$$

Where *EE* is the extraction efficiency, *a* represents the theoretical maximum sulfate removed in % at an infinite phase-volume ratio, *b* is the phase volume ratio required to remove 50% of the aqueous sulfate and *r* represents the phase-volume ratio. *b* and *r* are both dimensionless quantities in this analysis and values for *a* and *b* are shown in table 2.4.

Table 2.4: Fitting parameters for equation 2.8, describing sulfate extraction into the IL phases.

Ionic liquid	*a* (%)	*b*
Cyphos® 101	72.7	0.112
Aliquat® 336	99.9	0.036

2.3.3 Speciation of Aliquat® 336

As discussed previously in section 1.2.3, Aliquat® 336 can form reverse micelles which have been shown to be very useful for the separation and purification of proteins. This is achieved by dispersing Aliquat® 336 at 0.2 M in a hydrocarbon solvent that is a 4:1, vol:vol of *n*-octane and 1-decanol based on previously reported literature [128]. If the solvent is changed from octane/decanol to chloroform, the stronger solvent-solute interactions prevent formation of reverse micelles and instead the organic salt forms a a dispersion of ion pairs throughout the mixture [130].

To test if the liquid speciation of Aliquat® 336 has any effect on the sulfate extraction, 0.2 M solutions of Aliquat® 336 in chloroform or 4:1 octane/decanol were prepared and stored over water prior to use. These samples where then contacted with a 27.1 mM sodium sulfate solution at a phase volume ratio of 0.5 and the sulfate extraction analysed by XRF. An equivalent amount of water saturated Aliquat® 336 was also tested which is included in figure 2.7 at PVR = 0.045. The results of

this study are shown in figure 2.8.

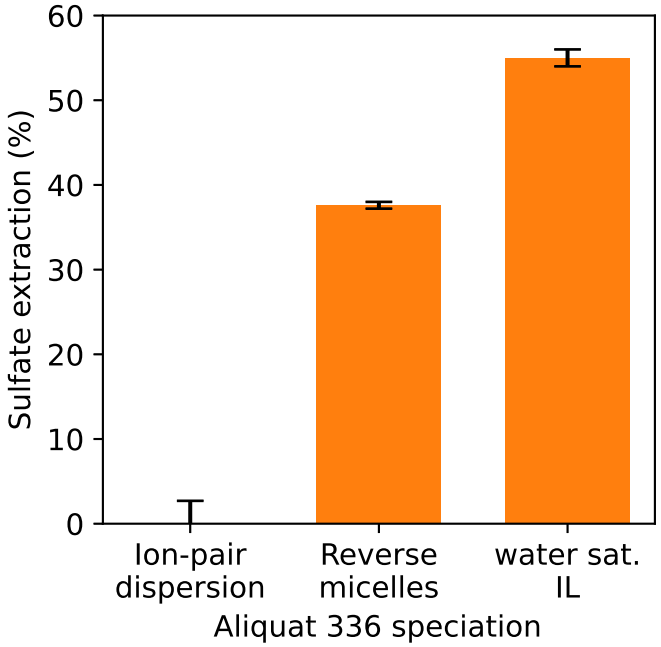

Figure 2.8: Sulfate extraction from a 27.1 mM Na_2SO_4 solution with different speciations of Aliquat® 336. Speciations are; ion-pair dispersion is 0.2 M in chloroform [130], reverse micelles is 0.2 M in 4:1 octane/decanol [128], and an equivalent amount of water saturated Aliquat® 336.

The ion-pair dispersion in chloroform shows no sulfate extraction whereas, the reverse micelle solution extracted 37.6% of the aqueous sulfate. The water saturated Aliquat® 336 outperformed both of these, extracting 55% of the aqueous sulfate. Clearly the morphology of the Aliquat® 336 plays an important role in the extraction of sulfate. A previous publication on the use of a guanidinium reverse micelle forming extractant for sulfate proposed a hydrogen bonded anion complexion mechanism to be responsible for the selectivity of sulfate over chloride [131]. Aliquat® 336 clearly does not bear a strong hydrogen bond donor group and provides evidence for an electrostatic selectivity as the divalent sulfate would be better at stabilising the positive head groups in the reverse micelle core. This is analogous to the selectivity that IX resins display for divalent ions in contact with low ionic strength solutions as they are able to screen the resin charge more effectively than monovalent ions [308, 309]. A significant degree of IX was observed from both the reverse micelle and water saturated IL as they equilibrated at $[N_{1888}]Cl_{0.8}[SO_4]_{0.1}$ and $[N_{1888}]Cl_{0.7}[SO_4]_{0.15}$ respectively.

2.3.4 Competitive chloride

As shown in section 1.2, sulfate is rarely found isolated in 'ideal' solutions and is usually accompanied by other anions such as chloride or phosphate etc. To test the effects of other potentially competing anions, sulfate extractions were performed on aqueous solutions with increasing concentrations of NaCl up to 536 mM. Again 27.1 mM Na_2SO_4 and a phase volume ratio of 0.5 was used, these concentrations mimic those found in sea water. The results are shown in figure 2.9.

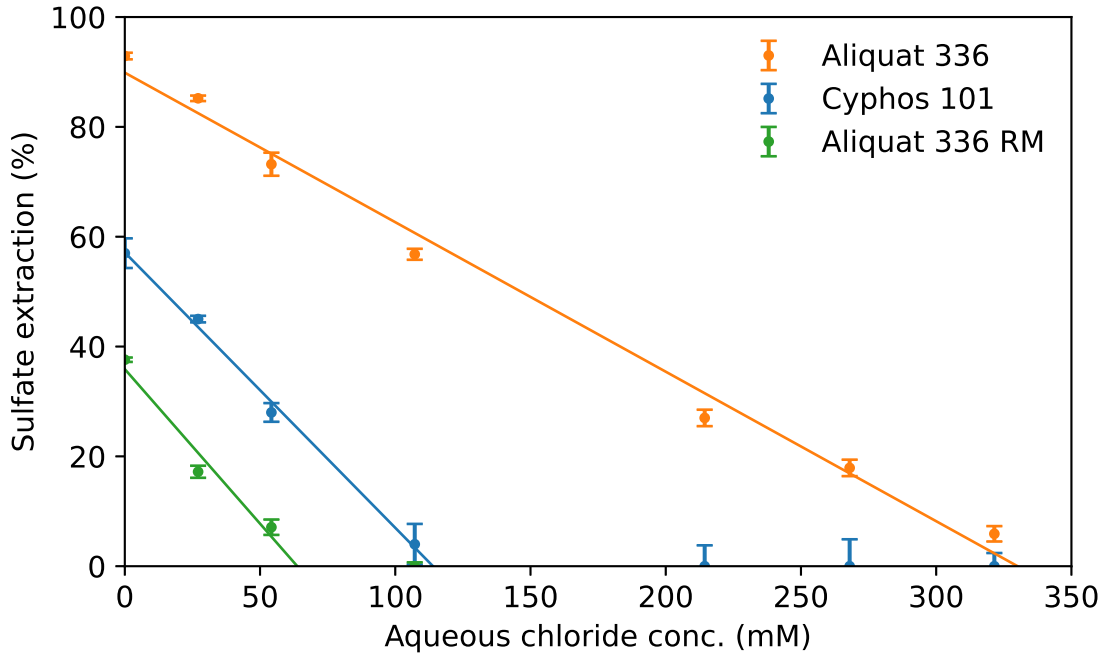

Figure 2.9: Sulfate removal from a 27.1 mM Na_2SO_4 solution while increasing the concentration of NaCl in the aqueous phase. RM = Reverse micelles of Aliquat® 336 at 0.2 M in 4:1 octane/decanol.

In all cases the presence of aqueous chloride inhibits the IX process and reduces the sulfate extraction. It is unclear whether the inhibition come from ion-pair extraction of Na^+ and Cl^- into the IL phase or if the increased ionic strength of the aqueous phase has a direct impact on the Gibbs free energy of the IX process. The relationship is approximately linear and the degree of inhibition can be fitted to equations 2.9 - 2.11 for Aliquat® 336 and Cyphos®101, as well as Aliquat® 336 in the form of reverse micelles where $[Cl^-]$ represents the aqueous chloride concentration mM. R^2 values for these equations are 0.9903, 0.9960 and 0.9634 respectively.

$$EE = -0.272[Cl^-] + 89.9 \tag{2.9}$$

$$EE = -0.501[Cl^-] + 57.1 \tag{2.10}$$

$$EE = -0.563[Cl^-] + 35.9 \quad (2.11)$$

The gradient in this case can be used as a measure of how selective the ILs are for sulfate over chloride. Neat Aliquat® 336 is more selective than Cyphos®101 as the methyl group may allow for better ordering of the charges which is stabilised better by sulfate than chloride. There is eight times less Aliquat® 336 in the reverse micelle series than in the neat IL so it is no surprise that it extracted less sulfate. However, it also displays the steepest gradient which shows that the reverse micelles are less selective than the neat ILs. Clearly this is still a long way off sulfate removal from sea water, however from this data, 16% of sulfate is still removed by neat Aliquat® 336 from a solution containing 10 times the concentration of competitive chloride, which is exceedingly rare in the literature, especially considering that 27.1 mM is a relatively high sulfate concentration compared to which is normally studied. For example, the highly selective reverse micelle forming guanidinium extractant reported by Williams *et al.* used an aqueous phase containing only 0.1 mM Na_2SO_4 and 10 mM NaCl [131].

The observed selectivity for sulfate over chloride in solutions of low ionic strength, that get reduced as the ionic strength of the solution increases is similar to many reports of strong anion exchangers [308, 309]. In IX resins, this selectivity arises from multivalent ions being better able to screen the charged surface of the resins. Williams *et al.* also suggested that their reverse micelle system extracts sulfate water clusters into the hydrocarbon phase, which negates the penalty of having to shed the hydration sphere and helps to stabilise the high charge density in the core of the reverse micelle [131]. In these ILs therefore, a similar mechanism for sulfate extraction is proposed where divalent sulfate is extracted into the IL phase where it can still hydrogen bond to the water in the IL phase. Additionally, the sulfate may be better able to stabilise domains of high charge density that must exist in a phase composed of charged cationic and anionic centres, long alkyl chains and water.

2.3.5 pH dependence of extraction

Acidification of the aqueous stream was suspected to be an effective method for improving the sulfate removal by protonation of sulfate to form the less hydrophilic hydrogen sulfate. To test this, 100 mL of an 'ideal' 27.1 mM Na_2SO_4 solution and 100 mL of a model sea water made from 27.1 mM Na_2SO_4 and 535 mM NaCl were acidified to pH 1 using 37% HCl. Acidification required 1 to 1.5 mL of acid solution so there was a negligible dilution effect on the sulfate concentration. Results from extracting the acidified aqueous solutions with water saturated Aliquat® 336 are shown in figure 2.10.

The addition of HCl to the 'ideal' solution has a negative effect on the sulfate re-

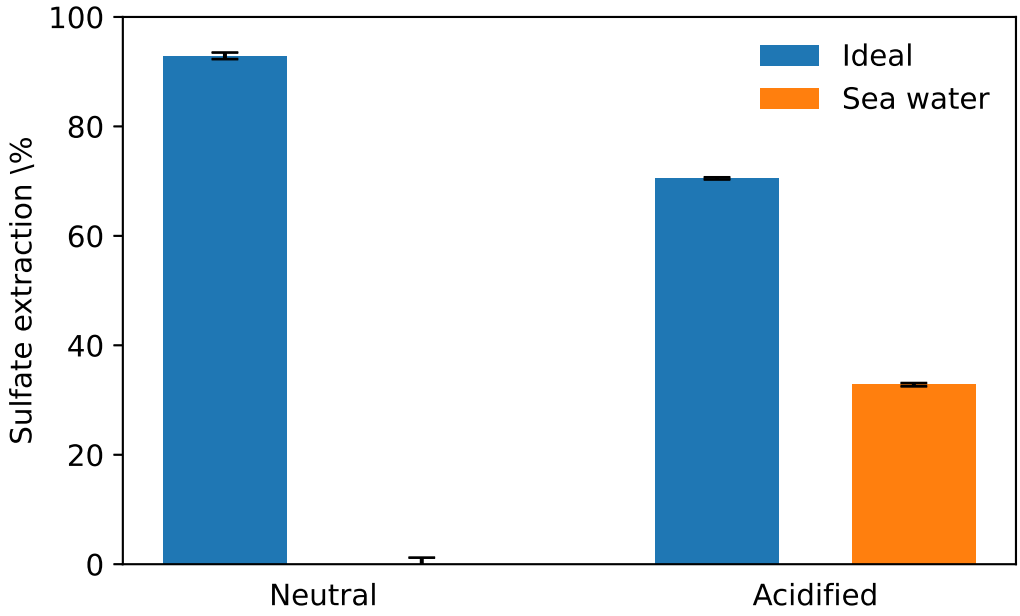

Figure 2.10: Sulfate removal by Aliquat® 336 from neutral and acidified (pH = 1) aqueous solutions. Ideal = 27.1 mM Na_2SO_4, Sea water = 27.1 mM Na_2SO_4 and 535 mM NaCl.

moval with the sulfate extraction reducing from 93 to 71%. This is counter-intuitive given that the hydration enthalpy of hydrogen sulfate is reported to be ΔG_{Hyd} = -330 kJ·mol^{-1} [310], similar to the value reported for chloride (-340 kJ·mol^{-1}). Considering only the aqueous phase, this is a much more favourable IX process of -10 kJ·mol^{-1} versus the +400 kJ·mol^{-1} that is lost in the exchange between sulfate and two chlorides. Acidification also increased the initial chloride concentration to 175 mM which as shown will have a negative effect on the extraction efficiency, reducing it by approximately 47.6%. It appears that for the ideal solution, the negative effect from the addition of the chloride overpowers any potential positive effect from sulfate protonation.

Opposite to this, the addition of HCl to the model sea water increases the sulfate removal from 0% to 32.8%. In this case the protonation outweighs the addition of more chloride and facilitates the migration of sulfate into the IL phase. Considering the similar free energies of hydration between chloride and hydrogen sulfate and the phase-volume ratio of 0.5, it appears that hydrogen sulfate is simply distributed evenly throughout the biphasic system with no preference for either phase as *ca.* one third of it resides in the IL phase.

2.3.6 Reusability

The ability to reuse the extracting phase is crucial for it being applicable in the real world. Unfortunately, no combination of water and/or acid and/or base washes would facilitate the reuse of Aliquat® 336 or Cyphos®101. They could potentially be regenerated via IX resin however this would be energy intensive as they would need diluted, ion-exchanged, the diluting solvent removed and then water saturated again. An alternative option would be barium precipitation, however this would also require the relatively viscous water saturated ILs to be filtered or centrifuged.

Fortunately, $[HN_{888}]Cl$ was able to be reused by successive washings with base and acid to deprotonate and reprotonate the amine, the same method used for weakly basic IX resins or Alamine 336 in metal recovery. $[HN_{888}]Cl$ was first contacted with a 27.1 M Na_2SO_4 in the usual way, the lower aqueous phase was then removed and the IL shaken with 7.5 wt% NaOH followed by 7.4 wt% HCl before contact with the next sulfate solution. 6 mL of each aqueous phase (sulfate, base and acid) was used at each stage and the samples were centrifuged to ensure complete phase separation. The results are shown in figure 2.11.

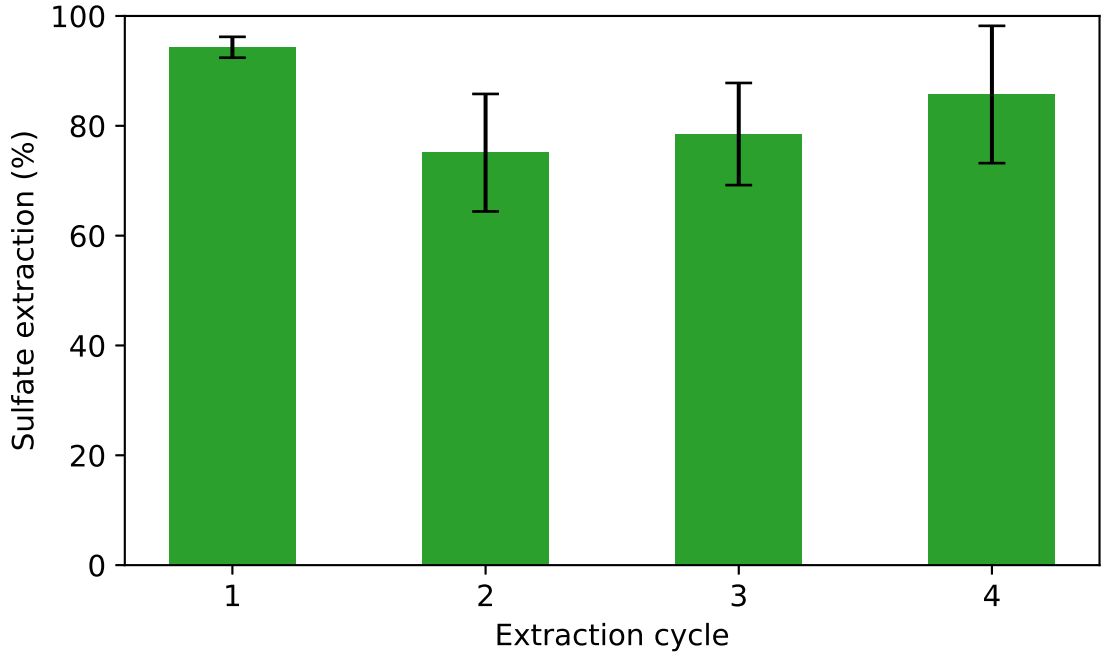

Figure 2.11: Sulfate removal from a 27.1 mM Na_2SO_4 solution across 5 cycles by $HN_{888}Cl$. Between cycles the IL was washed with two volume equivalents of 7.5 wt% NaOH and then 7.4 wt% HCl.

Initially, a drop in sulfate removal of 20% is observed, the large error bars then obscure any trend in the data between the second, third and fourth extraction cycle. Mechanical losses of the exacting phase would cause a decline in the extraction

efficiency each cycle while residual HCl brought forward into the sulfate extraction from the acid wash will provide a positive effect as shown from section 2.3.5. Differences in mechanical losses of the organic phase account for the variation in samples resulting in the large error bars causing a large uncertainty about the observed trend. Ignoring mechanical losses from this study, overtime the water solubility of $[HN_{888}]Cl$ would result in a steady reduction in sulfate removal, however this was not observed across four cycles.

2.3.7 Comparative Methods

Precipitation and IX resin methods of sulfate removal as discussed in section 1.2.1, were tested as a comparison to benchmark the ILs against. In this case, a molar excess of the precipitating agents ($BaCl_2$ and $Ca(OH)_2$) were added dry and the solutions filtered to removed any precipitate or residual solids before XRF analysis of the aqueous phase. The IX resins were hydrated with DI water prior to use and mixed with the aqueous solution so sulfate could equilibrate between the aqueous and resin phases. The results from this study are shown in figure 2.12.

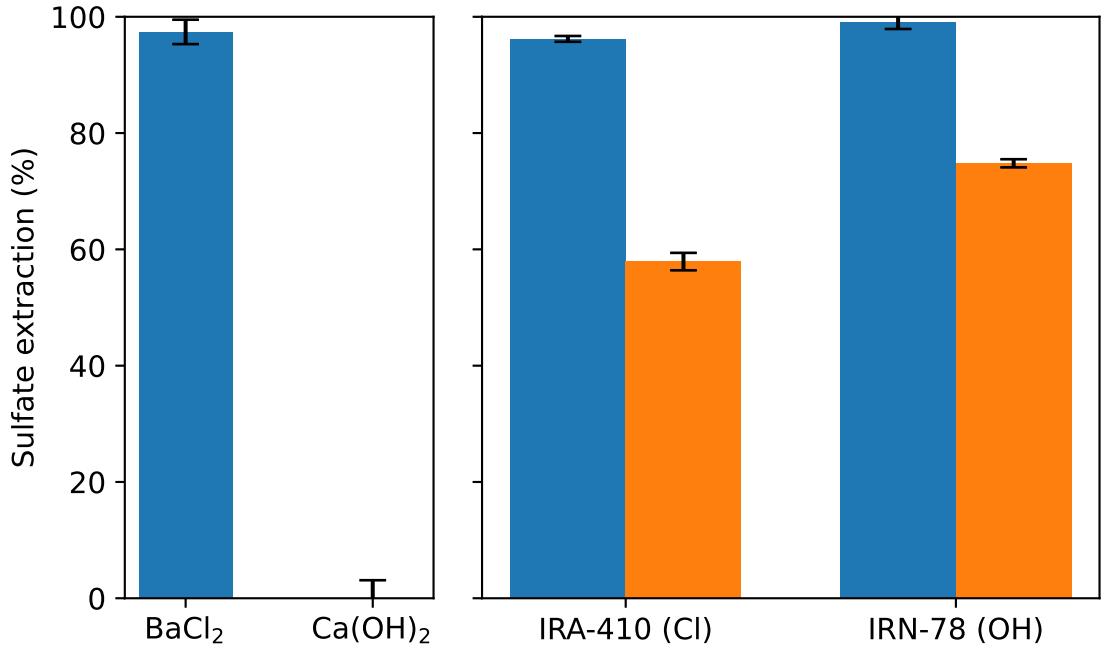

Figure 2.12: Aqueous sulfate removal via precipitation and IX methods. Blue = 'ideal' 27.1 mM Na_2SO_4, orange = model sea water, 27.1 mM Na_2SO_4 + 535 mM NaCl.

The addition of $BaCl_2$ removed 97% of the aqueous sulfate, in agreement with the reported solubility of $BaSO_4$ at 25 ℃ being 2.8 ppm (1.2 ppm sulfate) [311]. For reference, 27.1 mM sodium sulfate equates to 2,600 ppm sulfate. Opposite to

this, the addition of $Ca(OH)_2$ had no effect on the aqueous sulfate concentration although this is not entirely surprising as calcium precipitation is typically reported to reduce sulfate levels to approximately 2,000 ppm [312]. Although the presence of NaCl does have a minor effect on the solubility of both $BaSO_4$ and $CaSO_4$ through the uncommon ion effect, this has been shown to be very small and so precipitation methods were only tested on the ideal solutions [311, 313].

Amberlite™IRA-410 is a strongly basic anion Type II resin with two methyl groups and a hydroxyethyl group whereas IRN-78 is a strongly basic type I resin with three methyl groups. Both IX resins removed high levels of sulfate from both the ideal solution as excepted from IX resins in low ionic strength solutions as sulfate is better also to screen the surface charge on the resin [309]. In the model sea waters solutions, sulfate was still extracted but not as much as in the ideal solutions as the selectivity reverses in high ionic strength solutions. The hydroxide resin slightly outperforming the chloride resin as expected from the higher free enthalpy of hydration (ΔG_{Hyd} = -400 vs -340 kJ·mol^{-1} [80, 81]), however, the hydroxide loaded resin did also removed 85% of the aqueous chloride.

2.4 Conclusions

In conclusion it has been shown that long chain tetraalkyl ammonium and phosphonium chloride salts readily form aqueous biphasic systems and have the potential to be used as liquid anion exchangers. Less sterically hindered cations such as $[P_{1888}]^+$ are the most effective at exchanging the chloride for sulfate on a mol_{IL} per $mol_{sulfate}$ basis compared to more sterically hindered cation of Cyphos®101 ($[P_{66614}]^+$). Similar to solid IX resins, in solutions of low ionic strength they are selective for multivalent anions, however this selectivity reduces with increasing ionic strength of the aqueous phase as the IX process is inhibited by the presence of aqueous chloride. From competitive solutions, the sulfate removal can be enhanced through the addition of acid. $[HN_{888}]Cl$ also shows good recycling, with only a *ca.* 15% reduction in sulfate removal after 4 cycles.

It is suggested that the absorbed water helps to structure the IL phase similar to the formation of reverse micelles and that multivalent ions are better able to stabilise the areas of high charge density. This morphological stabilisation is the driving force for the ion-exchange process despite the differences in free energy of hydration between chloride and sulfate. Additionally, the water of saturation that is present in the IL phases can hydrogen bond to the sulfate allowing it to maintain at least part of the hydration sphere upon extraction.

Although these ILs have been demonstrated to be ineffective at sulfate removal from model sea water, they may still be applicable for other areas of anion extraction

such as paper mill [314] and nuclear waste [19]. In both of the industries, aqueous waste is produced in the form of sludge or slurries and so the use of liquid-liquid extraction would avoid the necessity for filtration that would be required prior to ion-exchange with a traditional solid resin.

2.5 Experimental

Materials and methods

Aliquat® 336, trioctylamine and trioctylphosphine were purchased from Tokyo Chemical Industry Ltd. Cyphos® 101 was kindly supplied by Solvay but found to contain residual acid from manufacturing, this was removed by dilution with DCM and washed with water until neutral. All other chemicals were used as supplied without further purification.

Microwave irradiation was performed using an Anton Paar Monowave 300. ED-XRF analysis was performed on a Rigaku NEX QC+ QuantEZ spectrometer run under a helium atmosphere. FT-IR was performed on a PerkinElmer Spectrum 100 spectrometer equipped with the universal ATR accessory. Density and viscosity was measured using an Anton Paar SVM 3001 kinematic viscometer. NMR was performed on a Bruker UltraShield Plus 400 MHz spectrometer. Samples mixed gently on a Stuart SRT6 roller mixer to avoid the formation of emulsions. Where error bars are presented, the data has been collected in triplicate with the points being displayed as the mean with error bars representing the 95% confidence interval [315].

Mutual solubility of water and ILs

IL solubility in water was determined by roller mixing approximately equal portions of water and IL overnight followed by centrifugation to ensure complete phase separation. The carbon content of the aqueous phase was then analysed by total organic content analysis to determine the amount of IL in the aqueous phase.

Water solubility in ILs was measured by accurately weighing an amount of water saturated IL before and after drying overnight under high-vac while being heated above the melting point of the dry IL. Neat ^{1}H NMR using a deuterated solvent capillary for a signal lock was also used to calculate the internal water by integration of water peaks and was found to be in good agreement with the drying procedure.

Extraction studies

Prior to extraction tests, all ILs were pre-equilibrated with DI water, centrifuged and stored over DI water to ensure saturation and complete phase separation before use. The general procedure for an extraction was to roller mix the already water saturated extracting phase (3 mL) and the desired anion containing aqueous phase (6 mL) overnight. The phases were then separated and 3 g of the aqueous phase

analysed by ED-XRF analysis using calibrations described later for sulfur and chlorine. The equilibration time was first examined with Cyphos® 101 with samples being contacted for specific durations up to 24 hours. Data shown in the appendix figure 6.6 demonstrates that roller mixing samples for 30 minutes is sufficient to reach equilibrium. The extractions were also performed at ambient lab conditions, around *ca.* 20 °C. The concentration of chloride and sulfate in IL phases cannot be measured directly as the high inherent chlorine peak in the ILs dominates the spectra and masks any sulfur signal, see appendix figure 6.8.

All IX resin extraction studies were performed by mixing of the resin and aqueous phase overnight to find an equilibrium rather than the usual column method. All resins were pre-wetted to ensure full swelling and hydration by soaking the IX resin (50 g) in DI water (200 mL) for 1 hour, this water was then drained and this soaking was repeated three times before use. The IX resins were then measured by wet bed volume and transferred to vials where excess water was removed before the addition of the sodium sulfate solutions to reduce any dilution effects from interspatial water.

Precipitation studies were performed by mixing the aqueous solutions with an excess of the precipitating agent overnight before filtering the solution twice to remove any particulates.

Hydrophobic IL-Cl Synthesis

$[P_{1888}]Cl$

This synthesis has been reported previously [316].

Trioctylphosphine (4.5 mL, 10 mmol), dimethylcarbonate (5.9 mL, 70 mmol) and methanol (5.9 mL) were added to a 30 mL microwave vial and the biphasic mixture heated to 140 °C under microwave irradiation for 24 h. After the reaction the solution was monophasic and 37% HCl (*ca.* 1 mL) was added dropwise to the vial with vigorous stirring which produced CO_2 and methanol via decomposition of the methylcarbonate anion. Five of batches were made and combined, DCM (100 mL) was then added, washed with water (3 x 50 mL), brine, dried with $MgSO_4$ and solvent removed under reduced pressure on a rotary evaporator to give a near quantitative yield of the product. ^{1}H NMR (400 MHz, DMSO-d_6) δ 2.20-2.10 (6 H, m), 1.78 (3 H, d, J = 14.1 Hz, $P-CH_3$), 1.51-1.41 (6 H, m), 1.40-1.32 (6 H, m), 1.32-1.20 (24 H, m), 0.86 (9 H, t, J = 6.9 Hz). $^{13}C\{^{1}H\}$ NMR (100 MHz, DMSO-d_6) δ 31.20 (s, 1C), 30.00 (d, J = 60.6 Hz, 1C), 28.26 (d, J = 72.2 Hz, 1C), 22.04 (s, 1C), 20.49 (d, J = 20 Hz, 1C), 19.06 (d, J = 192 Hz, 1C), 13.92 (s, 1C), 3.18 (d, J = 204 Hz, 1C). $^{31}P\{^{1}H\}$ NMR (162 MHz, DMSO-d_6) δ 32.29. HRMS (ESI, MeOH): *m/z* calcd for $[PC_{25}H_{54}]^{+}$: 385.40, found 385.3751.

[HN_{888}]Cl

Trioctylamine (87 mL, 200 mmol) was added to a 500 mL round-bottom flask followed by deionised water (50 mL) and the biphasic mixture stirred vigorously in an ice bath. 1 M HCl (250 mL, 250 mmol) was then added dropwise to the flask which immediately produced a white precipitate. The white precipitate melted as it warmed to room temperatures and was transferred to a separating funnel followed by diethyl ether (100 mL) and the organic phase washed with water (5 x 200 mL). The product was then dried under reduced pressure on a rotary evaporator to yield a white waxy solid (69.8 g, 89.5%). ^{1}H NMR (400 MHz, DMSO-d_6) δ 10.39 (1 H, s), 2.95 (6 H, quint, J = 8.4 Hz), 1.63 (6 H, m), 1.28 (30 H, m), 0.86 (9 H, t, J = 6.8 Hz). ^{13}C{^{1}H} NMR (100 MHz, DMSO-d_6) δ 51.59, 31.13, 28.42, 26.04, 22.71, 22.01, 13.88. HRMS (ESI, MeOH): *m/z* calcd for $[NC_{24}H_{52}]^{+}$: 354.41, found 354.4154.

[N_{2OH888}]Cl

Method adapted from previously reported literature [317].

Trioctylamine (53.05 g, 150 mmol), 2-bromoethanol (17 mL, 225 mmol) and toluene (250 mL) were added to a two-neck 500 mL round-bottom flask set up for reflux with a drying tube attached. The mixture was then stirred vigorously and heated to 100℃ for 3 days. Solvent and residual 2-bromoethanol were removed under reduced pressure to yield a red-brown oil. This was then dissolved in DCM (200 mL), and washed with 5 wt% NaOH solution (3 x 100 mL), distilled water (2 x 100 mL) and brine (100 mL). The organic layer was then dried over anhydrous sodium sulfate, filtered and the solvent removed under reduced pressure to yield a red-brown oil that solidified upon standing. Residual trioctylamine was then decanted off and the product dissolved in ethanol (500 mL) and passed through a chloride loaded Amberlite™IRA-402 ion-exchange resin (150 mL wet bed volume). The crude product was analysed by ED-XRF analysis and showed a 97% IX to chloride. Solvent was again removed under reduced pressure and the solid was recrystallized in dry diethyl ether for two days in the freezer. The ether solvent was removed by cannula and the process repeated twice more to yield white waxy-crystalline product that was dried under reduced pressure on the rotary evaporator (53.04 g, 81.4%). ^{1}H NMR (400 MHz; DMSO-d_6) δ 5.62 (1 H, br s, OH), 3.75 (2 H, s, CH_2OH), 3.33 (2 H, t, J = 4.8 Hz, NCH_2CH_2OH), 3.25 (6 H, m), 1.58 (6 H, m), 1.25 (30 H, m), 0.86 (9H, t, J = 6.8 H, CH_2CH_3). ^{13}C^{1}H NMR (100 MHz; DMSO-d_6) δ 59.36, 58.30, 54.46, 31.19, 28.47, 28.39, 25.74, 22.08, 21.05, 13.95. HRMS (ESI, MeOH): *m/z* calcd for $[NOC_{26}H_{56}]^{+}$: 398.44, found 398.4304.

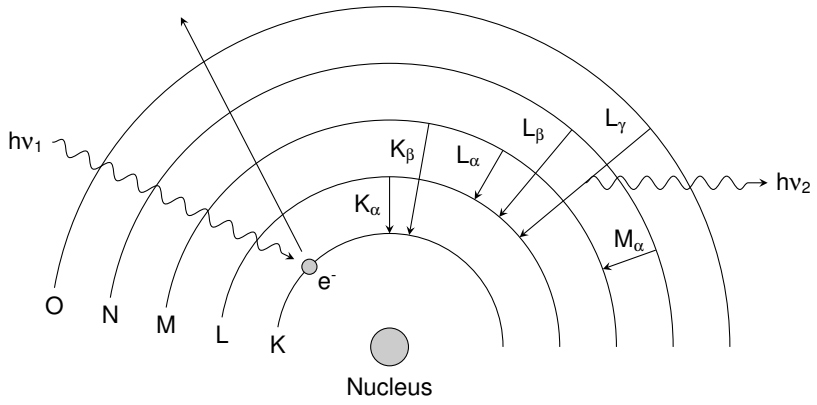

Figure 2.13: Atomic energy level transitions and their corresponding ED-XRF spectral lines. In this case an electron is shown to be ejected from the K shell and a subsequent L_γ relaxation is shown, this would also be accompanied by a K_α relaxation that has been omitted for clarity.

X-Ray Fluorescence

X-ray Fluorescence (XRF) analysis relies on the principle that every element (except H & He) when properly excited, will emit a unique set of characteristic X-rays. This allows for non-destructive, quantitative elemental analysis of samples as the energy of the emitted photons correspond to a specific element and the relative number of photons corresponds to the concentration.

Figure 2.13 shows how an incident X-ray ($h\nu_1$) can eject an inner electron from the nucleus if it is of sufficient energy, leaving an electron hole. The minimum energy required to eject an inner electron is known as the 'absorption edge', this can also be referred to more specifically as the 'K-edge' if the electron was ejected from the first shell (principle quantum number, n = 1) or the 'L-edge' from the second shell (n = 2) etc. Electrons in the outer shells will then relax to fill the hole, emitting a photon with a specific energy that corresponds to the difference in energy between the higher and lower energy levels. In the case of figure 2.13, the emitted photon $h\nu_2$ will have an energy corresponding to that of an O $\rightarrow$ L transition and denoted L_γ for that specific element and is usually expressed in units of keV. This is known as Siegbahn notation for spectral lines and can also include a subscript to denote the precise energy level taking the spin energy into account however, that level of precision is not necessary in this case. For this work the relevant transitions are; phosphorus K_α = 2.01 keV, K_β = 2.14 keV, sulfur K_α = 2.31 keV, K_β = 2.46 keV and chlorine K_α = 2.62 keV, K_β = 2.81 keV.

Table 2.5: Composition of standard solutions for ED-XRF calibration for sulfate and chloride at relevant concentrations to 'sea' water and an 'ideal' sea water that dose not contain competitive chloride.

Solution	Ideal		Sea	
	Sulfate / mM	Chloride / mM	Sulfate / mM	Chloride / mM
a	31.2	84.6	31.2	621
b	26.0	70.5	26.0	606
c	20.8	56.4	20.8	592
d	15.6	42.3	15.6	578
e	10.4	28.2	10.4	564
f	5.21	14.1	5.21	550
g	2.60	7.05	2.60	543
h	0	0	0	536

ED-XRF calibration

Here the 'ideal' calibration refers to a model sea water solution with respect to the concentration of sulfate but with no other anions present, the model sea water is thus the same concentrations of sulfate but also includes the presence of sea water levels of chloride. Standard stock solutions of sodium sulfate and sodium chloride were made up according to table 2.5. An empirical calibration was then made using the Nex software. 3 g of each aqueous solution was analysed for 3 minutes under a helium atmosphere using a silver cathode ray X-ray source running at 6.5 kV and 70 µA using no primary filter. For maximum resolution between the S and Cl peaks a shaping time of 4 µs was used and integration limits were set at 2.258 - 2.358 keV for the S K_α peak and 2.572 - 2.672 keV for the Cl K_α peak, the peak at $\approx$ 3 keV is the Ag L_α peak from the cathode ray tube. The integration of these peaks within the defined limits gives a peak intensity that can be plotted against the concentration according to equation 2.12.

$$I = ac + b \tag{2.12}$$

where I is the intensity of the K_α peak, c is the concentration of the species and a and b are constants that relate to the fluorescence of the element in that matrix and the background signal respectively. Raw spectra are shown in figures 2.14 and 2.15 and the linear relationship between concentration and response for both calibration series' is shown in figures 2.16 and 2.17. Values for the constants a and b as well as R^2 values for the linear regression are shown in table 2.6. Due to baseline effects from the Cl K_α peak, the observed sulfate response is slightly different in both calibrations. A comparison of the two sulfate calibrations is shown in figure 2.18.

Table 2.6: Equation constants for ED-XRF calibration of sulfate and chloride.

Constant	Ideal		Sea	
	S	Cl	S	Cl
a / cps·µA^{-1}·mM^{-1}	0.219	0.414	0.196	0.304
b / cps·µA^{-1}	2.970	6.488	3.557	41.36
R^2	0.9993	0.9993	0.9999	0.9880

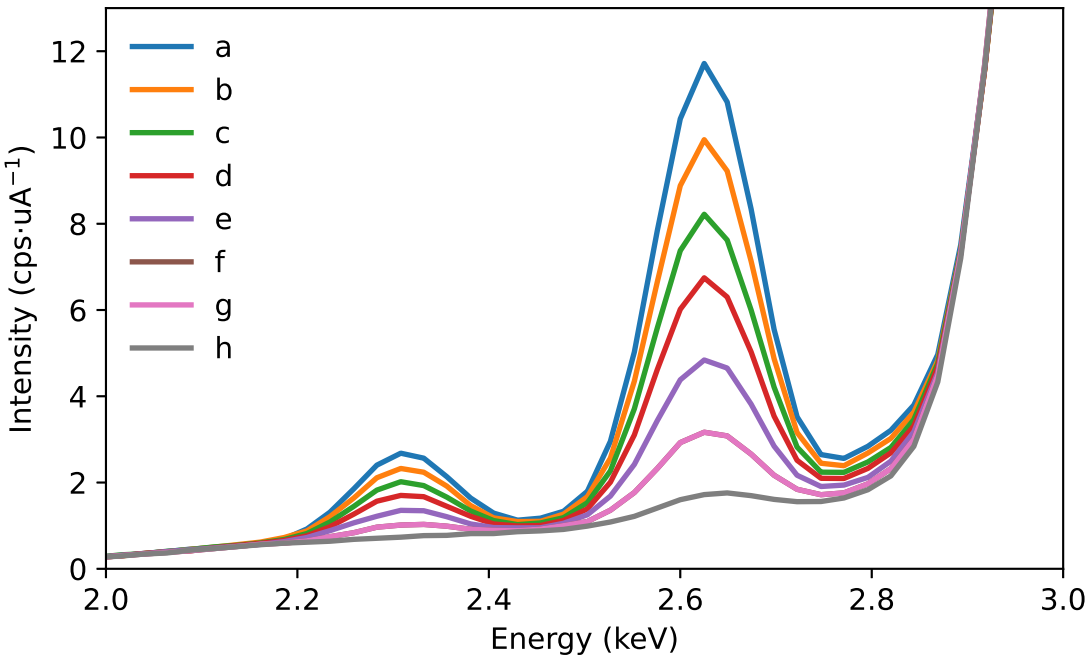

Figure 2.14: ED-XRF spectra for the ideal Na_2SO_4 calibration. From 0 - 31.2 mM Na_2SO_4 and 0 - 84.6 mM NaCl, showing peaks corresponding to the presence of sulfur and chlorine at 2.31 and 2.62 keV respectively.

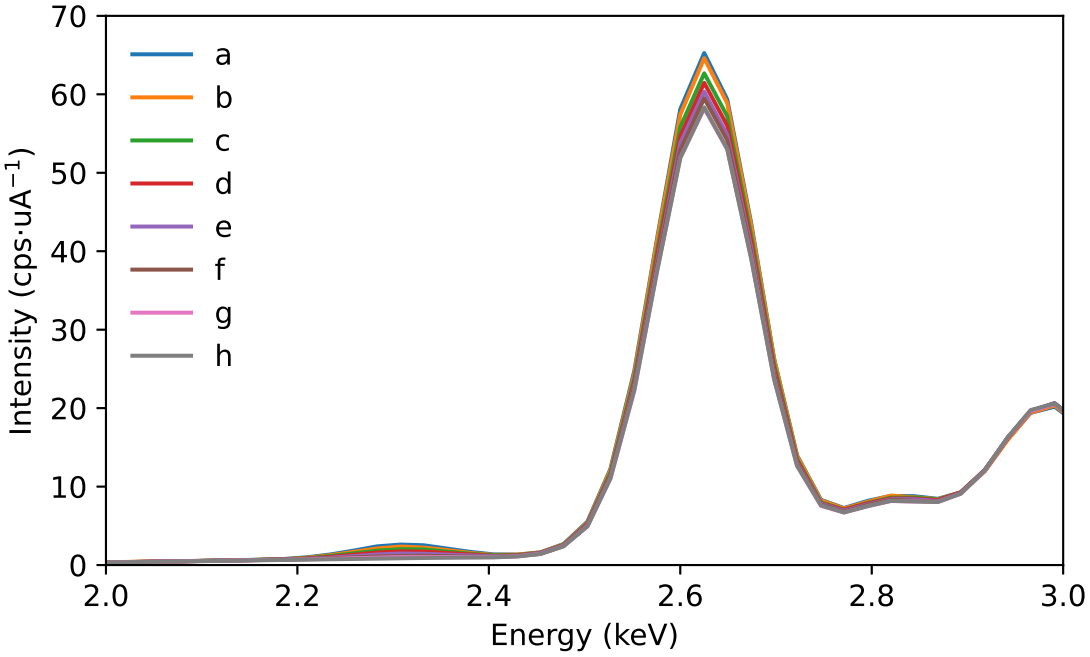

Figure 2.15: ED-XRF spectra for the model sea water calibration. From 0 - 31.2 mM Na_2SO_4 and 536 - 621 mM NaCl, showing peaks corresponding to the presence of sulfur and chlorine at 2.31 and 2.62 keV respectively.

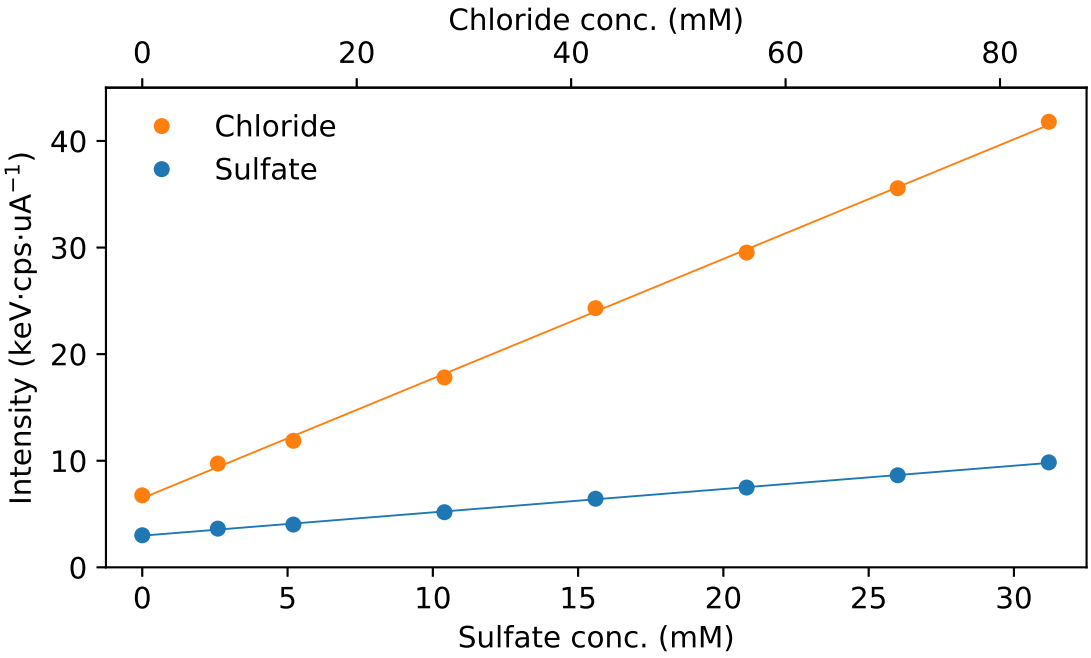

Figure 2.16: ED-XRF calibration of integrated peak area vs concentration. From 0 - 31.2 mM sulfate and 0 - 84.6 mM chloride.

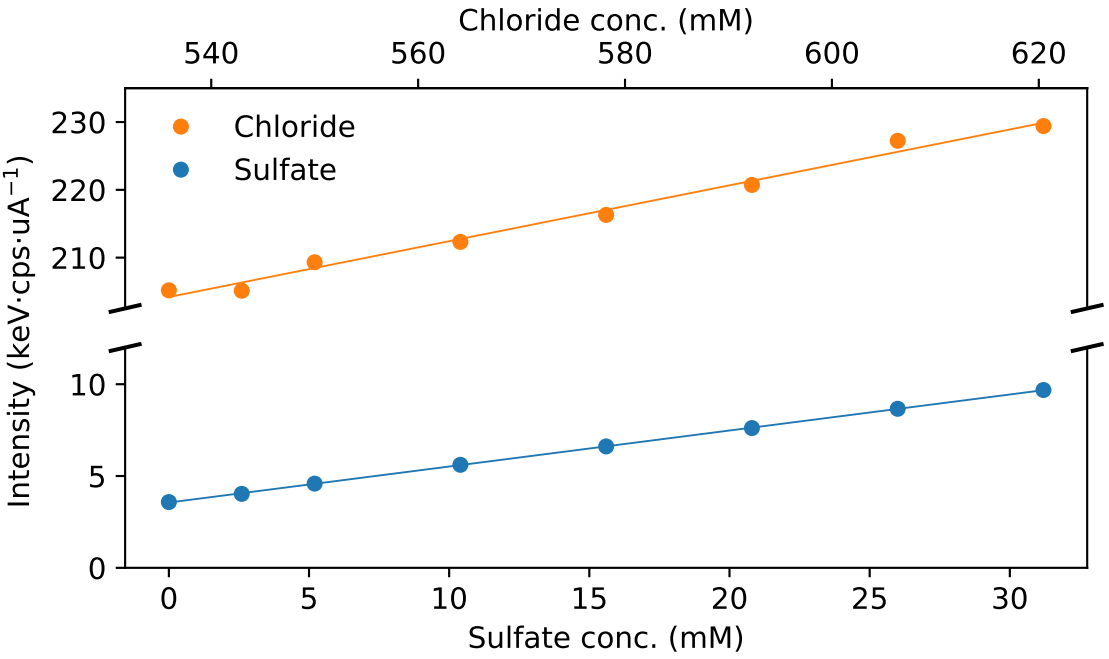

Figure 2.17: ED-XRF calibration of integrated peak area vs concentration. From 0 - 31.2 mM sulfate and 536 - 621 mM chloride.

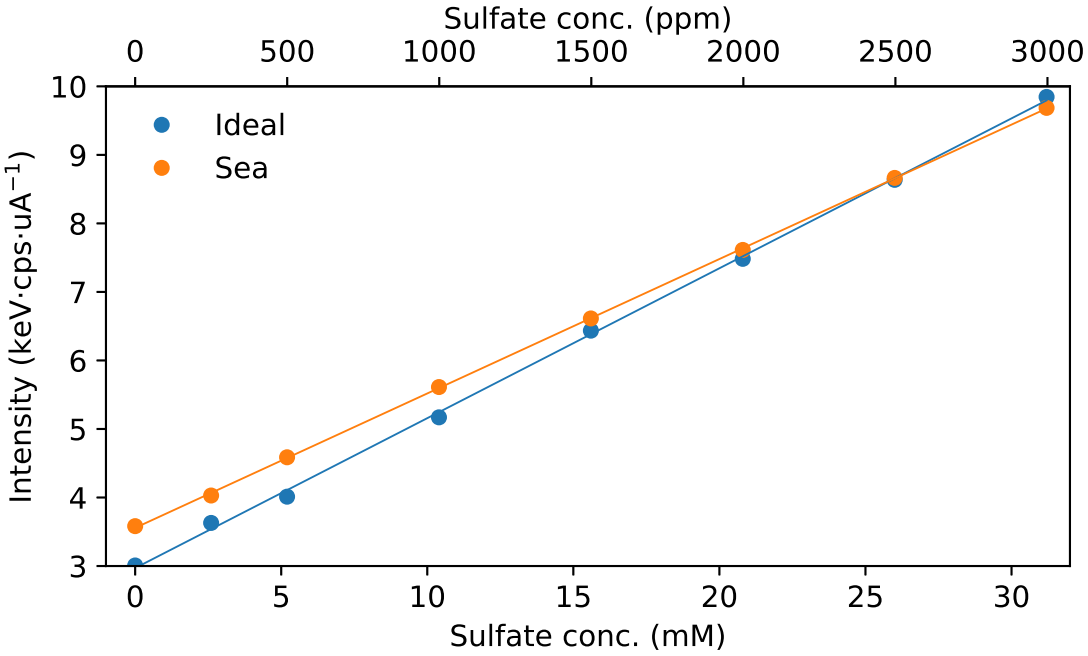

Figure 2.18: Comparison of the sulfate calibrations with the presence (sea) and absence (ideal) of 536 mM chloride.

3. Synergised Anion Exchange and Recognition

3.1 Introduction

To increase the affinity of Aliquat® 336 and Cyphos®101 for sulfate, a range of anion receptors were added to the water saturated ILs to act as extractants. In theory, the receptors could coordinate to the sulfate through hydrogen bond donation, resulting in a hydrophobic sulfate-receptor complex that preferentially distributes in the IL phase. This approach is not new and has been dubbed 'synergistic ion-exchange' by Borman *et al.* while characterising anion extracting phases that consisted of liquid anion exchangers such as Aliquat® 336 with *meso*-octamethylcalix[4]pyrrole in 1,2-dichloroethane [205]. The synergised extraction with *meso*-octamethylcalix[4]-pyrrole and Aliquat® 336 has been extensively studied due to the supramolecular organisation that occurs when this receptor is in solution with methyl bearing quaternary ammonium ions as described in section 1.3.2. Similar strategies have also been tested with IX resins where anion receptor groups are incorporated into the matrix of the resin to provide extra affinity for the target anion. Molecular imprinted polymers are a further development of this and are formed when the resin is cured with templating agents so clefts are formed that are specific to that target molecule [318].

The structures of the receptors examined here, combined with ILs, are shown in figure 3.1. Receptors **1** and **2** are are based on the *m*-xylyldiamine spacer and are from the first reported aqueous extraction of sulfate by Nishizawa *et al.* from 1995 to 1998 [179–181] Receptors **3**, **4** and **5** are based on the *o*-phenylenediamine spacer, first reported by Brooks *et al.* in 2005 [182, 183]. Finally, receptor **6** was first reported in 1995 by Raposo *et al.* [188] and then further developed by Wu *et al.* from 2008 onwards.

All six (thio)urea receptors were synthesised in good yields via the nucleophilic addition reaction between the corresponding primary amines and iso(thio)cyanates as shown in figure 3.2. Receptors **4** and **5** tended to precipitate as a mixture of mono and bis (thio)urea products when the synthesis was attempted in toluene.

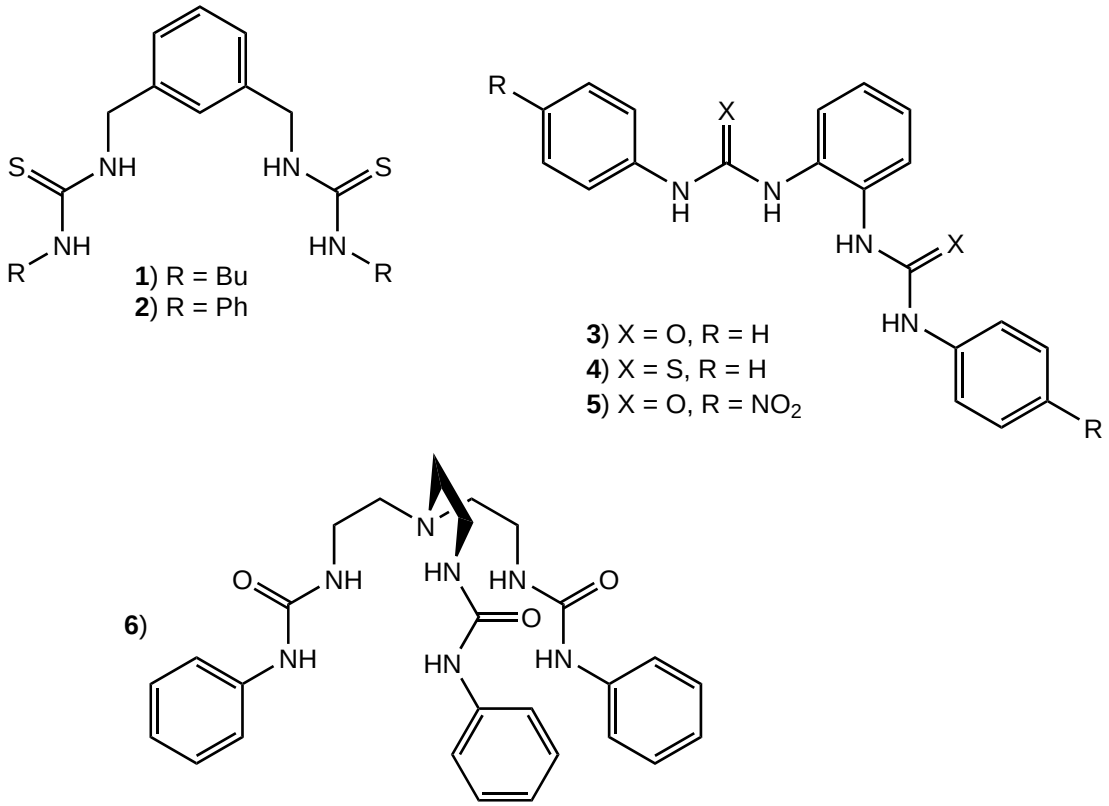

Figure 3.1: Structures of the anion receptors used in this work. **1** = 1,1'-(1,3-phenylenebis(methylene))bis(3-butylthiourea) [179], **2** = 1,1'-(1,3-phenylenebis(methylene))bis(3-phenylthiourea) [179], **3** = 1,1'-(1,2-phenylene)bis(3-phenylurea) [182], **4** = 1,1'-(1,2-phenylene)bis(3-phenylthiourea) [319], **5** = 1,1'-(1,2-phenylene)bis(3-(4-nitrophenyl)urea) [183], **6** = 1,1',1"-(nitrilotris(ethane-2,1-diyl))-tris(3-phenylurea) [320].

The solvent was then changed to DMF to keep the intermediate in solution which afforded the desired products. The urea receptors are stable solids that could be further purified by recrystallisation or washing in boiling acetone. This purification method was not possible for the thiourea receptors as they are susceptible thermal decomposition due to cyclisation that occurs readily at elevated temperatures [319], the decomposition process is shown in figure 3.3. This limits the ability to purify the thiourea receptors post-synthesis and so the purity of the starting materials and slow addition of the isothiocyanates is crucial to obtaining pure products.

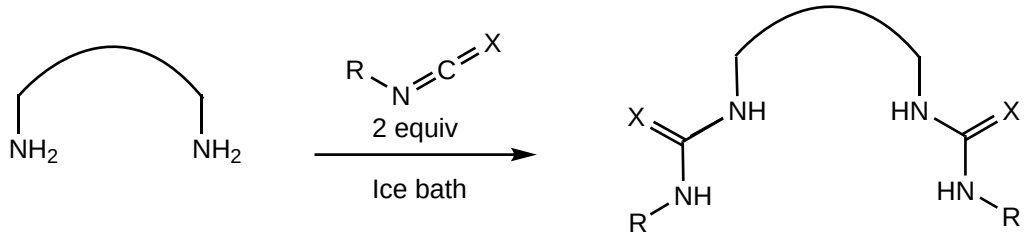

Figure 3.2: General reaction scheme for the synthesis of bis(thio)urea receptors **1** - **6**.

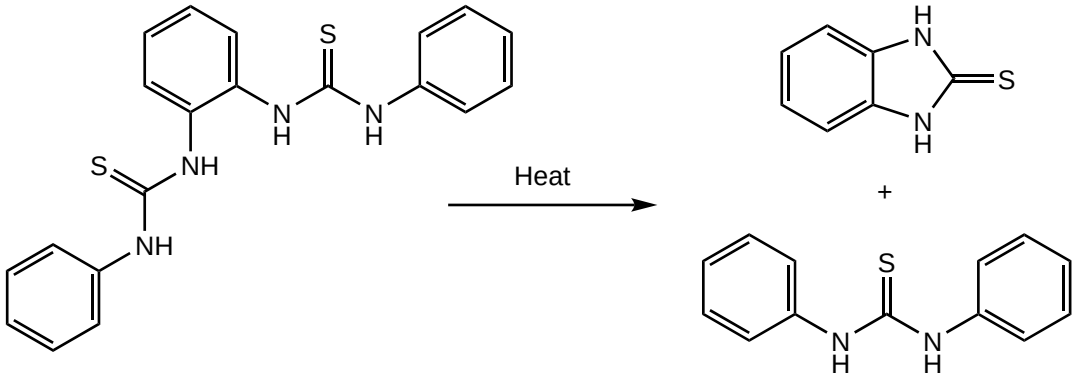

Figure 3.3: Thermal decomposition of receptor **4** was observed at temperatures of *ca.* 50-60℃ [319].

3.2 Solubility in ionic liquids

Due to the strong hydrogen bonding that exists between the (thio)urea groups in receptors **1** - **5**, they are only sparingly soluble in most common solvents other than dimethylformamide and dimethylsulfoxide. It was then surprising to find that these receptors were very soluble in water saturated Aliquat® 336 and Cyphos® 101. As shown in figure 3.4, a large amount of receptor **3** is soluble in water saturated Cyphos® 101 although the dissolution process is slow. During the dissolution process a small amount of water is also displaced from the IL phase.

The solubility limit for receptor **3** in Aliquat® 336 and Cyphos® 101 was determined by roller mixing each water saturated IL with daily additions of **3** until the solid persisted for a number of days. This process produced a heterogeneous mixture of water, **3** and an IL phase that had significantly increased in viscosity. The samples were then centrifuged and a sample of the IL phase was then diluted into fresh DMSO-d_6 and analysed by ^{1}H NMR. The composition of the mixtures is listed in table 3.1 and the full analysed ^{1}H NMR spectra are shown in the appendix, figures 6.10 and 6.11.

The concentration of receptor **3** in Aliquat® 336 equates to 0.372 M and the dissolution of **3** caused a *ca.* 9 wt% reduction in water capacity from 24.9 to 16 wt%. On the other hand, receptor **3** is far more soluble in Cyphos® 101, where

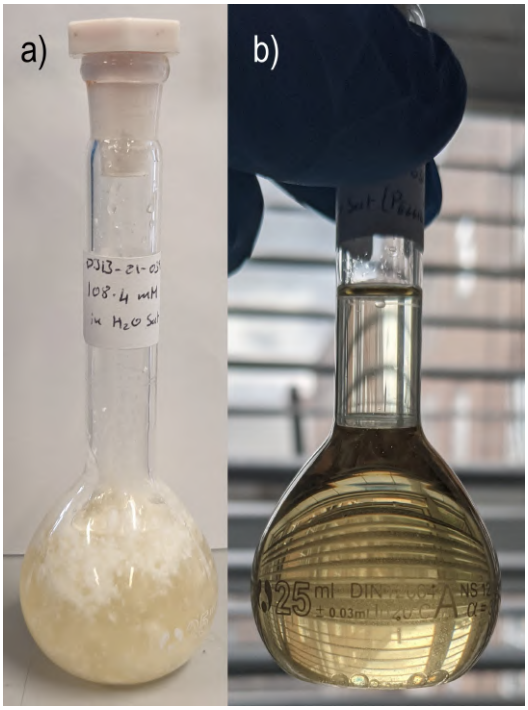

Figure 3.4: Pictures showing Receptor **3** in water saturated Cyphos®101 **a)** before roller mixing for two days and **b)** after mixing, showing full dissolution and a small amount of displaced aqueous phase.

Table 3.1: Molar ratio of IL:receptor:water at saturation point of receptor **3** in water saturated IL at room temperature. Determined by integration of ^{1}H NMR signals. Receptor **3** = 1,1'-(1,2-phenylene)bis(3-phenylurea)

System	Molar ratio			Mass ratio		
	IL	Receptor	Water	IL	Receptor	Water
Aliquat® 336	1	0.24	5.14	69.7	14.3	16.0
Cyphos® 101	1	0.675	1.63	66.4	29.9	3.8

the saturation amount equates to 0.776 M and again a *ca.* 10 wt% reduction in water capacity, from 14.1 down to 3.75 wt%. A large downfield shifting of the urea N−H protons was also observed in the ^{1}H NMR spectra as shown in figure 3.5. This change in chemical shift is the result of binding between receptor **3** and the chloride anion in the DMSO solution. This suggests that **3** will also bind to chloride anions in the neat IL phase as binding interactions are stronger in less polar solvents. Cyphos® 101 being more hydrophobic and having less water content therefore promotes chloride binding and improves the solubility of **3** in the IL. This also explains the displaced water that forms upon solvation of **3** as it competes with water for H-bonding, thus displacing some of the chloride's hydration sphere.

The amount of residual water left in the Cyphos®101 phases after adding different concentrations of receptors **2** and **3** was determined both by mass loss upon

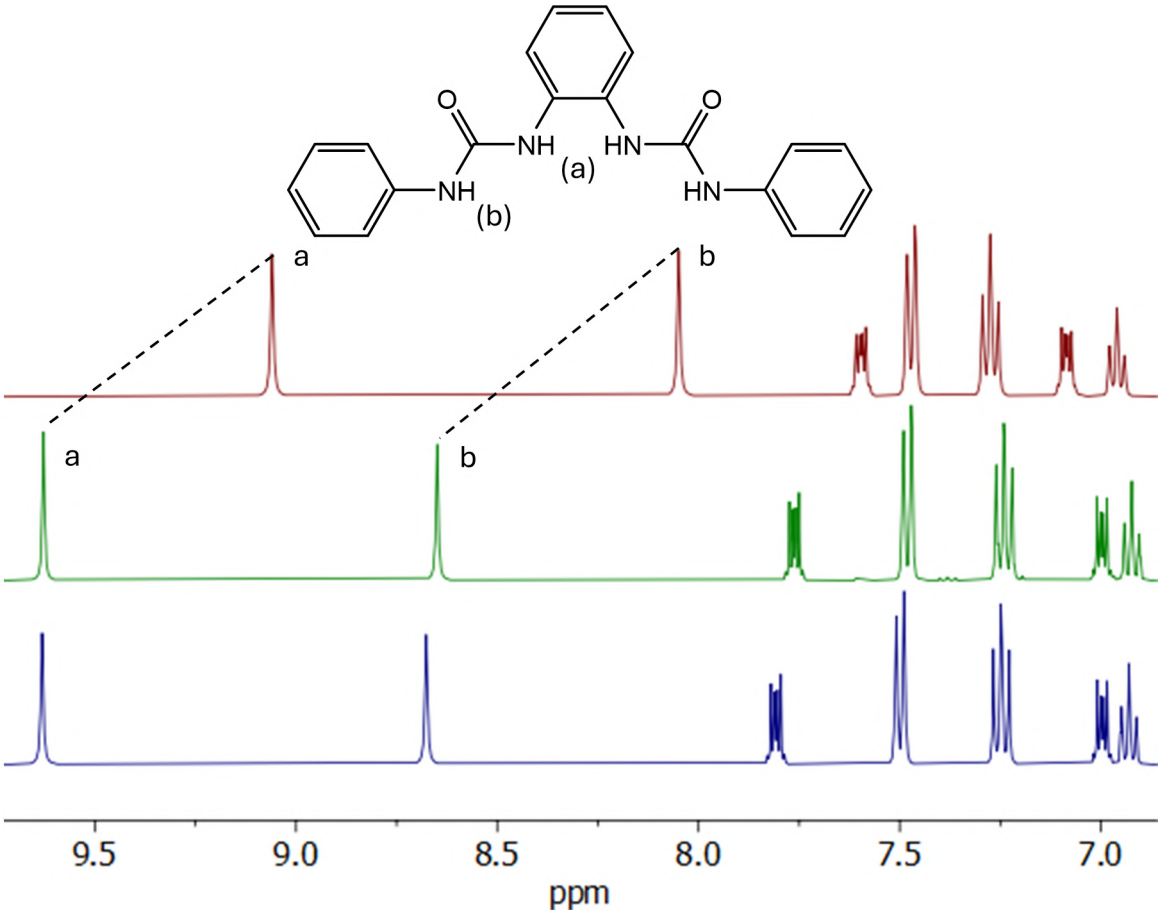

Figure 3.5: ^{1}H NMR spectra of (top) receptor **3** in DMSO, (middle) receptor **3** saturated Aliquat® 336 in DMSO and (bottom) receptor **3** saturated Cyphos® 101 in DMSO.

drying and quantitative ^{1}H NMR. The results are shown in figure 3.6. The water content of the IL phase reduces as more of receptor **3** is added to the IL phase. However, the phase behaviour between the IL, water and **3** can not be accurately described here as not enough data points were taken to construct a ternary phase diagram.

A large increase in viscosity was also observed upon solvation of **3** in both ILs. The viscosity of both ILs increases so much that they become gel-like in nature and resist flowing even when upturned. This limited the mass transfer of more **3** into the IL phase and resulted in very long equilibration times to determine the saturation limit. While this was not explored further, it was interesting to discover a thickening agent that does not induce any obvious physical or chemical cross-linking in the matrix that is typical of gels.

While *meso*-octamethylcalix[4]pyrrole is readily soluble in chlorinated organic solvents (in which the supramolecular organisation with Aliquat® 336 has been studied [205]), it was found to be insoluble in the selected ILs and so is not included in this study. At elevated temperatures of *ca.* 80 ℃, some solubility in water

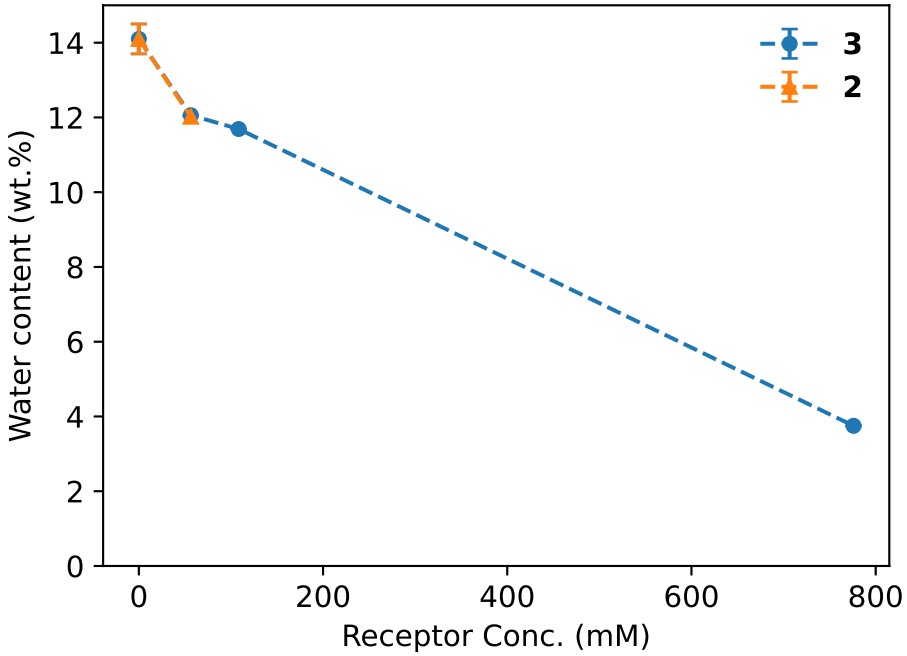

Figure 3.6: Change in saturated water content of Cyphos® 101 with increasing concentration of receptors **2** and **3**.

saturated Aliquat® 336 was observed, however it crystallised out of solution again upon cooling. Williams *et al.* replaced four of the methyl groups with hexyl chains to yield α,α',α",α'"-*meso*-tetrahexyltetramethylcalix[4]pyrrole, this was then shown to have a much higher solubility in organic solvents while retaining a similar anion binding strength [206]. Unfortunately this tetrahexyl derivative was not tested, however, it would be expected to show greater solubility in the highly alkylated ILs and greatly improve the performance of Aliquat® 336 via the supramolecular organisation discussed in section 1.3.2.

3.3 Binding studies

Receptors **1** to **6** have all been studied at length by many researchers as extractants, transmembrane transporters and scaffolds for supramolecular structures before and all of this stems from their ability to bind anions in solution. A selective overview of reported binding constants from the literature is shown in table 3.2. Receptors **1** - **5** are all relatively weak binding which makes them ideal for bolstering the anion affinity of an extracting phase and will not bind too strong as to prohibit any potential back extraction process. In 2005 Hay *et al.* benchmarked different spacial arrangements of urea to target different geometries of anions and showed that geometric selectivity between spherical anions like chloride and tetra-

hedral oxyanions is difficult to engineer due to the limited choices of covalent linkers and relatively small differences in conformational energies compared to the overall binding energies [321]. The *m*-xylyldiamine spacer of **1** and **2** does not allow for the optimal binding geometries of these bis(thiourea) receptors as the ureas are too far apart to bind on adjacent tetrahedral edges of an oxyanion such as sulfate, while the *o*-phenylenediamine spacer of **3**, **4** and **5** (although not included in Hay's paper as it had not been published on yet) aligns much better with adjacent tetrahedral edges. Even though the thiourea groups of **4** are more acidic than urea groups of **3**, weaker binding to many anions has been reported and it has been suggested that the size of the sulfur atom causes distortions in the receptor and prevents it from binding in one plane [183]. Receptor **6** is an order of magnitude stronger than the other receptors for both sulfate and chloride due to the increased flexibility of the tren spacer allowing for optimal binding geometry along three adjacent edges and three alkyl-phenyl-urea groups outweighing the binding of two more acidic diphenyl-urea groups. Additionally, receptor **2** has a reported sulfate binding constant in 1,2-dichloroethane of 2.5×10^6 by Shioya *et al.*, however this seems unprecedentedly large and inconsistent with the values shown in table 3.2.

Table 3.2: Reported first binding constants for receptors **1** - **6** in dimethyl sulfoxide.

Receptor	Binding constant (K_b / M^{-1})		Reference
	Sulfate	Chloride	
1	2[a]	9	[180]
2	–	10	[179]
3	10[a]	43	[182]
4	< 10[a]	18	[183]
5	–[a]	78	[183]
6	$> 10,000$	882	[191]

[a] Binding reported for hydrogen sulfate

It should be noted that in DMSO, receptors **1** - **5** show a preference for binding chloride over sulfate. In either Aliquat® 336 or Cyphos® 101 therefore, it could be expected that receptors **1** - **5** will preferentially bind to chloride, effectively inhibiting them from migrating into the aqueous phases, inhibiting the IX process and reducing the sulfate removal. It is also well known in the literature that anion binding is stronger in non-polar (and therefore non-competitive) solvents [322]. This is demonstrated by the large binding constant of **2** in 1,2-dichloroethane compared to the similar receptor **2** in DMSO.

In my hands, attempts to conduct binding studies of the receptors with either sulfate or chloride in DMSO were largely unsuccessful. Fresh DMSO-d_6 ampoules were used for each study as well as freshly purified and dried receptors and salts,

in some cases new NMR tubes that had been washed once with acetone were also used. NMR titrations showed a systematic increase in water during the course of the experiments as shown in figure 3.7, at the start of the experiment, the water peak integrated for 0.27, after 9 additions it increased to 0.52 and after 19 additions it had reached 0.84, all relative to the solvent peak which was set to 1. 0.5 wt% Water was added to new DMSO-d_6 ampoules in an attempt to reduce the relative rate change in water concentration during the experiment, however, this still did not produce accurate or consistent results. A batch method of sample preparation was also tried where twenty samples were prepared simultaneously from host and guest solutions, these were then sealed and immediately analysed. This should in theory, prevent systemic error that accumulates from the absorption of water but replace it with a random error from small differences in sample preparation. This also gave inconsistent results although some of these studies were partially successful. The combination of these receptors being weakly binding to sulfate and chloride, as well as the strength of binding in DMSO being very sensitive to the amount of competitive water present due to absorption from humidity resulted in inconsistent and unreliable data.

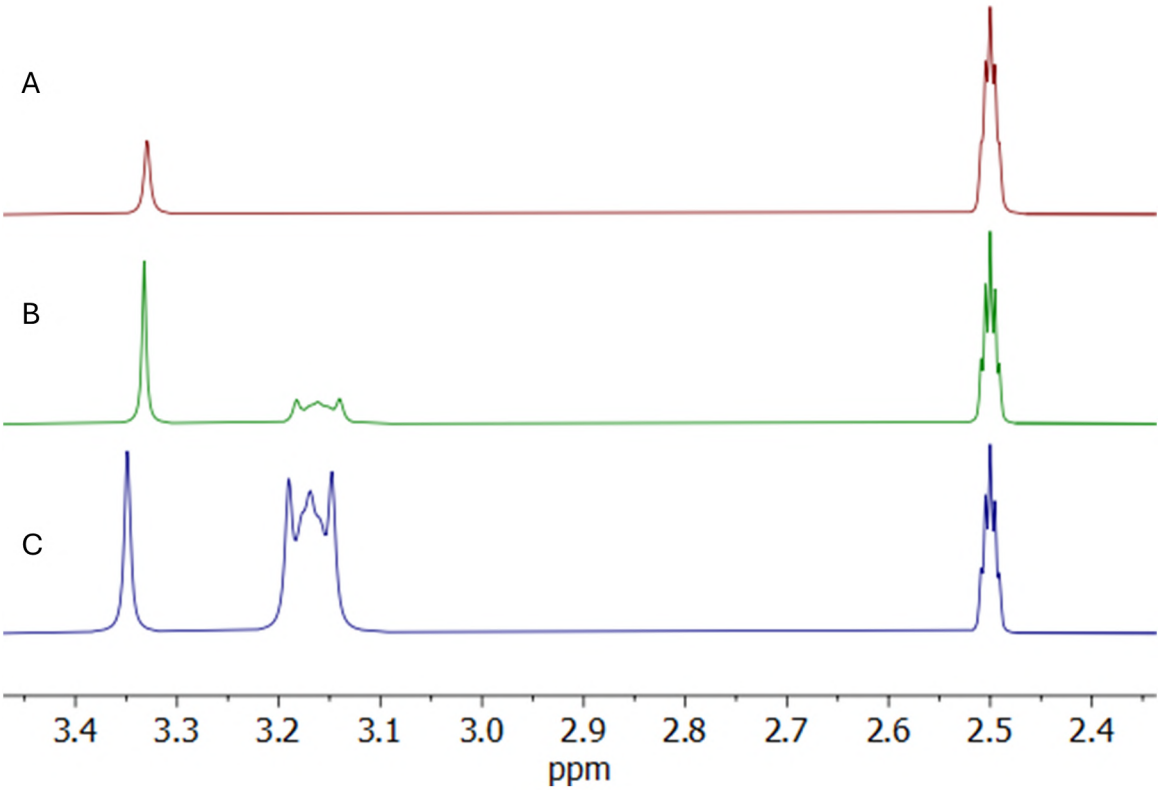

Figure 3.7: Increase in water peak over the course of a binding study between receptor **3** and Tetrapropylammonium chloride showing an increase in the water peak at 3.35 ppm. A = Start of the binding study, B = after 9 additions, C = after 19 additions.

A plot of the N−H signals from the urea groups in receptor **3** is shown in 3.8. The steady downfield shifting of the urea protons shows an increase in hydrogen bonding in the sample between the receptors and the added anions. It is obvious from the plot that addition of chloride results in a larger downfield shift which is indicative of stronger hydrogen bonding and stronger binding to the receptor than sulfate which only produces a small downfield shift in the urea protons.

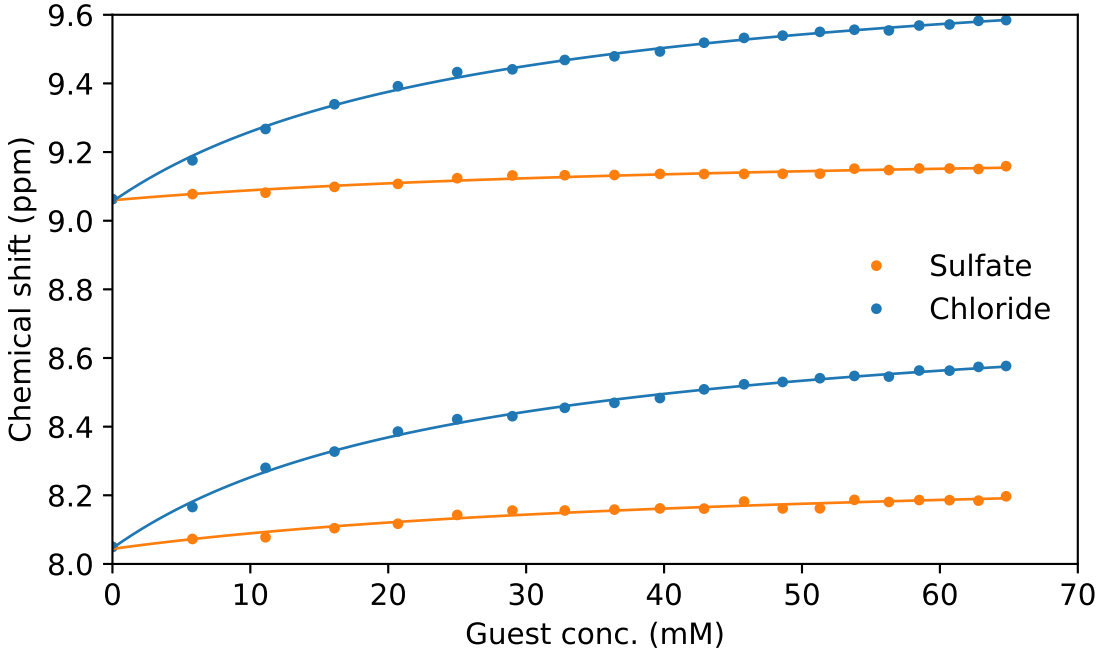

Figure 3.8: Change in chemical shift of the urea N−H signals in receptor **3** (at 10 mM in DMSO-d_6) with increasing sulfate or chloride concentration.

Equation 3.1 was used to generate smooth lines for figure 3.8 as well as for similar plots of receptors **2**, **5** and **6** in the appendix, figures 6.12 - 6.24.

$$\delta_{obs} = \delta_H + \frac{\delta_{HG}[G]_0 a}{1 + [G]_0 a} \tag{3.1}$$

Here, δ_{obs}, δ_H and δ_{HG} are the chemical shifts of the observed species, host and host-guest complex respectively, $[G_0]$ is the initial concentration of guest and a is a fitting parameter that relates to the binding constant.

Receptor **5** showed clear binding to both sulfate and chloride, however, the rate of association and disassociation for both anions (sulfate shown in appendix figure 6.20) in DMSO-d_6 appears to be approximately the same as the NMR timescale so both residual free host and the equilibrium host-guest complex peaks can be observed in figure 3.9. This shows that a portion of the population of receptor **5** is not contributing to the observed chemical shift (δ_{obs}), this effectively lowers $[H_0]$ and increases the host-guest ratio. This heterogeneity in the population of **5** explains

why the calculated binding constants in table 3.3 are higher than those reported in the literature.

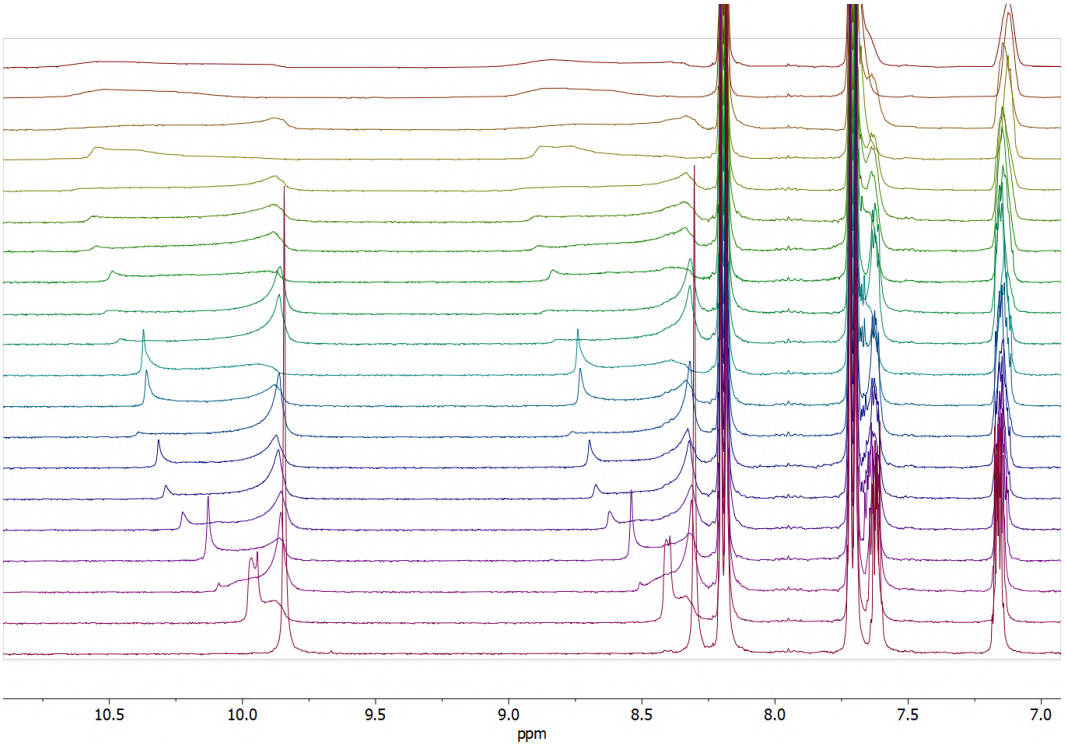

Figure 3.9: Receptor **5** at 1 mM in DMSO-d_6, with increasing concentrations of tetrapropylammonium chloride up to 45 mM.

The binding constants that were (somewhat) successfully measured and analysed using the online Bindfit tool [172], are shown in table 3.3. The values for receptors **2**, **3** and **4** are comparable with those reported in the literature, while the values for **6** were measured to be much lower than reported. Values for sulfate binding with receptors **2** and **4** did successfully converge, with K_b values that were several orders of magnitude below zero. Again, receptor **6** is the only receptor that was found to bind stronger to sulfate than chloride in DMSO. While the strength of chloride binding by **6** was *ca.* half of the reported value, the sulfate binding constant was an order of magnitude lower than the reported value. Both of these binding constants for **6**, as well as those calculated for **5** have an extremely large error associated with them.

Table 3.3: Measured Binding constants for receptor **2** - **6** in dimethyl sulfoxide (DMSO-d_6). Anions were added as tetrapropyl or tetrabutyl ammonium salts.

Receptor	Binding constant (K_b / M^{-1})		Method
	Sulfate	Chloride	
2	< 0	$2 \pm 3\%$	Batch
3	$25 \pm 5\%$	$56 \pm 2\%$	Titration
4	< 0[ab]	$0.4 \pm 3.4\%$[b]	Batch
5	$5 \pm 14\%$[c]	$763 \pm 19\%$[c]	Batch
6	$756 \pm 39\%$	$466 \pm 20\%$	Titration

[a] 0.5 wt% water added to solvent
[b] Hydrogen sulfate
[c] Rate of binding was on the NMR timescale

3.4 Sulfate extraction

To test if the addition of receptors **1** - **6** increase the sulfate removal ability of Aliquat® 336 and Cyphos®101, they were added at a concentration of 54.4 mM to the IL phases which were then contacted with 27.1 mM Na_2SO_4 solutions. The same 1:2, IL:Aq phase volume ratio was used as in chapter 2 and the concentrations were chosen so that there was approximately a 1:1 molar ratio of sulfate to receptor in each extraction system. Assuming no secondary equilibria such as the formation of 2:1 complexes, the IX mechanism should follow equation 3.2. As shown from the previous sections, it is likely that the receptors (L) are initially bound to chloride in the IL, but during the IX process, the receptors complex to sulfate and extract it into the IL phase. The results for the Cyphos® 101 series is shown in figure 3.10 and the series with Aliquat® 336 is shown in figure 3.11. For both data sets the '0' value represents the neat IL without any receptor added. Receptors **1**, **2** and **4** all contain thiourea groups that will interfere with the XRF analysis as it cannot differentiate between sulfate and thiourea sulfur atoms To account for this, they were all tested for leaching into DI water and their leaching values used to correct the extraction values. The solubility of the receptors in DI water is assumed to be higher than in NaCl and Na_2SO_4 due to their Hofmeister salting out properties, this may result in an over correction with the results being slightly lower than the actual sulfate extraction value.

$$LCl^-_{(IL)} + Cl^-_{(IL)} + [SO_4]^{2-}_{(aq)} \rightleftharpoons L[SO_4]^{2-}_{(IL)} + 2\,Cl^-_{(aq)} \tag{3.2}$$

In every case, the addition of receptors to the ILs was beneficial for the removal of aqueous sulfate. Cyphos® 101, which started with a fairly low level of sulfate removal, was improved at least by 2.6% with **1** and at most by 14.6% with **3**. Aliquat®

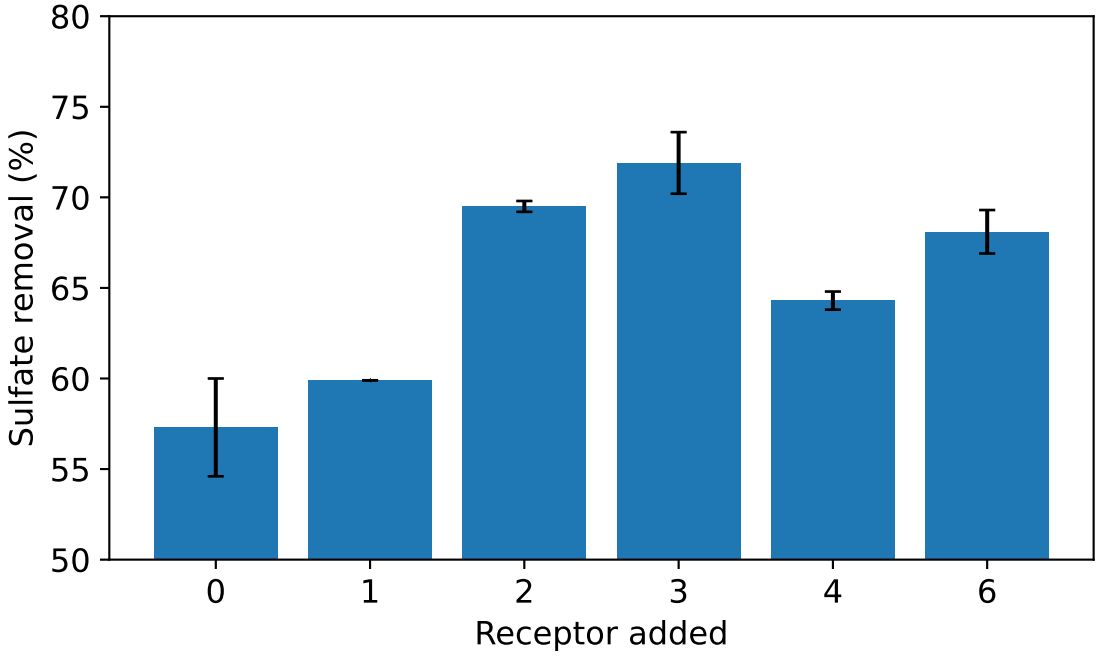

Figure 3.10: Sulfate removal from a 27.1 mM Na_2SO_4 solution with receptors **1** - **6** at 54.4 mM in water saturated Cyphos® 101 using a 1:2, IL:Aq phase volume ratio.

336 already had a higher baseline sulfate removal than Cyphos® 101 (89.1% compared to 57.3%), and so it was only improved at worst by 1.6% with **6** and at best by 8.2% with **5**. In general this follows the trend that an increase in sulfate bindings as observed in DMSO (tables 3.2 and 3.3) showed a corresponding increase in sulfate removal with the ILs. There are two exceptions to this, receptors **5** showed the largest improvement in Aliquat® 336 despite reported to have no affinity for hydrogen sulfate and to only weakly bind to sulfate in DMSO. The other exception is receptor **6**, which is the strongest binding of all the receptors and the only receptor to show a preference for sulfate in DMSO. This did allow for a large increase in sulfate removal when used with Cyphos® 101, however, this did not translate to Aliquat® 336 where **6** was the worst performing of all the receptors. The origin of the difference in sulfate extraction ability of **6** in the two ILs is not clear and could stem from several factors including the conformation freedom of **6** to bind multiple anions and the difference in water content and thus competitiveness of the surrounding IL environment.

While it may seem odd, the fact that the addition of these receptors improves the sulfate removal is genuinely surprising as it shows a large reversal in selectivity between the binding in DMSO and binding in the ILs, particularly since chloride is far more abundant in the IL phase than the extracted sulfate (*ca.* 35 molar equivalents). These results are strikingly similar to the work of Borman *et al.* [200] where *meso*-octamethylCalix[4]pyrrole shows a reversal of selectivity between nitrate and

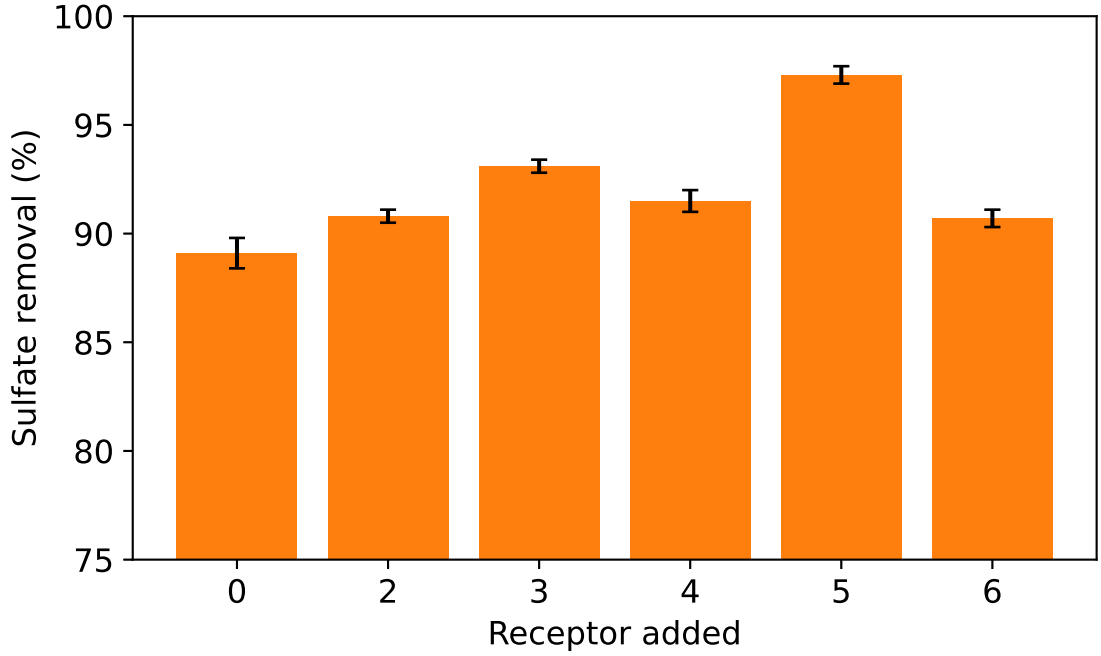

Figure 3.11: Sulfate removal from a 27.1 mM Na_2SO_4 solution with receptors **2** - **6** at 54.4 mM in water saturated Aliquat® 336 using a 1:2, IL:Aq phase volume ratio.

sulfate in chloroform in the presence of a methylammonium cation due to the calix-[4]pyrrole acting as an ion-pair receptor. In the case of receptors **1** to **6** however, there is no such obvious synergy between the receptors and the IL. There is also no significant change in the chloride:sulphate IX ratio from the neat IL, all receptor extractions showed IX ratio between 2.1 and 2.25, in agreement with the neat ILs for this concentration of Na_2SO_4 as shown previously in figure 2.5. This suggests that the mechanism of sulfate extraction does not change but it is simply enhanced by the addition of receptors **1** to **6**.

Figure 3.12 shows the sulfate removal of Cyphos® 101 with increasing concentrations of receptor **3**. These concentrations represent 1 and 2 molar equivalents of **3** to sulfate in each extraction system. At 54.4 mM, a 14.6% increase in sulfate removal was observed and at 108.2 mM, only a further 6.2% sulfate removal was observed. This shows that increasing the concentration of **3** does increase the sulfate extraction but with diminishing returns. Again, there was no significant change in IX ratio of sulfate to chloride across the range of receptors and concentrations of **3** suggesting that the receptors do not change the mechanism of sulfate extraction.

In general, if a receptor binds stronger to one anion over another, although the absolute binding strength and degree of selectivity can change in different solvents, the direction of the selectively does not usually change [322]. Only two reports of a solvent induced reversal of anion binding selectively has been found in the literature. Firstly, a bicyclic polypeptide antibiotic thiostrepton was found to only

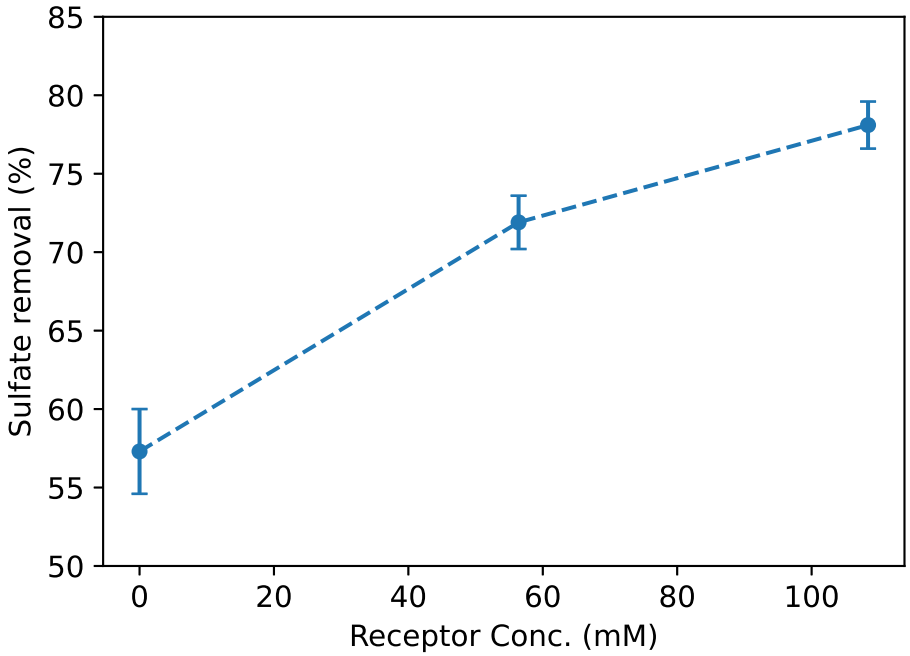

Figure 3.12: Sulfate removal from a 27.1 mM Na_2SO_4 solution with receptor **3** at 54.4 and 108.4 mM in Cyphos® 101.

bind fluoride and acetate in DMSO but preferentially binds to chloride and sulfate in chloroform [323]. Then a tetraurea picket porphyrin was shown to preferentially bind dihydrogen phosphate in chloroform but chloride in DMSO via co-operative binding of the DMSO solvent [324]. Other methods to induce a reversal in anion selectivity have been reported, several by the simultaneous binding of a metal ion [325, 326] and there are many reports of changes in pH changing the selectivity of binding, especially in biological systems. It should also be noted that this is not direct evidence of the receptors binding to sulfate in the IL phases and the increase in sulfate removal may be due to other effects such as water exclusion, bringing the cationic centres closer together and therefore preferring the divalent sulfate for charge stabilisation.

3.5 Conclusions

To conclude, bis and tris(thio)urea receptors **1** to **6** are all remarkably soluble in the hydrated ionic liquid phases of Cyphos® 101 and Aliquat® 336. Complexion of the receptors to the chloride of the ILs is thought to aid in the solvation of the receptors. Binding of the receptors to the chloride displaces water from the hydration shell and reduces the total water content of the IL phase which also contributes to a significant increase in viscosity of the IL phase at high receptor concentrations.

In all cases, the addition of these receptors into the IL phases improved the sulfate removal with a higher concentration of receptor being beneficial to the extraction process. Receptors **1** to **5** bind more strongly to chloride than sulfate in DMSO-d_6, however, this selectivity appears to reverse in the IL phases as the addition of the these receptors to the ILs increases the sulfate extraction from aqueous solutions, despite the presence of excess chloride as the IL anion. It is unclear whether this is a result of direct binding to the sulfate as receptor **6**, the strongest sulfate receptor and the only receptor to selectively bind sulfate over chloride in DMSO, showed the least improvement in sulfate extraction in the Aliquat® 336.

3.6 Experimental

All chemicals were procured from licensed chemical suppliers such as Merck, Fluorochem, Tokyo Chemical Industry. *m*-Xylyldiamine and pyrrole was redistilled prior to use. Tetrapropylammonium chloride is hygroscopic and was dried in a vacuum oven overnight at 50℃ prior to use. Bis(tetrabutylammonium) sulfate ($[TBA]_2[SO_4]$), although reportedly used by many sources that do not state a supplier [187, 191, 196], was not found to be available anywhere except as a 50 wt% aqueous solution. This solution was dried by rotary evaporation to afford a white crystalline solid assumed to be pure tetrabutylammonium sulfate (although drying may also produce a mixture of $[TBA][HSO_4]$ and [TBA]OH). This ($[TBA]_2[SO_4]$) was also dried in a vacuum oven overnight at 50℃ prior to use. All other general procedures were described previously in section 2.5.

Synthesis of receptors

1,1'-(1,3-phenylenebis(methylene))bis(3-butylthiourea) (1)

Synthesis adapted from previously reported procedures [179].

m-Xylylenediamine (0.3 mL, 2 mmol) was dissolved in toluene (10 mL) followed by the addition of butylisothiocyanate (0.9 mL, 7.2 mmol), immediately producing a precipitate. The mixture was stirred at 60℃ for 1 h after which time the precipitate was collected by filtration, recrystallised from ethanol and dried under high vacuum overnight to yield a white solid (0.5231 g, 71.3%). ^{1}H NMR (400 MHz; DMSO-d_6) δ 7.73 (2 H, s), 7.45 (2 H, s), 7.28 (1 H, t, J = 7.9 Hz), 7.17 (3 H, t, J = 6.0 Hz), 4.63 (4 H, s), 3.37 (4 H, s), 1.46 (4 H, quint, J = 7.3 Hz), 1.34-1.22 (4 H, m), 0.88 (6 H, t, J = 7.3 Hz). ^{13}C^{1}H NMR (100 MHz; DMSO-d_6) δ 182.66, 139.45, 128.22, 126.22, 125.78, 46.96, 43.25, 30.87, 19.58, 13.74. Calc. for $C_{18}H_{30}N_4S_2$: C, 58.98; H, 8.25; N, 15.28; S, 17.49%, found: C, 59.22; H, 8.2; N, 15.05; S, 17.56%. HRMS (ESI, DMSO): *m/z* calcd for $C_{18}H_{31}N_4S_2^+$ $[M + H]^+$: 367.198, found 367.1973.

1,1'-(1,3-phenylenebis(methylene))bis(3-phenylthiourea) (2)

Synthesis adapted from previously reported procedures [179].

m-Xylyldiamine (10 mmol, 1.3600 g) was diluted in DCM (50 mL), stirred and cooled in an ice bath. A solution of phenylisothiocyanate (30 mmol, 4.0557 g) in DCM (25 mL) was then added dropwise to the cooled diamine solution. The solution was then allowed to warm to room temp and left to stir for 48 h after which time a large mass of white precipitate had formed. The precipitate was filtered and dried under high vacuum to yield a white solid (3.866 g, 95.1%). ^{1}H NMR (400

MHz; DMSO-d_6) δ 9.67 (2 H, s), 8.22 (2 H, s), 7.50 (4 H, dd, *J* = 8.4 Hz), 7.38 (6 H, tt, *J* = 7.4 Hz), 7.29 (2 H, dd, *J* = 8.7 Hz), 7.17 (2 H, tt, *J* = 7.4 Hz), 4.81 (4 H, d, *J* = 5.6 Hz). $^{13}C^{1}H$ NMR (100 MHz; DMSO-d_6) δ 180.75, 139.12, 139.03, 128.58, 128.20, 126.35, 125.98, 124.22, 123.31, 47.16. Calc. for $C_{22}H_{22}N_4S_2$: C, 64.99; H, 5.45; N, 13.78; S, 15.77%, found: C, 65.85; H, 5.51; N, 13.36; S, 15.04%. HRMS (ESI, DMSO): *m/z* calcd for $C_{22}H_{23}N_4S_2^+$ $[M + H]^+$: 407.138, found 407.1382.

1,1'-(1,2-phenylene)bis(3-phenylurea) (3)

Synthesis adapted from previously reported procedures [182].

o-Phenylenediamine (20mmol, 2.1664 g) was dissolved in toluene (50 mL) and phenylisocyanate (5.3 mL, 48 mmol) was added. Immediately a white precipitate formed. The solution was stirred vigorously and heated to 60℃ overnight before being cooled on an ice bath and the white precipitate collected. The product was then washed with boiling acetone and dried under high vacuum overnight to yield a white solid (5.0172 g, 72.4%). ^{1}H NMR (400 MHz; DMSO-d_6) δ 9.06 (2 H, s), 8.05 (2 H, s), 7.60 (2 H, m), 7.47 (4 H, dd, *J* = 8.8Hz), 7.28 (4 H, tt, *J* = 8 Hz), 7.08 (2 H, m), 6.96 (2 H, tt, *J* = 7.6 Hz). $^{13}C^{1}H$ NMR (100 MHz; DMSO-d_6) δ 153.16, 139.81, 131.25, 128.72, 123.97, 123.91, 121.72, 118.13. Calc. for $C_{20}H_{18}N_4O_2$: C, 69.35; H, 5.24; N, 16.17%, found: C, 70.49; H, 5.17; N, 16.2%. HRMS (ESI, DMSO): *m/z* calcd for $C_{20}H_{18}N_4O_2Na^+$ $[M + Na]^+$: 369.13, found 369.1335.

1,1'-(1,2-phenylene)bis(3-phenylthiourea) (4)

Synthesised following previously reported procedures [319].

o-Phenylenediamine (10 mmol, 1.081 g) was dissolved in DMF (30 mL), stirred and cooled in an ice bath. A solution of phenylisothiocyanate (30 mmol, 4.0557 g) in DMF (20 mL) was then added dropwise to the cooled diamine solution. The solution was then allowed to warm to room temp and left to stir for 16 h after this time it was poured into DI water (200 mL) forming a white precipitate which was then collected by filtered and washed with DCM. The product was then dried under high vacuum to yield a white solid (3.1607 g, 83.5%). ^{1}H NMR (400 MHz; DMSO-d_6) δ 10.02 (2 H, s), 9.21 (2 H, s), 7.48 (2 H, m), 7.44 (4 H, dd, *J*= 8.4 Hz), 7.32 (4 H, tt, *J* = 7.6 Hz), 7.26 (2 H, m), 7.14 (2 H, tt, *J* = 7.2 Hz). $^{13}C^{1}H$ NMR (100 MHz; DMSO-d_6) δ 179.96, 138.90, 134.60, 128.62, 128.07, 126.25, 124.83, 123.80 Calc. for $C_{20}H_{18}N_4S_2$: C, 63.46; H, 4.79; N, 14.8; S, 16.94%, found: C, 63.82; H, 5.15; N, 13.34; S, 15.08%. HRMS (ESI, DMSO): *m/z* calcd for $C_{20}H_{18}N_4S_2Na^+$ $[M + Na]^+$: 401.09, found 401.0839.

1,1'-(1,2-phenylene)bis(3-(4-nitrophenyl)urea) (5)

Synthesis adapted from previously reported methods [183].

o-Phenylenediamine (10 mmol, 1.081 g) was dissolved in DMF (25 mL), stirred and cooled in an ice bath. A solution of 4-nitrophenylisocyanate (30 mmol, 4.924 g) in DMF (50 mL) was then added dropwise to the cooled diamine solution. The solution was then allowed to warm to room temp and left to stir for 16 h, after this time it was poured into DI water (200 mL) forming an orange precipitate which was then collected by filtered and washed with DCM. The product was then dried under high vacuum to yield a orange solid (3.5348 g, 81.0%). ^{1}H NMR (400 MHz; DMSO-d_6) δ 9.83 (2 H, s, NH), 8.29 (2 H, s, NH), 8.19 (4 H, d, *J* = 8 Hz), 7.71 (4 H, d, *J* = 8 Hz), 7.62 (2 H, m), 7.17 (2 H, m). ^{13}C^{1}H NMR (100 MHz; DMSO-d_6) δ 152.68, 146.46, 141.01, 131.02, 125.18, 124.76, 124.48, 117.46. Calc. for $C_{20}H_{16}N_6O_6$: C, 55.05; H, 3.7; N, 19.26%, found: C, 54.42; H, 4.08; N, 18.58%. HRMS (ESI, DMSO): *m/z* calcd for $C_{20}H_{16}N_6O_6Na^+$ $[M + Na]^+$: 459.1, found 459.1050.

1,1',1''-(nitrilotris(ethane-2,1-diyl))tris(3-phenylurea) (6)

Synthesis adapted from previously reported methods [320].

Tris(2-aminoethyl)amine (1.2 mL, 8 mmol) was dissolved in toluene (40 mL) followed by phenylisocyanate (3.2 mL, 30 mmol), immediately a white precipitate formed. The solution was stirred vigorously and heated to 60℃ for 1 h after which time the precipitate was collected and dried under high vacuum overnight to yield a white powder (3.8858 g, 96.4%). ^{1}H NMR (400 MHz; DMSO-d_6) δ 8.51 (3 H, s), 7.38 (6 H, dd, *J* = 8.4 Hz), 7.20 (6 H, tt, *J* = 8.4 Hz), 6.88 (3 H, tt, *J* = 7.2 Hz), 6.17 (3 H, t, *J* = 5.5 Hz), 3.20, (6 H, q, *J* = 6.3 Hz), 2.60 (6 H, t, *J* = 6.7 Hz). ^{13}C^{1}H NMR (100 MHz; DMSO-d_6) δ 151.31, 140.45, 128.59, 121.00, 117.74, 53.95, 37.52. Calc. for $C_{29}H_{33}N_7O_3$: C, 64.39; H, 6.61; N, 19.47%, found: C, 64.34; H, 6.32; N, 19.1%. HRMS (ESI, DMSO): *m/z* calcd for $C_{29}H_{34}N_7O_3^+$ $[M + H]^+$: 504.268, found 504.2723.

Binding studies

Two different methods were attempted for binding studies as described below. For different hosts, the concentration of host and guest solutions were changed to get an appropriate range of host to guest ratios depending on the binding strength. The ^{1}H NMR spectra were all calibrated to the solvent signal at 2.50 ppm and the chemical shifts of the hosts urea N−H protons were plotted against the guest concentration and the data analysed by Bindfit v0.5 at supramolecular.org [172].

Titration method

The general procedure was to make 10 mL of a 10 mM host (receptor) solution using fresh DMSO-d_6 solvent. A guest (anion) solution (5 mL) was then made containing 150 mM of the desired guest as the tetrapropyl or tetrabutyl ammonium salt, and the host solution was used as the solvent to ensure both solutions contain the same concentration of host. The host solution (0.5 mL) was then added to a clean NMR tube and analysed by ^{1}H NMR. The guest solution (20 µL) was then pipetted into the NMR tube and the mixture analysed again. This was repeated twenty times to obtain spectra with a range of guest concentrations up to 6.5x that of the host.

Batch method

For the batch method, host and guest solutions were both made up separately using fresh DMSO-d_6 solvent. Twenty NMR tubes were then filled with the same amount of host solution (usually 100 µL) followed by an increasing amount of guest solution. The samples were then topped up with DMSO-d_6 to the same volume, the tubes sealed and submitted for ^{1}H NMR analysis.

Sulfate extractions

Sulfate extractions were performed in triplicate in the same way as described in chapter 2. Prior to extraction, stock solutions were made of the receptor in the IL phase, usually 54.4 mM, corresponding to a 1:1 sulfate:receptor ratio in the system considering the 0.5 phase-volume ratio.

For receptors that contain sulfur, a triplicate of samples made with the desired receptor in IL and DI water. The sulfur content of the aqueous phase was then analysed by ED-XRF as described in section 2.5. This is used for a correction to account for leaching of the receptor during extraction as per equation 3.3. The leaching of **1**, **2** and **4** into DI water was measured to be between 200 and 250 ppm in all cases.

$$\%Removal = \frac{[S]_{final} - [S]_{leaching}}{[S]_{initial}} \times 100 \tag{3.3}$$

4. Ionic Liquids as Chemisorbants for Flue Gas Carbon Capture

4.1 Introduction

As discussed in section 1.5, ionic liquids are particularly well suited for use as media for gas capture or separations due to their negligible vapour pressure preventing contamination of the resulting gas streams. It has been 25 years since ILs were first identified as being strong physisorbants for CO_2 [231], and 22 years since the first report of a chemisorbant IL for CO_2 was made [235]. The need for CO_2 capture in the modern world is a certainty if future generations are to thrive [327, 328] and a considerable amount of effort has been put into studying this challenge from the ionic liquids community in an attempt to develop new materials that will facilitate this global clean up operation [10, 329].

The aim of this chapter is to investigate the use of chemisorbant ionic liquids for flue gas capture of CO_2. Typical flue gas composition is *ca.* 80 % N_2, 15 % CO_2 and 5 % water (in vol%) and can be upwards of 120℃. Initially, a range of chemisorbant ionic liquids (mostly protic ILs) were screened for CO_2 absorption under both dry and wet (<5 wt% water) conditions. From this, [DBUH][Im] was identified as a potential candidate and investigated further with the use of FT-IR, NMR and TGA-MS. [DBUH][Im] was also shown not to corrode 316 stainless steel and finally a process diagram was detail showing how this IL could be used in a post-combustion CO_2 capture process. The results from this work have been filed for patent by Chevron Energy Corp. in the US filing office under the title of 'Energy Efficient Post-Combustion CO_2 Capturing Process using Ionic Liquid Absorbent' *Attorney Docket No. 70205.0674USP1 (T-11879)*.

For absolute clarity of units, in this chapter when CO_2 uptake capacities are displayed in units of $g{\cdot}kg^{-1}$, this means grams of CO_2 per kilogram of ionic liquid, not per kilogram of resultant absorbed material. This is especially important for capacities reported for ILs with added water to simulate the effect of a humid gas stream, in these cases the weight of water was not included in the 'per kilogram' term of the calculation. Additionally, if a material in this section is referred to solely

as a salt, it is implied to be a solid under the given conditions as opposed to a liquid salt which is referred to as an IL.

4.2 Carbon dioxide uptake studies

4.2.1 Screening of selected Ionic Liquids

A short series of ionic liquids were selected from the literature based on their reported CO_2 capacities, viscosities and material cost. Structures of the ions used in this study are shown in figure 4.1 and a brief overview of the literature that inspired this series is also given here.

[TMGH][Im] was reported by Lei *et al.* in 2014 with an impressive working capacity of 192 g·kg^{-1} (0.8 mol·mol^{-1}) and absorption-desorption temperatures of 35 ℃ and 65 ℃ respectively [252]. [DBUH][Im] was first reported as a useful IL solvent for the synthesis of furanones from CO_2 [255], but the first reported study of its CO_2 chemisorption ability was by Zhu *et al.* in 2017 [256]. They tested a series of DBU based protic ILs with functionalised imidazole anions and found that imidazole and 4-methylimidazole were the best performing, [DBUH][Im] was shown to have a working capacity of *ca.* 140 g·kg^{-1} (0.7 mol·mol^{-1}) when cycled between 40 ℃ and 80 ℃. 3-(Dimethylammonium)propylamine 2-fluorophenolate was reported by Zhao *et al.* in 2018, reporting impressive capacities of *ca.* 140 g·kg^{-1} (0.8 mol·mol^{-1}) and good recycling between 30 and 80 ℃ [261]. The phenolate ([PhO]) series of ILs were taken from various sources, with conflicting reports about capacity as previously discussed in section 1.5 [253, 258].

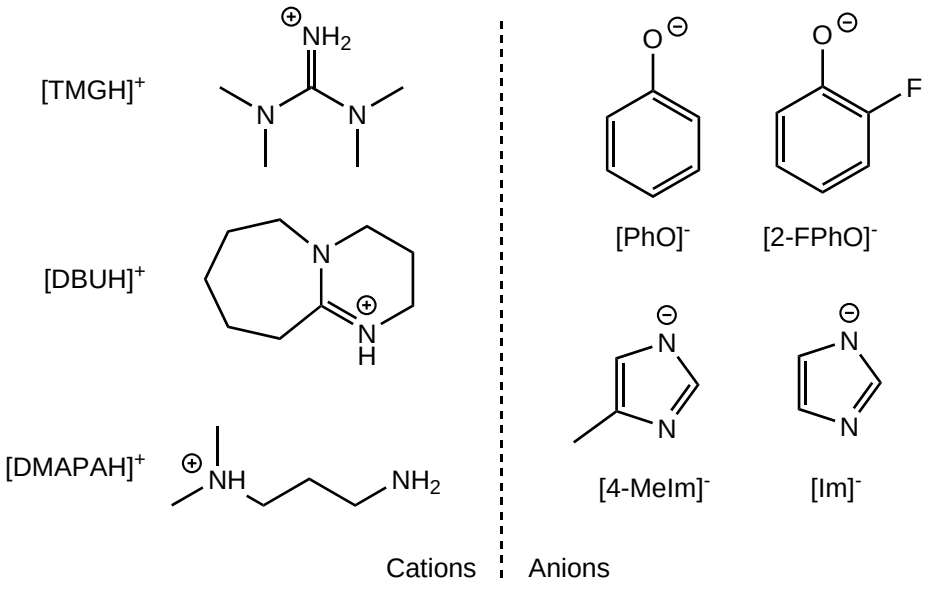

Figure 4.1: Structures of the cations and anions studied in this work.

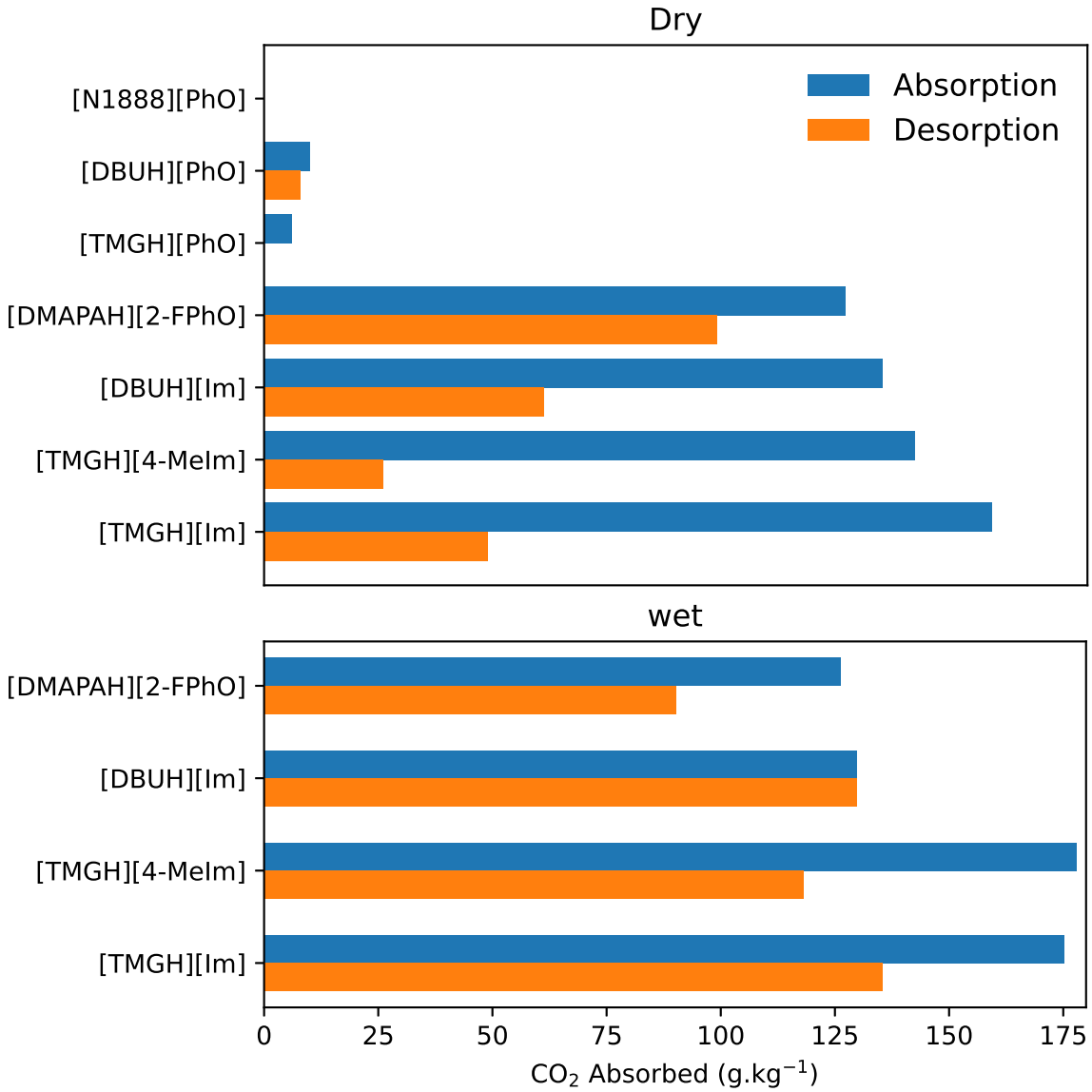

Figure 4.2: CO_2 absorbed by each IL after absorption at 30 ℃ and residual CO_2 remaining after desorption at 80 ℃ (above) under dry conditions or (below) with the addition of 5wt% water to the IL to simulate wet conditions.

Initially, the ILs were tested for CO_2 absorption using a dry gas stream after the ILs had been dried under reduced pressure overnight. These results are shown in the top chart of figure 4.2 where the absorption bar represent the amount of CO_2 absorbed by the IL at 30 ℃ and the desorption bar represents the amount of CO_2 that remained absorbed in the IL after heating to 80 ℃ and held at that temperature until no off-gas was observed. The temperatures of 30 and 80 ℃ were chosen as they roughly match the absorption and desorption temperatures reported in the respective publications for each IL.

No CO_2 uptake was observed for $[N_{1888}][PhO]$, although this exact combination of cation and anion had not been reported in the literature, phenolates have been reported many times with conflicting capacities [82]. Values for dry gas absorption

for [DBUH][PhO] and [TMGH][PhO] agree well with reported literature values of *ca.* 25 and 10 $g \cdot kg^{-1}$ [253, 330]. The dry absorption capacity of [DBUH][Im] agreed with the values reported by Zhu *et al.* [256]. Similarly, [DMAPAH][2-FPhO] and [TMGH][Im] were slightly less but still in reasonable agreement with the reported values [252, 253, 261]. For [DBUH][Im], [DMAPAH][2-FPhO] and [TMGH][Im], heating to 80℃ showed a much lower degree of desorption than is reported.

If no pre-drying stages are present, flue gas can contin up to *ca.* 15 vol% water [270], and since all ILs are hygroscopic, it would be expected that an IL would absorb this water from the gas stream. These conditions were simulated by the addition of 5 wt% water to the dried ILs before each absorption experiment, it is also important to note that 5 wt% is less than stoichiometric amount of water for all of the ILs. The phenolate ILs were not tested under wet conditions since their capacities under dry conditions were much lower than the others. These 'wet' uptake results are shown in the bottom chart of figure 4.2. [DMAPAH][2-FPhO] showed almost no change with the addition of water as there was very little change in either the absorption or desorption capacities. [DBUH][Im] also showed no significant change in absorption upon the addition of water, however, the $[TMGH]^+$ ILs both showed an improvement in CO_2 uptake. The effect of water on [DBUH][Im] and the $[TMGH]^+$ ILs became more apparent upon heating to 80℃ as the absorbed CO_2 was not as easily released compared to the dry experiments.

It is also worth noting some important and obvious information that is clearly missing from the publications on [DBUH][Im] and [TMGH][Im]. During the initial screening of [TMGH][Im], it was obvious that even after drying under reduced pressure overnight, residual water in the IL was enough to induce crystallisation. For the dry sample after CO_2 absorption, initially and increase in viscosity was observed, however after standing for some time, the sample began to crystallise. For the 5 wt% water sample, crystallisation is immediate. Figure 4.3 shows a picture of the physical change upon CO_2 absorption when in the presence of 5 wt% water. Lei *et al.* published the first report on [TMGH][Im] and part of their study included the effect of moisture on the CO_2 capture process where they report *'At the end of absorption experiment, the effect of moisture on CO_2 absorption capacity of [TMG][IM] is not obvious, the absorption capacity of [TMG][IM] decreases slightly with the increase the moisture of CO_2'* [252]. A similar lack of physical change reporting can be found in Li *et al.*'s publication on the same PIL [253]. Zhu *et al.* also omitted any observations of physical changes for [DBUH][Im], they only report on the decrease in capacity [256]. In this study, [DBUH][Im] also displayed an increase in viscosity upon dry CO_2 absorption and solidified into a waxy solid upon CO_2 absorption at 30℃ in the presence of water.

[TMGH][4-MeIm] was included in the 'wet' absorption study in an attempt to sup-

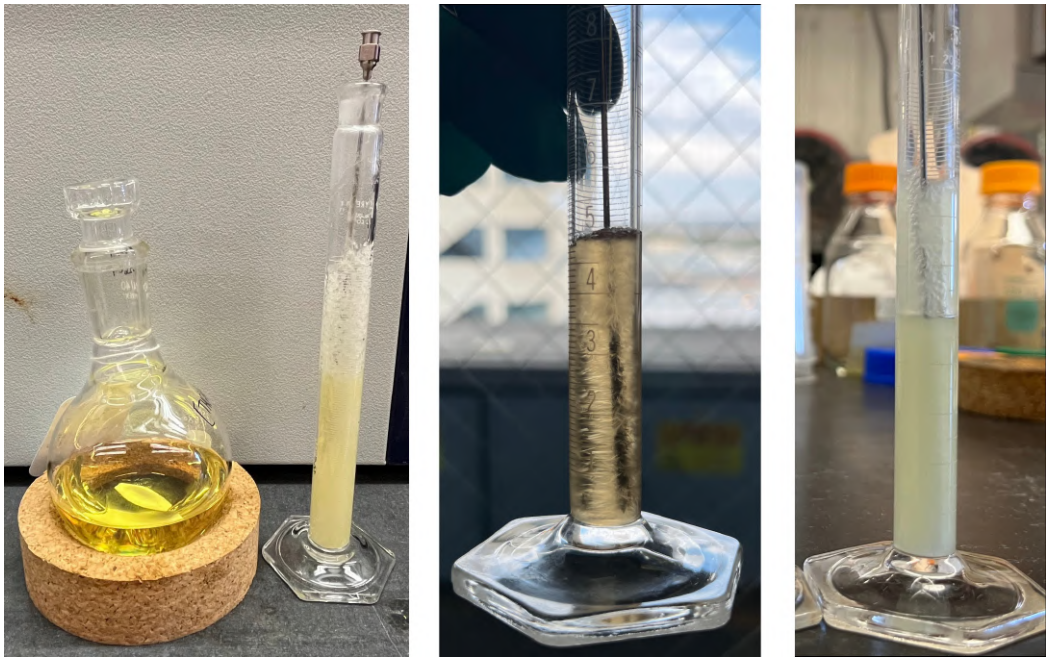

Figure 4.3: (left and middle) Pictures of neat protic ionic liquid [TMGH][Im] in the round bottom flask crystallising upon CO_2 absorption when in the presence of 5 wt% water in the measuring cylinders. (right) Solidification of [DBUH][Im] upon CO_2 absorption in the presence of 5 wt% water [252, 256].

press crystallisation of [TMGH][Im] by reducing the potential for hydrogen bonding through the C4 and C5 protons on the imidazolide anion. Unfortunately this failed as the IL also crystallised in the presence of water and CO_2, qualitatively however, it appeared to crystallise less readily than [TMGH][Im]. Heldebrant *et al.* have previously discussed the hydrogen bonding potential between carboxylates and the $[TMGH]^+$/$[DBUH]^+$ cations [254]. The authors suggest that the greater enthalpy of CO_2 binding is a result of the increased H-bonding potential of the $[TMGH]^+$ salts relative to the $[DBUH]^+$ salts. While they do not report a phase change in their 'organic liquid' systems, their hypothesis is supported qualitatively here as the waxy precipitate produced from the [DBUH][Im] IL upon CO_2 absorption in the presence of water, melted at a much lower temperature (*ca.* 80 °C), compared to the crystals produced by [TMGH][Im] under the same conditions (>80 °C).

Similarly, Oncsik *et al.* reported on a series of diamino protic ILs with remarkable capacities for CO_2 capture [260]. Following the reported procedure, N,N-dimethylethylenediamine and imidazole were mixed at room temperature until they formed a homogenous liquid, the mixture was then dried under moderate vacuum overnight. By morning a large mass of crystals had formed as shown in figure 4.4. This clearly shows that the mixture is not a protic ionic liquid but instead a solution of imidazole in the diamine as a significant amount of diamine was removed under reduced pressure. This is also supported by the difference in acidity, Stoimenovsk

et al. have explored how large the $\Delta pK_{a\,(aq)}$ should be between the acid and base components to form a PIL, where a $\Delta pK_{a\,(aq)}$ of 2 is required to achieve 90% proton transfer for primary amines, whereas tertiary amines require a $\Delta pK_{a\,(aq)}$ of 6 to achieve the same level of ionisation [331]. For [DMEDAH][Im], the $pK_{a\,(aq)}$ of imidazole is reported to be 14.5 [332] whereas the ammonium ion is more acidic with a $pK_{a\,(aq)}$ of *ca.* 10.8 [333], giving a $\Delta pK_{a\,(aq)}$ of -3.7, suggesting no significant ionisation would occur.

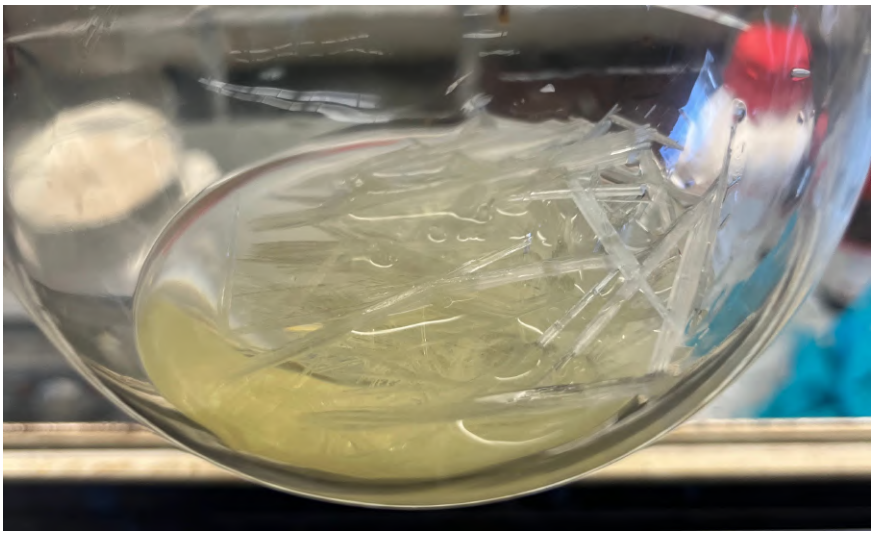

Figure 4.4: Picture of imidazole crystallising out of solution after drying the reported protic IL, [DMEDAH][Im], under reduced pressure overnight [260].

Other acid-base combinations were explored in an attempt to tune the physical properties and CO_2 capacity of the ILs. 1,2,4-Triazole and benzimidazole were both tried as acids to pair with DBU, structures of these anions are shown in figure 4.5. The triazolide salt was a low viscosity liquid, however, TGA revealed a low thermal stability as shown in the appendix figure 6.25, and so it was not investigated as the triazolide anion was suspected to have a low degree of thermal stability. The benzimidazolide salt on the other hand formed a solid at room temperature and so was not investigated further. Seo *et al.* have previously reported on both the $[P_{2222}]^+$ and $[P_{4444}]^+$ benzimidazolide salts which are both solid at room temperature, however they liquefy upon exposure to CO_2 [334]. This [DBUH][BnIm] salt may therefore still have potential for the CO_2 capture process outlined later in section 4.5. Additionally, 1,2,4-triazole (4-Triz) was also paired with TMG however the resulting [TMGH][4-Triz] was a crystalline solid at room temperature so it was also not tested for CO_2 uptake.

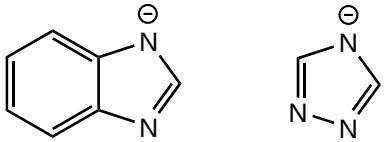

Figure 4.5: Structures of the benzimidazolide and 1,2,4-Triazolide anions that were also investigated.

4.2.2 Absorption vs temperature

From the scoping study, [DBUH][Im] and [TMGH][4-MeIm] were identified as having the potential for use with a higher temperature swing absorption (TSA) cycle, where absorption could be performed at *ca.* 80 °C. The rational being that, although the specific heat capacity does increase slightly with temperature, the specific heat capacities of many common ILs are less than half that of water [335], which equates to a large energy saving compared to aqueous amine scrubbers. Ficke *et al.* have also shown the molar heat capacity of some IL-water systems to be approximately linear, proportional to the mole fraction of both components [336]. Couple this with the fact that flue gas is normally emitted at high temperatures of *ca.* 120 °C and at emission sites such as a refinery, there is usually a plentiful amount of low grade heat available on site to facilitate a higher temperature TSA.

To investigate the capacity of these ILs at higher temperatures, samples were saturated with CO_2 at 30 °C, either dry or with the addition of 5 or 9 wt% water which represents less then and greater than stoichiometric amount of water. The samples were then heated at 10 °C intervals and held until no off-gas was observed, and the residual CO_2 capacity was determined. The results for [TMGH][4-MeIm] are shown in figure 4.6 and the results of [DBUH][Im] are shown in figure 4.7.

For [TMGH][4-MeIm], 5 wt% water equates to 0.58 molar equivalents whereas 9 wt% water corresponds to a slight excess at 1.08 molar equivalents. The dry sample absorbed 0.64 mol·mol^{-1} CO_2 and the majority of the captured CO_2 desorbed below 80 °C with only a small amount of residual CO_2 remaining at 110 °C, this is consistent with literature values and the initial screening study. The 9 wt% water sample absorbed significantly more CO_2 with 0.87 mol·mol^{-1} at 30 °C but desorbed almost no CO_2 upon heating to 80 °C. Thereafter, the desorption process began, with 0.5 mol·mol^{-1} CO_2 remaining at 110 °C. The capacity of 5 wt% water sample was approximately halfway between the other two samples. The presence of water therefore shows two effects here; first, it increases the total CO_2 capacity at 30 °C and second, it subsequently requires much higher temperatures for desorption which suggests a change in the capture mechanism.

CO_2 desorption from [DBUH][Im] under wet and dry conditions was examined between 30 and 200 °C in order to explore whether complete CO_2 stripping could

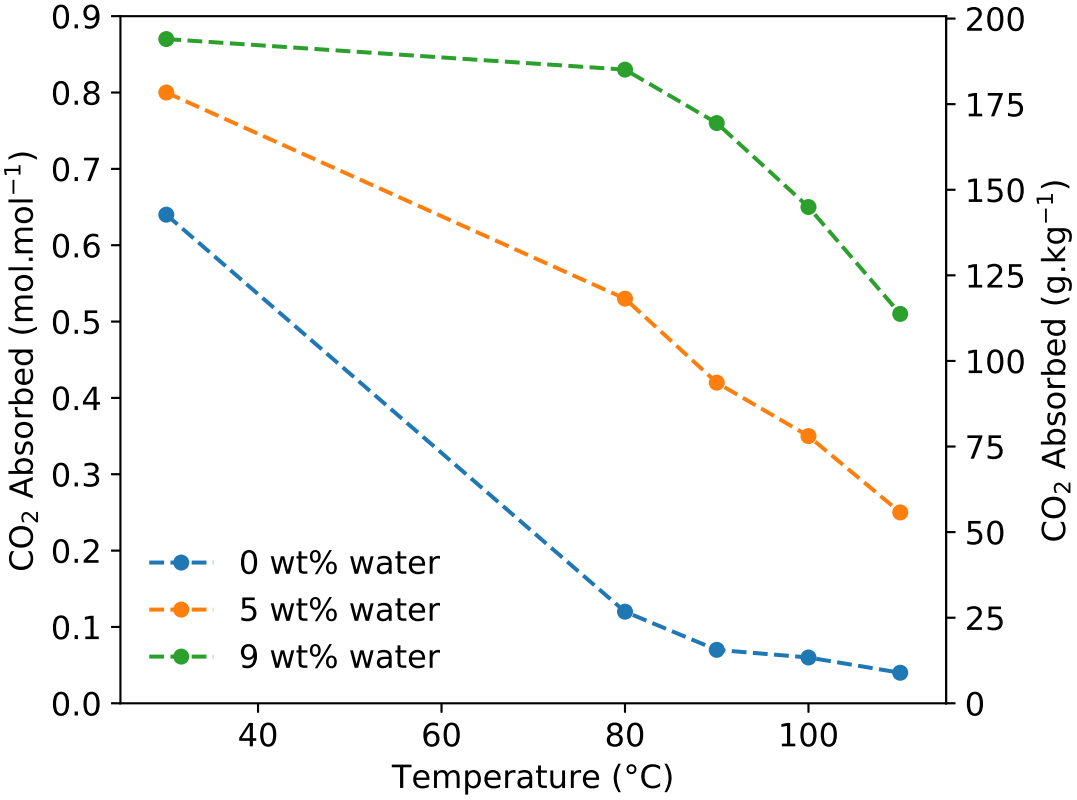

Figure 4.6: CO_2 absorption at 30 °C and the residual CO_2 remaining at each temperature increment for [TMGH][4-MeIm] with various water compositions.

be obtained at elevated temperatures given the retention of CO_2 in [DBUH][Im] with 5 wt% water at 80 °C as shown in figure 4.2. It is important to note that the sample began to darken in colour when being heated from 160 to 170 °C, probably from the onset of thermal decomposition of the IL. This corresponds both with the drop in capacity observed in all samples, as the assumptions made in the study as outlined in section 4.7 do not account for thermal decomposition.

For [DBUH][Im], 5 wt% water equates to 0.64 molar equivalents whereas 9 wt% water equates to 1.21. In this case, the dry sample absorbed 0.68 mol·mol^{-1} of CO_2 at 30 °C but only half of this was released on heating to 80 °C. Desorption continued steadily on stepping the temperature up to 140 °C where it plateaued with a residual 25 g·kg^{-1} (0.125 mol·mol^{-1}) CO_2 in the IL before a second drop corresponding with the sample darkening in colour. The 9 wt% water sample (1.21 molar equivalents) absorbed 0.75 mol·mol^{-1} at 30 °C, and similar to [TMGH][4-MeIm], very little was desorbed at 80 °C. On heating above 80 °C, CO_2 loss occurs through two desorption steps, the first gradual desorption region between 80 and 160 °C where *ca.* half of the absorbed CO_2 was stripped, followed by a much sharper desorption beyond 160 °C where the sample also began to darken in colour. Here, the 5 wt% sample

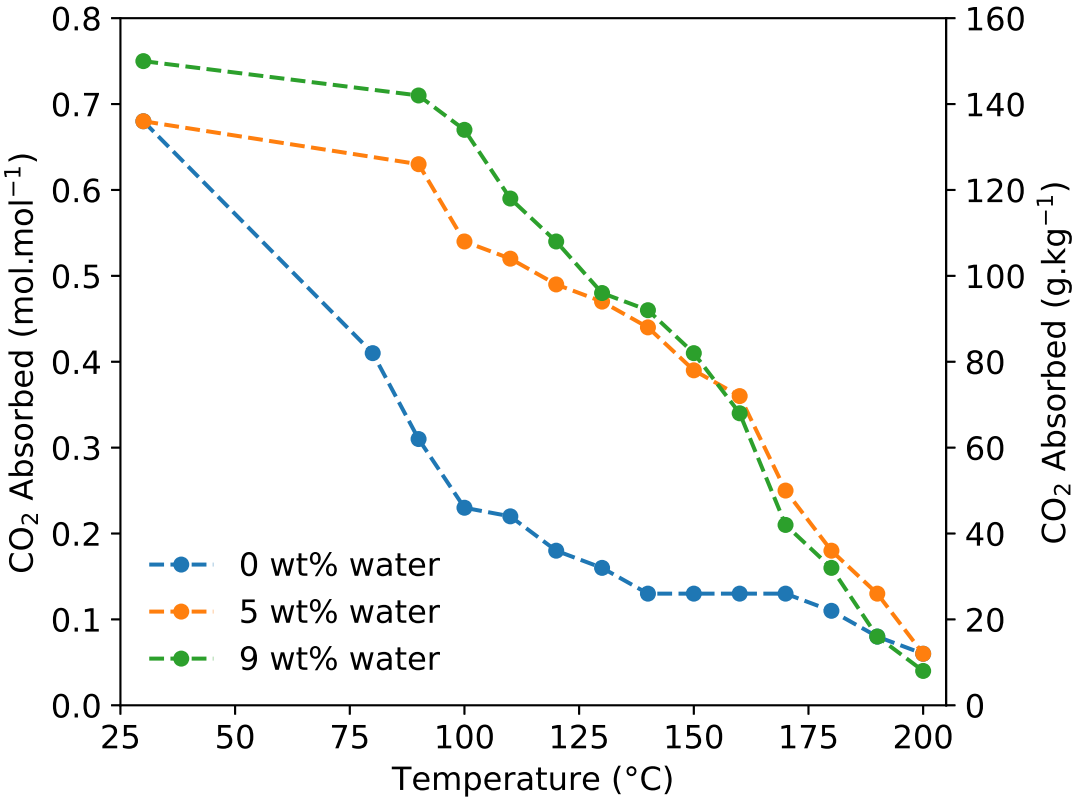

Figure 4.7: CO_2 absorption by [DBUH][Im] at 30 °C and the residual CO_2 remaining in the IL at each temperature increment with various water compositions.

started with the same capacity as the dry sample but little desorption was observed at 80 °C and the capacity converged with the 9 wt% sample at 130 °C. Water therefore had a similar effect on both ILs by increasing the capacity and subsequently requiring a higher temperature for desorption.

Both of these studies conflict with the reports of Lei *et al.* [252] and Zhu *et al.* [256] where a decrease in capacity was reported for [TMGH][Im] and [DBUH][Im] respectively. In both cases they passed pure CO_2 through a water bubbler and measured the CO_2 absorption over time at 30 and 40 °C respectively. This has the same effect in both ILs, causing a reduction in uptake kinetics and a reduction in the total CO_2 capacity although the effect was much more pronounced in [DBUH][Im]. Li *et al.* however, did report an increase in CO_2 capacity upon the addition of water for [TMGH][Im], up to a maximum of *ca.* 0.81 mol·mol^{-1} at 7.5 wt% [253]. The data reported by Li *et al.* is in good agreement with the data presented here considering the slight modification of the IL by the addition of the methyl group and that absorption here was conducted at 10 °C lower temperature.

The increase in CO_2 capacity displayed here by [TMGH][4-MeIm] upon the addition of water, and the higher temperatures required for desorption suggest that in

the presence of water, both of these ILs capture CO_2 via a bicarbonate mechanism as described in section 1.5.3. As already discussed, Heldebrant *et al.* suggested that the H-bonding between the $[TMGH]^+$ cation and carboxylates increased the CO_2 absorption enthalpy and subsequently increased the capacity. The formation of bicarbonate was also reported by Li *et al.* for [TMGH][Im] where they reported that higher regeneration temperatures are required to recycle the IL in the presence of water, although they did not investigate what temperature is required [253]

4.2.3 Absorption vs water content

Based on the previous section, [DBUH][Im] appears to have a difference in CO_2 capacity of *ca.* 70 $g{\cdot}kg^{-1}$ (0.35 $mol{\cdot}mol^{-1}$) between 80 and 160 °C. Additionally, both 'wet' samples were observed to be low viscosity, homogenous liquids above 90 °C, whereas the [TMGH][4-MeIm] still contained a crystalline precipitate at 110 °C. To further explore a high temperature absorption process for [DBUH][Im], absorption and desorption temperatures of 95 and 160 °C were chosen for further testing. In this case, the water content was increased from 9 wt% to 20 wt% to ensure equimolar amount of water throughout the absorption process. The results from this study are shown in figure 4.8.

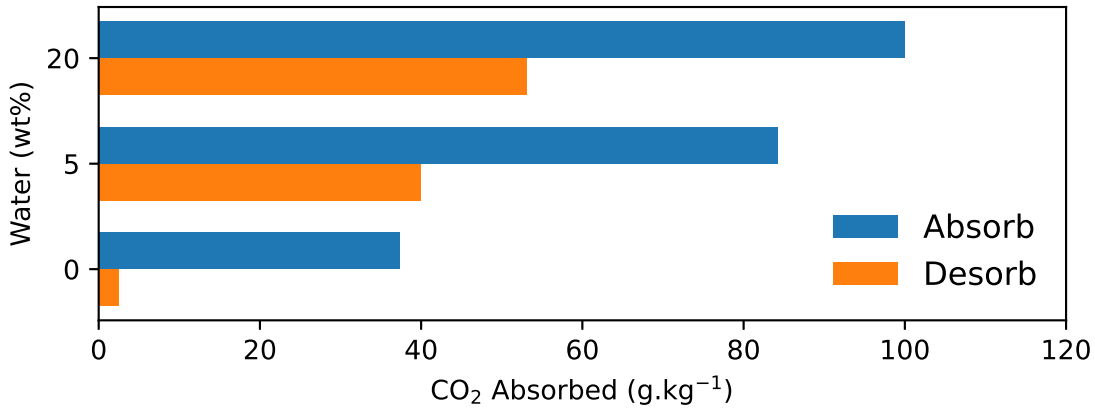

Figure 4.8: CO_2 absorption at 95 °C vs water weight added to [DBUH][Im]. The samples were then desorbed by heating to 160 °C.

The results show that in the absence of water, *ca.* 40 $g{\cdot}kg^{-1}$ of CO_2 is absorbed at 95 °C and the IL is nearly totally regenerated upon desorption at 160 °C. The addition of 5 wt% water approximately doubles the absorption to 85 $g{\cdot}kg^{-1}$ but then only half of this is desorbed as the IL retains 40 $g{\cdot}kg^{-1}$. Increasing the water content further to 20 wt% also produces a further increase in absorption up to 100 $g{\cdot}kg^{-1}$ but again, only half of the absorbed CO_2 is released upon heating to 160 °C.

Li *et al.* have shown that increasing the water content in [TMGH][Im] at 30 °C causes an increase in the CO_2 absorption up to a maximum at 0.82 mol·mol^{-1} at 7.5 wt% [253]. Above this water content only served to dilute the IL and did not further affect the mol·mol^{-1} absorption of CO_2. Li *et al.* also tested the recyclability of [TMGH][Im] with 20 wt% water and showed a reduction in working capacity after four cycles due to a build up of bicarbonate that could not be desorbed under their regeneration conditions of 60 °C and reduced pressure. In contrast, data in figure 4.8 shows that at 80 °C and under wet conditions, [DBUH][Im] can absorb 100 g·kg^{-1} and half of this can be desorbed upon heating to 160 °C, suggesting a working capacity of *ca.* 50 g·kg^{-1}. These conditions are not usually considered in the chemisorbant IL literature where lower temperature is generally considered more viable, but they are conditions that are relevant to industrial flue gas capture.

4.2.4 Reusability

To test the reusability of [DBUH][Im] and confirm the estimated working capacity of *ca.* 50 g·kg^{-1} from the previous section, 5 absorption-desorption cycles were conducted at 95 and 160 °C respectively with 20 wt% water. To quantify the amount of CO_2 desorbed by the IL, the off-gas was bubbled through a 1 M solution of sodium hydroxide, and so by measuring the pH before and after desorption, a rough calculation of the quantity of CO_2 can be calculated [337]. Results from this study are shown in figure 4.9.

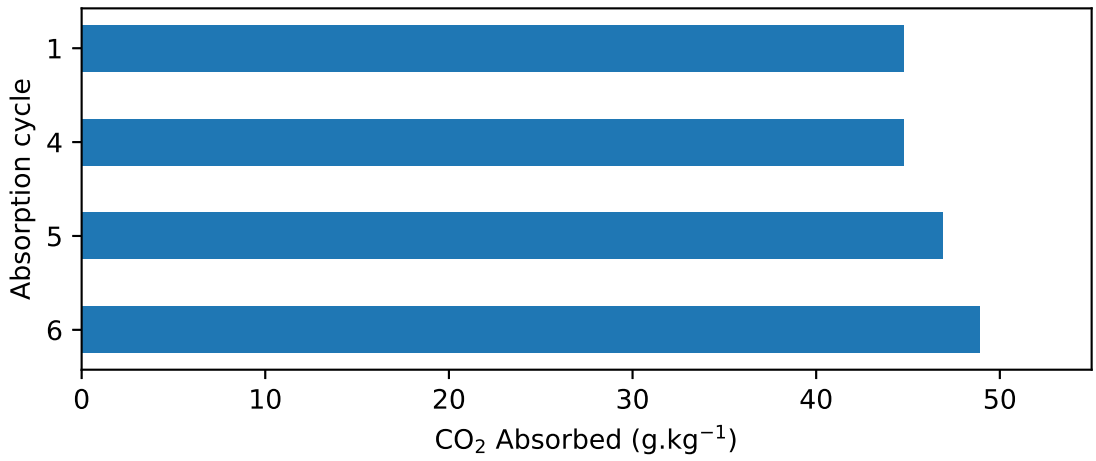

Figure 4.9: CO_2 released from a sample of [DBUH][Im] with 20 wt% water across six absorption-desorption cycles at 95 and 160 °C.

Cycles 1, 4, 5 and 6 all show working capacities between 45 and 50 g·kg^{-1} which is in agreement with the previous section (4.2.3). The slight increase in working capacity across the cycles is probably due to experimental error due to inaccuracies

in the pH probe and residual CO_2 in the headspace at the end of the desorption process. Across the six cycles, the sample remained visibly unchanged in colour and there was no sign of decomposition by NMR analysis as shown in appendix figure 6.26, demonstrating good stability of the IL under these conditions. Cycles 2 and 3 showed a significant reduction in CO_2 capacity from the first cycle although this is thought to be due to depletion in the hydroxide concentration allowing CO_2 to pass through the solution without being absorbed. Fresh sodium hydroxide solutions were used for cycles 4 through 6 which showed the expected desorption values. Full results are shown in appendix figure 6.27.

4.2.5 Absorption vs time

To investigate the kinetics of CO_2 absorption of wet [DBUH][Im] at 95℃, 100% and 15% CO_2 (N_2 balance) streams were used to simulate the conditions of real flue gas. As we are working under the assumption that the flue gas will be wet, the worst case scenario of 20 wt% water was used in this study which equates to a large excess of water at 3 molar equivalents. A dry sample was not included as similar studies of the dry [DBUH][Im] have been reported previously [256], additionally, dry [DBUH][Im] is expected to have a very low capacity for CO_2 at 95℃ as seen in figure 4.8. Raw data showing the change in mass as a function of time when using a 100% N_2 gas stream was used as a control experiment to account for water loss is shown in the appendix figure 6.28 and the results from this study are shown in figure 4.10.

The control expeiment showed a constant rate of water loss of 2.6 $\mu g \cdot min^{-1}$ over the 30 minute duration of the experiment. As others have shown, the addition of ionic liquid components to water significantly increases the boiling point of the mixture and reduced the vapour pressure of water due to the formation of strong hydrogen bonds between the water and IL ions [338, 339]. This shows that the absorption of CO_2 can be reasonably measured in the presence of water by taking into account the rate of water loss from the sample.

With neat CO_2, rapid CO_2 uptake into the [DBUH][Im]/20 wt% water mixture is observed, with equilibration to *ca.* 120 $g \cdot kg^{-1}$ (0.58 $mol \cdot mol^{-1}$) CO_2 in less than 10 minutes. With a more dilute gas stream of 15% CO_2, 85% N_2, equilibration is much slower, reaching *ca.* 100 $g \cdot kg^{-1}$ (0.5$mol \cdot mol^{-1}$) after 30 minutes. Over the next 3 hours, the capacity slowly increased to 0.551 $mol \cdot mol^{-1}$. The first three data points of the 100% CO_2 sample and the first five points of the 15% CO_2 sample show a linear increase in CO_2 absorption. Figure 4.11 shows these data points plotted with a line of best fit based on equations 4.1 and 4.2 with R^2 values of 0.9995 and 0.9985 respectively.

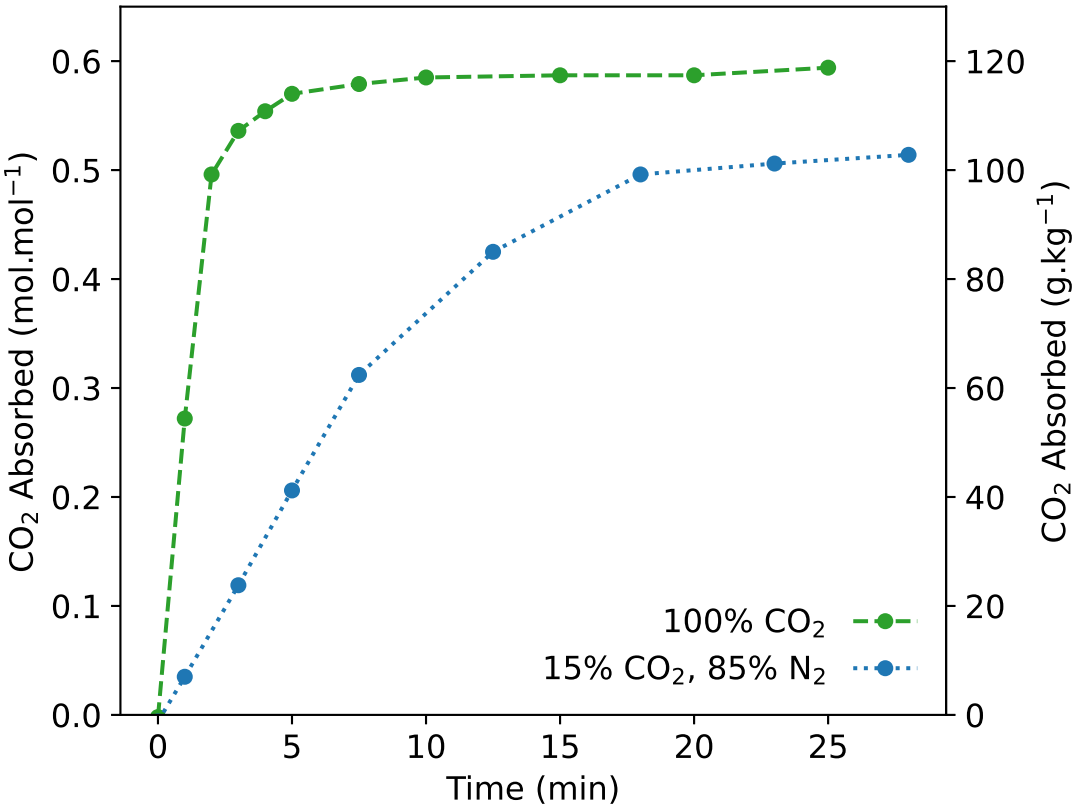

Figure 4.10: CO_2 absorption vs time of [DBUH][Im] with 20 wt% water at 95℃ and gas compositions at a flow rate of 0.1 L·min^{-1}.

$$q = 0.0413t \tag{4.1}$$

$$q = 0.2529t \tag{4.2}$$

Here, q is the amount of CO_2 absorbed in mmol·mol^{-1} and t is the time in minutes. normalisation of the gradients so the 100% gas stream is 1, yields a gradient of 0.163 for the 15% CO_2 stream. This demonstrates first order reaction kinetics with respect to CO_2, where the rate of absorption is linearly dependant on the partial pressure of CO_2 in the gas stream.

Li *et al.* reported similar results for [TMGH][Im], where lower partial pressures of CO_2 resulted in lower absorption capacities and slower uptake kinetics. They also reported the kinetics to be substantially faster in the presence of water (up to 25 wt%) which suppressed the increase in viscosity observed for [TMGH][Im] under dry conditions. For [DBUH][Im], the presence of 20 wt% water and the high absorption temperature prevents solidification of the absorbed species and keeps viscosity low to achieve relatively fast uptake kinetics.

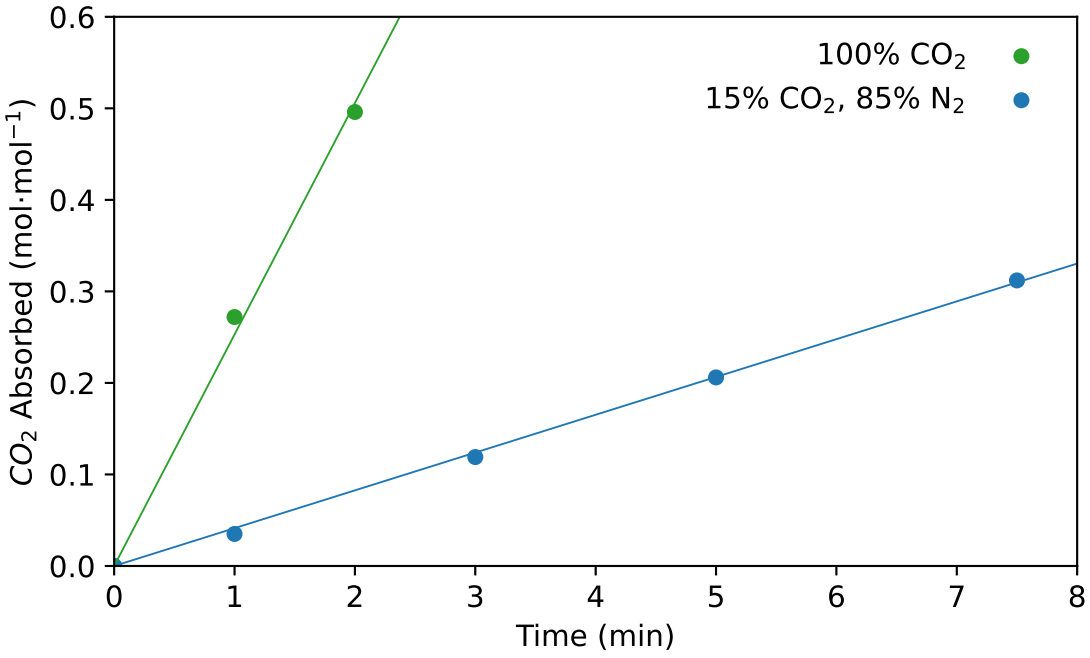

Figure 4.11: Initial linear region of CO_2 absorption by [DBUH][Im] with 20 wt% water at 95℃ and gas compositions at a flow rate of 0.1 L·min^{-1}.

4.3 Analysis of Absorption

4.3.1 TGA-MS

As discussed in section 4.2.2, [DBUH][Im] was observed to darken in colour above 160℃ and the presence of water hindered the desorption of absorbed CO_2. To investigate this, thermogravimetric analysis (TGA) coupled with mass spectroscopy (MS) was used to measure the desorption temperature of the dry and wet CO_2 loaded samples as well as the thermal stability of the wet IL. TGA-MS analysis for a sample of [DBUH][Im] with 10 wt% water added is shown in the appendix figure 6.29. It shows water beginning to leave the sample around 100℃ with a 10% mass loss being achieved at 176℃, although this cannot be fully ascribed to water loss.

Figure 4.12 shows TGA-MS results for dry, CO_2 absorbed [DBUH][Im]. It shows that regeneration under dry conditions is achievable at 95℃ by the significant amount of CO_2 being released from the sample at that temperature. After this desorption step the sample is then relatively stable until the next drop in sample mass that starts around 160℃. A small amount of water is detected from the sample at 100℃ which is likely from water absorption between sample preparation and analysis as it took several days for the sample to be analysed.

Figure 4.13 then shows the results for a sample of [DBUH][Im] with 5 wt% water (0.64 molar equivalents) after being exposed to CO_2 absorption. In this case, there

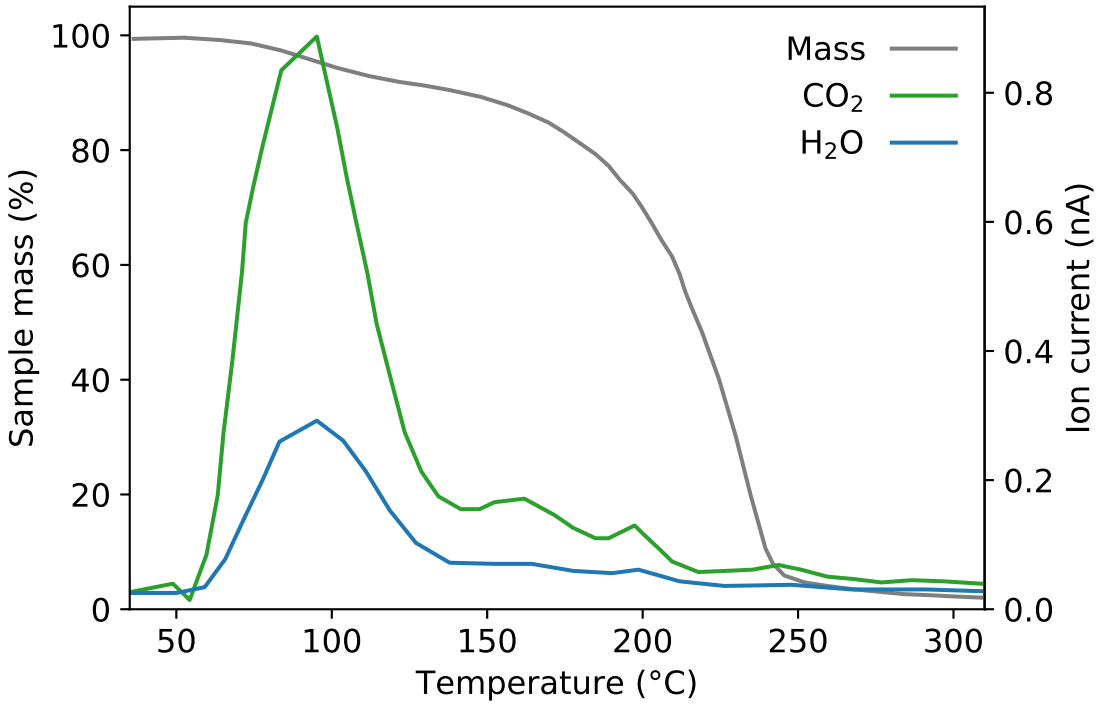

Figure 4.12: TGA-MS analysis of dry [DBUH][Im] after CO_2 absorption showing mass loss profile (grey) and evolution of CO_2 (green) and water (blue).

are two clear desorption steps, the first at 95℃, and the second at 110℃. This agrees with the results from section 4.2.2 where two desorption steps were also observed suggesting that there are different capture mechanisms under wet and dry conditions. The majority of CO_2 desorption occurs during the first step whereas water is released in approximately equal amounts in both steps.

Finally, figure 4.14 shows TGA-MS analysis of [DBUH][Im] with 9 wt% water (1.21 molar equivalents) after CO_2 absorption. In this case there only one significant desorption step at 102℃ that is also accompanied by desorption of water which is in agreement with section 4.2.2.

As shown from section 4.2.3, when there is enough water present, only half of the absorbed CO_2 will be released upon heating to 160℃. It appears that the absorbed CO_2 remaining upon desorption is absorbed semi-permanently, as it is only released upon thermal decomposition of the IL. This is shown in both of the wet samples where there is a small but noticeable increase in CO_2 released at approximately 160-170℃ that is missing from the dry sample. This may suggest that divalent carbonate is formed upon heating to 160℃ which cannot by desorbed without thermal degradation also occurring.

Zhu *et al.* have also investigated the thermal stability of dry [DBUH][Im] and reported an onset decomposition temperature of just 128 ℃ for the dry IL with a

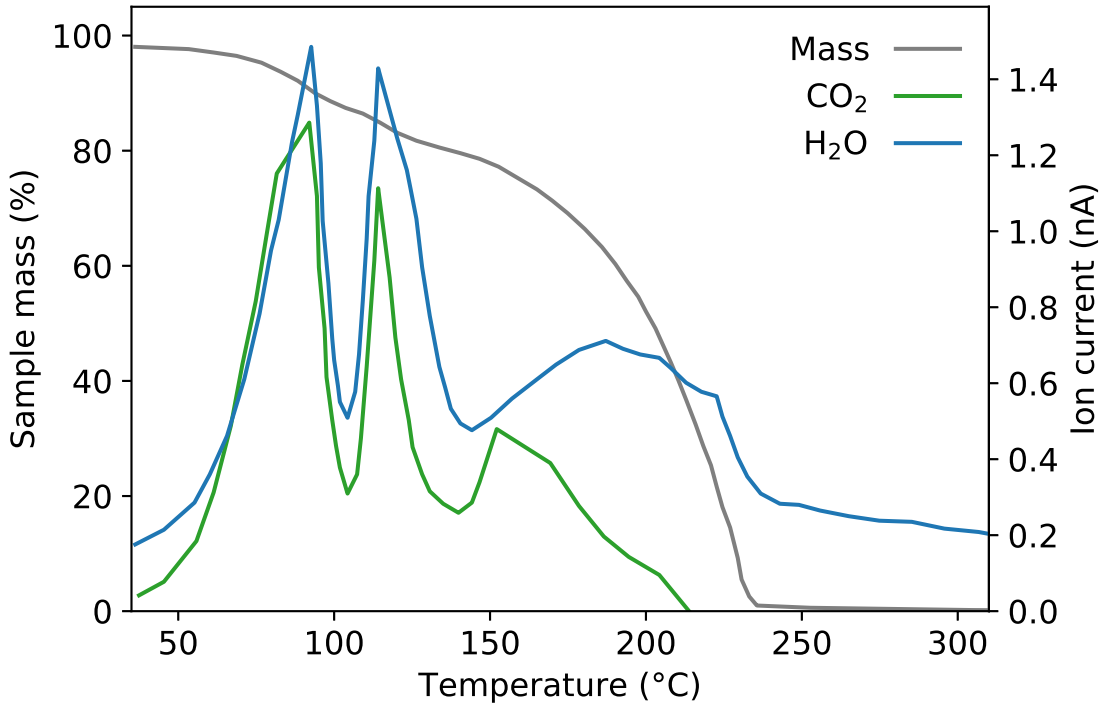

Figure 4.13: TGA-MS analysis of [DBUH][Im] with 5 wt% water added after CO_2 absorption showing mass loss profile (grey) and evolution of CO_2 (green) and water (blue).

heating rate of 10 °C·min^{-1} [256]. The results shown here suggest that the presence of water or CO_2 absorption can help to stabilise the IL as the onset degradation temperature of the IL appears to be *ca.* 160 °C, which agrees with the colour change observed in section 4.2. Similar to the findings of Li *et al.*, the presence of water in the system requires higher temperatures for regeneration [253] and based on the absorption studies here, the base IL cannot be totally regenerated at these higher temperatures. However, the demonstrated working capacity of 45 - 50 g·kg^{-1} is on par with most aqueous amines technologies [224].

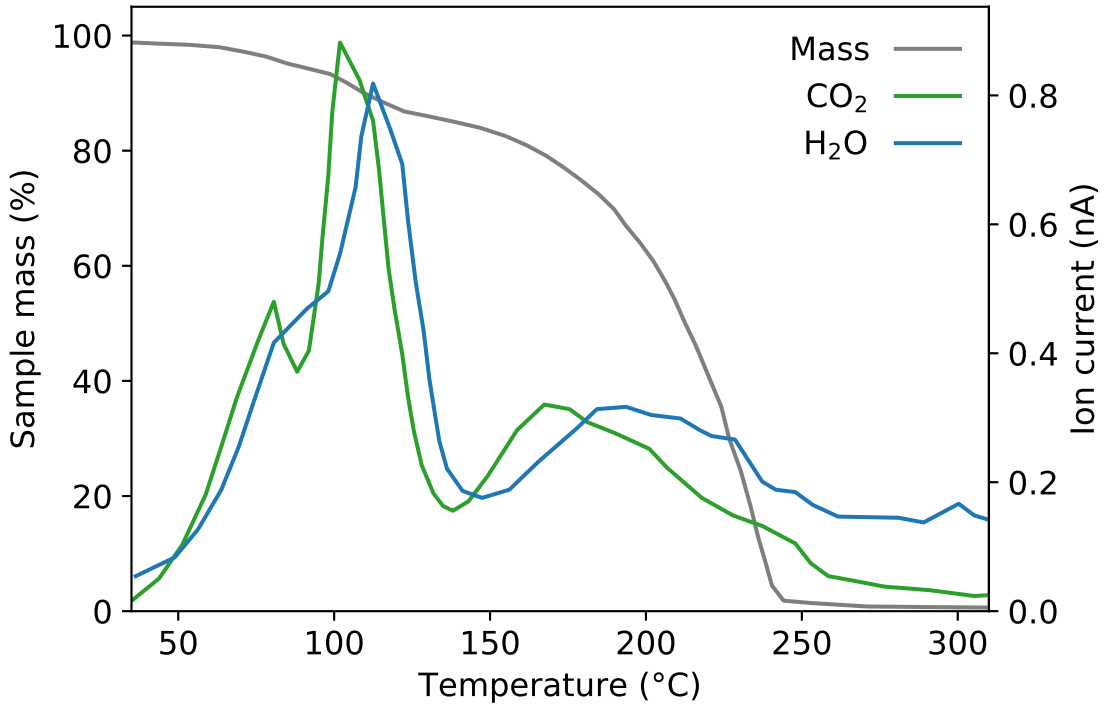

Figure 4.14: TGA-MS analysis of [DBUH][Im] with 10 wt% water added after CO_2 absorption showing mass loss profile (grey) and evolution of CO_2 (green) and water (blue).

4.3.2 FT-IR

To investigate the CO_2 absorption mechanism of [DBUH][Im] under dry and wet conditions, samples of the IL, as well as the CO_2 absorbed samples were analysed by FT-IR. Upon absorption of CO_2 under dry conditions, two new peaks appear in the carbonyl region at 1700 and 1643 cm^{-1}, as well as three peaks in the fingerprint region at 1289, 1044 and 771 cm^{-1}. These peaks are annotated in figure 4.15. Absorption under wet conditions produces the same peak at 1643 cm^{-1}, however, instead of the peak at 1700 cm^{-1}, a new peak at 1570 cm^{-1} appears.

Figure 4.16 shows the carbonyl region for [DBUH][Im] and the two CO_2 absorbed samples. [DBUH][Im] shows only one strong sharp peak in the carbonyl region at 1606 cm^{-1} from the C=N bond stretch. This peak is only slightly shifted from neat DBU where it appears at 1610 cm^{-1}, also shown in the appendix figure 6.30.

As other researchers have previously reported, this suggests that under dry conditions, CO_2 binds directly to the imidazolide anion, forming a carbamate which is responsible for the peak at 1700 cm^{-1} [252, 253, 256]. While under wet conditions bicarbonate is formed and is responsible for the peak at 1570 cm^{-1} [253]. The peak at 1643 cm^{-1} has been reported by some researchers to be from the $[DBUH]^+$

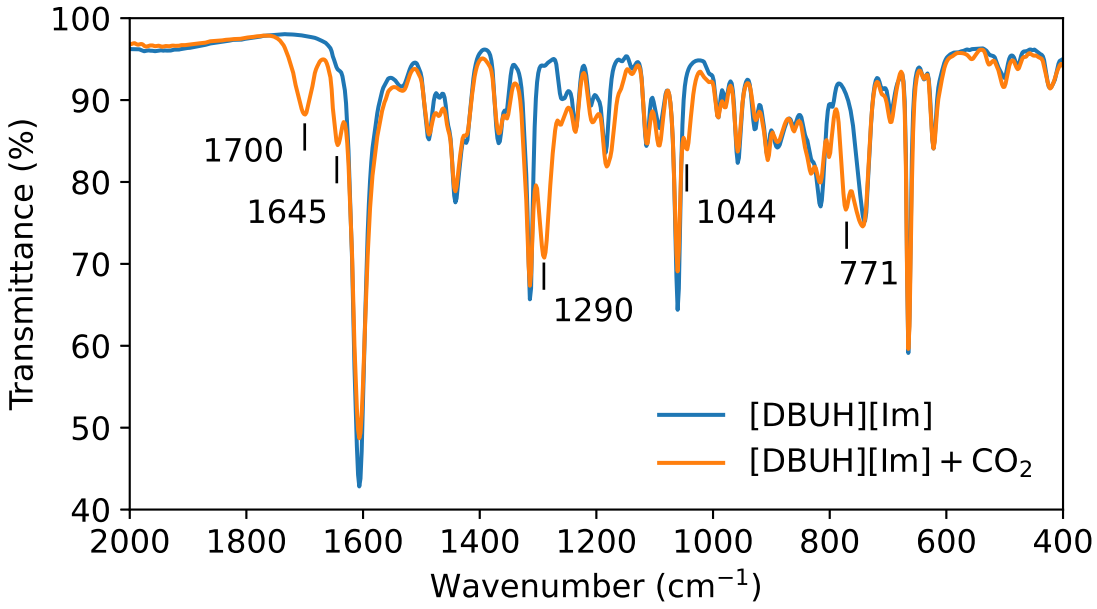

Figure 4.15: Annotated FT-IR spectra of the protic ionic liquid [DBUH][Im] after CO_2 absorption, showing all of the emerging peaks.

ion [340, 341], although this is a large shift from the observed 1606 cm^{-1} peak of neat [DBUH][Im]. This may suggest that the protic IL [DBUH][Im] is really just a mixture of imidazole in DBU and that ionisation does not occur until CO_2 absorption, however this does not seem likely due to the relatively small size of the 1643 cm^{-1} peak under dry absorption conditions. Additionally, Shah Miran *et al.* have reported IR spectra for a series of protonated DBU ILs and suggest the the formation of new peaks between 3000 and 3400 cm^{-1} to be from protonation of DBU [342]. Similar weak peaks are seen in the [DBUH][Im] spectra at 2594, 2681 and 3106 cm^{-1} which are not present in neat DBU as shown in appendix figure 6.32.

To investigate this 1643 cm^{-1} peak further, a sample of waxy solid $[DBUH]^+$ bicarbonate was prepared by bubbling CO_2 through a mixture of DBU and water [340] and the FT-IR spectra is shown in figure 4.17. This sample also shows both new peaks at 1643 cm^{-1} and 1570 cm^{-1} confirming that imidazole is not involved either directly or through hydrogen bonding. Spectra of [DBUH][Im] with an excess (10 wt%) of water does not show a symmetric stretching peak of water at 1630 cm^{-1} (presumably to extensive hydrogen bonding to the IL) or the unknown peak at 1643 cm^{-1}, only peak broadening towards higher wavenumbers. The mixing of DBU and water is exothermic which is indicative of proton transfer and ionisation to form [DBUH][OH] in solution, so the lack of a peak at 1643 cm^{-1} suggests it is not from the $[DBUH]^+$ cation. Excess water is therefore not responsible for this peak either which means that bicarbonate and/or carbonate must be responsible for the peaks

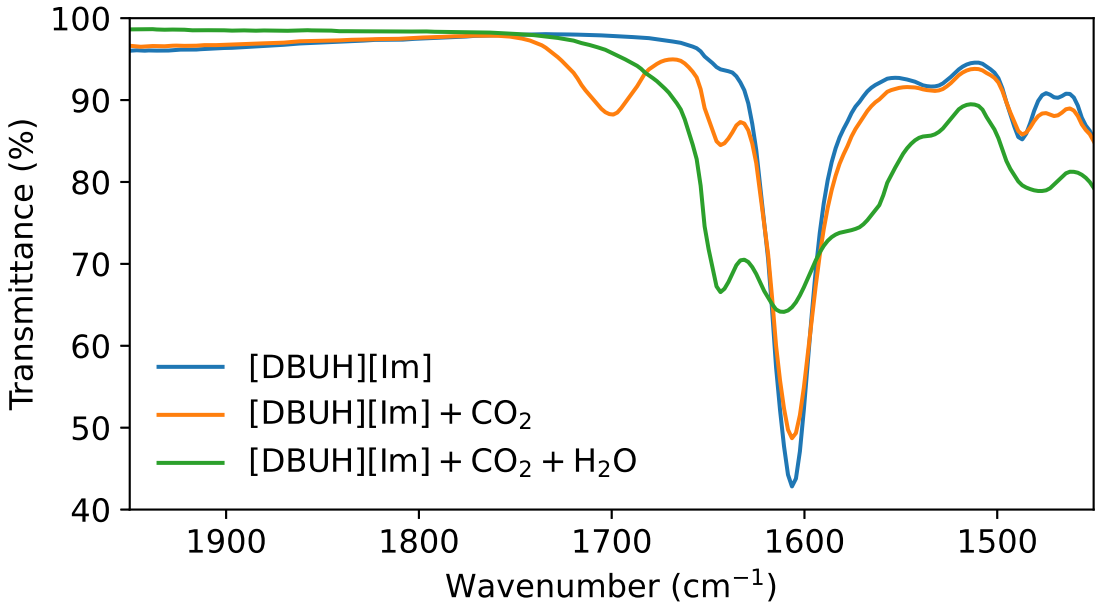

Figure 4.16: Carbonyl region of the FT-IR spectra of the protic ionic liquid [DBUH[Im]] overlaid with the IL after CO_2 bubbling in the absence and presence of water.

at 1570 cm^{-1} *and* 1643 cm^{-1}. Yuan *et al.* has also published on a bicarbonate based IL which shows similar peaks from 1600 - 1700 cm^{-1} [343], similar peaks are also seen in bicarbonate-water clusters as reported by Garand *et al.* [344], . The presence of this peak in the dry, CO_2 absorbed sample may be due to a small amount of water in the sample, possibly even being absorbed during analysis due to the hygroscopic nature of the sample.

Finally, a sample of wet [DBUH][Im] that heated to 160℃ to strip CO_2 from the sample was analysed and the carbonyl region is shown in figure 4.18. Although the peaks are suppressed, the persistence of both peaks 1700 cm^{-1} and 1643 cm^{-1} after desorption, clearly show that the base IL of [DBUH][Im] is not regenerated upon heating. Rather, two molecules of bicarbonate can react to release water and CO_2 while also forming divalent carbonate which maintains charge balance and is responsible for the persistent peaks.

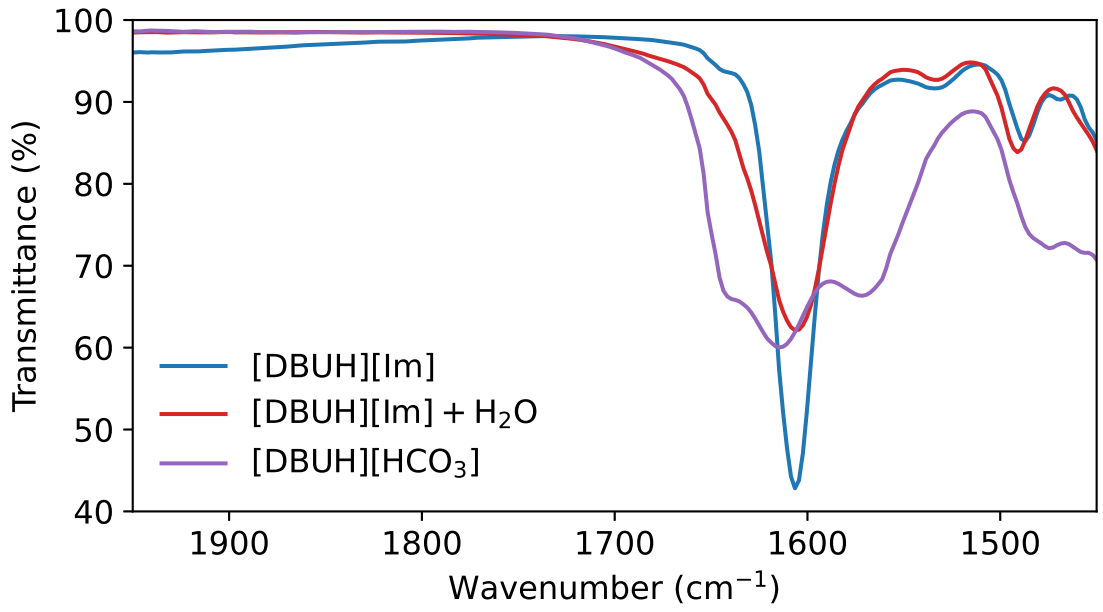

Figure 4.17: Carbonyl region of the FT-IR spectra of DBU and [DBUH][Im] after CO_2 bubbling in the presence of water.

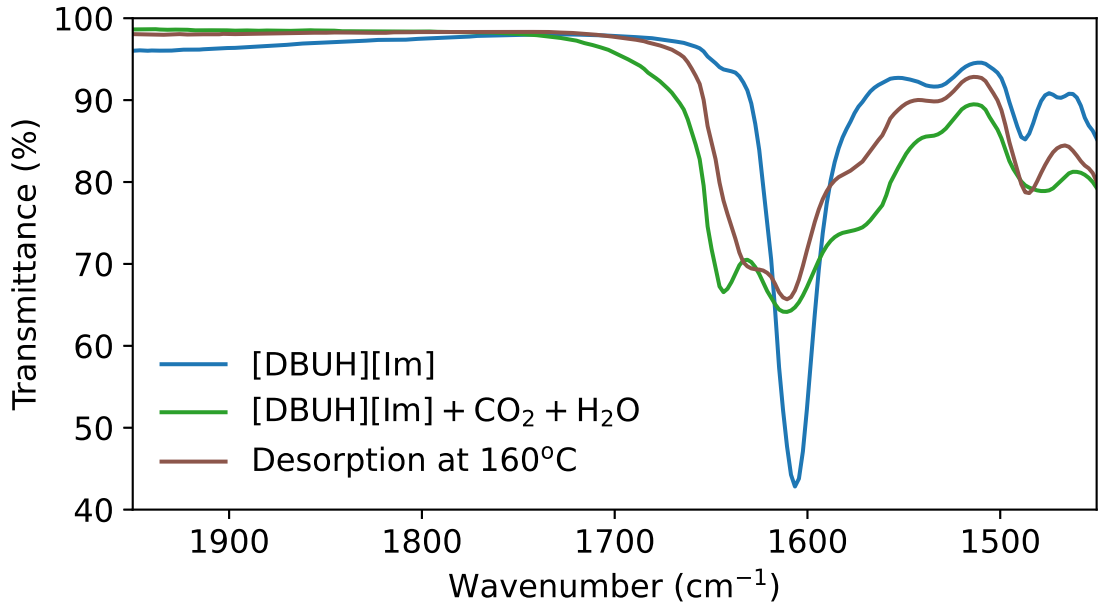

Figure 4.18: FT-IR spectra of the protic ionic liquid [DBUH[Im]] overlaid with the IL after CO_2 bubbling in the presence of water and then heated to 160℃.

4.3.3 NMR

The mechanism for absorption and desorption of CO_2 by dry and wet [DBUH][Im] was also analysed by ^1H and ^{13}C NMR spectroscopy to better understand the results of the FT-IR and TGA-MS analysis. Initial NMR investigations were performed using neat samples, prepared in an NMR tube, using a $CDCl_3$ capillary to provide the signal lock. This method avoids having to dissolve aliquots of the samples into other NMR solvents which could shift the position of any equilibria within the samples. Both CO_2 absorbed samples were analysed at 40 ℃ due to the increased viscosity and/or solidification upon CO_2 absorption. This is why these spectra have broader signals than the CO_2 lean samples.

^1H NMR spectra of wet (10 wt%) and dry [DBUH][Im], before and after CO_2 absorption are shown in figure 4.19. Upon CO_2 absorption in the dry sample, there is little change in the spectra except for a slight upfield shifting of the N^+-H signal of $[DBUH]^+$ at 14 ppm due to a reduction in hydrogen bonding to the anion. Spectra C shows the addition of 10 wt% of water to the IL which suppresses the peak at 14 ppm due to proton dynamics on the NMR timescale. Additionally, a new broad peak at 5.75 ppm appears belonging to the water. Finally, absorption of CO_2 by the wet sample shows a reduction of the water peak and the formation of bicarbonate via a signal at 9.75 ppm.

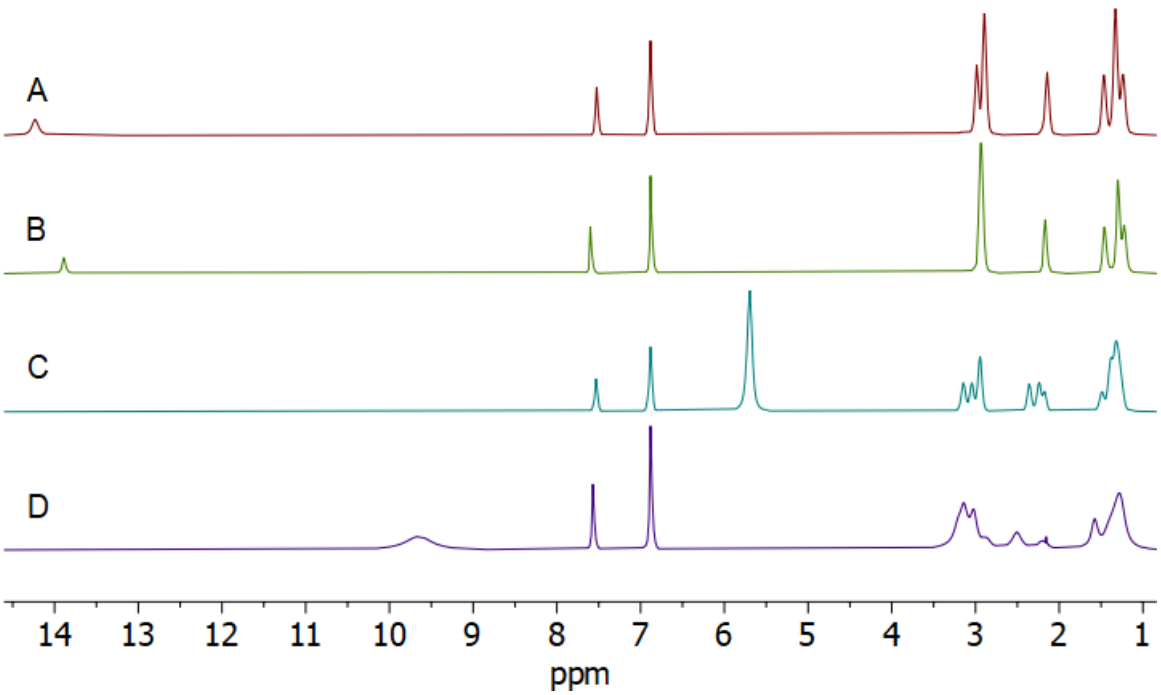

Figure 4.19: Neat ^1H NMR spectra of [DBUH][Im] using $CDCl_3$ capillaries. A = neat, B = CO_2 absorbed, C = 10 wt% water, D = 10 wt% water + CO_2. A & C run at 25 ℃, B & C run at 40 ℃.

Figure 4.20 shows ^{13}C NMR spectra for the same four samples. For clarity, only the relevant downfield portion of the spectra is shown here, the full ^{13}C spectra is shown in appendix figure 6.36. The splitting of the imidazole peaks at 124 and 136 ppm upon CO_2 absorption also occurs in the DBU peaks as can be seen in the full spectra. This suggests a change in environment for half of the sample which is indicative of a phase change. The absorbed sample is a waxy solid at room temperature although 40 °C was thought to have been enough to liquefy the sample, solids in an NMR experiment also tend to have very broad peaks due to reduced diffusion within the sample. An alternative or complimentary explanation is that the absorption of CO_2 reduces the polarity of the solvent enough to induce a liquid-liquid phase separation. Jessop *et al.* have studied a large number of such 'switchable-polarity solvents' which include ionic liquids or organic liquid mixtures of DBU and either alcohols or amines [345].

For [DBUH][Im], after CO_2 absorption under dry conditions, ignoring the peak splitting just discussed, one new signal appears at 150 ppm, due to the formation of the carbamate anion. Addition of water to [DBUH][Im] produced a small peak at 177 ppm and upon CO_2 absorption two additional peaks appear between 161 and 166 ppm. Physically absorbed CO_2 usually appears around 125 ppm [346] which does not appear here so physical absorption contributes a negligible amount to the total capacity under these conditions.

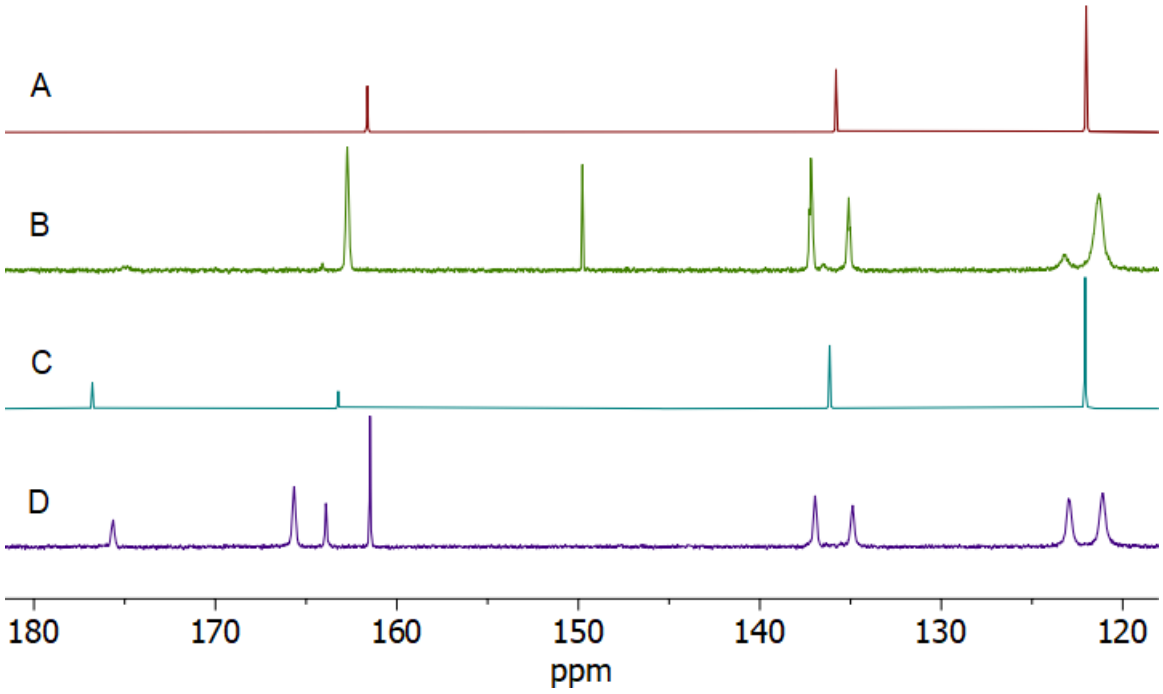

Figure 4.20: Neat ^{13}C NMR spectra of [DBUH][Im] using $CDCl_3$ capillaries. A = neat, B = CO_2 absorbed, C = 10 wt% water, D = 10 wt% water + CO_2. A & C run at 25 °C, B & C run at 40 °C.

No reports have been found in the relevant literature about such a peak at 176 or 177 ppm although several researchers have reported on the formation of a bicarbonate peak between 160 and 165 ppm [253, 340]. As this could be due to IL solvent environment, samples of wet [DBUH][Im] before and after absorption as well as after desorption were diluted in $CDCl_3$ and analysed by ^{13}C NMR as shown in figure 4.21, the full spectra are shown in appendix 6.37. Water from the samples that was not miscible in $CDCl_3$ was separated prior to analysis.

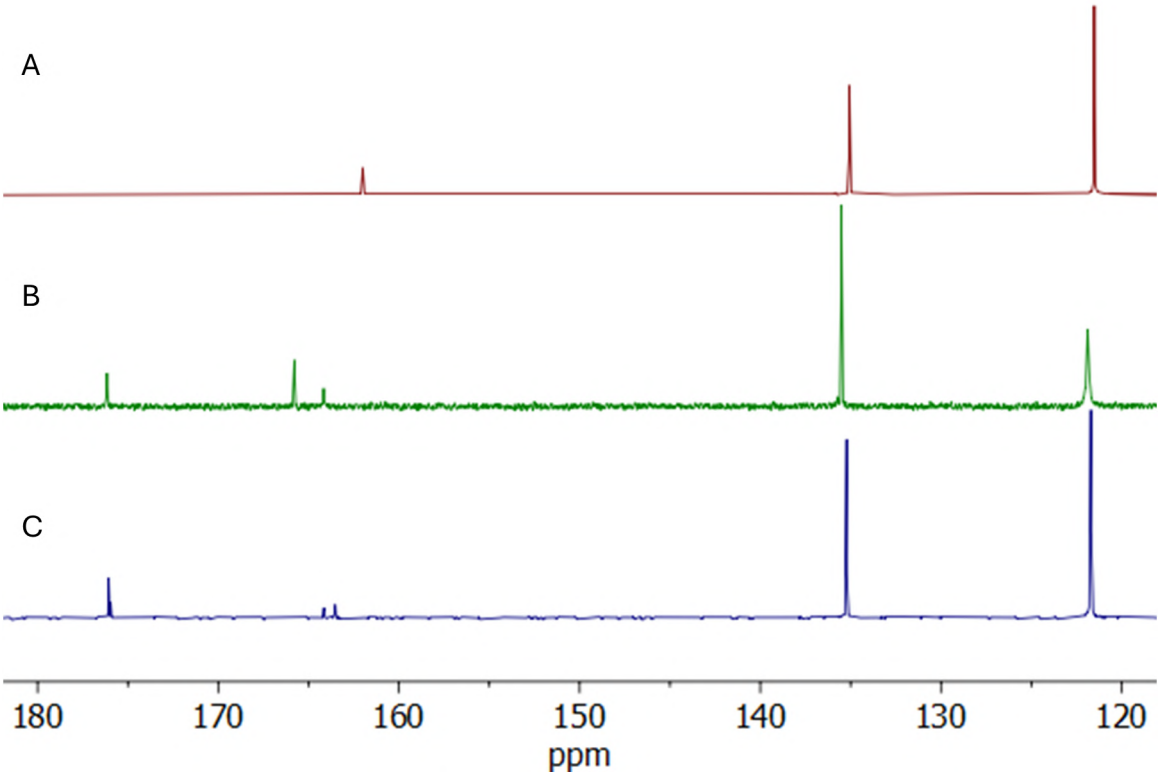

Figure 4.21: ^{13}C NMR spectra taken in $CDCl_3$. A = [DBUH][Im] with 20 wt% water, B = after CO_2 absorption at 95℃ and C = after desorption at 160℃.

This method of NMR sample preparation greatly simplified the spectra as there is no longer any splitting of the imidazole or DBU, leaving only three peaks of interest in the downfield spectra. The central carbon of DBU is at 161 ppm in the DBU spectra A, this shifts to slightly higher δ of 163 ppm upon CO_2 absorption. Samples B and C both show two new peaks at 164/165 ppm and 176 ppm, in the absorbed sample, the 165 ppm peak is more prominent, whereas in the desorbed sample, the 176 ppm peak is more prominent.

Yoo *et al.* have previously explored the mechanism of CO_2 absorption in aqueous sodium hydroxide solutions [337]. They show that initially, hydroxide will react with CO_2 to form bicarbonate, but due to the amphoteric nature of bicarbonte, a side reaction occurs in which bicarbonte is deprotonated to form divalent carboante and water. In the first half of the absorption, any CO_2 absorbed is deprotonated and

forms divalent carbonate, and only beyond 0.5 mol·mol^{-1} is bicarbonate formed in significant amounts. A scheme for this reaction is shown in figure 4.22.

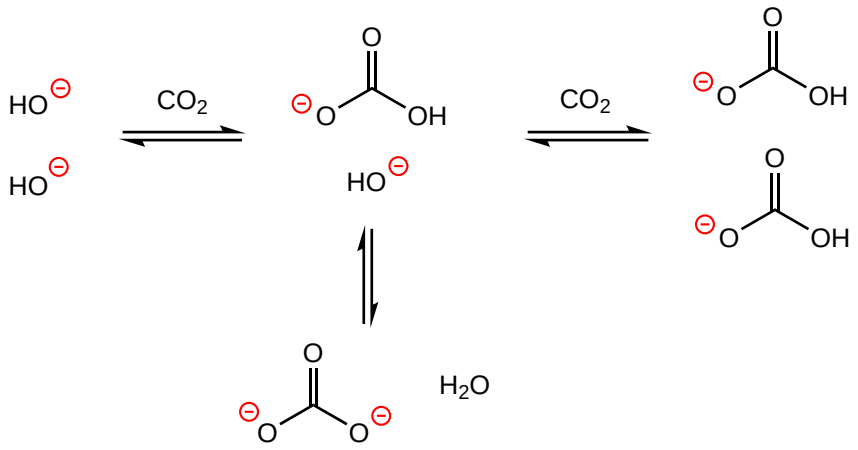

Figure 4.22: Mechanism of CO_2 absorption by sodium hydroxide showing the secondary equilibria whereby bicarbonate can be deprotonated into dianionic carbonate [337].

The ^{13}C NMR spectra in figures 4.20 and 4.21 suggest that this side reaction is also occurring in the wet [DBUH][Im] system with the peak at 165 ppm belonging to bicarbonate, while the peak at 176 ppm is carbonate. When the IL is saturated with CO_2 at *ca.* 0.6 mol·mol^{-1}, the equilibrium is towards bicarbonate but then upon desorption, the equilibrium shifts towards carbonate. Sample C in figure 4.20 shows a peak at 176 ppm suggesting a small amount of CO_2 absorption under ambient conditions and that all of it is in the form of carbonate. The two peaks appearing at 164 and 166 ppm in Sample D may be bicarbonate in two different environments, the same way the imidazole and upfield DBU peaks are observed to split.

To summarise the absorption mechanism, [DBUH][Im] shows two distinct CO_2 absorption mechanisms in the presence, or absence, of water as depicted in figure 4.23. Under dry conditions, CO_2 binds directly to the anion forming a carbamate which can be regenerated at relatively low temperatures. When there is equimolar water in the system however, CO_2 can be absorbed at elevated temperatures of *ca.* 90 °C and is initially absorbed to bicarbonate and then deprotonated to form carbonate. At higher capacities, the majority of the absorbed CO_2 is in the form of bicarbonate. This wet absorption mechanism requires higher temperatures for regeneration of *ca.* 160 °C and will not full regenerate due to the formation of carbonate as per the mechanism shown in figure 4.24. This is the usual thermal decomposition pathway for any bicarbonate salt [347].

Aqueous hydroxide solutions have been researched for decades as potential reusable absorbents where the carbonate species are usually precipitated and dis-

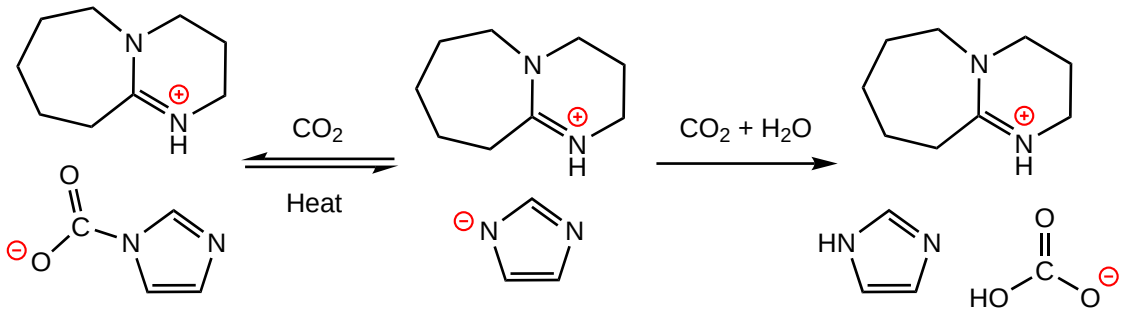

Figure 4.23: CO_2 Absorption pathways of [DBUH][Im] with and without the presence of water.

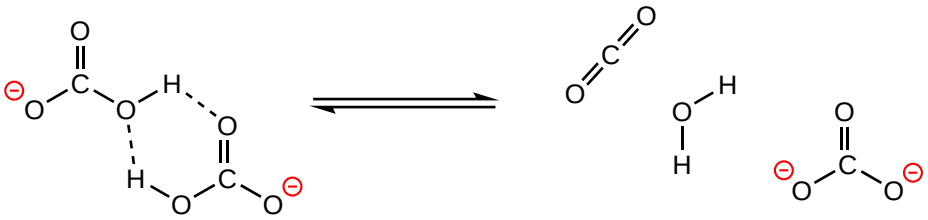

Figure 4.24: Mechanism of bicarbonate thermal decomposition into CO_2, water and divalent carbonate [347].

posed of as solid products [348]. Metal oxides are also commonly reported as solid absorbents for CO_2 as they form metal carbonates under ambient conditions which can then be regenerated by heating to much higher temperatures of 300-500 °C [349]. Metal oxide processes can also be formulated into molten salt systems but these systems still cycle between metal oxides and carbonates [350]. There seems to be a gap in the literature for carbonate materials that react with water and CO_2 to form two equivalents of bicarbonate that can then be regenerated at much lower temperatures of *ca.* 150 °C. The effective CO_2 absorbing material here may be considered to be a carbonate ionic liquid (although it is technically a mixture and the neat material may not melt below 100 °C) that absorbed CO_2 by the above method, also shown in equation 4.3.

$$[DBUH]_2[CO_3] + H_2O + CO_2 \rightleftharpoons 2\,[DBUH][HCO_3] \tag{4.3}$$

4.4 Corrosion study

Several hundred papers are published each year on the use of ILs as corrosion inhibitors [351] as their low vapour pressure can prolong their lifespan however, some ILs, especially those containing coordinating anions such as chloride can promote steel corrosion. [DBUH][Im] has not been tested for this purpose yet but imidazole derivatives are also investigated as inhibitors [352]. On the other hand,

DBU has been shown to promote the formation of magnetite (Fe_3O_4) under hot conditions and in the presence of water.

To determine if the [DBUH][Im] has any corrosive properties on steel, four corrosion studies were conducted, two at 95℃ and two at 150℃, each of which had either neat [DBUH][Im] or [DBUH][Im] with 10wt% water and fully saturated with CO_2. The samples containing the tokens and IL were then placed in convection ovens for three weeks.

After just four hours at 160℃, a sample of [DBUH][Im] had turned black and was showing significant signs of thermal decomposition. The study was therefore repeated at 150℃, after this time the IL had also significantly darkened. The stainless steel tokens however were completely unchanged after the three week period, no measurable change in size, shape or weight. ED-XRF analysis of both the IL and token showed no significant changes in composition, all deviations being within the error of the instrument. SEM analysis was conducted on the token that had been exposed to [DBUH][Im] at 150℃, the pictures shown in figure 4.25 clearly show no significant change in the surface features of the token.

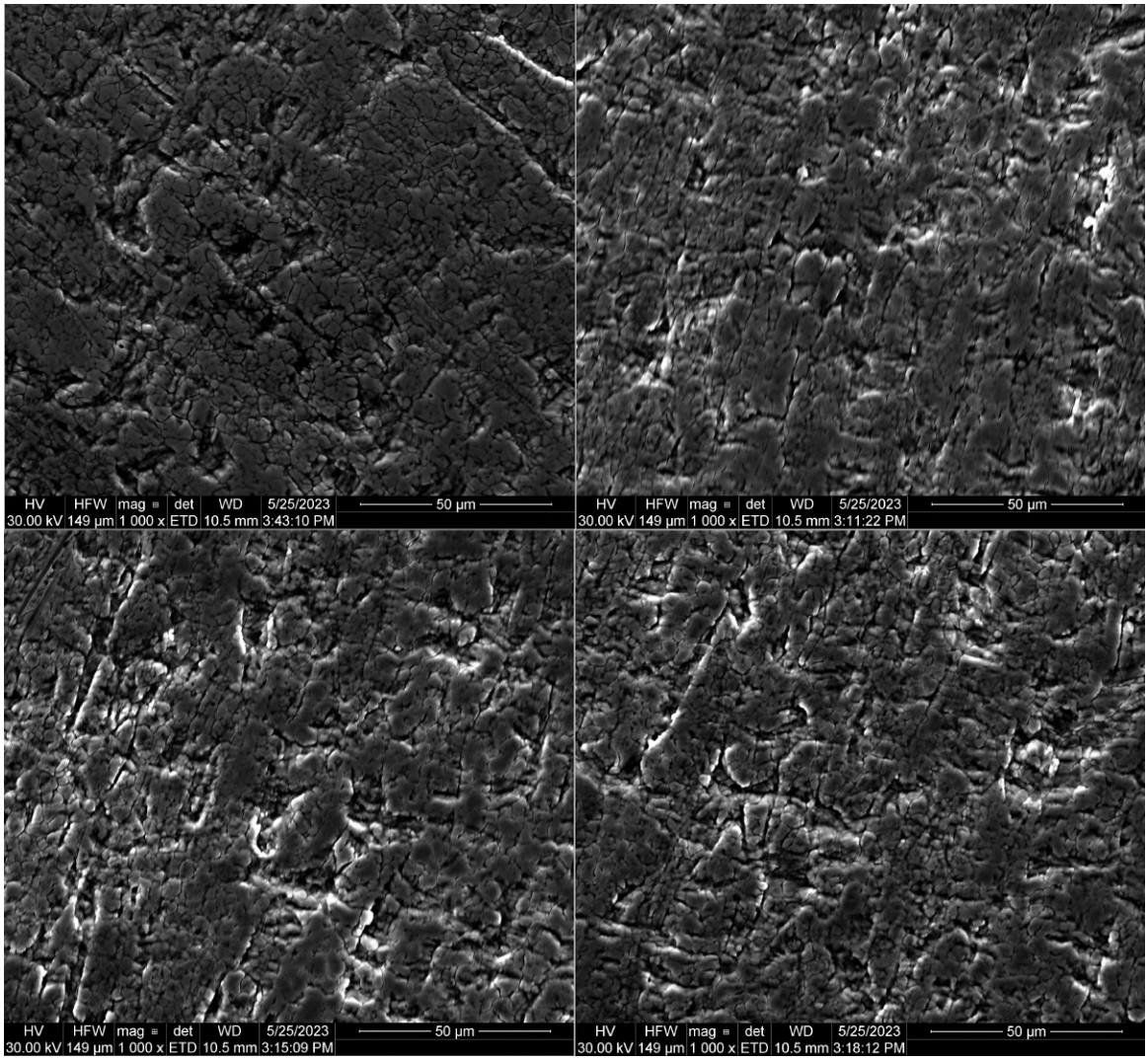

Figure 4.25: Scanning electron microscopy pictures of 316 stainless steel tokens before (top left) and after (top right and bottom two) showing no major change in surface features after three weeks of exposure to [DBUH][Im] at 150 °C.

4.5 Post-combustion carbon capture process

Based on the above work, a high temperature flue gas scrubbing process was designed and a patent applied for with the US patent office. A schematic of the process diagram is shown in figure 4.26. In essence, the protic ionic liquid [DBUH][Im] is circulated through an absorber at 95 °C where it is contacted with hot, wet flue gas. Under these conditions CO_2 is absorbed forming predominantly bicarbonate and the CO_2 rich IL is circulated into a regeneration unit where it is heated to 160 °C. The gas that makes it through the absorber can then be considered CO_2 lean and vented to the atmosphere. In the regeneration unit, excess water is removed and thermal decomposition of bicarbonate is induced which releases the absorbed CO_2 and carbonate is formed. The off-gas can be considered CO_2 rich and depending

on the composition, could be used for conversion or sequestration. The CO_2 lean IL is then circulated from the regenerator back to the absorber. Along the way it passes through a heat exchanger to transfer heat from the lean IL to the rich IL, utilising some waste heat.

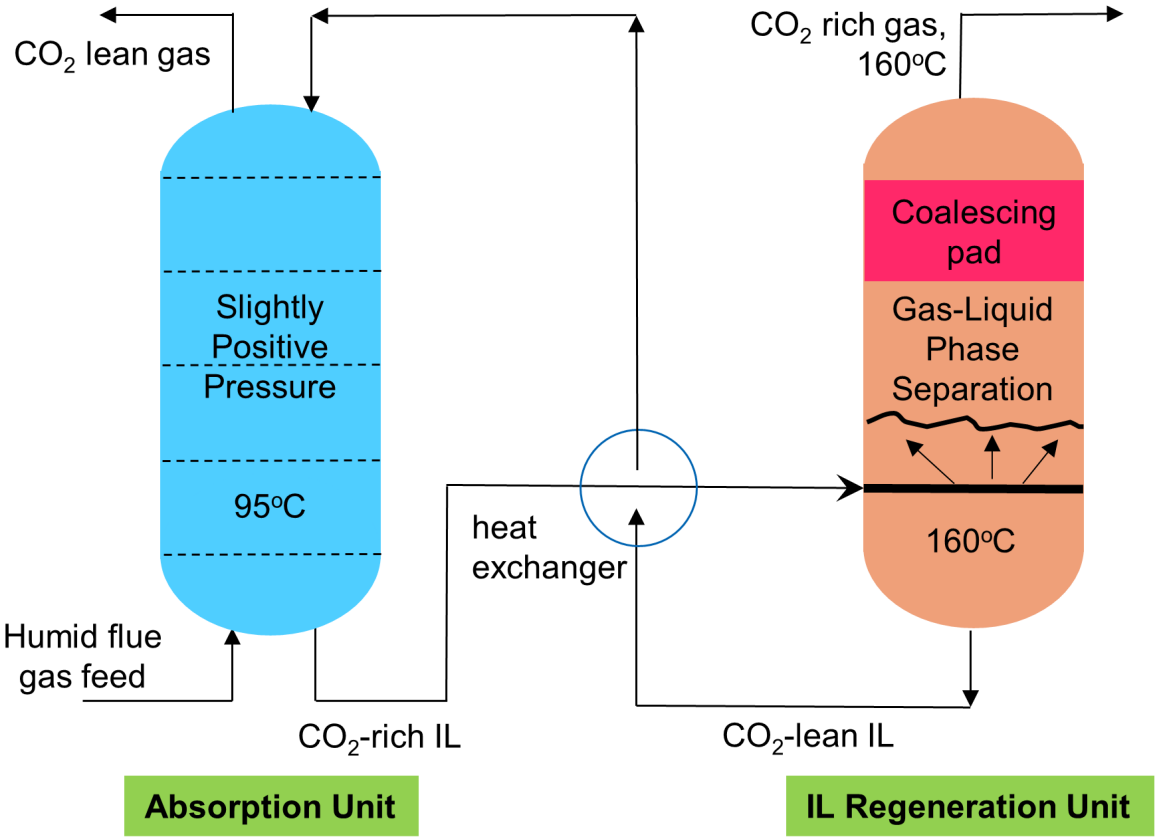

Figure 4.26: Process diagram showing how [DBUH][Im] could be used in a high temperature CO_2 scrubbing process from flue gas.

The viscosity of the CO_2 rich IL was not measurable due to off-gassing during the measurement although it will vary with water content and CO_2 loading. However, the viscosity of the desorbed IL at 95 ℃ was measured to be only 6.6 cSt, due to the presence of divalent carbonate and lack of residual water at this stage, it can be assumed that this will be more viscous than the CO_2 IL. For reference, neat [DBUH][Im] has a viscosity of 3 cSt at 95 ℃ and 1.2 cSt at 160 ℃.

As discussed above, during the first absorption cycle, CO_2 is absorbed along with water to form bicarbonate and the imidazole counterion gets protonated to become a neutral species as per figure 4.27. Upon desorption, two bicarbonate anions will then react to form divalent carbonate, water and CO_2 which will be released into the CO_2 rich gas stream. Successive absorption-desorption cycles thereafter will follow the mechanism shown in figure 4.28 where the divalent carbonate acts as the base, deprotonating water to form hydroxide that can then capture more CO_2. For simplicity in these figures, a 1 $mol \cdot mol^{-1}$ capacity is depicted

although it is important to keep in mind that the maximum observed absorption at 95℃ was *ca.* 0.6 mol·mol^{-1}.

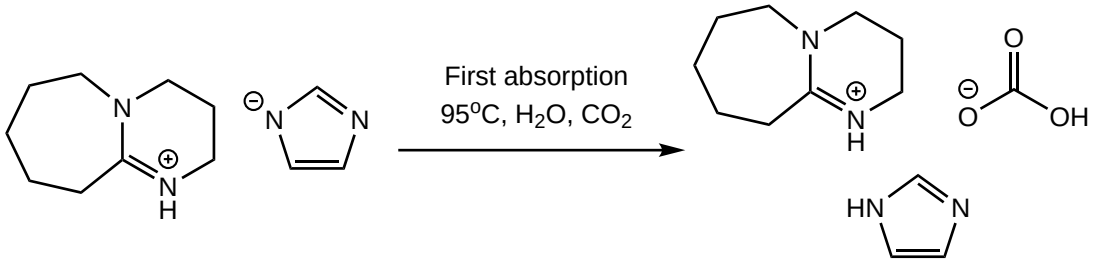

Figure 4.27: First absorption of CO_2 by [DBUH][Im].

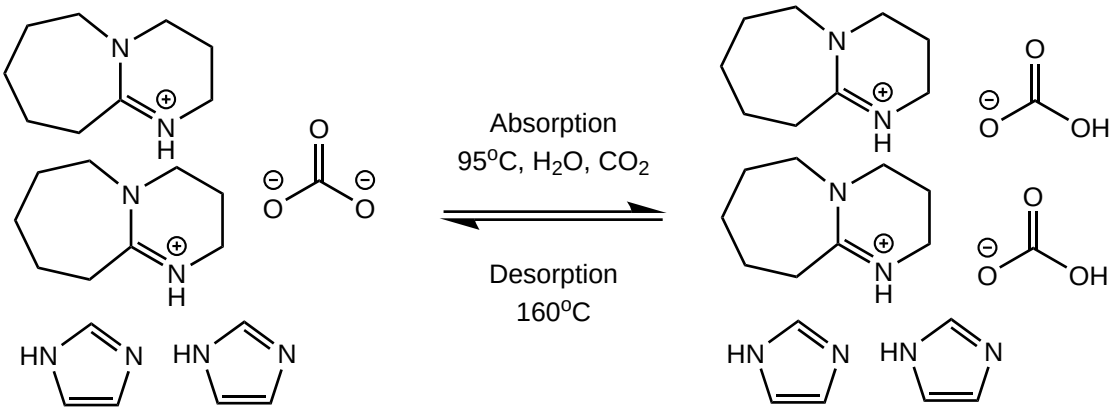

Figure 4.28: Repeated absorption-desorption cycles of [DBUH][Im].

Clearly there is still room for improvement in the process design, most notably the 160℃ regeneration temperature which will slowly degrade the IL over time as shown from the corrosion study. Additionally, imidazole is thought to be a bystander in the process, where it has a net negative effect on the g·kg^{-1}/g·$^{-1}$ capacity. Perhaps its presence forms a eutectic which improves fluidity as imidazole is a common component in eutectic solvent formulation [353]. There are some reports that aqueous imidazole solutions can bind CO_2, due to being amphoteric, it can capture CO_2 through a ternary mechanism involving water and resulting in bicarbonate formation [354]. In the case of wet [DBUH][Im] at elevated temperatures however, it seems unlikely to be contributing to CO_2 absorption as much as other components of the mixture and due to being neutral upon protonation, may be sufficiently volatile to contaminate the produced CO_2 gas stream.

Any sufficiently low melting carbonate salt with a suitable thermally stable cation should be suitable for this type of process. Several examples exist in the literature for bicarbonate ILs where they're either used as synthetic precursors [355, 356], stabilisers for high explosives [343] and for CO_2 conversion [357]. A similar example of a bicarbonate IL was reported by Zhao *et al.* where they use an imidazolium

bicarbonate IL as a dehydrating agent to deprotonate water and form a similar carbene-CO_2 adduct reported by Holbrey *et al.* [241], the adduct activates the CO_2 so that is can then be converted into dimethyl carbonate [358]. Unfortunately, no previous reports have been found on divalent carbonate ILs, and although it was never isolated, $[DBUH]_2[CO_3]$ may be the first of this class of ILs.

A summary of the pros and cons of this process are outlined below:

Benefits

1. High temperature and humid conditions significantly reduce the viscosity of ILs and increases the kinetics of absorption/desorption, solving two of the biggest problems in IL carbon capture.

2. Comparable working CO_2 capacity to aqueous amines in terms of $g \cdot kg^{-1}$.

3. Specific heat capacity is estimated to be half that of water.

4. No need to dry the gas stream or to cool it below 95°C.

5. Low volatility of IL components limits contamination of produced gas streams (although neutral imidazole may also contamine the CO_2 stream in this case).

Drawbacks

1. If the system is ever turned off, CO_2 rich [DBUH][Im] may begin to solidify in the system and require heating to liquefy, although this may be solved by pumping all of the IL in the regeneration tank prior to shutdown so it can be re-melted.

2. Effect of other impurities such as H_2S, SOx, NOx etc. are unknown.

3. Relatively expensive starting materials compared to aqueous amines.

4. Higher operational thermal energy demands than other ILs but still less than aqueous amines (this can come from reused low grade heat depending on the site).

4.6 Conclusions

While the experimental methods were admittedly rudimentary, the idea is still viable that high temperature, TSA cycling may mitigate the two biggest shortcomings in chemisorbant ILs: their high viscosity, and the presence of water causing bicarbonate formation. Although the staring materials are more expensive, wet [DBUH][Im] has demonstrated a working capacity that is comparable to aqueous

amines with an estimated specific heat capacity approximately half that of the water and a smaller temperature swing between absorption and desorption temperatures. Additionally, this system is effective at high temperatures where conventional alkanolamines are too volatile, and under wet conditions were many reported ‘dry’ ILs are ineffective. Finally, this system was shown to be non-corrosive to 316 stainless steel and stable across six absorption cycles. There is undoubtedly room for improvement, but this shows that liquid carbonate based absorbents may be a viable material for carbon capture from flue gas.

4.7 Experimental

All chemicals were sourced from Sigma-Aldrich. CO_2 cylinders were supplied by BOC. TGA-MS was run on a Netzsch STA 449 F3 Jupiter simultaneous TGA-DTA/DSC that was coupled with a Netzsch QMS 403 Aeolos II mass sepc. TGA experiments were run at 5℃ per min under a simulant air stream of 80% N_2 and 20% O_2. All other methods were the same as previous chapters.

Synthesis of ILs

The general synthetic procedure for all of the PILs tested was the same. The 'acid' component (imidazole, 4-methylimidazole, phenol or 2-fluorophenol) was added to a round bottom flask and cooled in an ice bath. An equimolar amount of the 'base' component was then added dropwise with vigorous stirring.

Synthesis of [DBUH][Im]

Imidazole (13.4112 g, 0.197 mol) was added to a flask and cooled in an ice bath. DBU (30 mL, 0.197 mol) was then added slowly and the resulting mixture allowed to warm to room temperature and stirred for 24 h. The resulting clear yellow solution is then dried at 40℃ under reduced pressure overnight, yielding the product as clear yellow liquid in quantitative yields. ^{1}H NMR (400 MHz; CDCl3) δ 13.46 (1H, br s), 7.49 (1H, s), 6.90 (2H, s), 3.08 (6H, m), 2.26 (2H, br s), 1.66 (2H, quint), 1.50(4H, br s), 1.44(2H, br s). ^{13}C^{1}H NMR (100 MHz; CDCl3) δ 162.01, 135.07, 121.52, 77.16, 52.66, 48.08, 42.91, 36.19, 29.32, 28.03, 25.52, 21.93.

Synthesis of [N1888][PhO]

Sodium hydroxide (6.0045 g, 0.15 mol) and phenol (11.7855 g, 0.125 mol) were added to a beaker and dissolved in ice water (300 mL). Aliquat 336 ([N1888]Cl) was then dissolved in DCM (300 mL) and the two solutions were shaken in a separating funnel. The organic layer was separated, washed with DI water (2 x 200 mL), dried with magnesium sulfate and the solvent removed under reduced pressure to yield a clear yellow liquid in near quantitative yields. ^{1}H NMR (400 MHz; DMSO-d_6) δ 7.02 (2H, t, *J* = 7.6 Hz), 6.80, (2H, d, *J* = 7.6 hz), 6.57 (1H, t, *J* = 7.2 Hz), 3.22 (6H, m), 2.97, (3H, s), 1.58 (7H, m), 1.26 (41H, m), 0.87 (10H, m). ^{13}C^{1}H NMR (100 MHz; DMSO-d_6) δ 159.93, 128.65, 116.37, 115.96, 60.62, 60.34, 47.41, 39.52, 32.48, 31.19, 31.08, 28.80, 28.70, 28.58, 28.36, 25.70, 25.45, 21.99, 21.95, 21.28, 13.80.

Synthesis of [DBUH][PhO]

Phenol (31.4600 g, 0.3343 mol) was added to round bottom flask and placed in an ice bath to cool. DBU (50 mL, 0.03343 mol) was then added dropwise to the flask with vigorous stirring. Once the addition was complete, the mixture was then dried under reduced pressure overnight to yield the clear pale yellow liquid product in quantitative yields. ^{1}H NMR (400 MHz; CDCl3) δ 13.26 (1H, br s), 7.12 (2H, m), 6.82 (2H, m), 6.66 (1H, t, J = 7.2 Hz), 3.28 (2H, m), 3.23 (4H, t, J = 6.2 Hz), 2.47 (2H, m), 1.82 (2H, m), 1.60 (6H, m). ^{13}C^{1}H NMR (100 MHz; CDCl3) δ 163.2, 160.8, 129.3, 117.0, 116.7, 53.2, 48.4, 41.8, 35.0, 29.6, 28.1, 25.4, 21.7.

Synthesis of [TMGH][PhO]

Phenol (37.5069 g, 0.3985 mol) was added to round bottom flask and placed in an ice bath to cool. 1,1,3,3-Tetramethylguanidine (50 mL, 0.3985 mol) was then added dropwise to the flask with vigorous stirring. Once the addition was complete, the mixture was then dried under reduced pressure overnight to yield the clear pale yellow liquid product in quantitative yields. ^{1}H NMR (400 MHz; CDCl3) δ 7.08 (2H, t), 6.79 (2H, d), 6.68 (1H, t), 2.69 (12H, s). ^{13}C^{1}H NMR (100 MHz; CDCl3) δ 165.71, 157.33, 128.36, 117.56, 115.04, 38.27.

Synthesis of [DMAPAH][2-FPhO]

N,N-Dimethylaminopropylamine (50 mL, 0.3921 mol) was added to a round bottom flask and placed in an ice bath to cool. 2-Fluorophenol (35 mL, 0.3921 mol) was then added dropwise which produced white fumes so the addition was slowed substantially. The product was then obtained as a clear dark yellow liquid in a quantitative yield. ^{1}H NMR (400 MHz; DMSO-d_6) δ 7.03 (1H, m), 6.89 (2H, m), 6.63 (1H m), 5.07 (3H, br s), 2.58 (2H, t,J = 7.2 Hz), 2.21 (2H, t, J = 7.2 Hz), 1.49 (2H, quint, J = 6.8 Hz). ^{13}C^{1}H NMR (100 MHz; DMSO-d_6) δ 153.01, 150.61, 147.03, 124.40, 124.37, 118.28, 117.39, 115.71, 115.53, 56.89, 45.11, 30.10.

Synthesis of [TMGH][4-MeIm]

4-Methylimidazole (32.7026 g, 0.3983 mol) was added to round bottom flask and placed in an ice bath to cool. 1,1,3,3-Tetramethylguanidine (50 mL, 0.3985 mol) was then added dropwise to the flask with vigorous stirring. Once the addition was complete, the mixture was then dried under reduced pressure overnight to yield the clear pale yellow liquid product in quantitative yields. ^{1}H NMR (400 MHz; DMSO-d_6) δ 8.59 (2H, br s), 7.63 (1H, s), 7.01 (2H, s), 2.62 (12H, s). ^{13}C^{1}H NMR (100 MHz; DMSO-d_6) δ 166.14, 135.09, 121.62, 39.01.

Synthesis of [TMGH][Im]

Imidazole (37.9815 g, 0.5579 mol) was added to round bottom flask and placed in an ice bath to cool. 1,1,3,3-Tetramethylguanidine (70 mL, 0.5579 mol) was then added dropwise to the flask with vigorous stirring. Once the addition was complete, the mixture was then dried under reduced pressure overnight to yield the clear yellow liquid product in quantitative yields. ^{1}H NMR (400 MHz; DMSO-d_6) δ 7.45 (1H, s), 6.67 (1H, s), 2.61 (12H, s), 2.12 (3H, s). ^{13}C^{1}H NMR (100 MHz; DMSO-d_6) δ 166.79, 134.25, 118.13, 39.00, 11.66.

Absorption experiments

For initial screening studies of dry ILs, 5 g of each IL was added to a tall (*ca.* 30 cm) measuring cylinder which was sealed with parafilm and placed in a water bath at a set temperature. Pure CO_2 was then gently bubbled through a long needle into the sample which vented through a small needle at the top of the cylinder. A schematic of this is shown in figure 4.29. After 5 minute intervals the samples were then removed, dried with paper towels and weighed until no further weight increase was measured to determine the CO_2 uptake. For samples where water has been added to simulate the effects of humid gas streams, the same method is used but with the addition of water to the IL before being placed in the water bath. For repeated cycles, the desired amount of water was replenished between cycles.

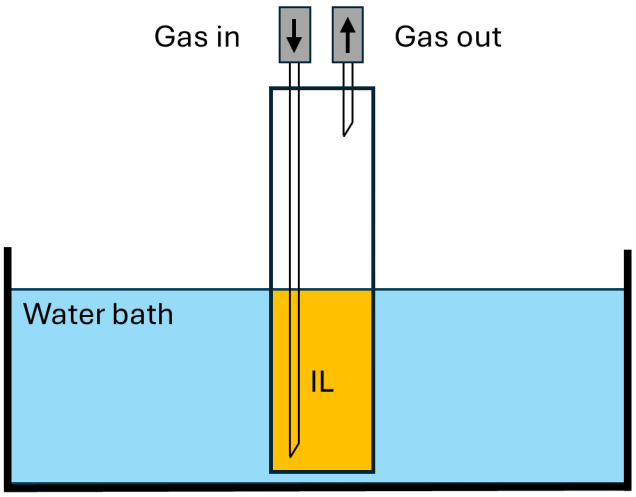

Figure 4.29: Diagram of the method used to determine CO_2 absorption capacities of the ILs during the screening study.

Assumptions

For dry samples of IL, no assumptions need made. If there is a measured increase in mass upon bubbling CO_2 through the IL then all of that gained mass can be

attributed to either chemically or physically absorbed CO_2. Similarly, during desorption, if there is a measured mass loss then this is ascribed to the desorption of CO_2 up to the decomposition temperature of the IL.

If there is water present then certain assumptions must be made. During absorption at low temperatures (*ca.* room temperature), there is assumed to be no mass loss of water during the absorption step. For absorption at higher temperatures, a control experiment was performed where an identical sample was bubbled with the same flow rate of nitrogen and this is used to account for loss of water during the course of the experiment. This is shown graphically in appendix figure 6.28 and the rate of water loss was found to be a steady rate of 0.0026 $g \cdot min^{-1}$

For the all desorption experiments in the presence of water, several assumptions were made and are listed below:

1. If there is water present in the sample, the CO_2 will be captured preferentially as bicarbonate, rather than the less stable carbamate/carbonate anions that forms via the nucleophilic attack of the IL anion on CO_2.

2. If there is less than excess water present, CO_2 will first be captured as bicarbonate until the water has been consumed, then residual IL can absorb more CO_2 via carbamate/carbonate formation. Additionally, upon desorption, CO_2 will be released from the decomposition of the carbamate/carbonate species, then from the bicarbonate.

3. If there is excess water, then this mass will be lost first, before any bicarbonate decomposition can occur.

4. The desorption of CO_2 when it is assumed to be captured as bicarbonate, will result in an equal molar loss of H_2O and CO_2.

Corrosion studies

316 Stainless steel tokens of *ca.* 1 mm thickness and 12.5 mm diameter were submerged in *ca.* 5 g of IL and kept in a conventional oven at either 95℃ or 150℃ for three weeks. The IL samples used were either neat [DBUH][Im] or [DBUH][Im] with 10wt% water added that had then been loaded with CO_2 via bubbling pure CO_2 through the sample using a needle for 15 mins The tokens were then rinsed with water and dried before being measured using vernier calipers to determine any decrease in token size, analysed by XRF to determine any metal leaching into the IL and finally analysed by SEM analysis to observe any surface changes.

5. Conclusions & Future Work

5.1 Conclusions

The initial aim of this research was to examine potential applications for ionic liquids in industrial pollution management. Initial research was focused on the removal of aqueous sulfate from competitive sources but this was later broadened to also include the separation of carbon dioxide from flue gas.

Chapter two was aimed at accessing the potential for ionic liquids to be used as hydrophobic liquid anion exchangers. Two commercially available ionic liquids, Cyphos® 101 and Aliquat® 336, as well as three prepared salts, $[HN_{888}]Cl$, $[P_{1888}]Cl$ and $[N_{2OH888}]Cl$, all of which mimic the functionality found in common solid anion exchange resins. All of these ionic liquids were found to form aqueous biphasic systems when in contact with an aqueous solution, absorbing significant amounts of water into the ionic liquid phase due to the presence of the hydrophilic chloride anion. In contact with an aqueous sulfate solution, all five will exchange chloride for sulfate, effectively extracting it from an aqueous phase. Cyphos® 101 was found to be the worst performing of the series while the other four all performed broadly similar with moderate degrees of sulfate extraction. The effects of sulfate concentration, phase volume ratio, competitive chloride and pH were all tested and finally $[HN_{888}]Cl$ was shown to be reusable across four cycles. The driving force for the ion exchange process is unclear but comparing to recent literature, it seems plausible that the divalent sulfate is better able to structure the ionic liquid phase into regions of high and low charge density when in contact with low ionic strength solutions whereas this segregation of domains is less well defined at higher ionic strengths.

Chapter three built on the work of chapter 2 and explored the use weak (thio)urea anion receptors as extractants to enhance the sulfate removal that was demonstrated in chapter two by the two commercially available ionic liquids; Cyphos® 101 and Aliquat® 336. The receptors were all found to be highly soluble in the ionic liquids and their addition resulted in the exclusion of water from the the ionic liquids and a subsequent increase in viscosity of the ionic liquid phase. This is thought to be from binding of the receptors to the chloride anions, displacing some of the chloride's hydration shell. Binding studies showed that five of the six receptors would

bind stronger to chloride than they would to sulfate when in a highly polar DMSO solvent. However, this selectivity appeared to reverse in the ionic liquid phase as in every case, the addition of a receptor caused an increase in aqueous sulfate extraction.

Chapter four shifted focus to the development of a chemisorbant ionic liquid process for the removal of CO_2 from flue gas. The only limitation that was set out was that the system must work under humid conditions. Initially, a small series of ionic liquids were tested for CO_2 absorption under dry conditions and with the addition of water to mimic the effects of humidity. From this study, [DBUH][Im] was shown as a potential candidate for a high temperature absorption-desorption cycle under humid conditions. Further absorption-desorption experiments and spectroscopic analysis showed that in the presence of water, CO_2 was absorbed in the form of bicarbonate. Desorption from this point then causes two bicarbonate anions to decompose into CO_2, H_2O and divalent carbonate, successive absorption-desorption cycles then swing between carbonate and bicarbonate species. The use of high temperatures and humid conditions significantly reduce the viscosity of [DBUH][Im] and increases the kinetics of absorption/desorption, solving two of the biggest problems in ionic liquid carbon capture Finally, a chemisorbant flue gas capture process was designed based on this work which was been submitted for filing at the US patent office by Chevron.

5.2 Future Work

Potential places for future work by chapter are listed below.

1. Ionic Liquid Chlorides as Liquid Anion Exchangers
    (a) Development of dications or polycations
    (b) Use of different anions in place of chloride
    (c) Extraction of other anions such as carbonate, phosphate, nitrate etc.
    (d) Solubility of ILs in water as a function of temperature
2. Synergised Anion Exchange and Recognition
    (a) Binding study of receptors in an IL phase
    (b) Ternary phase diagram of receptor **3**-water-IL system
    (c) Analysis of binding strength of sulfate and chloride in DMSO vs sulfate extraction efficiency
3. Ionic Liquids as Chemisorbants for Flue Gas Carbon Capture

(a) Closed system gas uptake measurements to measure more accurate absorption vs temperature isotherms

(b) Physical characterisation of neat [DBUH][HCO_3] and [DBUH]$_2$[CO_3] to potentially remove the need for imidazole

(c) Testing other cations such as $[P_{4444}]^+$ or $[P_{66614}]^+$ with the carbonate anion to test carbonate-bicarbonate cycling

6. Appendix

Ionic Liquid Chlorides as Liquid Anion Exchangers

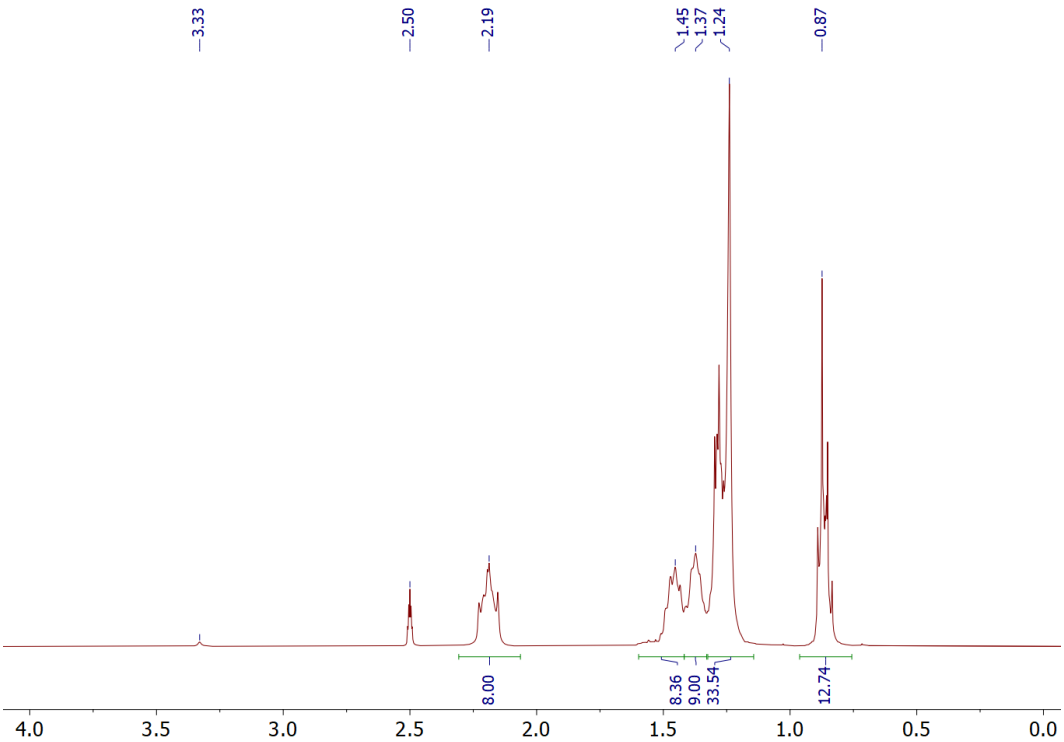

Figure 6.1: ^{1}H NMR spectra of Cyphos® 101 in DMSO-d_6.

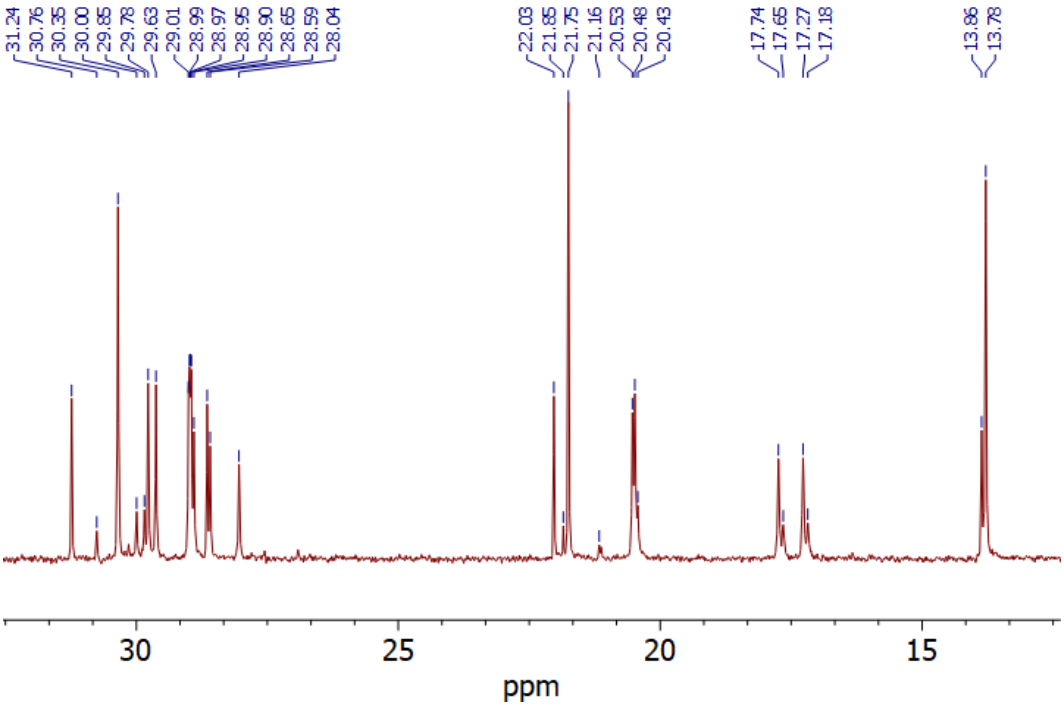

Figure 6.2: ^{13}C NMR spectra of Cyphos® 101 in DMSO-d_6.

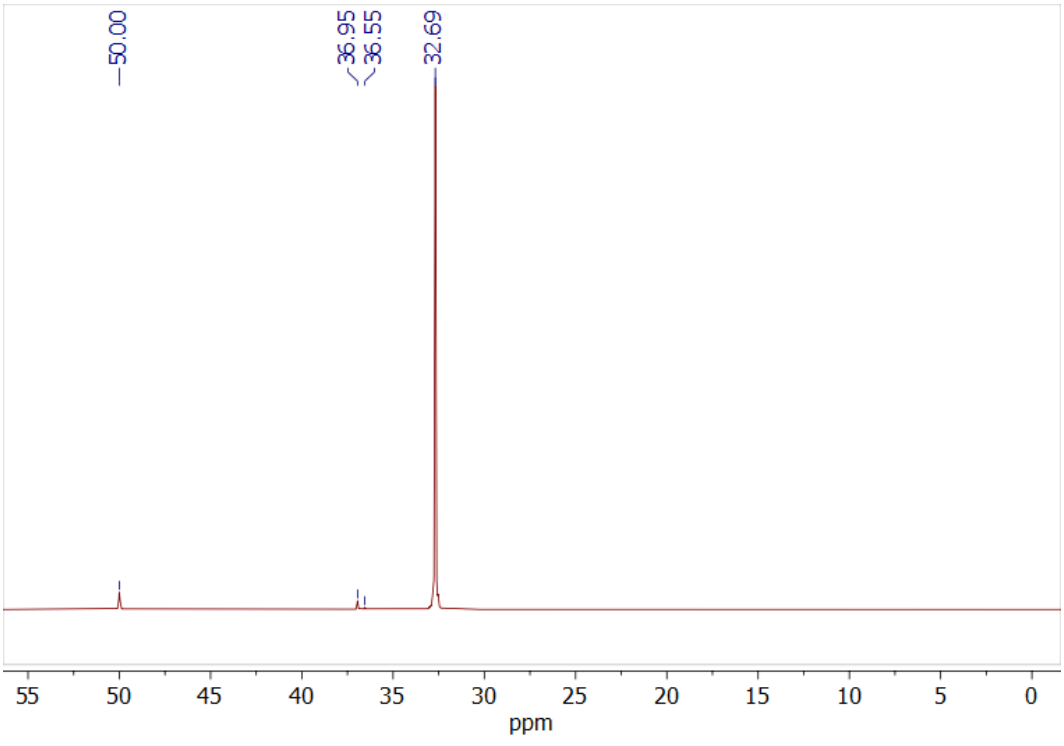

Figure 6.3: ^{31}P NMR spectra of Cyphos® 101 in DMSO-d_6.

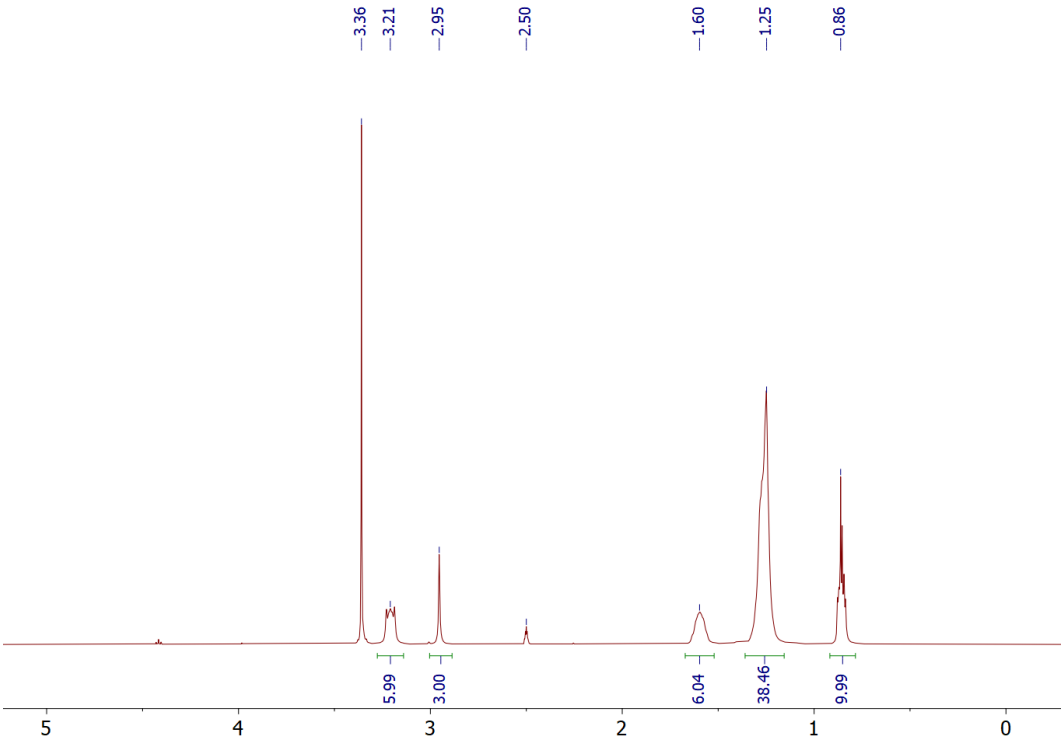

Figure 6.4: ^{1}H NMR spectra of Cyphos® 101 in DMSO-d_6.

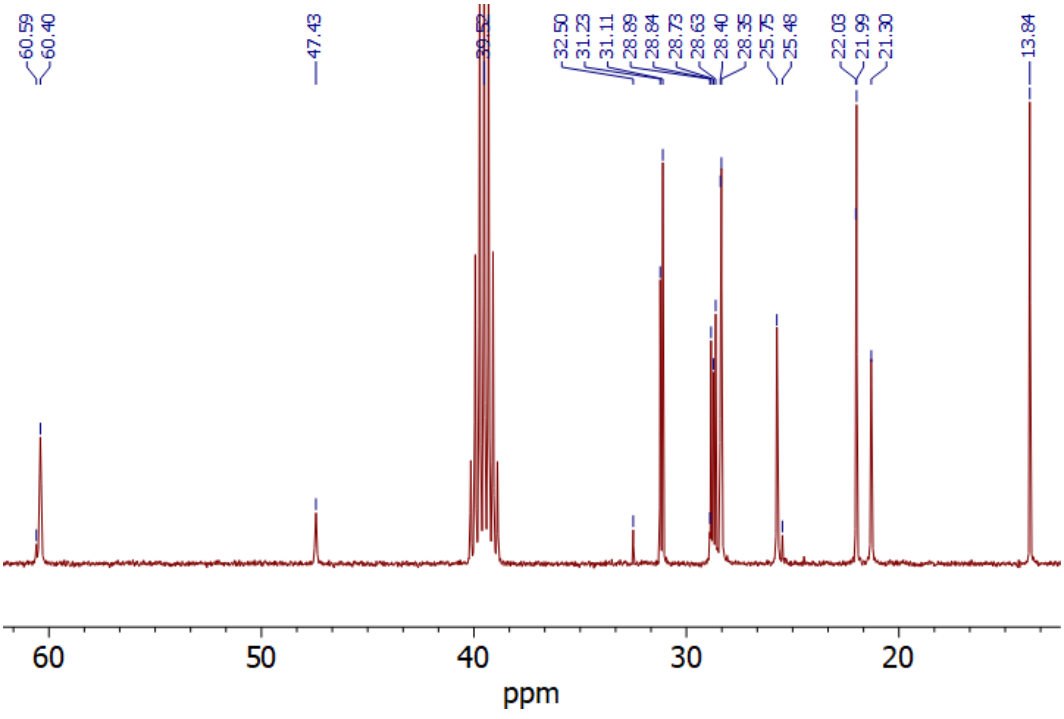

Figure 6.5: ^{13}C NMR spectra of Aliquat® 336 in DMSO-d_6.

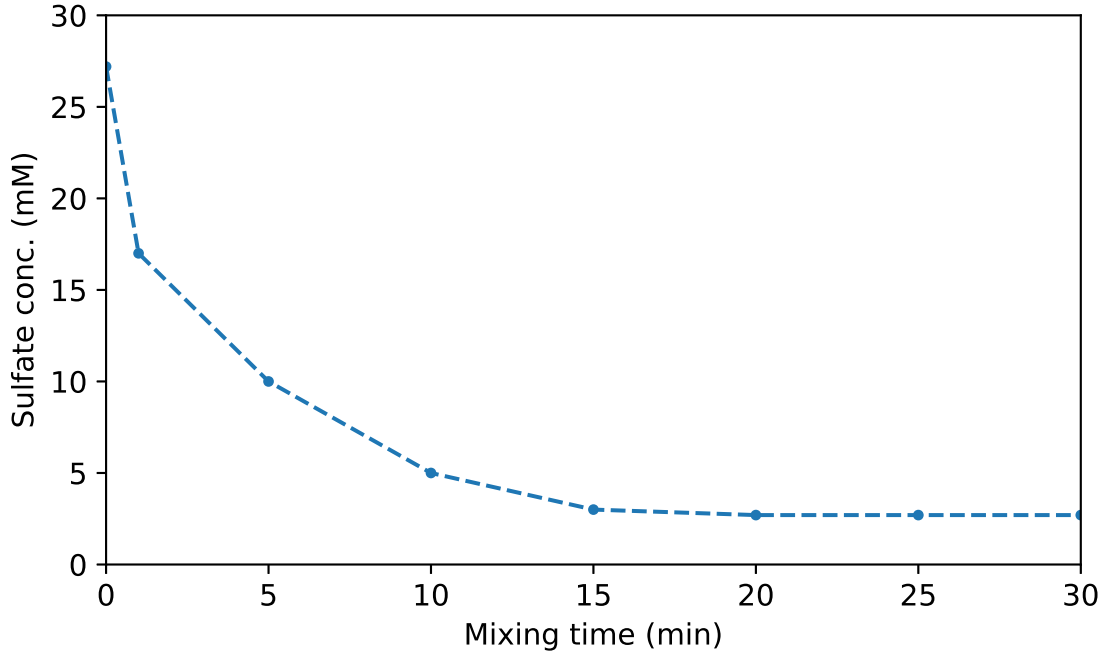

Figure 6.6: Sulfate concentration as a function of roller mixing time with $[P_{66614}]Cl$ using a phase volume ratio of 0.5. Data collected for times up to 24 hours. This analysis was performed on an inaccurate calibration so absolute sulfate concentration values are incorrect but time taken to reach equilibrium will remain the same.

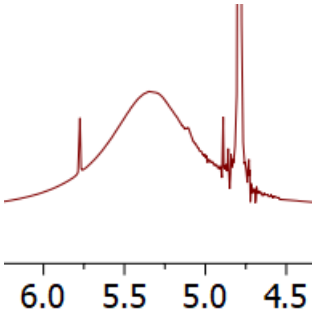

Figure 6.7: Zoomed in neat ^{1}H NMR of $[HN_{888}]Cl$ showing the saturated water peak.

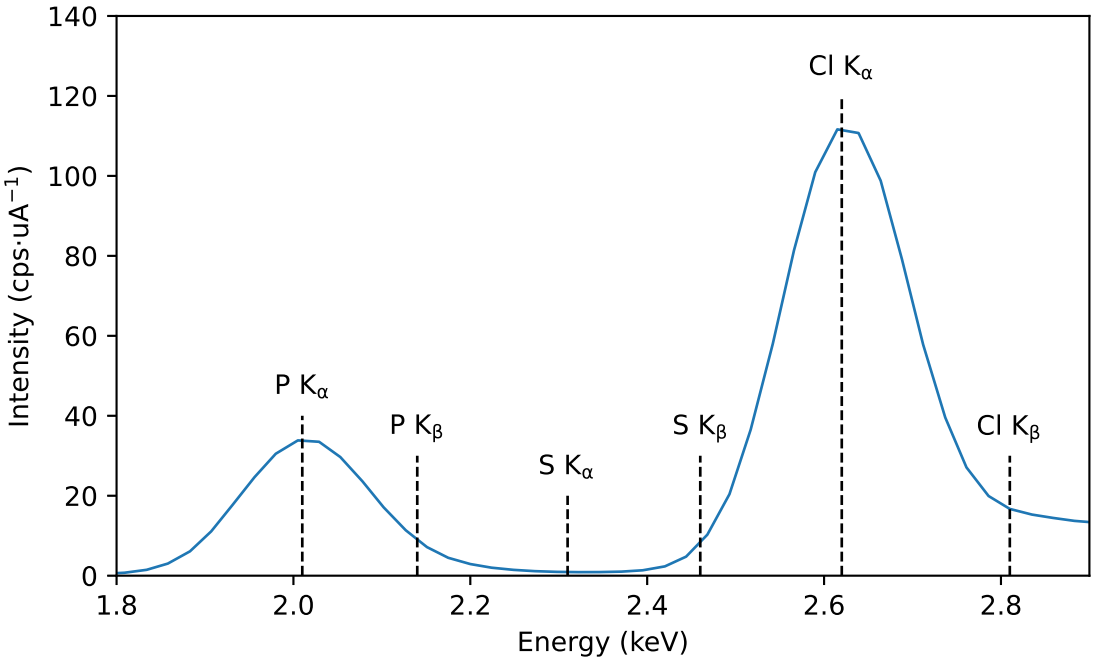

Figure 6.8: ED-XRD spectra of water saturated Cyphos® 101 showing the relevant phosphorus, sulfur and chlorine peaks.

Table 6.1: Optimized values from non-liner fitting to 4 significant figures.

	a	*b*	*c*	*d*
Cyphos® 101	91.62	−0.021 98	12.34	0.006 004
Aliquat® 336	110.9	−0.006 927	−12.69	−0.1142
$[HN_{888}]Cl$	108.2	−0.006 200	−21.57	−0.1100
$[P_{1888}]Cl$	105.3	−0.006 038	−3.396	−0.045 75
$[N_{2OH888}]Cl$	111.3	−0.006 567	−13.57	−0.1135
Amberlite® IRA-410	104.9	−0.001 602	−15.96	−0.057 49

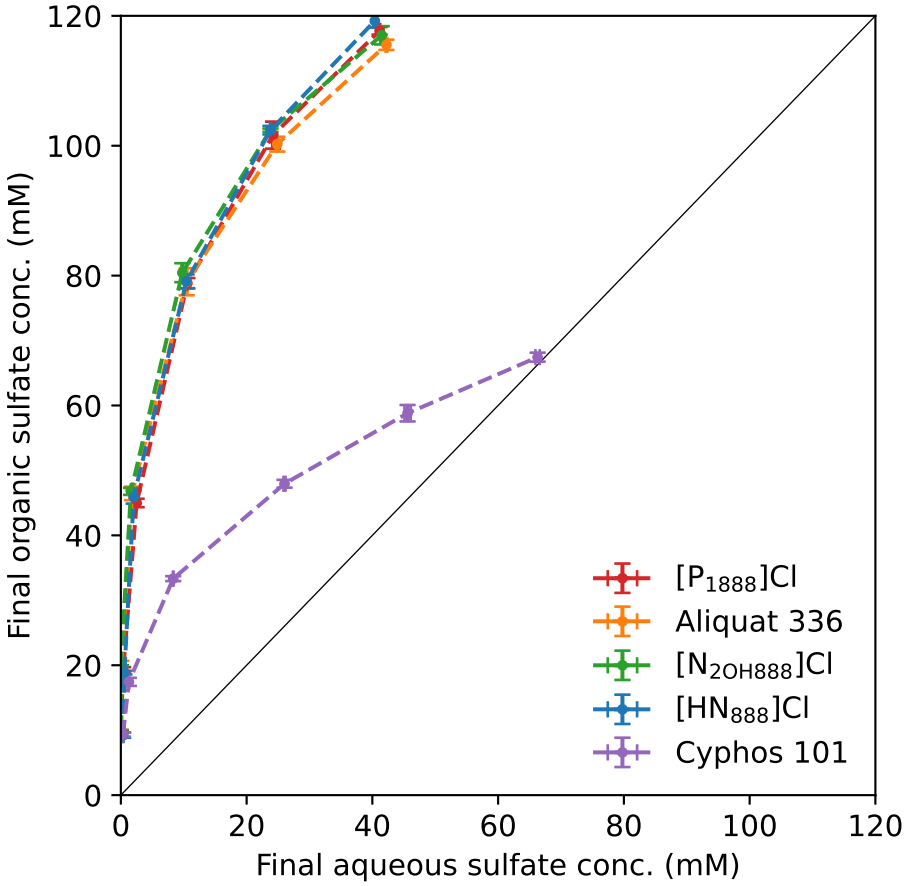

Figure 6.9: Plot of the equilibrium concentration of sulfate between the aqueous and organic phases.

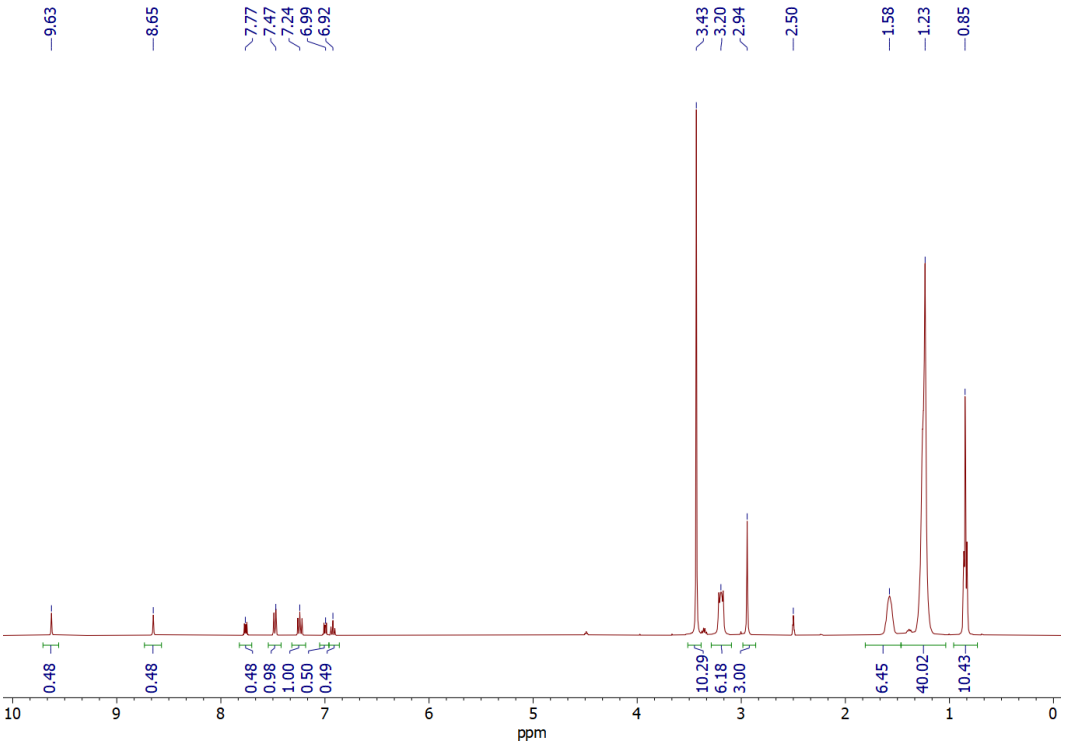

Figure 6.10: ^{1}H NMR spectra of **3** and water saturated Aliquat® 336 in DMSO-d_6. Integrals normalised to the ammonium methyl group at 2.94 ppm.

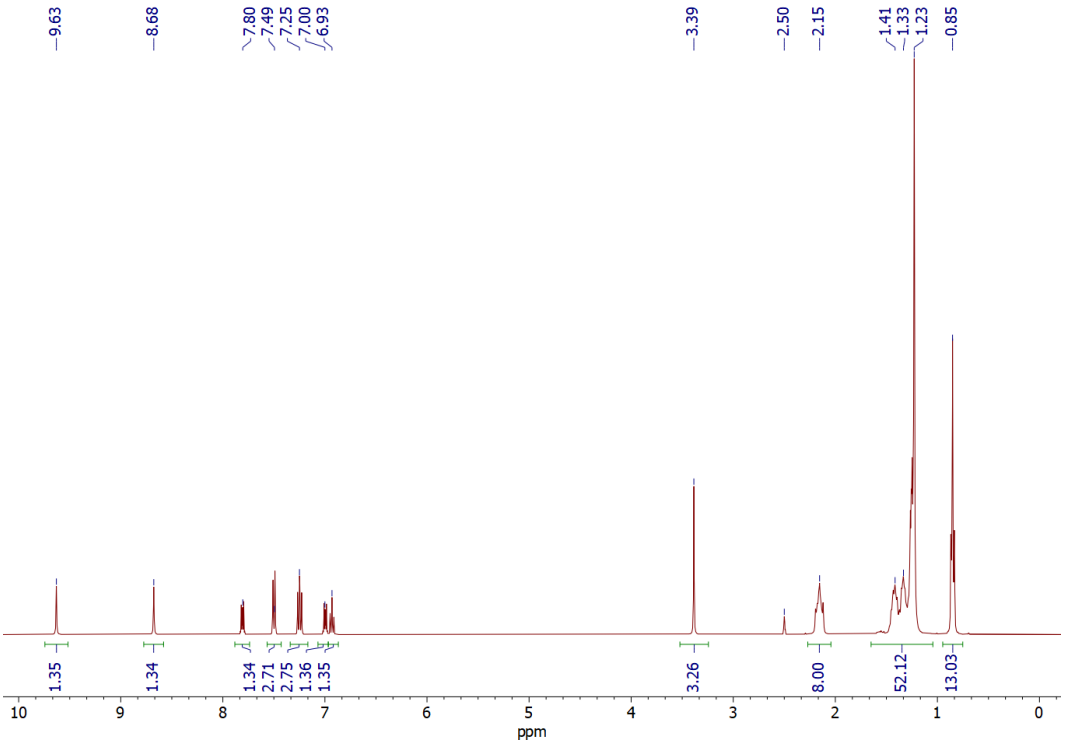

Figure 6.11: ^{1}H NMR spectra of **3** and water saturated Cyphos® 101 in DMSO-d_6. Integrals normalised to the four methylene CH_2's at 2.15 ppm.

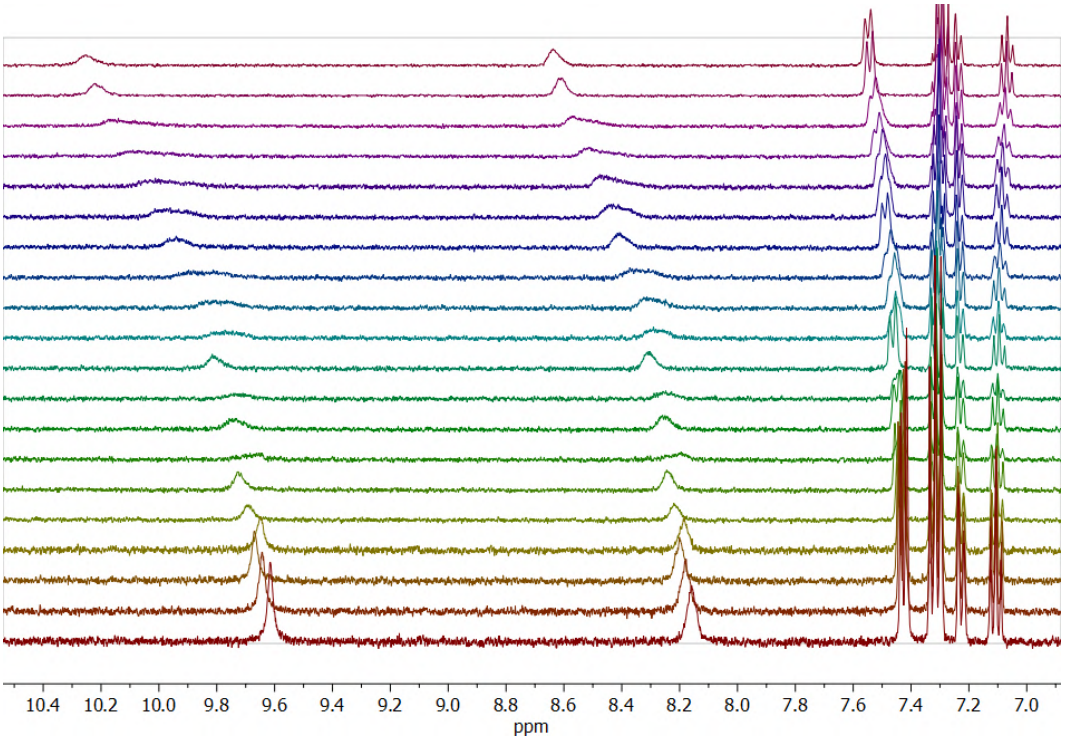

Figure 6.12: Receptor **2** at 1 mM in DMSO-d_6, with increasing concentrations of tetrapropylammonium chloride up to 45 mM.

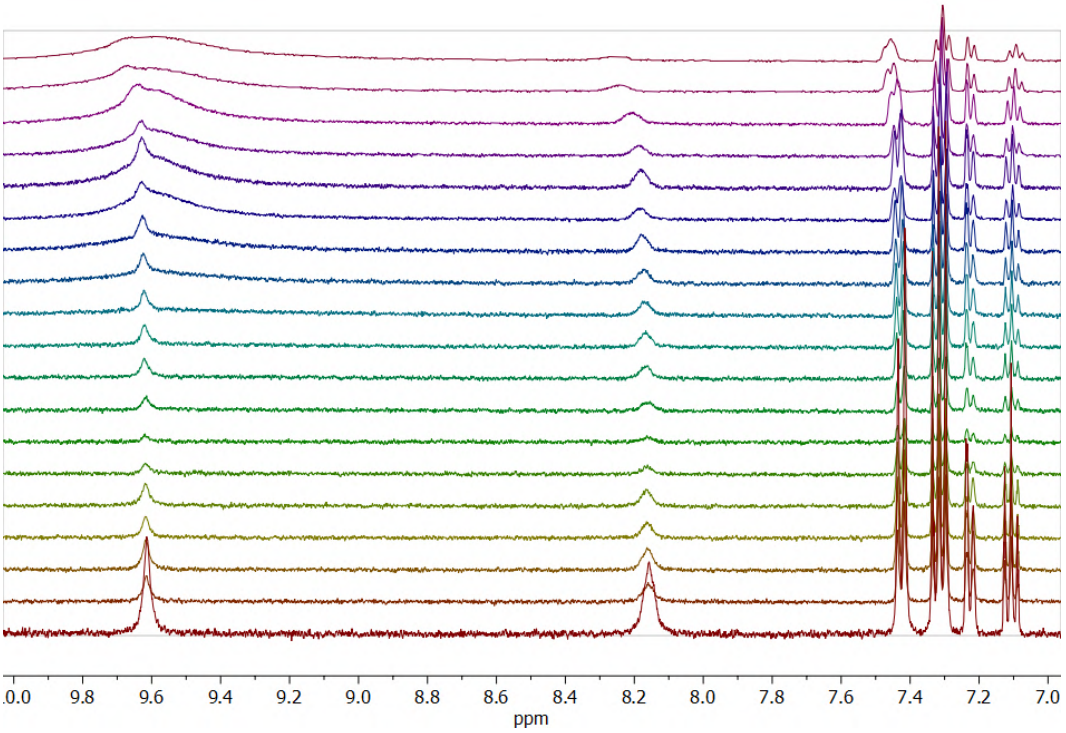

Figure 6.13: Receptor **2** at 1 mM in DMSO-d_6, with increasing concentrations of bis(tetrabutylammonium) sulfate up to 45 mM.

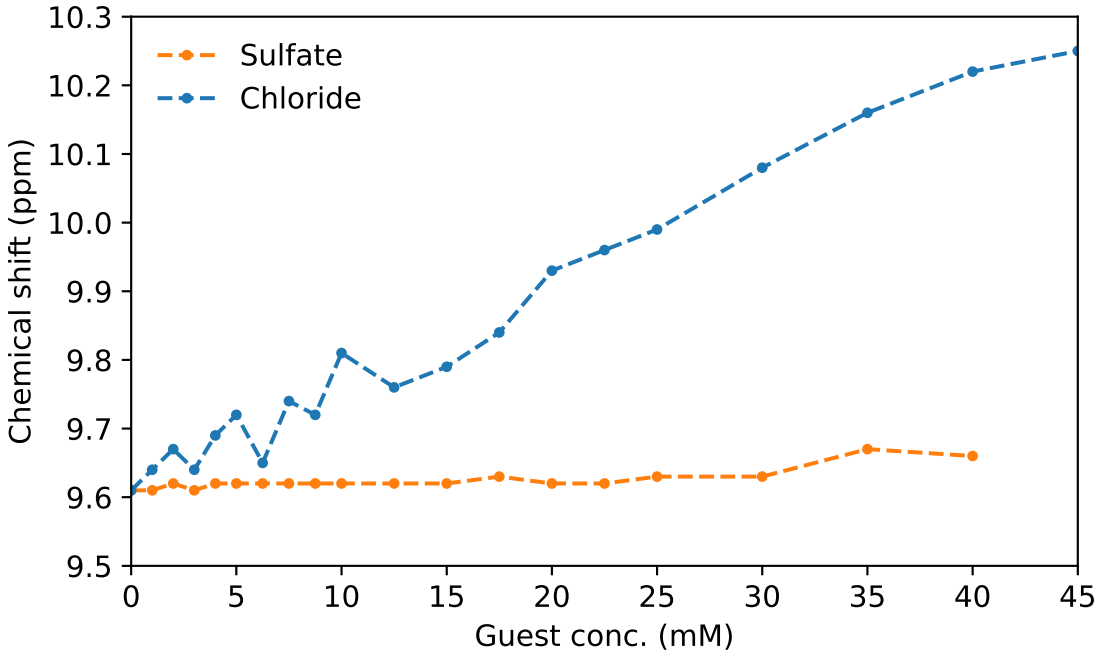

Figure 6.14: Change in chemical shift of the N−H signals in receptor **2** (at 1 mM) with increasing sulfate or chloride concentration.

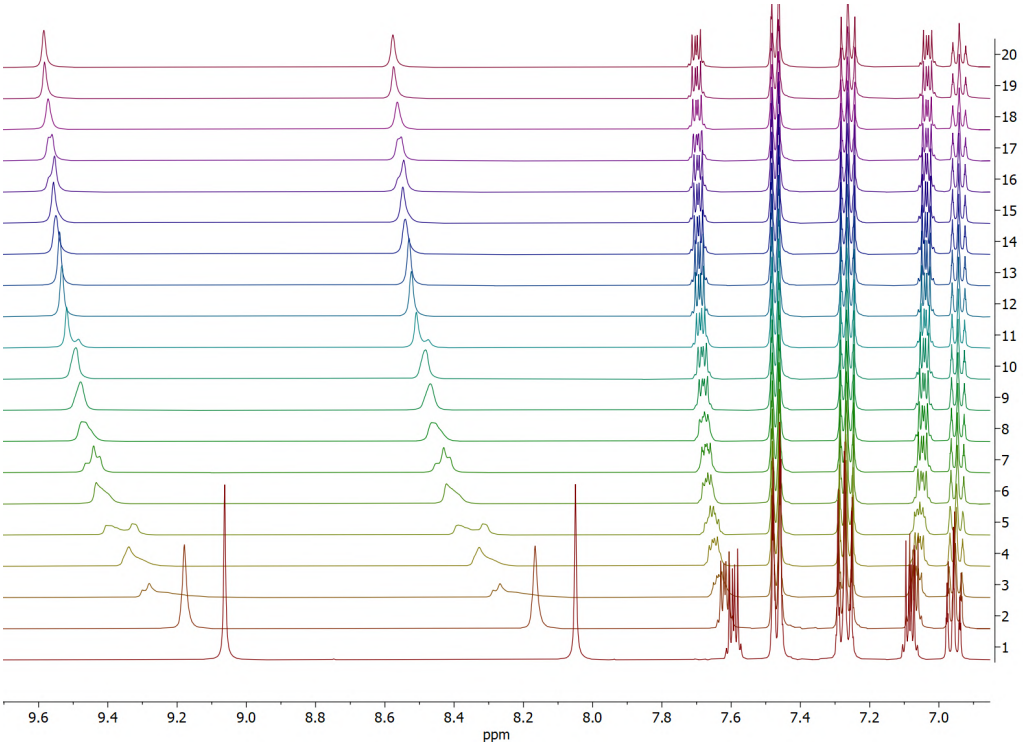

Figure 6.15: Receptor **3** at 10 mM in DMSO-d_6, with increasing concentrations of tetrapropylammonium chloride up to 65 mM.

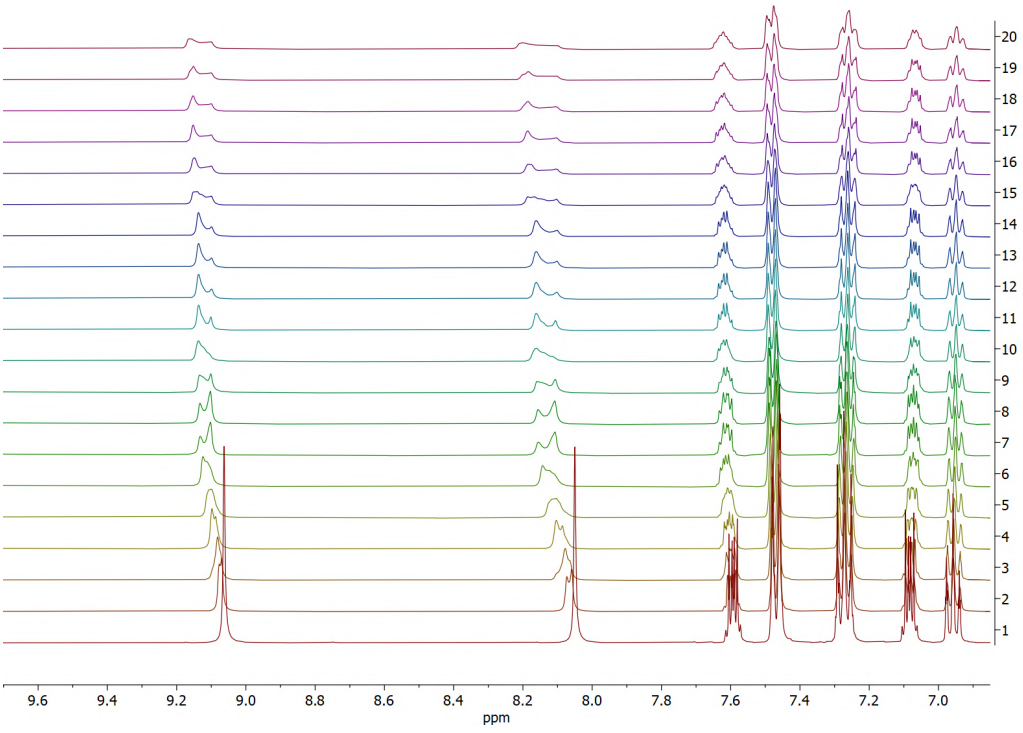

Figure 6.16: Receptor **3** at 10 mM in DMSO-d_6, with increasing concentrations of bis(tetrabutylammonium) sulfate up to 65 mM.

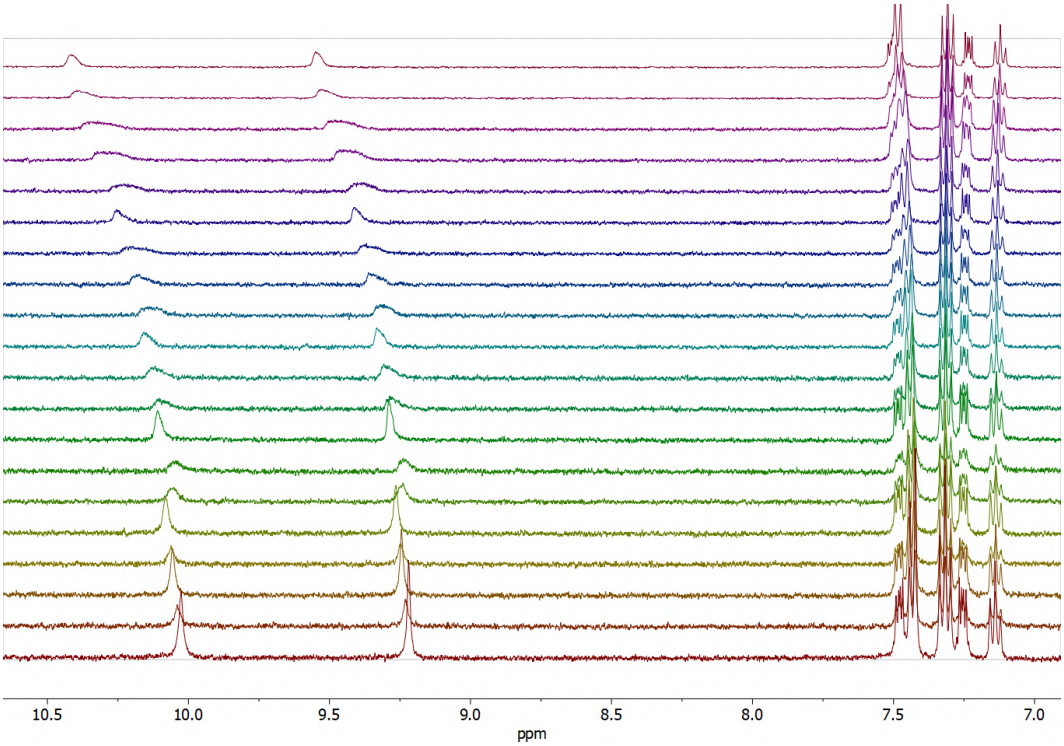

Figure 6.17: Receptor **4** at 1 mM in DMSO-d_6, with increasing concentrations of tetrapropylammonium chloride up to 45 mM.

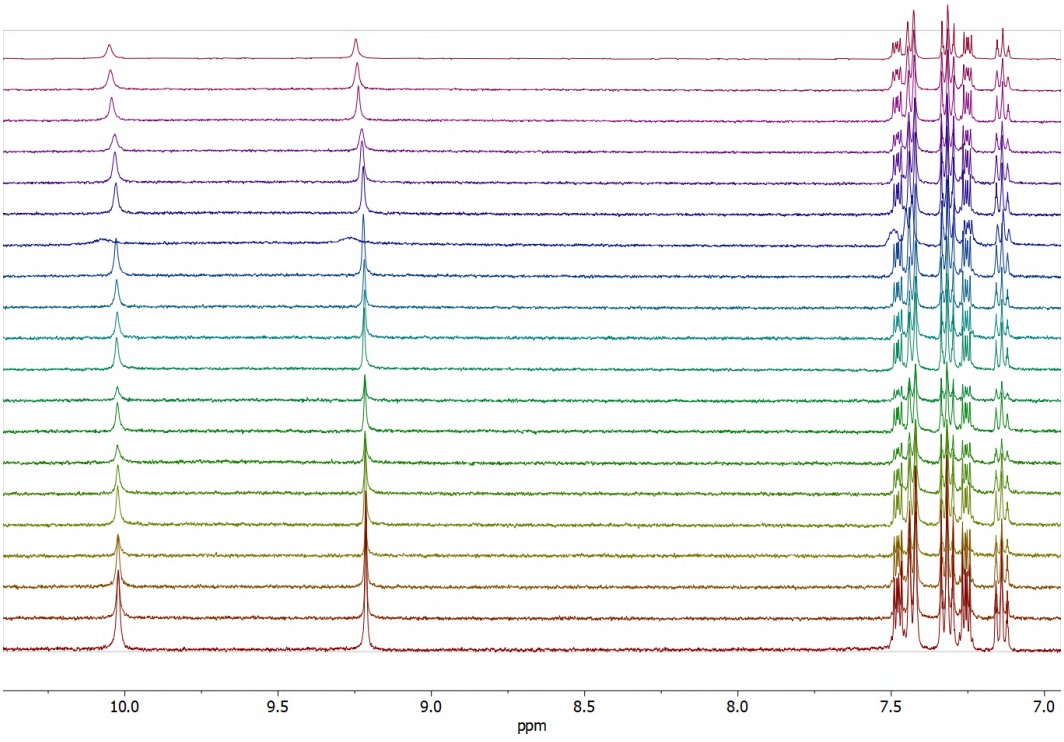

Figure 6.18: Receptor **4** at 1 mM in DMSO-d_6, with increasing concentrations of tetrabutylammonium hydrogen sulfate up to 45 mM.

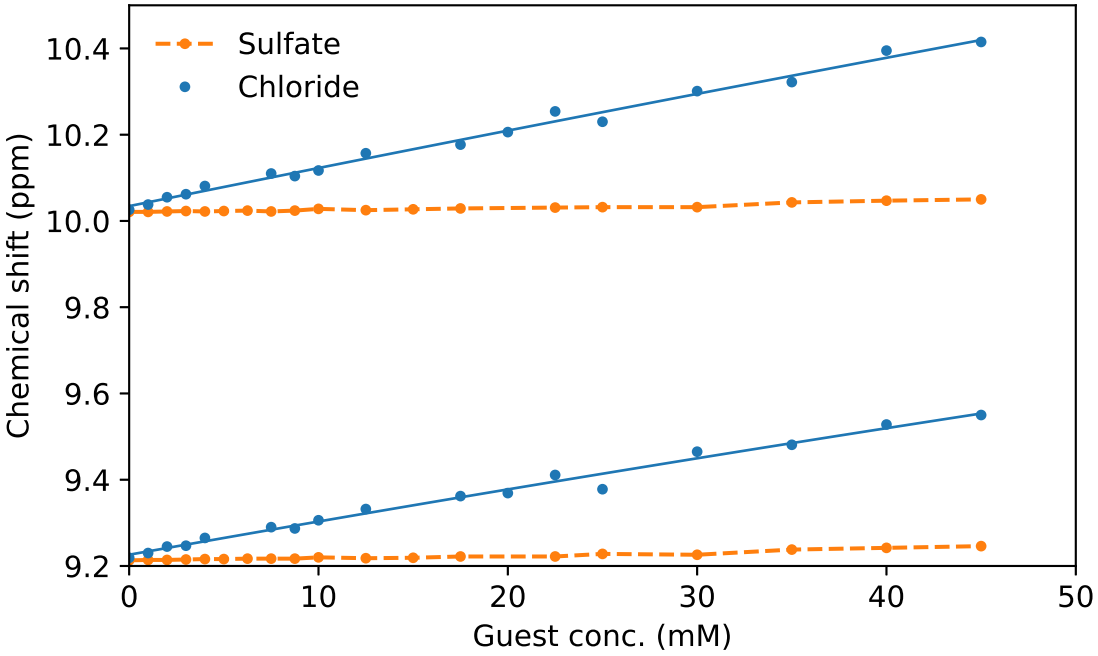

Figure 6.19: Change in chemical shift of the N−H signals in receptor **4** (at 1 mM) with increasing sulfate or chloride concentration.

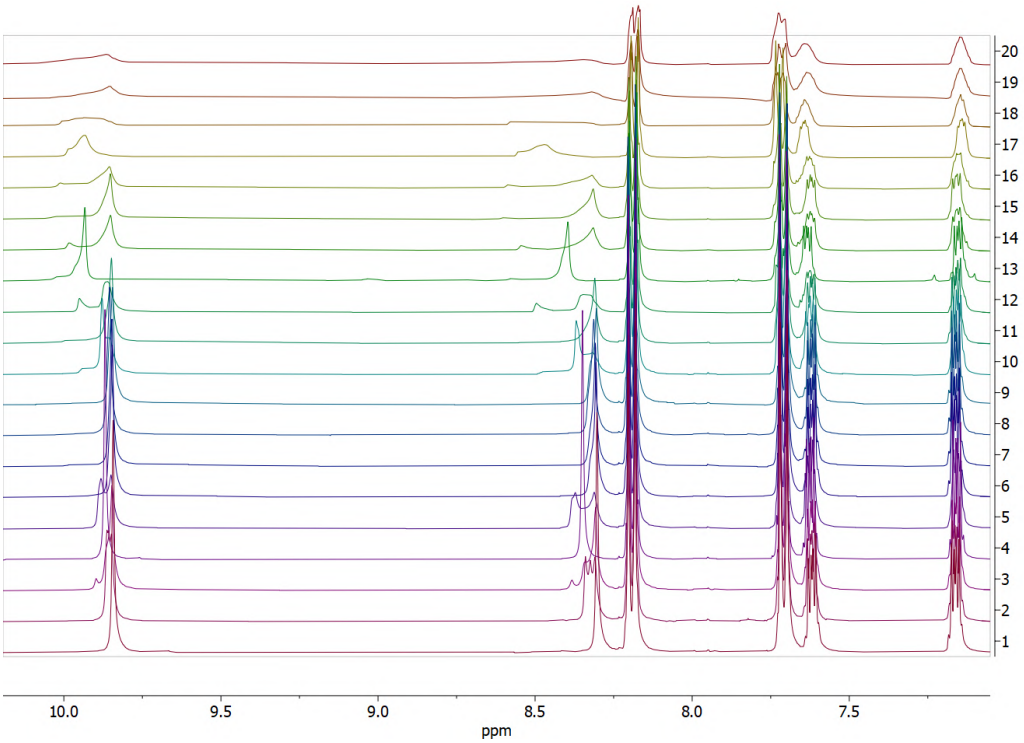

Figure 6.20: Receptor **5** at 1 mM in DMSO-d_6, with increasing concentrations of bis(tetrabutylammonium) sulfate up to 45 mM.

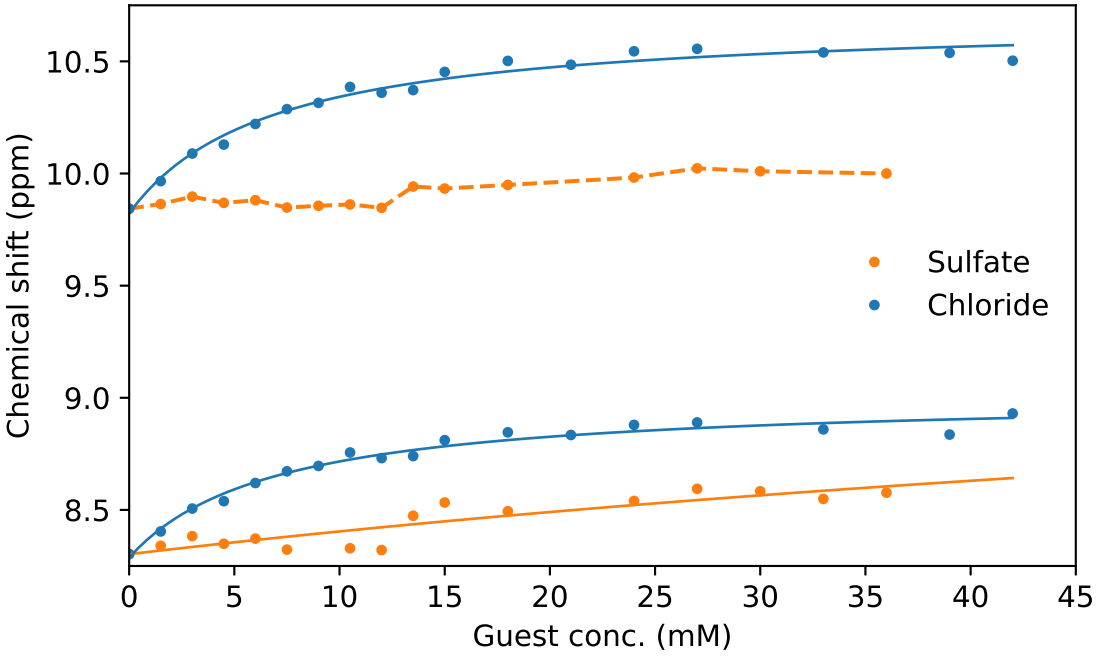

Figure 6.21: Change in chemical shift of the N−H signals in receptor **5** (at 10 mM) with increasing sulfate or chloride concentration.

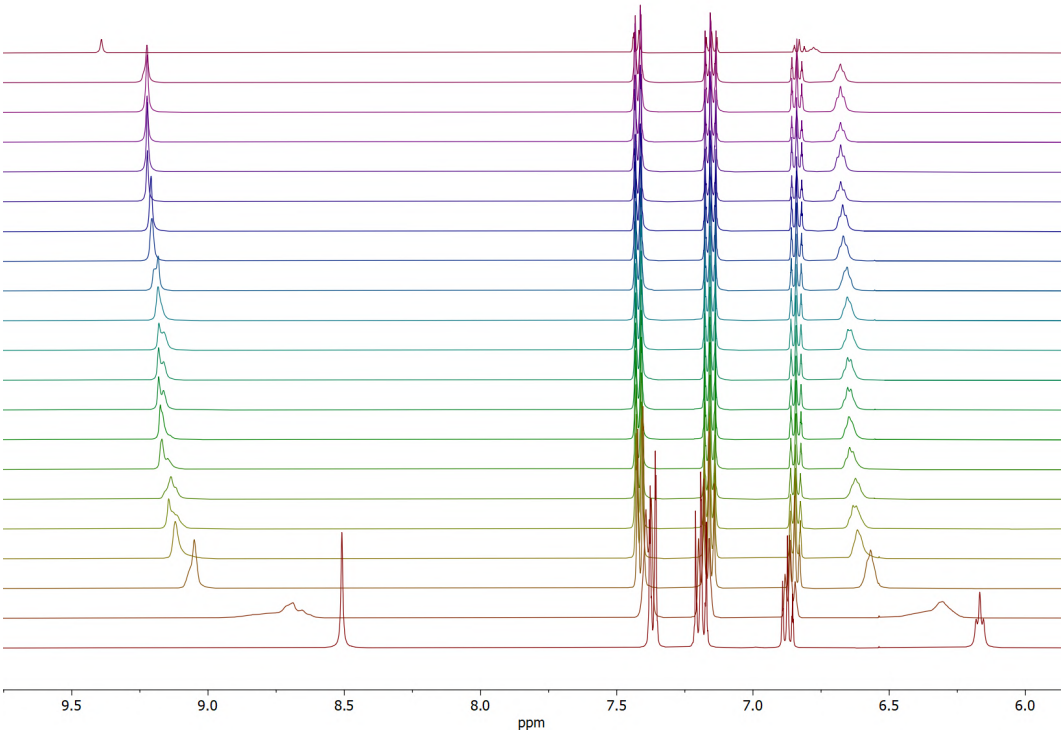

Figure 6.22: Receptor **6** at 1 mM in DMSO-d_6, with increasing concentrations of tetrapropylammonium chloride up to 45 mM.

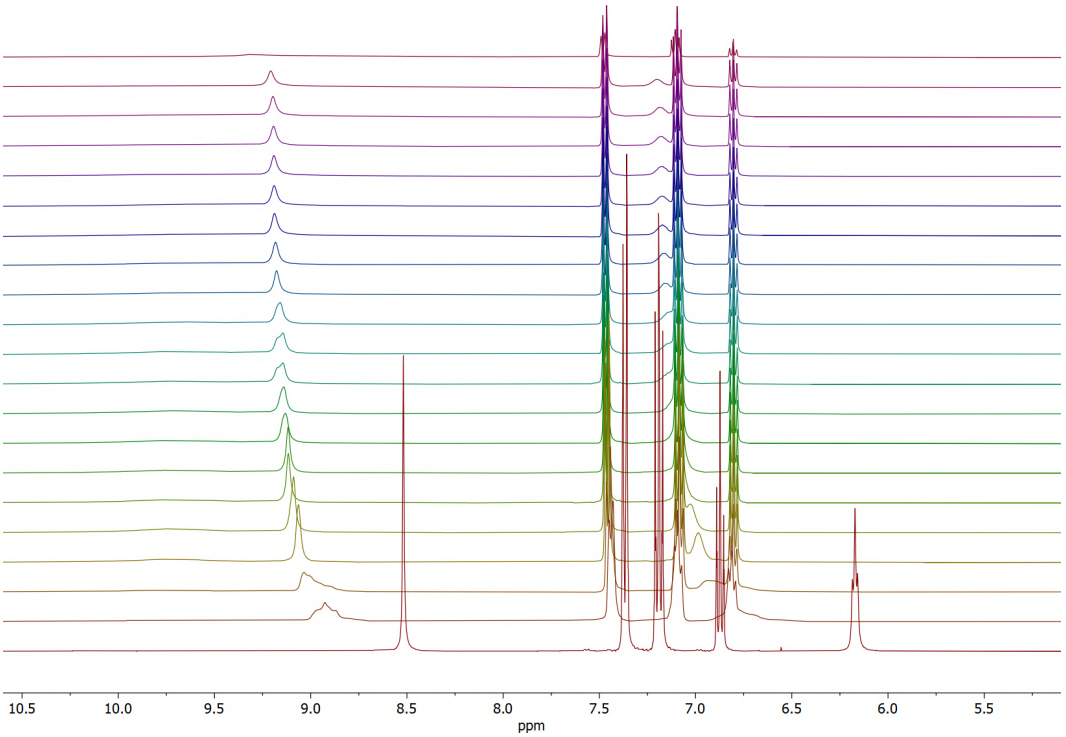

Figure 6.23: Receptor **6** at 1 mM in DMSO-d_6, with increasing concentrations of bis(tetrabutylammonium) sulfate up to 45 mM.

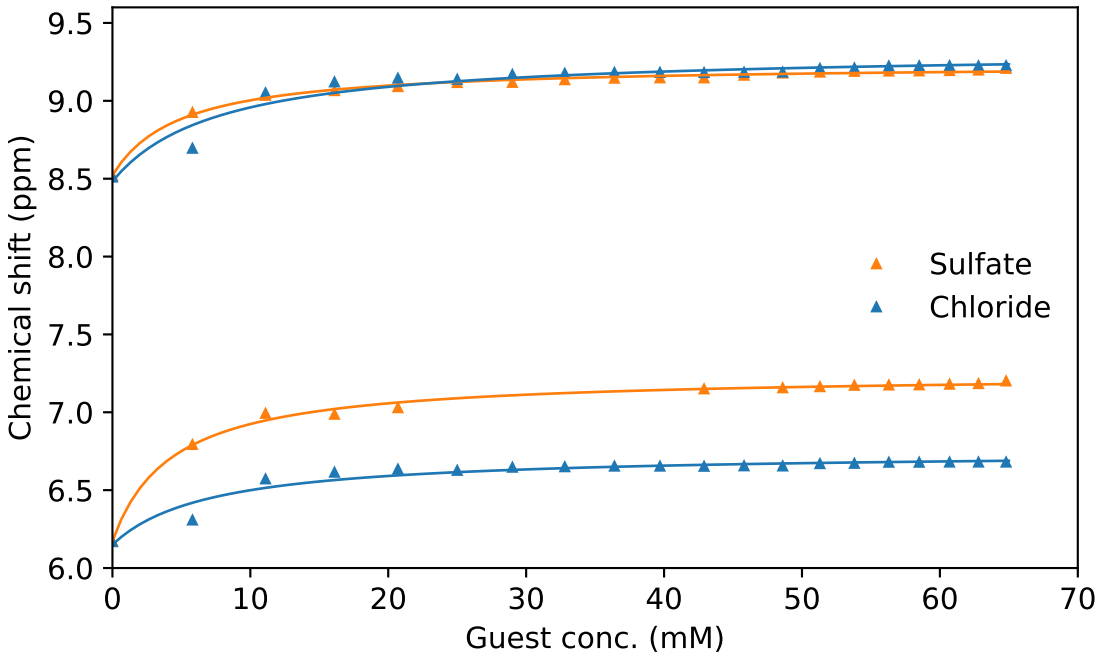

Figure 6.24: Change in chemical shift of the N−H signals in receptor **6** (at 10 mM) with increasing sulfate or chloride concentration.

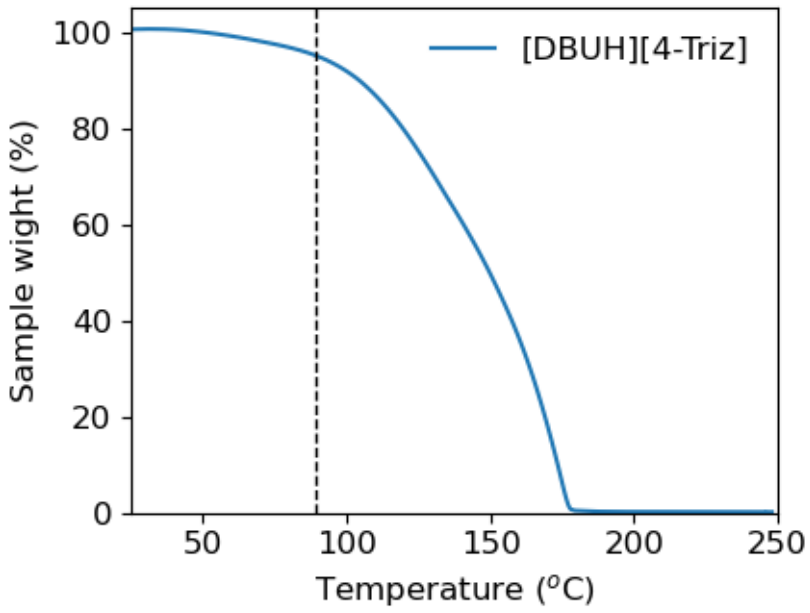

Figure 6.25: TGA of [DBUH][4-Triz] showing 5 wt% mass loss at 89℃.

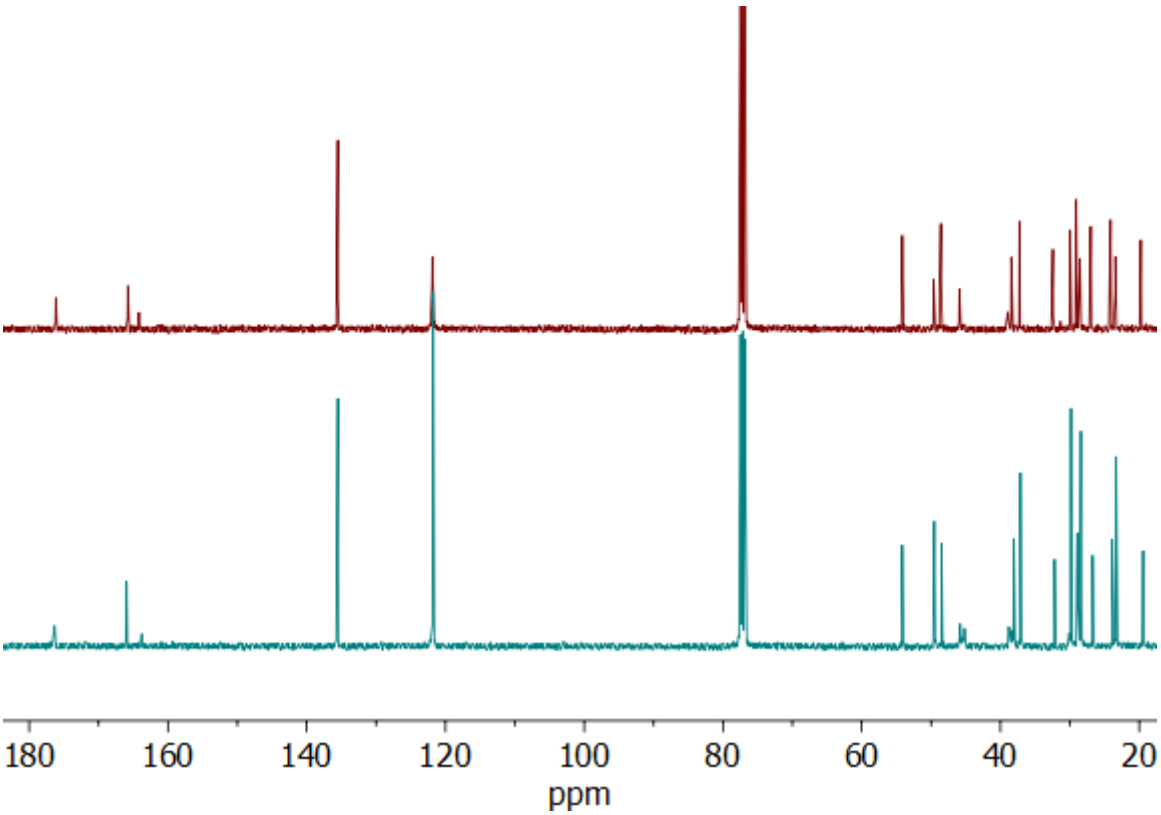

Figure 6.26: ^{13}C NMR spectra (top) before and (below) after 5 absorption-desorption cycles at 95 and 160 ℃ respectively and the addition of 20 wt% water.

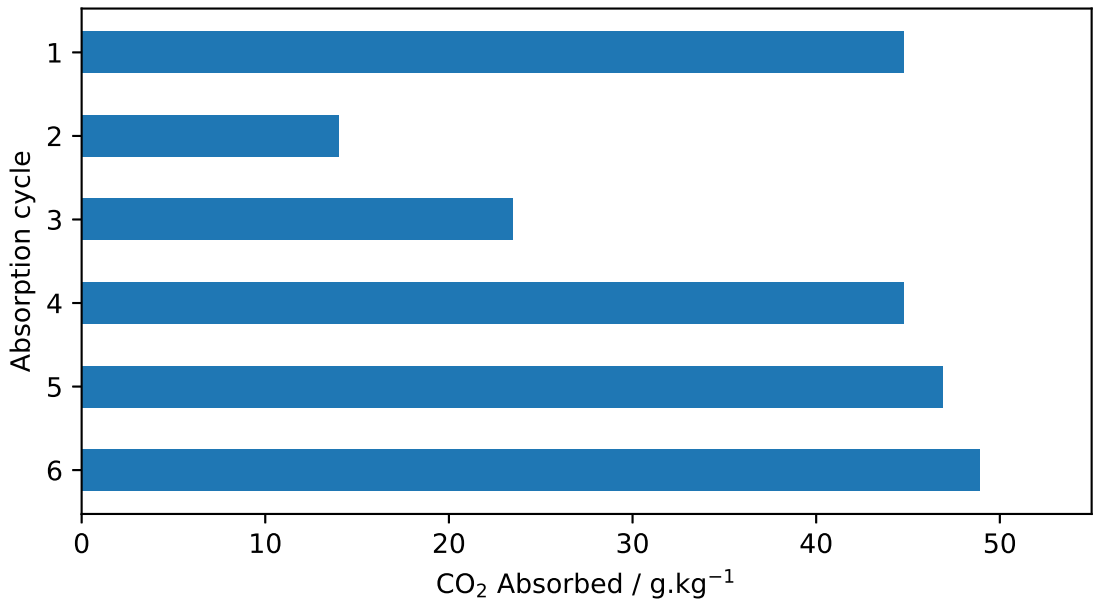

Figure 6.27: CO_2 released from a sample of [DBUH][Im] with 20 wt% water across six absorption-desorption cycles at 95 and 160 ℃.

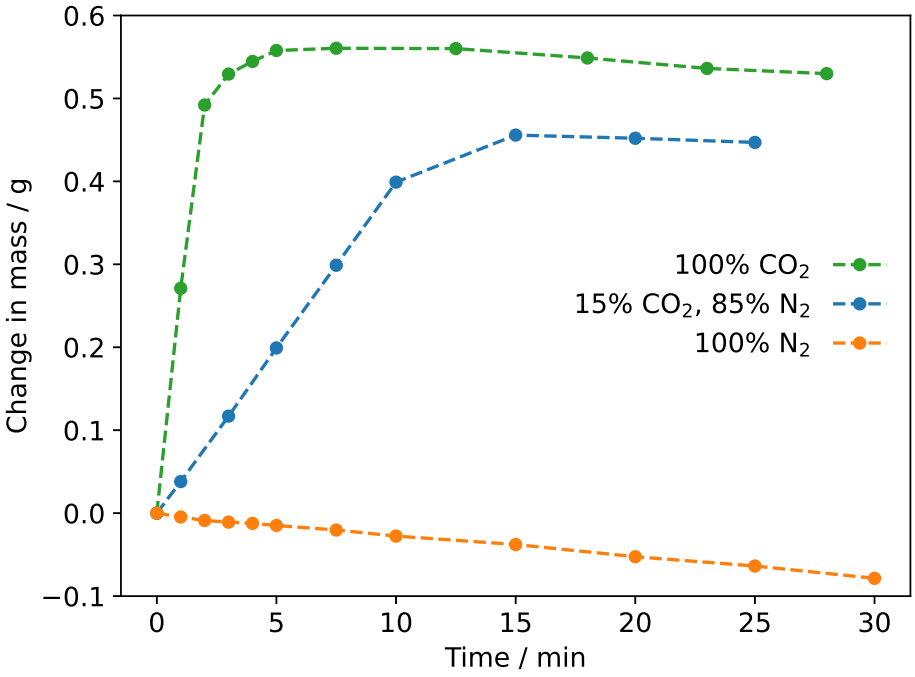

Figure 6.28: Change in mass of [DBUH][Im] (5 g) with 20 wt% water (1.25 g) at 95℃ and various gas compositions at a flow rate of 0.1 L·min^{-1}.

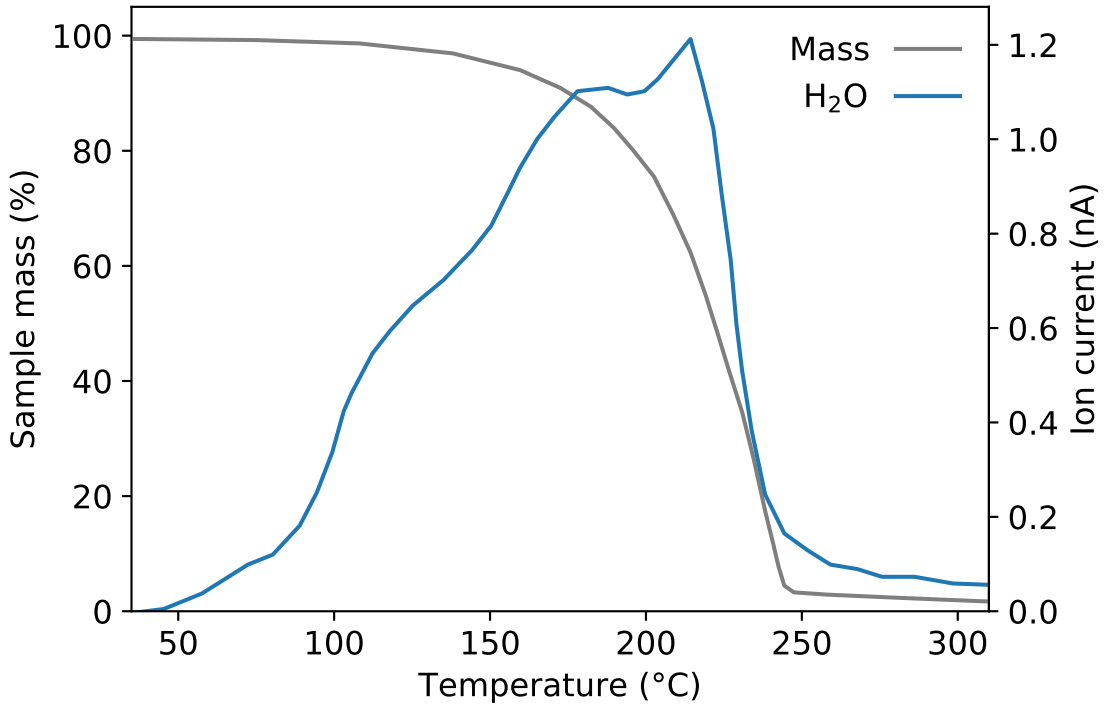

Figure 6.29: TGA-MS of [DBUH][Im] with 10 wt% water added.

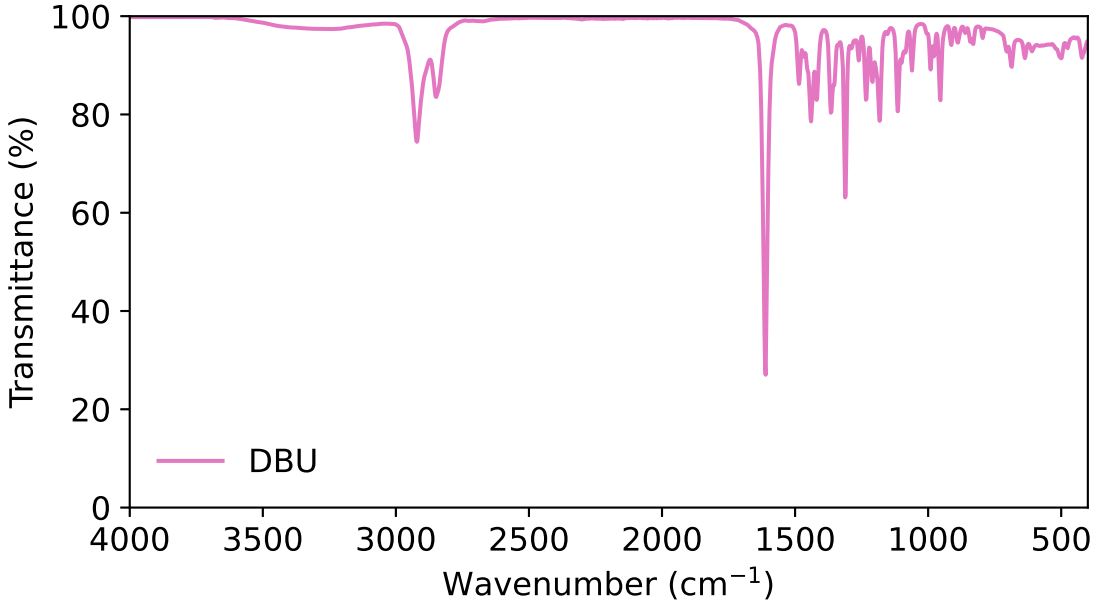

Figure 6.30: FT-IR spectra of 1,8-Diazabicyclo(5.4.0)undec-7-ene (DBU).

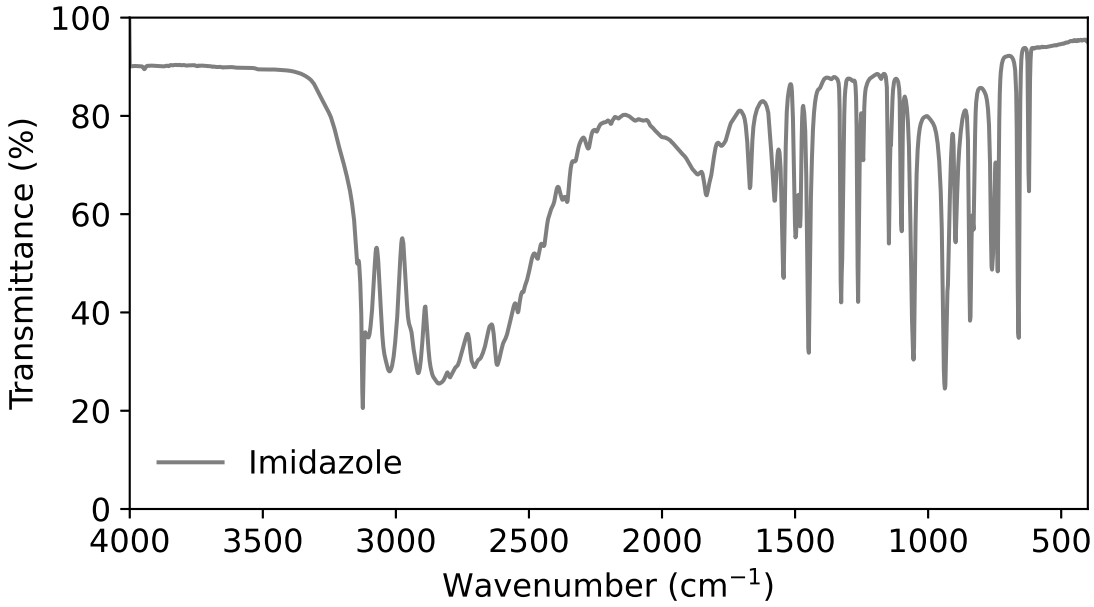

Figure 6.31: FT-IR spectra of imidazole.

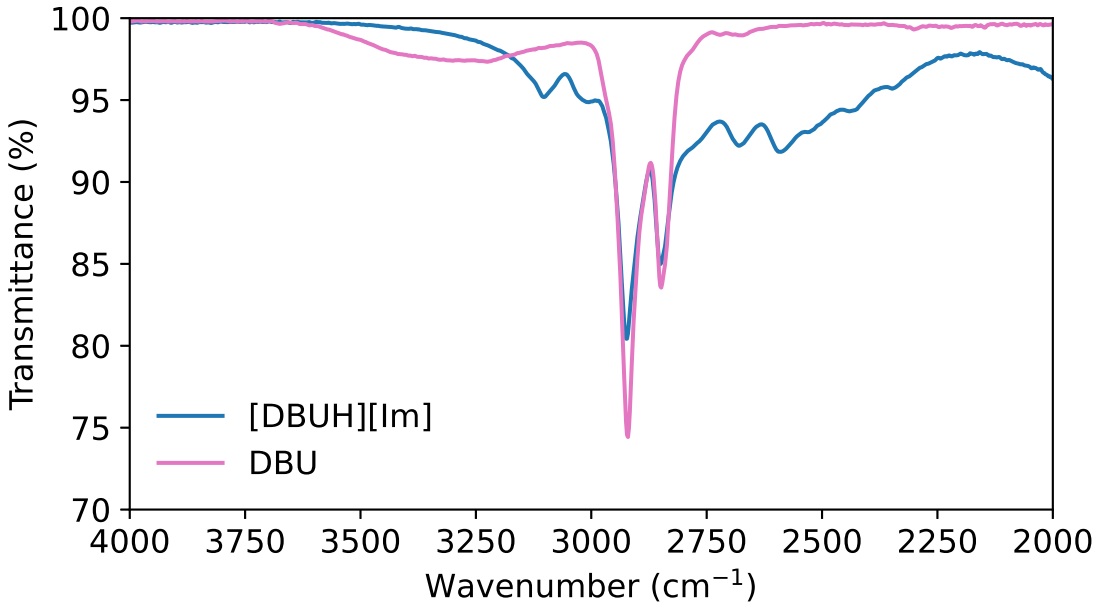

Figure 6.32: FT-IR spectra of neat DBU vs the protic ionic liquid [DBUH][Im] showing the formation of N−H signals at 2594, 2681 and 3106 cm^{-1}.

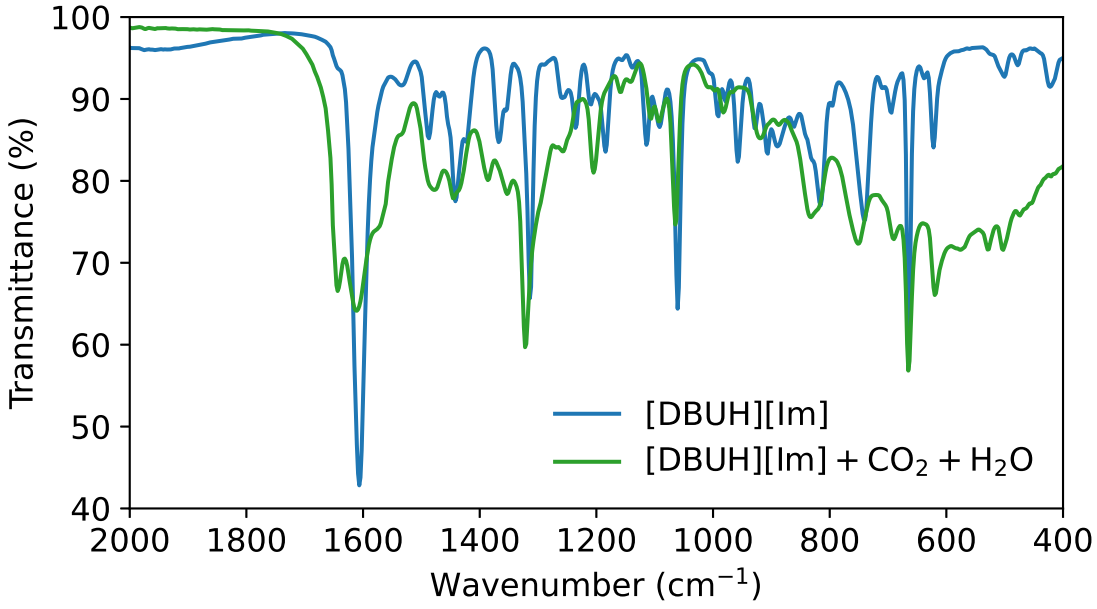

Figure 6.33: Overlaid full FT-IR spectra of the protic ionic liquid [DBUH][Im] before and after the addition of 10 wt% water and CO_2 absorption.

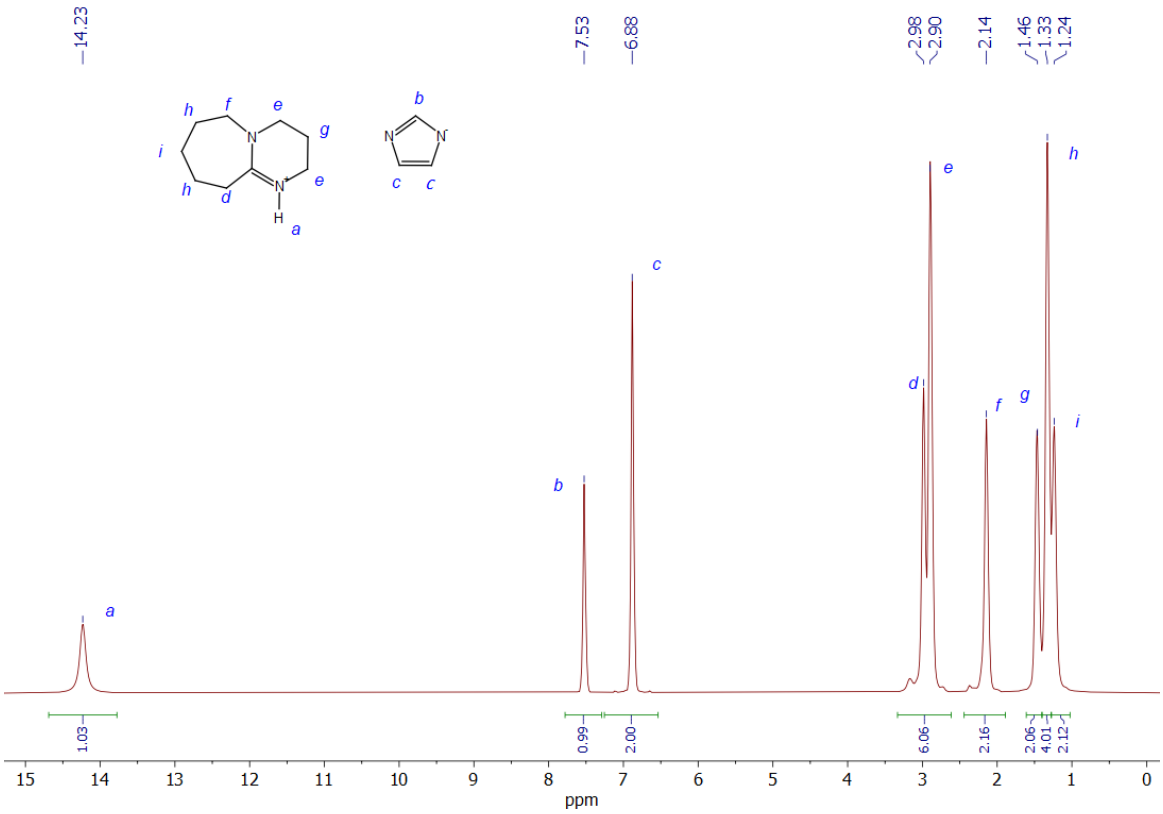

Figure 6.34: Annotated neat ^{13}C NMR spectra of [DBUH][Im] with a $CDCl_3$ capillary.

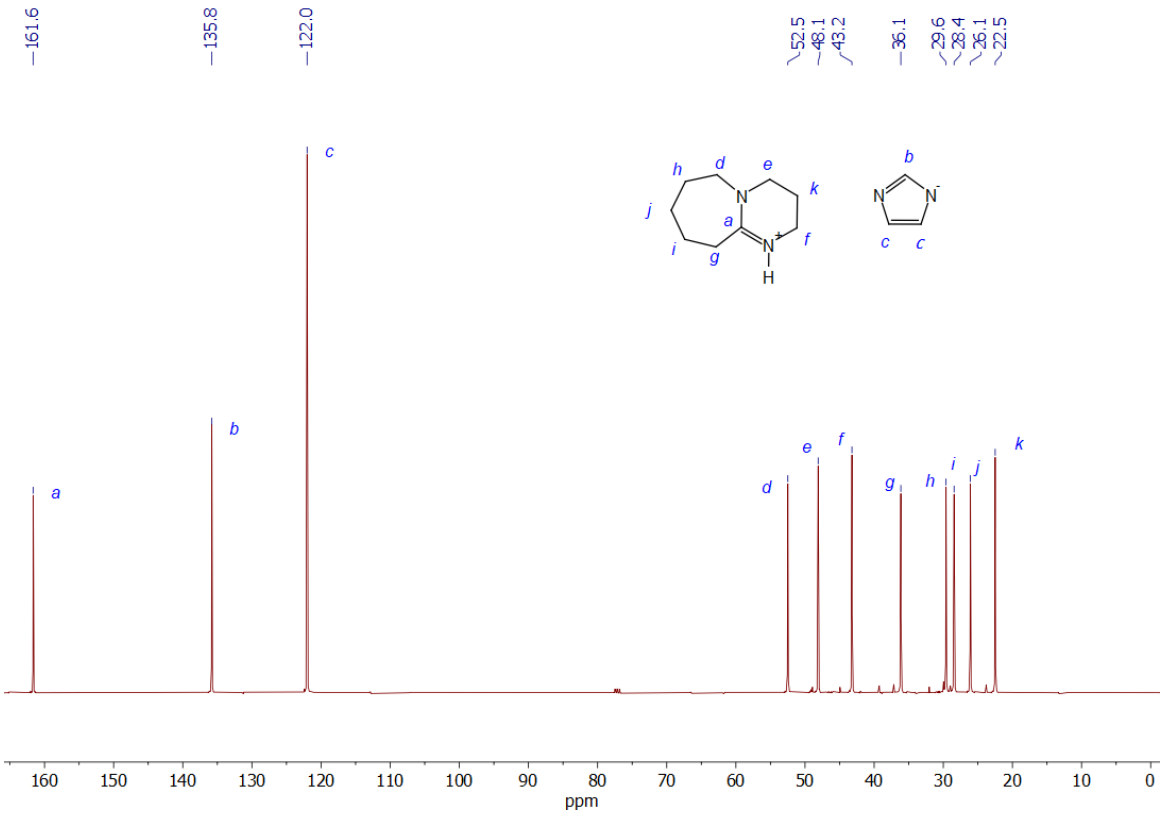

Figure 6.35: Annotated neat ^{13}C NMR spectra of [DBUH][Im] with a $CDCl_3$ capillary.

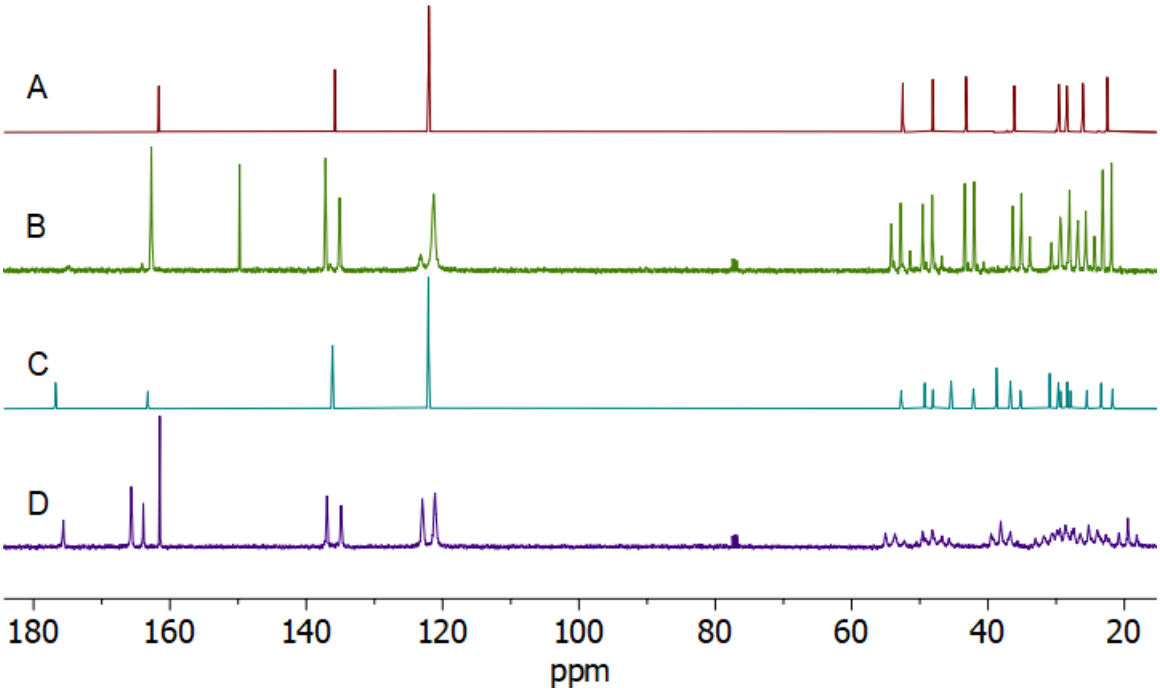

Figure 6.36: Neat ^{13}C NMR spectra of [DBUH][Im] with $CDCl_3$ capillaries. A = neat, B = CO_2 absorbed, C = 10 wt% water, D = 10 wt% water + CO_2. A & C ran at 25℃, B & C ran at 40℃.

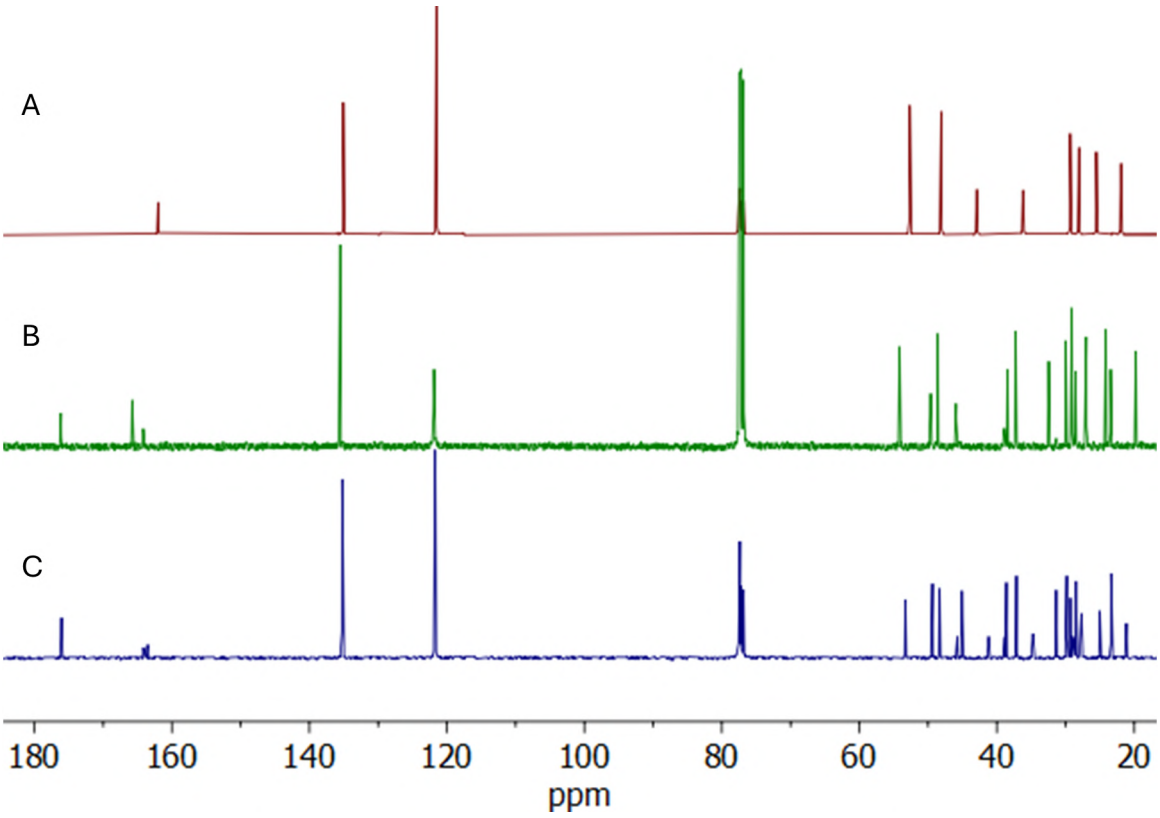

Figure 6.37: ^{13}C NMR spectra of [DBUH][Im] in $CDCl_3$. A = before absorption in the presence of water, B = after CO_2 absorption in the presence of water at 95℃, C = after desorption at 160℃.

7. Bibliography

[1] "Designer Solvents", *Chem. Eng. News Archive*, 1998, **76**, 32–37.

[2] T. Welton, "Ionic liquids: a brief history", *Biophys. Rev.*, 2018, **10**, 691–706.

[3] M. Tariq, M. G. Freire, B. Saramago, J. A. P. Coutinho, J. N. C. Lopes and L. P. N. Rebelo, "Surface tension of ionic liquids and ionic liquid solutions", *Chem. Soc. Rev.*, 2012, **41**, 829–868.

[4] *Ionic Liquids in Organic Synthesis*, ed. S. V. Malhotra, ACS Symp. Ser., 2007, vol. 950.

[5] F. Philippi, D. Rauber, K. L. Eliasen, N. Bouscharain, K. Niss, C. W. M. Kay and T. Welton, "Pressing matter: why are ionic liquids so viscous?", *Chem. Sci.*, 2022, **13**, 2735–2743.

[6] M. J. Earle, J. M. S. S. Esperança, M. A. Gilea, J. N. Canongia Lopes, L. P. N. Rebelo, J. W. Magee, K. R. Seddon and J. A. Widegren, "The distillation and volatility of ionic liquids", *Nature*, 2006, **439**, 831–834.

[7] R. S. Kalb, in *Commercial Applications of Ionic Liquids*, ed. M. B. Shiflett, Springer International Publishing, Cham, 2020, pp. 261–282.

[8] B. Azimi, H. Maleki, V. Gigante, R. Bagherzadeh, A. Mezzetta, M. Milazzo, L. Guazzelli, P. Cinelli, A. Lazzeri and S. Danti, "Cellulose-based fiber spinning processes using ionic liquids", *Cellulose*, 2022, **29**, 3079–3129.

[9] F. Hermanutz, M. P. Vocht and M. R. Buchmeiser, in *Commercial Applications of Ionic Liquids*, ed. M. B. Shiflett, Springer International Publishing, Cham, 2020, pp. 227–259.

[10] W. F. Elmobarak, F. Almomani, M. Tawalbeh, A. Al-Othman, R. Martis and K. Rasool, "Current status of CO2 capture with ionic liquids: Development and progress", *Fuel*, 2023, **344**, 128102.

[11] A. R. Abouelela, S.-y. Tan, G. H. Kelsall and J. P. Hallett, "Toward a Circular Economy: Decontamination and Valorization of Postconsumer Waste Wood Using the ionoSolv Process", *ACS Sustainable Chem. Eng.*, 2020, **8**, 14441–14461.

[12] Y. Zheng, D. Wang, S. Kaushik, S. Zhang, T. Wada, J. Hwang, K. Matsumoto and R. Hagiwara, “Ionic Liquid Electrolytes for Next-generation Electrochemical Energy Devices”, *EnergyChem*, 2022, **4**, 100075.

[13] L. M. Haverhals, D. P. Durkin and P. C. Trulove, in *Commercial Applications of Ionic Liquids*, ed. M. B. Shiflett, Springer International Publishing, Cham, 2020, pp. 211–226.

[14] A. J. Greer, J. Jacquemin and C. Hardacre, “Industrial Applications of Ionic Liquids”, *Molecules*, 2020, **25**, 5207.

[15] V. Vchirawongkwin, B. M. Rode and I. Persson, “Structure and dynamics of sulfate ion in aqueous solution-an ab initio QMCF MD simulation and large angle X-ray scattering study”, *J. Phys. Chem. B*, 2007, **111**, 4150–4155.

[16] Y. Marcus, “Thermodynamics of solvation of ions. Part 5.—Gibbs free energy of hydration at 298.15 K”, *J. Chem. Soc., Faraday Trans.*, 1991, **87**, 2995–2999.

[17] M. J. King, W. G. Davenport and M. S. Moats, in *Sulfuric Acid Manufacture (Second Edition)*, ed. M. J. King, W. G. Davenport and M. S. Moats, Elsevier, Oxford, Second Edition, 2013, pp. 1–9.

[18] L. E. Apodaca, G. E. d’Aquin and R. C. Fell, in *Handbook of Industrial Chemistry and Biotechnology*, ed. J. A. Kent, T. V. Bommaraju and S. D. Barnicki, Springer International Publishing, Cham, 2017, pp. 1241–1266.

[19] B. A. Moyer, R. Custelcean, B. P. Hay, J. L. Sessler, K. Bowman-James, V. W. Day and S. O. Kang, “A case for molecular recognition in nuclear separations: Sulfate separation from nuclear wastes”, *Inorg. Chem.*, 2013, **52**, 3473–3490.

[20] M. S. H. Bader, “Sulfate scale problems in oil fields water injection operations”, *Desalination*, 2006, **201**, 100–105.

[21] W. A. M. Fernando, I. M. S. K. Ilankoon, T. H. Syed and M. Yellishetty, “Challenges and opportunities in the removal of sulphate ions in contaminated mine water: A review”, *Miner. Eng.*, 2018, **117**, 74–90.

[22] D. Zak, M. Hupfer, A. Cabezas, G. Jurasinski, J. Audet, A. Kleeberg, R. McInnes, S. M. Kristiansen, R. J. Petersen, H. Liu and T. Goldhammer, “Sulphate in freshwater ecosystems: A review of sources, biogeochemical cycles, ecotoxicological effects and bioremediation”, *Earth Sci. Rev.*, 2021, **212**, 103446.

[23] *Sulfate in Drinking-water*, World Health Organization, 2004.

[24] *Guidelines for drinking-water quality*, World Health Organization, Geneva, Fourth edition incorporating the first addendum., 2017, 11541 pp.

[25] A. G. Dickson and C. Goyet, in *Handbook of Methods for the Analysis of the Various Parameters of the Carbon Dioxide System in Sea Water*, Department of Energy, 2nd edn., 1994, vol. 2, ch. 5.

[26] M. El-Said, M. Ramzi and T. Abdel-Moghny, "Analysis of oilfield waters by ion chromatography to determine the composition of scale deposition", *Desalination*, 2009, **249**, 748–756.

[27] P. Kinnunen, H. Kyllönen, T. Kaartinen, J. Mäkinen, J. Heikkinen and V. Miettinen, "Sulphate removal from mine water with chemical, biological and membrane technologies", *Water Sci. Technol.*, 2018, **2017**, 194–205.

[28] W. Liamleam and A. P. Annachhatre, "Electron donors for biological sulfate reduction", *Biotechnol. Adv.*, 2007, **25**, 452–463.

[29] H. Runtti, E.-T. Tolonen, S. Tuomikoski, T. Luukkonen and U. Lassi, "How to tackle the stringent sulfate removal requirements in mine water treatment—A review of potential methods", *Environ. Res.*, 2018, **167**, 207–222.

[30] R. J. Bowell, mine water 2004 - Proceedings International Mine Water Association Symposium 2, Newcastle upon Tyne, 2004, vol. 2, pp. 75–91.

[31] *Treatment of Sulphate in Mine Effluents, 2003*, https://www.inap.com.au/wp-content/uploads/Treatment_of_Sulphate_in_Mine_Effluents_-_Lorax_Report.pdf (visited on 06/28/2024).

[32] S.-Q. Chen, W. Zhao and B. Wu, "Separation of Sulfate Anion From Aqueous Solution Governed by Recognition Chemistry: A Minireview", *Front. Chem.*, 2022, **10**, 905563.

[33] M. A. Reinsel, "A New Process for Sulfate Removal From Industrial Waters", *National Meeting of the American Society for Surface Mining and Reclamation*, 1999, 546–550.

[34] W. Dou, Z. Zhou, L. M. Jiang, A. Jiang, R. Huang, X. Tian, W. Zhang and D. Chen, "Sulfate removal from wastewater using ettringite precipitation: Magnesium ion inhibition and process optimization", *J. Environ. Manage.*, 2017, **196**, 518–526.

[35] R. C. Ropp, in *Encyclopedia of the Alkaline Earth Compounds*, ed. R. Ropp, Elsevier, Amsterdam, 2013, ch. 3, pp. 105–197.

[36] W. Zhang, Y. Zhou, J. Zhu and Y. Pan, "New clean process for barium sulfide preparation by barite reduction with elemental sulfur", *Ind. Eng. Chem. Res.*, 2014, **53**, 5646–5651.

[37] A. Oskarsson, in *Handbook on the Toxicology of Metals (Fifth Edition)*, ed. G. F. Nordberg and M. Costa, Academic Press, Fifth Edition, 2022, pp. 91–100.

[38] S. Ananda, Z. Shaohua and L. Liang, "Fatal barium chloride poisoning: four cases report and literature review", *Am. J. Forensic Med. Pathol.*, 2013, **34**, 115–118.

[39] S. Jun-Feng, L. Dao-Ping, L. Chun-He, L. Jian-Dong and X. Xiong-Jian, "Critical care management of patients with barium poisoning: a case series", *Chin. Med. J.*, 2020, **133**, 724–725.

[40] R. B. Fischer and T. B. Rhinehammer, "Rapid Precipitation of Barium Sulfate", *Anal. Chem.*, 1952, **25**, 1544–1548.

[41] M. Mulder, in *Basic Principles of Membrane Technology*, Springer Netherlands, Dordrecht, 1991, pp. 198–280.

[42] Y.-N. Wang and R. Wang, in *Membrane Separation Principles and Applications*, ed. A. F. Ismail, M. A. Rahman, M. H. D. Othman and T. Matsuura, Elsevier, 2019, ch. 1, pp. 1–45.

[43] Y. Roy, D. M. Warsinger and J. H. Lienhard, "Effect of temperature on ion transport in nanofiltration membranes: Diffusion, convection and electromigration", *Desalination*, 2017, **420**, 241–257.

[44] N. S. Suhalim, N. Kasim, E. Mahmoudi, I. J. Shamsudin, A. W. Mohammad, F. Mohamed Zuki and N. L.-A. Jamari, "Rejection Mechanism of Ionic Solute Removal by Nanofiltration Membranes: An Overview", *Nanomaterials*, 2022, **12**, 437.

[45] L. F. Greenlee, D. F. Lawler, B. D. Freeman, B. Marrot and P. Moulin, "Reverse osmosis desalination: Water sources, technology, and today's challenges", *Water Res.*, 2009, **43**, 2317–2348.

[46] *World's Largest Reverse Osmosis Desalination Plant: ACWA Power's Rabigh 3 IWP Project*, https://energyindustryreview.com/environment/worlds-largest-reverse-osmosis-desalination-plant-acwa-powers-rabigh-3-iwp-project/ (visited on 10/30/2023).

[47] *Specialty Membranes XUS180808 Ultra-High Pressure RO Element*, https://www.dupont.com/products/dupontspecialtymembranesxus180804andxus180802ultrahighpressureoelement.html (visited on 10/30/2023).

[48] A. Panagopoulos, K. J. Haralambous and M. Loizidou, "Desalination brine disposal methods and treatment technologies - A review", *Science of the Total Environment*, 2019, **693**, 133545.

[49] G. Muyzer and A. J. M. Stams, “The ecology and biotechnology of sulphate-reducing bacteria”, *Nat. Rev. Microbiol.*, 2008, **6**, 441–454.

[50] G. S. Lollar, O. Warr, J. Telling, M. R. Osburn and B. S. Lollar, “‘Follow the Water’: Hydrogeochemical Constraints on Microbial Investigations 2.4 km Below Surface at the Kidd Creek Deep Fluid and Deep Life Observatory”, *Geomicrobiol. J.*, 2019, **36**, 859–872.

[51] F. de Dardel and T. V. Arden, in *Ullmann’s Encyclopedia of Industrial Chemistry*, John Wiley & Sons, Ltd, 2008.

[52] K. W. Pepper, H. M. Paisley and M. A. Young, “833. Properties of ion-exchange resins in relation to their structure. Part VI. Anion-exchange resins derived from styrene-divinyl-benzene copolymers”, *J. Chem. Soc.*, 1953, 4097–4105.

[53] *Our Technologies to Treat Sulphate*, https://www.bqewater.com/technology-solutions/sulphate/ (visited on 11/05/2023).

[54] T. Doughty and P. Littlejohn, 27th International Applied Geochemistry Symposium, 2015.

[55] S. Demcak, M. Balintova and P. Pavlikova, “Study of Sorption Properties of Various Wood Sawdust for Sulphate Remomal”, *In conference proceedings of People, Buildings and Environment 2016, an international scientific conference*, 2016, **4**, 206–211.

[56] W. E. Marshall and L. H. Wartelle, “An anion exchange resin from soybean hulls”, *J. Chem. Technol. Biotechnol.*, 2004, **79**, 1286–1292.

[57] W. Cao, Z. Dang, X. Q. Zhou, X. Y. Yi, P. X. Wu, N. W. Zhu and G. N. Lu, “Removal of sulphate from aqueous solution using modified rice straw: Preparation, characterization and adsorption performance”, *Carbohydr. Polym.*, 2011, **85**, 571–577.

[58] A. Stojanovic and B. K. Keppler, “Ionic Liquids as Extracting Agents for Heavy Metals”, *Sep. Sci. Technol.*, 2012, **47**, 189–203.

[59] H. Zhao, S. Xia and P. Ma, “Use of ionic liquids as ’green’ solvents for extractions”, *J. Chem. Technol. Biotechnol.*, 2005, **80**, 1089–1096.

[60] C. H. C. Janssen, N. A. Macías-Ruvalcaba, M. Aguilar-Martínez and M. N. Kobrak, “Metal extraction to ionic liquids: the relationship between structure, mechanism and application”, *Int. Rev. Phys. Chem.*, 2015, **34**, 591622.

[61] S. Dai, Y. H. Ju and C. E. Barnes, “Solvent extraction of strontium nitrate by a crown ether using room-temperature ionic liquids”, *J. Chem. Soc., Dalton Trans.*, 1999, 1201–1202.

[62] M. L. Dietz and J. A. Dzielawa, “Ion-exchange as a mode of cation transfer into room-temperature ionic liquids containing crown ethers: implications for the ‘greenness’ of ionic liquids as diluents in liquid-liquid extraction”, *Chem. Commun.*, 2001, 2124–2125.

[63] M. L. Dietz, J. A. Dzielawa, I. Laszak, B. A. Young and M. P. Jensen, “Influence of solvent structural variations on the mechanism of facilitated ion transfer into room-temperature ionic liquids”, *Green Chem.*, 2003, **5**, 682–685.

[64] X. Sun, H. Luo and S. Dai, “Ionic Liquids-Based Extraction: A Promising Strategy for the Advanced Nuclear Fuel Cycle”, *Chem. Rev.*, 2012, **112**, 2100–2128.

[65] A. E. Visser, R. P. Swatloski, W. M. Reichert, R. Mayton, S. Sheff, A. Wierzbicki, J. H. Davis, Jr. and R. D. Rogers, “Task-specific ionic liquids for the extraction of metal ions from aqueous solutions”, *Chem. Commun.*, 2001, 135–136.

[66] D. Parmentier, T. Vander Hoogerstraete, S. J. Metz, K. Binnemans and M. C. Kroon, “Selective Extraction of Metals from Chloride Solutions with the Tetraoctylphosphonium Oleate Ionic Liquid”, *Ind. Eng. Chem. Res.*, 2015, **54**, 5149–5158.

[67] V. A. Cocalia, M. P. Jensen, J. D. Holbrey, S. K. Spear, D. C. Stepinski and R. D. Rogers, “Identical extraction behavior and coordination of trivalent or hexavalent f-element cations using ionic liquid and molecular solvents”, *Dalton Trans.*, 2005, 1966–1971.

[68] M. K. Jha, A. Kumari, R. Panda, J. Rajesh Kumar, K. Yoo and J. Y. Lee, “Review on hydrometallurgical recovery of rare earth metals”, *Hydrometallurgy*, 2016, **165**, 2–26.

[69] F. Xie, T. A. Zhang, D. Dreisinger and F. Doyle, “A critical review on solvent extraction of rare earths from aqueous solutions”, *Miner. Eng.*, 2014, **56**, 10–28.

[70] B. Galan, A. M. Urtiaga, A. I. Alonso, J. A. Irabien and M. I. Ortiz, “Extraction of Anions with Aliquat 336: Chemical Equilibrium Modeling”, *Ind. Eng. Chem. Res.*, 1994, **33**, 1765–1770.

[71] S. E. Pepper and M. D. Ogden, “Perrhenate extraction studies by Cyphos 101-IL; screening for implementation in technetium removal”, *Sep. Purif. Technol.*, 2013, **118**, 847–852.

[72] J. E. Quinn, M. D. Ogden and K. Soldenhoff, “Solvent Extraction of Uranium (VI) from Chloride Solutions using Cyphos IL-101”, *Solvent Extr. Ion Exch.*, 2013, **31**, 538–549.

[73] K. Friess, in *Encyclopedia of Membranes*, ed. E. Drioli and L. Giorno, Springer Berlin Heidelberg, Berlin, Heidelberg, 2015, pp. 1–3.

[74] K. Sarangi, E. Padhan, P. V. R. B. Sarma, K. H. Park and R. P. Das, “Removal/recovery of hydrochloric acid using Alamine 336, Aliquat 336, TBP and Cyanex 923”, *Hydrometallurgy*, 2006, **84**, 125–129.

[75] J. Coca, F. V. Díez and M. A. Morís, “Solvent extraction of molybdenum and tungsten by Alamine 336 and DEHPA”, *Hydrometallurgy*, 1990, **25**, 125–135.

[76] G. Ramadevi, T. Sreenivas, A. S. Navale and N. P. H. Padmanabhan, “Solvent extraction of uranium from lean grade acidic sulfate leach liquor with alamine 336 reagent”, *J. Radioanal. Nucl. Chem.*, 2012, **294**, 13–18.

[77] *Tokyo Chemical Industry Co., methyltri-n-octylammonium chloride*, https://www.tcichemicals.com/OP/en/p/T1365 (visited on 11/29/2022).

[78] Y.-L. Li, Q.-X. Li, L.-F. Zhi and M.-H. Zhang, “Synthesis, Characterization and Surface Activity of Trioctyl Hydroxyethyl Ammonium Chloride”, *Tenside, Surfactants, Deterg.*, 2011, **48**, 305–307.

[79] Y. Li, Q. Li, L. Zhi and M. Zhang, “Synthesis, characterization and surface-activity of hydroxyethyl group-containing quaternary ammonium surfactants”, *J. Surfactants Deterg.*, 2011, **14**, 529–533.

[80] K. Gloe, H. Stephan and M. Grotjahn, “Where is the Anion Extraction Going?”, *Chem. Eng. Technol.*, 2003, **26**, 1107–1117.

[81] J. A. Mejias and S. Lago, “Calculation of the absolute hydration enthalpy and free energy of H^+ and OH^-”, *J. Chem. Phys.*, 2000, **113**, 7306–7316.

[82] T. B. Lee, S. Oh, T. R. Gohndrone, O. Morales-Collazo, S. Seo, J. F. Brennecke and W. F. Schneider, “CO2 Chemistry of Phenolate-Based Ionic Liquids”, *J. Phys. Chem. B*, 2016, **120**, 1509–1517.

[83] O. Hollóczki and L. Nyulászi, in *Electronic Effects in Organic Chemistry*, ed. B. Kirchner, Springer Berlin Heidelberg, Berlin, Heidelberg, 2014, pp. 1–24.

[84] S. Wellens, B. Thijs and K. Binnemans, “How safe are protic ionic liquids? Explosion of pyrrolidinium nitrate”, *Green Chem.*, 2013, **15**, 3484–3485.

[85] B. Wang, Y. Feng, X. Qi, M. Deng, J. Tian and Q. Zhang, “Designing Explosive Poly(Ionic Liquid)s as Novel Energetic Polymers”, *Chem. Eur. J.*, 2018, **24**, 15897–15902.

[86] S.-H. Liu, C.-C. Chen, B. Zhang and J.-H. Wu, “Fire and explosion hazards of 1-ethyl-3-methylimidazolium bis(trifluoromethylsulfonyl)imide”, *RSC Adv.*, 2020, **10**, 22468–22479.

[87] M. G. Freire, A. F. M. Cláudio, J. M. M. Araújo, J. A. P. Coutinho, I. M. Marrucho, J. N. C. Lopes and L. P. N. Rebelo, “Aqueous biphasic systems: a boost brought about by using ionic liquids”, *Chem. Soc. Rev.*, 2012, **41**, 4966–4995.

[88] M. W. Beijerinck, “Ueber eine eigentiimlichkeit derlöslichenstärke”, *Zentralblatt für Bakteriologie, Parasiten und Infektionskrankenheiten*, 1896, **2**, 697–699.

[89] A. Hamta and M. R. Dehghani, “Application of polyethylene glycol based aqueous two-phase systems for extraction of heavy metals”, *J. Mol. Liq.*, 2017, **231**, 20–24.

[90] C. Y. Khripin, J. A. Fagan and M. Zheng, “Spontaneous Partition of Carbon Nanotubes in Polymer-Modified Aqueous Phases”, *J. Am. Chem. Soc.*, 2013, **135**, 6822–6825.

[91] H. Hustedt, K. H. Kroner, U. Menge and M.-R. Kula, “Protein recovery using two-phase systems”, *Trends Biotechnol.*, 1985, **3**, 139–144.

[92] I. Kaplanow, F. Goerzgen, J. Merz and G. Schembecker, “Mass Transfer of Proteins in Aqueous Two-Phase Systems”, *Sci. Rep.*, 2019, **9**, 3692–3698.

[93] M. Dilip, S. T. Griffin, S. K. Spear, C. Rijksen, H. Rodríguez and R. D. Rogers, “Dual Nature of Polyethylene Glycol-Based Aqueous Biphasic Extraction Chromatographic (ABEC) Resins: Uptakes of Perchlorate versus Mercury(II)”, *Ind. Eng. Chem. Res.*, 2008, **47**, 7390–7396.

[94] N. Dubouis, C. Park, M. Deschamps, S. Abdelghani-Idrissi, M. Kanduč, A. Colin, M. Salanne, J. Dzubiella, A. Grimaud and B. Rotenberg, “Chasing Aqueous Biphasic Systems from Simple Salts by Exploring the LiTFSI/LiCl/-H_2O Phase Diagram”, *ACS Cent. Sci.*, 2019, **5**, 640–643.

[95] W. J. R. Gilbert, J. Safarov, D. L. Minnick, M. A. Rocha, E. P. Hassel and M. B. Shiflett, “Density, Viscosity, and Vapor Pressure Measurements of Water + Lithium Bis(trifluoromethylsulfonyl)imide Solutions”, *J. Chem. Eng. Data*, 2017, **62**, 2056–2066.

[96] F. Lo Celso, A. Triolo and R. Triolo, “Phase separation in multi-component mixtures: the four-component case”, *Physica A*, 2002, **304**, 299–307.

[97] K. E. Gutowski, G. A. Broker, H. D. Willauer, J. G. Huddleston, R. P. Swatloski, J. D. Holbrey and R. D. Rogers, "Controlling the Aqueous Miscibility of Ionic Liquids: Aqueous Biphasic Systems of Water-Miscible Ionic Liquids and Water-Structuring Salts for Recycle, Metathesis, and Separations", *J. Am. Chem. Soc.*, 2003, **125**, 6632–6633.

[98] M. G. Freire, J. F. B. Pereira, M. Francisco, H. Rodríguez, L. P. N. Rebelo, R. D. Rogers and J. A. P. Coutinho, "Insight into the Interactions That Control the Phase Behaviour of New Aqueous Biphasic Systems Composed of Polyethylene Glycol Polymers and Ionic Liquids", *Chem. Eur. J.*, 2012, **18**, 1831–1839.

[99] S. Sharma, A. S. Ivanov and C. J. Margulis, "A Brief Guide to the Structure of High-Temperature Molten Salts and Key Aspects Making Them Different from Their Low-Temperature Relatives, the Ionic Liquids", *J. Phys. Chem. B*, 2021, **125**, 6359–6372.

[100] G. M. Kontogeorgis, A. Holster, N. Kottaki, E. Tsochantaris, F. Topsøe, J. Poulsen, M. Bache, X. Liang, N. S. Blom and J. Kronholm, "Water structure, properties and some applications - A review", *Chem. Thermodyn. Therm. Anal.*, 2022, **6**, 100053.

[101] K. P. Gregory, G. R. Elliott, H. Robertson, A. Kumar, E. J. Wanless, G. B. Webber, V. S. J. Craig, G. G. Andersson and A. J. Page, "Understanding specific ion effects and the Hofmeister series", *Phys. Chem. Chem. Phys.*, 2022, **24**, 12682–12718.

[102] R. Hayes, G. G. Warr and R. Atkin, "Structure and Nanostructure in Ionic Liquids", *Chem. Rev.*, 2015, **115**, 6357–6426.

[103] J. C. Araque, J. J. Hettige and C. J. Margulis, "Modern Room Temperature Ionic Liquids, a Simple Guide to Understanding Their Structure and How It May Relate to Dynamics", *J. Phys. Chem. B*, 2015, **119**, 12727–12740.

[104] T. Murphy, R. Atkin and G. G. Warr, "Scattering from ionic liquids", *Curr. Opin. Colloid Interface Sci.*, 2015, **20**, 282–292.

[105] O. Nordness and J. F. Brennecke, "Ion Dissociation in Ionic Liquids and Ionic Liquid Solutions", *Chem. Rev.*, 2020, **120**, 12873–12902.

[106] E. J. R. Sudholter, J. B. F. N. Engberts and W. H. De Jeu, "Thermotropic liquid-crystalline behavior of some single- and double-chained pyridinium amphiphiles", *J. Phys. Chem.*, 1982, **86**, 1908–1913.

[107] Y. Matsunaga and T. Tsujimura, "The Thermotropic Liquid-Crystalline Behavior of Alkylammonium Naphthalenesulfonates", *Mol. Cryst. Liq. Cryst.*, 1991, **200**, 103–108.

[108] A. Kanazawa, O. Tsutsumi, T. Ikeda and Y. Nagase, “Novel Thermotropic Liquid Crystals without a Rigid Core Formed by Amphiphiles Having Phosphonium Ions”, *J. Am. Chem. Soc.*, 1997, **119**, 7670–7675.

[109] C. J. Bowlas, D. W. Bruce and K. R. Seddon, “Liquid-crystalline ionic liquids”, *Chem. Commun.*, 1996, 1625–1626.

[110] A. E. Bradley, C. Hardacre, J. D. Holbrey, S. Johnston, S. E. J. McMath and M. Nieuwenhuyzen, “Small-Angle X-ray Scattering Studies of Liquid Crystalline 1-Alkyl-3-methylimidazolium Salts”, *Chem. Mater.*, 2002, **14**, 629–635.

[111] J. N. A. Canongia Lopes and A. A. H. Pádua, “Nanostructural Organization in Ionic Liquids”, *J. Phys. Chem. B*, 2006, **110**, 3330–3335.

[112] C. Hardacre, J. D. Holbrey, C. L. Mullan, T. G. A. Youngs and D. T. Bowron, “Small angle neutron scattering from 1-alkyl-3-methylimidazolium hexafluorophosphate ionic liquids ([$C_n$mim][PF_6], n=4, 6, and 8)”, *J. Chem. Phys.*, 2010, **133**, 074510.

[113] A. Kaintz, G. Baker, A. Benesi and M. Maroncelli, “Solute Diffusion in Ionic Liquids, NMR Measurements and Comparisons to Conventional Solvents”, *J. Phys. Chem. B*, 2013, **117**, 11697–11708.

[114] J. J. Hettige, J. C. Araque and C. J. Margulis, “Bicontinuity and Multiple Length Scale Ordering in Triphilic Hydrogen-Bonding Ionic Liquids”, *J. Phys. Chem. B*, 2014, **118**, 12706–12716.

[115] J. C. Araque, S. K. Yadav, M. Shadeck, M. Maroncelli and C. J. Margulis, “How Is Diffusion of Neutral and Charged Tracers Related to the Structure and Dynamics of a Room-Temperature Ionic Liquid? Large Deviations from Stokes-Einstein Behavior Explained”, *J. Phys. Chem. B*, 2015, **119**, 7015–7029.

[116] Z. Hu and C. J. Margulis, “Heterogeneity in a room-temperature ionic liquid: Persistent local environments and the red-edge effect”, *Proc. Natl. Acad. Sci.*, 2006, **103**, 831–836.

[117] A. Triolo, O. Russina, B. Fazio, R. Triolo and E. Di Cola, “Morphology of 1-alkyl-3-methylimidazolium hexafluorophosphate room temperature ionic liquids”, *Chem. Phys. Lett.*, 2008, **457**, 362–365.

[118] T. L. Greaves, D. F. Kennedy, S. T. Mudie and C. J. Drummond, “Diversity Observed in the Nanostructure of Protic Ionic Liquids”, *J. Phys. Chem. B*, 2010, **114**, 10022–10031.

[119] C. Tanford, *The hydrophobic effect: formation of micelles and biological membranes*, John Wiley & Sons Inc., Somerset. NJ, 1973.

[120] J. N. Israelachvili, D. J. Mitchell and B. W. Ninham, "Theory of self-assembly of hydrocarbon amphiphiles into micelles and bilayers", *J. Chem. Soc., Faraday Trans. 2*, 1976, **72**, 1525–1568.

[121] R. Nagarajan, "Molecular Packing Parameter and Surfactant Self-Assembly: The Neglected Role of the Surfactant Tail", *Langmuir*, 2002, **18**, 31–38.

[122] R. Zana, M. Benrraou and R. Rueff, "Alkanediyl-α,ω-bis(dimethylalkylammonium bromide) Surfactants. 1. Effect of the Spacer Chain Length on the Critical Micelle Concentration and Micelle Ionization Degree", *Langmuir*, 1991, **7**, 1072–1075.

[123] M.-L. Arsene, I. Răut, M. Călin, M.-L. Jecu, M. Doni and A.-M. Gurban, "Versatility of Reverse Micelles: From Biomimetic Models to Nano (Bio)Sensor Design", *Processes*, 2021, **9**, 345.

[124] H.-F. Eicke and H. Christen, "Is water critical to the formation of micelles in apolar media??", *Helv. Chim. Acta*, 1978, **61**, 2258–2263.

[125] R. Urano, G. A. Pantelopulos and J. E. Straub, "Aerosol-OT Surfactant Forms Stable Reverse Micelles in Apolar Solvent in the Absence of Water", *J. Phys. Chem. B*, 2019, **123**, 2546–2557.

[126] A. I. Rusanov, "On the Thermodynamics of Reverse Micelles: Effect of Water on Micellization", *Colloid J.*, 2020, **82**, 560–566.

[127] C. Jolivalt, M. Minier and H. Renon, "Extraction of α-chymotrypsin using reversed micelles", *J. Colloid Interface Sci.*, 1990, **135**, 85–96.

[128] Z. Dövyap, E. Bayraktar and Ü. Mehmetoğlu, "Amino acid extraction and mass transfer rate in the reverse micelle system", *Enzyme Microb. Technol.*, 2006, **38**, 557–562.

[129] B. de Oliveira and R. Bertazzoli, "On the role of the surfactant aliquat® 336 on the kinetics of oxygen reduction reaction and on the rate of hydrogen peroxide electrosynthesis", *J. Electroanal. Chem.*, 2007, **611**, 126–132.

[130] D. Hayati and C. Robert W., "The extraction of zinc(II) from chloride solutions by methyltrioctylammonium and methyltridecylammonium chlorides dissolved in chloroform and other diluents and a comparison with Aliquat 336", *Aust. J. Chem.*, 1982, **35**, 1087–1093.

[131] N. J. Williams, C. A. Seipp, K. A. Garrabrant, R. Custelcean, E. Holguin, J. K. Keum, R. J. Ellis and B. A. Moyer, “Surprisingly selective sulfate extraction by a simple monofunctional di(imino)guanidinium micelle-forming anion receptor”, *Chem. Commun.*, 2018, **54**, 10048–10051.

[132] H. E. Simmons and C. H. Park, “Macrobicyclic amines. I. Out-in isomerism of 1,(k+ 2)-diazabicyclo [klm] alkanes”, *J. Am. Chem. Soc.*, 1968, **90**, 2428–2429.

[133] C. H. Park and H. E. Simmons, “Macrobicyclic amines. II. out-out in-in Prototropy in 1, (k + 2)-diazabicyclo [k.l.m] alkaneammonium ions”, *J. Am. Chem. Soc.*, 1968, **90**, 2429–2431.

[134] C. H. Park and H. E. Simmons, “Macrobicyclic amines. III. Encapsulation of halide ions by in,in-1,(k + 2)-diazabicyclo[k.l.m.]alkane ammonium ions”, *J. Am. Chem. Soc.*, 1968, **90**, 2431–2432.

[135] J. M. Lehn, “Cryptates: the chemistry of macropolycyclic inclusion complexes”, *Acc. Chem. Res.*, 1978, **11**, 49–57.

[136] P. A. Gale, in *Encyclopedia of Supramolecular Chemistry*, 2004, vol. 1, pp. 31–41.

[137] E. A. Katayev, Y. A. Ustynyuk and J. L. Sessler, “Receptors for tetrahedral oxyanions”, *Coord. Chem. Rev.*, 2006, **250**, 3004–3037.

[138] S. Kubik, “Anion recognition in water”, *Chem. Soc. Rev.*, 2010, **39**, 3648–3663.

[139] P. Dydio, D. Lichosyt and J. Jurczak, “Amide- and urea-functionalized pyrroles and benzopyrroles as synthetic, neutral anion receptors”, *Chem. Soc. Rev.*, 2011, **40**, 2971–2985.

[140] I. Ravikumar and P. Ghosh, “Recognition and separation of sulfate anions”, *Chem. Soc. Rev.*, 2012, **41**, 3077–3098.

[141] V. Blažek Bregović, N. Basarić and K. Mlinarić-Majerski, “Anion binding with urea and thiourea derivatives”, *Coord. Chem. Rev.*, 2015, **295**, 80–124.

[142] C. Jia, W. Zuo, D. Zhang, X. J. Yang and B. Wu, “Anion recognition by oligo-(thio)urea-based receptors”, *Chem. Commun.*, 2016, **52**, 9614–9627.

[143] J. Zhao, D. Yang, X. J. Yang and B. Wu, “Anion coordination chemistry: From recognition to supramolecular assembly”, *Coord. Chem. Rev.*, 2019, **378**, 415–444.

[144] L. K. Macreadie, A. M. Gilchrist, D. A. McNaughton, W. G. Ryder, M. Fares and P. A. Gale, “Progress in anion receptor chemistry”, *Chem*, 2022, **8**, 46–118.

[145] K. Bowman-James, “Alfred Werner revisited: The coordination chemistry of anions”, *Acc. Chem. Res.*, 2005, **38**, 671–678.

[146] P. Gilli, L. Pretto, V. Bertolasi and G. Gilli, “Predicting Hydrogen-Bond strengths from Acid-Base molecular properties. the pKa slide rule: Toward the solution of a Long-Lasting problem”, *Acc. Chem. Res.*, 2009, **42**, 33–44.

[147] P. A. Gale, J. T. Davis and R. Quesada, “Anion transport and supramolecular medicinal chemistry”, *Chem. Soc. Rev.*, 2017, **46**, 2497–2519.

[148] N. Busschaert, C. Caltagirone, W. Van Rossom and P. A. Gale, “Applications of Supramolecular Anion Recognition”, *Chem. Rev.*, 2015, **115**, 8038–8155.

[149] A. Pal, M. Karmakar, S. R. Bhatta and A. Thakur, “A detailed insight into anion sensing based on intramolecular charge transfer (ICT) mechanism: A comprehensive review of the years 2016 to 2021”, *Coord. Chem. Rev.*, 2021, **448**, 214167.

[150] N. Gimeno and R. Vilar, “Anions as templates in coordination and supramolecular chemistry”, *Coord. Chem. Rev.*, 2006, **250**, 3161–3189.

[151] S. Beckendorf, S. Asmus and O. G. Mancheño, “H-Donor Anion Acceptor Organocatalysis—The Ionic Electrophile Activation Approach”, *ChemCatChem*, 2012, **4**, 926–936.

[152] B. Schiøtt, B. B. Iversen, G. K. H. Madsen, F. K. Larsen and T. C. Bruice, “On the electronic nature of low-barrier hydrogen bonds in enzymatic reactions”, *Proc. Natl. Acad. Sci.*, 1998, **95**, 12799–12802.

[153] G. Gilli and P. Gilli, “Towards an unified hydrogen-bond theory”, *J. Mol. Struct.*, 2000, **552**, 1–15.

[154] V. W. Day, M. A. Hossain, S. O. Kang, D. Powell, G. Lushington and K. Bowman-James, “Encircled Proton”, *J. Am. Chem. Soc.*, 2007, **129**, 8692–8693.

[155] M. Rozenberg, A. Loewenschuss and C. J. Nielsen, “H-Bonding of Sulfuric Acid with Its Decomposition Products: An Infrared Matrix Isolation and Computational Study of the $H_2SO_4{\cdot}H_2O{\cdot}SO_3$ Complex”, *J. Phys. Chem. A*, 2016, **120**, 3450–3455.

[156] *Hans Reich’s Collection. Bordwell pKa Table*, https://organicchemistrydata.org/hansreich/resources/pka/.

[157] E. Rossini, A. D. Bochevarov and E. W. Knapp, “Empirical Conversion of pKa Values between Different Solvents and Interpretation of the Parameters: Application to Water, Acetonitrile, Dimethyl Sulfoxide, and Methanol”, *ACS Omega*, 2018, **3**, 1653–1662.

[158] X. Ni, X. Li, Z. Wang and J.-P. Cheng, “Squaramide Equilibrium Acidities in DMSO”, *Org. Lett.*, 2014, **16**, 1786–1789.

[159] N. Busschaert, I. L. Kirby, S. Young, S. J. Coles, P. N. Horton, M. E. Light and P. A. Gale, “Squaramides as Potent Transmembrane Anion Transporters”, *Angew. Chem. Int. Ed.*, 2012, **51**, 4426–4430.

[160] D. Quiñonero, R. Prohens, C. Garau, A. Frontera, P. Ballester, A. Costa and P. M. Deyà, “A theoretical study of aromaticity in squaramide complexes with anions”, *Chem. Phys. Lett.*, 2002, **351**, 115–120.

[161] N. Busschaert, R. B. P. Elmes, D. D. Czech, X. Wu, I. L. Kirby, E. M. Peck, K. D. Hendzel, S. K. Shaw, B. Chan, B. D. Smith, K. A. Jolliffe and P. A. Gale, “Thiosquaramides: pH switchable anion transporters”, *Chem. Sci.*, 2014, **5**, 3617–3626.

[162] S. Nishizawa, Y.-Y. Cui, M. Minagawa, K. Morita, Y. Kato, S. Taniguchi, R. Kato and N. Teramae, “Conversion of thioureas to fluorescent isothiouronium-based photoinduced electron transfer sensors for oxoanion sensing”, *J. Chem. Soc., Perkin Trans. 2*, 2002, 866–870.

[163] A. Casula, P. Begines, A. Bettoschi, J. G. Fernandez-Bolaños, F. Isaia, V. Lippolis, Ó. López, G. Picci, M. Andrea Scorciapino and C. Caltagirone, “Selenoureas for anion binding as molecular logic gates”, *Chem. Commun.*, 2017, **53**, 11869–11872.

[164] M. J. Spooner and P. A. Gale, “A tripodal tris-selenourea anion transporter matches the activity of its thio- analogue but shows distinct selectivity”, *Supramol. Chem.*, 2018, **30**, 514–519.

[165] G. Ciancaleoni, “Cooperativity between hydrogen- and halogen bonds: the case of selenourea”, *Phys. Chem. Chem. Phys.*, 2018, **20**, 8506–8514.

[166] S. A. Boer, E. M. Foyle, C. M. Thomas and N. G. White, “Anion coordination chemistry using O-H groups”, *Chem. Soc. Rev.*, 2019, **48**, 2596–2614.

[167] L. M. Eytel, H. A. Fargher, M. M. Haley and D. W. Johnson, “The road to aryl CH anion binding was paved with good intentions: fundamental studies, host design, and historical perspectives in CH hydrogen bonding”, *Chem. Commun.*, 2019, **55**, 5195–5206.

[168] A. J. Arduengo, “Looking for Stable Carbenes: The Difficulty in Starting Anew”, *Acc. Chem. Res.*, 1999, **32**, 913–921.

[169] H. Du and X. Qian, “The effects of acetate anion on cellulose dissolution and reaction in imidazolium ionic liquids”, *Carbohydr. Res.*, 2011, **346**, 1985–1990.

[170] K. Hirose, “A Practical Guide for the Determination of Binding Constants”, *J. Inclusion Phenom. Macrocyclic Chem.*, 2001, **39**, 193–209.

[171] P. Thordarson, “Determining association constants from titration experiments in supramolecular chemistry”, *Chem. Soc. Rev.*, 2011, **40**, 1305–1323.

[172] *supramolecular.org*, http://supramolecular.org (visited on 09/12/2023).

[173] C. Hübler, “SupraFit - An Open Source Qt Based Fitting Application to Determine Stability Constants from Titration Experiments”, *Chem. Methods*, 2022, **2**, e202200006.

[174] M. J. Hynes, “EQNMR: a computer program for the calculation of stability constants from nuclear magnetic resonance chemical shift data”, *J. Chem. Soc., Dalton Trans.*, 1993, 311–312.

[175] D. Brynn Hibbert and P. Thordarson, “The death of the Job plot, transparency, open science and online tools, uncertainty estimation methods and other developments in supramolecular chemistry data analysis”, *Chem. Commun.*, 2016, **52**, 12792–12805.

[176] R. G. LeBel and D. A. I. Goring, “Density, Viscosity, Refractive Index, and Hygroscopicity of Mixtures of Water and Dimethyl Sulfoxide”, *J. Chem. Eng. Data*, 1962, **7**, 100–101.

[177] F. A. Quiocho and P. S. Ledvina, “Atomic structure and specificity of bacterial periplasmic receptors for active transport and chemotaxis: variation of common themes”, *Mol. Microbiol.*, 1996, **20**, 17–25.

[178] J. H. Jing and A. Q. Florante, “A Nonconservative Serine to Cysteine Mutation in the Sulfate-Binding Protein, a Transport Receptor”, *Science*, 1991, **251**, 1479–1481.

[179] P. Bühlmann, S. Nishizawa, K. P. Xiao and Y. Umezawa, “Strong hydrogen bond-mediated complexation of $H_2PO_4^-$ by neutral bis-thiourea hosts”, *Tetrahedron*, 1997, **53**, 1647–1654.

[180] S. Nishizawa, P. Bühlmann, M. Iwao and Y. Umezawa, “Anion recognition by urea and thiourea groups: Remarkably simple neutral receptors for dihydrogenphosphate”, *Tetrahedron Lett.*, 1995, **36**, 6483–6486.

[181] T. Shioya, S. Nishizawa and N. Teramae, “Anion recognition at the liquid-liquid interface. Sulfate transfer across the 1,2-dichloroethane-water interface facilitated by hydrogen- bonding ionophores”, *J. Am. Chem. Soc.*, 1998, **120**, 11534–11535.

[182] S. J. Brooks, P. A. Gale and M. E. Light, “Carboxylate complexation by 1,1’-(1,2-phenylene)bis(3-phenylurea) in solution and the solid state”, *Chem. Commun.*, 2005, 4696–4698.

[183] S. J. Brooks, P. R. Edwards, P. A. Gale and M. E. Light, “Carboxylate complexation by a family of easy-to-make ortho-phenylenediamine based bisureas: studies in solution and the solid state”, *New J. Chem.*, 2006, **30**, 65–70.

[184] R. Li, Y. Zhao, S. Li, P. Yang, X. Huang, X. J. Yang and B. Wu, “Tris chelating phosphate complexes of bis(thio)urea ligands”, *Inorg. Chem.*, 2013, **52**, 5851–5860.

[185] S. J. Moore, C. J. E. Haynes, J. González, J. L. Sutton, S. J. Brooks, M. E. Light, J. Herniman, G. J. Langley, V. Soto-Cerrato, R. Pérez-Tomás, I. Marques, P. J. Costa, V. Félix and P. A. Gale, “Chloride, carboxylate and carbonate transport by ortho-phenylenediamine-based bisureas”, *Chem. Sci.*, 2013, **4**, 103–117.

[186] C. Jia, B. Wu, S. Li, Z. Yang, Q. Zhao, J. Liang, Q. S. Li and X. J. Yang, “A fully complementary, high-affinity receptor for phosphate and sulfate based on an acyclic tris(urea) scaffold”, *Chem. Commun.*, 2010, **46**, 5376–5378.

[187] Y. Zhang, R. Zhang, Y. Zhao, L. Ji, C. Jia and B. Wu, “Anion binding of tris-(thio)urea ligands”, *New J. Chem.*, 2013, **37**, 2266–2270.

[188] C. Raposo, M. Almaraz, M. Martín, V. Weinrich, M. L. Mussóns, V. Alcázar, M. C. Caballero and J. R. Morán, “Tris(2-aminoethyl)amine, a Suitable Spacer for Phosphate and Sulfate Receptors”, *Chem. Lett.*, 1995, **24**, 759–760.

[189] R. Custelcean, “Urea-functionalized crystalline capsules for recognition and separation of tetrahedral oxoanions”, *Chem. Commun.*, 2013, **49**, 2173–2182.

[190] A. Rajbanshi, B. A. Moyer and R. Custelcean, “Sulfate Separation from Aqueous Alkaline Solutions by Selective Crystallization of Alkali Metal Coordination Capsules”, *Cryst. Growth Des.*, 2011, **11**, 2702–2706.

[191] N. Busschaert, M. Wenzel, M. E. Light, P. Iglesias-hern, P. Ricardo and P. A. Gale, “Structure-Activity Relationships in Tripodal Transmembrane Anion Transporters: The Effect of Fluorination”, *J. Am. Chem. Soc.*, 2011, **133**, 14136–14148.

[192] B. Akhuli, I. Ravikumar and P. Ghosh, “Acid/base controlled size modulation of capsular phosphates, hydroxide encapsulation, quantitative and clean extraction of sulfate with carbonate capsules of a tripodal urea receptor”, *Chem. Sci.*, 2012, **3**, 1522–1530.

[193] P. Bose, R. Dutta, S. Santra, B. Chowdhury and P. Ghosh, “Combined Solution-Phase, Solid-Phase and Phase-Interface Anion Binding and Extraction Studies by a Simple Tripodal Thiourea Receptor”, *Eur. J. Inorg. Chem.*, 2012, **2012**, 5791–5801.

[194] C. Jia, B. Wu, S. Li, X. Huang, Q. Zhao, Q. S. Li and X. J. Yang, “Highly efficient extraction of sulfate ions with a tripodal hexaurea receptor”, *Angew. Chem. Int. Ed.*, 2011, **50**, 486–490.

[195] S.-Q. Chen, S.-N. Yu, W. Zhao, L. Liang, Y. Gong, L. Yuan, J. Tang, X.-J. Yang and B. Wu, “Recognition-guided sulfate extraction and transport using tripodal hexaurea receptors”, *Inorg. Chem. Front.*, 2022, **9**, 6091–6101.

[196] L. Qin, S. J. N. Vervuurt, R. B. P. Elmes, S. N. Berry, N. Proschogo and K. A. Jolliffe, “Extraction and transport of sulfate using macrocyclic squaramide receptors”, *Chem. Sci.*, 2020, **11**, 201–207.

[197] A. Baeyer, “Polymerisation der Propargylsaure”, *Ber. Dtsch. Chem. Ges.*, 1886, **19**, 2184–2185.

[198] C. J. Fowler, T. J. Haverlock, B. A. Moyer, J. A. Shriver, D. E. Gross, M. Marquez, J. L. Sessler, M. A. Hossain and K. Bowman-James, “Enhanced anion exchange for selective sulfate extraction: Overcoming the Hofmeister bias”, *J. Am. Chem. Soc.*, 2008, **130**, 14386–14387.

[199] B. A. Moyer, F. V. Sloop, C. J. Fowler, T. J. Haverlock, H.-A. Kang, L. H. Delmau, D. M. Bau, A. M. Hossain, K. Bowman-James, J. A. Shriver, N. L. Bill, M. Marquez, V. M. Lynch and J. L. Sessler, “Enhanced liquid-liquid anion exchange using macrocyclic anion receptors: effect of receptor structure on sulphate-nitrate exchange selectivity”, *Supramol. Chem.*, 2010, **22**, 653–671.

[200] C. J. Borman, R. Custelcean, B. P. Hay, N. L. Bill, J. L. Sessler and B. A. Moyer, “Supramolecular organization of calix[4]pyrrole with a methyltrialkylammonium anion exchanger leads to remarkable reversal of selectivity for sulfate extraction vs. nitrate”, *Chem. Commun.*, 2011, **47**, 7611–7613.

[201] R. Custelcean, L. H. Delmau, B. A. Moyer, J. L. Sessler, W.-S. Cho, D. Gross, G. W. Bates, S. J. Brooks, M. E. Light and P. A. Gale, “Calix[4]pyrrole: An Old yet New Ion-Pair Receptor”, *Angew. Chem.*, 2005, **117**, 2593–2598.

[202] J. L. Sessler, D. E. Gross, W.-S. Cho, V. M. Lynch, F. P. Schmidtchen, G. W. Bates, M. E. Light and P. A. Gale, “Calix[4]pyrrole as a Chloride Anion Receptor: Solvent and Countercation Effects”, *J. Am. Chem. Soc.*, 2006, **128**, 12281–12288.

[203] D. E. Gross, F. P. Schmidtchen, W. Antonius, P. A. Gale, V. M. Lynch and J. L. Sessler, “Cooperative Binding of Calix[4]pyrrole-Anion Complexes and Alkylammonium Cations in Halogenated Solvents”, *Chem. Eur. J.*, 2008, **14**, 7822–7827.

[204] M. P. Wintergerst, T. G. Levitskaia, B. A. Moyer, J. L. Sessler and L. H. Delmau, “Calix[4]pyrrole: A New Ion-Pair Receptor As Demonstrated by Liquid-Liquid Extraction”, *J. Am. Chem. Soc.*, 2008, **130**, 4129–4139.

[205] C. J. Borman, P. V. Bonnesen and B. A. Moyer, “Selectivity Control in Synergistic Liquid-Liquid Anion Exchange of Univalent Anions via Structure-Specific Cooperativity between Quaternary Ammonium Cations and Anion Receptors”, *Anal. Chem.*, 2012, **84**, 8214–8221.

[206] N. J. Williams, V. S. Bryanstev, R. Custelcean, C. A. Seipp and B. A. Moyer, “α,α’,α",α’"-meso-tetrahexyltetramethyl-calix[4]pyrrole: an easy-to-prepare, isomerically pure anion extractant with enhanced solubility in organic solvents”, *Supramol. Chem.*, 2016, **28**, 176–187.

[207] P. A. Gale, J. L. Sessler, V. Král and V. Lynch, “Calix[4]pyrroles: Old Yet New Anion-Binding Agents”, *J. Am. Chem. Soc.*, 1996, **118**, 5140–5141.

[208] S. Peng, Q. He, G. I. Vargas-Zúñiga, L. Qin, I. Hwang, S. K. Kim, N. J. Heo, C.-H. Lee, R. Dutta and J. L. Sessler, “Strapped calix[4]pyrroles: from syntheses to applications”, *Chem. Soc. Rev.*, 2020, **49**, 865–907.

[209] S. K. Kim, J. Lee, N. J. Williams, V. M. Lynch, B. P. Hay, B. A. Moyer and J. L. Sessler, “Bipyrrole-Strapped Calix[4]pyrroles: Strong Anion Receptors That Extract the Sulfate Anion”, *J. Am. Chem. Soc.*, 2014, **136**, 15079–15085.

[210] R. Custelcean, N. J. Williams and C. A. Seipp, “Aqueous Sulfate Separation by Crystallization of Sulfate-Water Clusters”, *Angew. Chem. Int. Ed.*, 2015, **54**, 10525–10529.

[211] J. D. Einkauf, V. S. Bryantsev, B. A. Moyer and R. Custelcean, “A Photoresponsive Receptor with a 105 Magnitude of Reversible Anion-Binding Switching”, *Chem. Eur. J.*, 2022, **28**, e202200719.

[212] J. E. Bara, in *Ionic Liquids for Environmental Issues*, Royal Society of Chemistry, 2023.

[213] M. Ramdin, T. W. de Loos and T. J. H. Vlugt, “State-of-the-Art of CO2 Capture with Ionic Liquids”, *Ind. Eng. Chem. Res.*, 2012, **51**, 8149–8177.

[214] M. Aghaie, N. Rezaei and S. Zendehboudi, “A systematic review on CO2 capture with ionic liquids: Current status and future prospects”, *Renewable Sustainable Energy Rev.*, 2018, **96**, 502–525.

[215] X. Zhang, X. Zhang, H. Dong, Z. Zhao, S. Zhang and Y. Huang, “Carbon capture with ionic liquids: overview and progress”, *Energy Environ. Sci.*, 2012, **5**, 6668–6681.

[216] S. D. Kenarsari, D. Yang, G. Jiang, S. Zhang, J. Wang, A. G. Russell, Q. Wei and M. Fan, “Review of recent advances in carbon dioxide separation and capture”, *RSC Adv.*, 2013, **3**, 22739–22773.

[217] Y. Fu, Z. Yang, S. M. Mahurin, S. Dai and D. en Jiang, “Ionic liquids for carbon capture”, *MRS Bull.*, 2022, **47**, 1–10.

[218] D. Hospital-Benito, J. Lemus, C. Moya, R. Santiago, V. R. Ferro and J. Palomar, “Techno-economic feasibility of ionic liquids-based CO2 chemical capture processes”, *Chem. Eng. J.*, 2021, **407**, 127196.

[219] R. R. Bottoms, “Process for Separating Acid Gases”, 1930, US Pat. 1783901.

[220] G. T. Rochelle, “Amine Scrubbing for CO2 Capture”, *Science*, 2009, **325**, 1652–1654.

[221] H. M. Stowe and G. S. Hwang, “Fundamental Understanding of CO2 Capture and Regeneration in Aqueous Amines from First-Principles Studies: Recent Progress and Remaining Challenges”, *Ind. Eng. Chem. Res.*, 2017, **56**, 6887–6899.

[222] G. Rochelle, E. Chen, S. Freeman, D. Van Wagener, Q. Xu and A. Voice, “Aqueous piperazine as the new standard for CO2 capture technology”, *Chem. Eng. J.*, 2011, **171**, 725–733.

[223] M. R. M. Abu-Zahra, L. H. J. Schneiders, J. P. M. Niederer, P. H. M. Feron and G. F. Versteeg, “CO2 capture from power plants: Part I. A parametric study of the technical performance based on monoethanolamine”, *nt. J. Greenhouse Gas Control*, 2007, **1**, 8th International Conference on Greenhouse Gas Control Technologies, 37–46.

[224] I. M. Bernhardsen and H. K. Knuutila, “A review of potential amine solvents for CO2 absorption process: Absorption capacity, cyclic capacity and pKa”, *Int. J. Greenhouse Gas Control*, 2017, **61**, 27–48.

[225] Z. L. Ooi, P. Y. Tan, L. S. Tan and S. P. Yeap, “Amine-based solvent for CO2 absorption and its impact on carbon steel corrosion: A perspective review”, *Chin. J. Chem. Eng.*, 2020, **28**, 1357–1367.

[226] K. Li, W. Leigh, P. Feron, H. Yu and M. Tade, “Systematic study of aqueous monoethanolamine (MEA)-based CO2 capture process: Techno-economic assessment of the MEA process and its improvements”, *Appl. Energy*, 2016, **165**, 648–659.

[227] M. R. M. Abu-Zahra, J. P. M. Niederer, P. H. M. Feron and G. F. Versteeg, “CO2 capture from power plants: Part II. A parametric study of the economical performance based on mono-ethanolamine”, *nt. J. Greenhouse Gas Control*, 2007, **1**, 8th International Conference on Greenhouse Gas Control Technologies, 135–142.

[228] P. Luis, “Use of monoethanolamine (MEA) for CO2 capture in a global scenario: Consequences and alternatives”, *Desalination*, 2016, **380**, 93–99.

[229] S. F. R. Taylor, M. McClung, C. McReynolds, H. Daly, A. J. Greer, J. Jacquemin and C. Hardacre, “Understanding the Competitive Gas Absorption of CO2 and SO2 in Superbase Ionic Liquids”, *Ind. Eng. Chem. Res.*, 2018, **57**, 17033–17042.

[230] K. Huang, Y. T. Wu and S. Dai, “Sigmoid Correlations for Gas Solubility and Enthalpy Change of Chemical Absorption of CO2”, *Ind. Eng. Chem. Res.*, 2015, **54**, 10126–10133.

[231] L. A. Blanchard, D. Hancu, E. J. Beckman and J. F. Brenneceke, “Green processing using ionic liquids and CO2”, *Nature*, 1999, **399**, 28–29.

[232] J. E. Bara, T. K. Carlisle, C. J. Gabriel, D. Camper, A. Finotello, D. L. Gin and R. D. Noble, “Guide to CO_2 separations in imidazolium-based room-temperature ionic liquids”, *Ind. Eng. Chem. Res.*, 2009, **48**, 2739–2751.

[233] M. S. Shannon, J. M. Tedstone, S. P. O. Danielsen, M. S. Hindman, A. C. Irvin and J. E. Bara, “Free volume as the basis of gas solubility and selectivity in imidazolium-based ionic liquids”, *Ind. Eng. Chem. Res.*, 2012, **51**, 5565–5576.

[234] C. Cadena, J. L. Anthony, J. K. Shah, T. I. Morrow, J. F. Brennecke and E. J. Maginn, “Why is CO2 so Soluble in Imidazolium-Based Ionic Liquids?”, *J. Am. Chem. Soc.*, 2004, **126**, 5300–5308.

[235] E. D. Bates, R. D. Mayton, I. Ntai and J. H. Davis, “CO2 Capture by a Task-Specific Ionic Liquid”, *J. Am. Chem. Soc.*, 2002, **124**, 926–927.

[236] J. H. Davis, “Task-specific ionic liquids”, *Chem. Lett.*, 2004, **33**, 1072–1077.

[237] B. E. Gurkan, J. C. D. Fuente, E. M. Mindrup, L. E. Ficke, B. F. Goodrich, E. A. Price, W. F. Schneider and J. F. Brennecke, “Equimolar CO2 Absorption by Anion-Functionalized Ionic Liquids”, *J. Am. Chem. Soc.*, 2010, **132**, 2116–2117.

[238] B. F. Goodrich, J. C. De La Fuente, B. E. Gurkan, Z. K. Lopez, E. A. Price, Y. Huang and J. F. Brennecke, “Effect of water and temperature on absorption of CO2 by amine-functionalized anion-tethered ionic liquids”, *J. Phys. Chem. B*, 2011, **115**, 9140–9150.

[239] K. E. Gutowski and E. J. Maginn, “Amine-Functionalized Task-Specific Ionic Liquids: A Mechanistic Explanation for the Dramatic Increase in Viscosity upon Complexation with CO2 from Molecular Simulation”, *J. Am. Chem. Soc.*, 2008, **130**, 14690–14704.

[240] S. A. Freeman, R. Dugas, D. H. Van Wagener, T. Nguyen and G. T. Rochelle, “Carbon dioxide capture with concentrated, aqueous piperazine”, *Int. J. Greenhouse Gas Control*, 2010, **4**, The Ninth International Conference on Greenhouse Gas Control Technologies, 119–124.

[241] J. D. Holbrey, W. M. Reichert, I. Tkatchenko, E. Bouajila, O. Walter, I. Tommasi and R. D. Rogers, “1,3-Dimethylimidazolium-2-carboxylate: the unexpected synthesis of an ionic liquid precursor and carbene-CO2 adduct”, *Chem. Commun.*, 2003, 28–29.

[242] C. Wang, H. Luo, X. Luo, H. Li and S. Dai, “Equimolar CO2 capture by imidazolium-based ionic liquids and superbase systems”, *Green Chem.*, 2010, **12**, 2019–2023.

[243] F. Philippi, D. Rauber, O. Palumbo, K. Goloviznina, J. McDaniel, D. Pugh, S. Suarez, C. C. Fraenza, A. Padua, C. W. M. Kay and T. Welton, “Flexibility is the key to tuning the transport properties of fluorinated imide-based ionic liquids”, *Chem. Sci.*, 2022, **13**, 9176–9190.

[244] L. Conte, G. Gambaretto, G. Caporiccio, F. Alessandrini and S. Passerini, “Perfluoroalkanesulfonylimides and their lithium salts: synthesis and characterisation of intermediates and target compounds”, *J. Fluorine Chem.*, 2004, **125**, 243–252.

[245] G. Gurau, H. Rodríguez, S. P. Kelley, P. Janiczek, R. S. Kalb and R. D. Rogers, “Demonstration of Chemisorption of Carbon Dioxide in 1,3-Dialkylimidazolium Acetate Ionic Liquids”, *Angew. Chem. Int. Ed.*, 2011, **50**, 12024–12026.

[246] B. Gurkan, B. F. Goodrich, E. M. Mindrup, L. E. Ficke, M. Massel, S. Seo, T. P. Senftle, H. Wu, M. F. Glaser, J. K. Shah, E. J. Maginn, J. F. Brennecke and W. F. Schneider, "Molecular Design of High Capacity, Low Viscosity, Chemically Tunable Ionic Liquids for CO2 Capture", *J. Phys. Chem. Lett.*, 2010, **1**, 3494–3499.

[247] S. Seo, M. Quiroz-Guzman, M. A. Desilva, T. B. Lee, Y. Huang, B. F. Goodrich, W. F. Schneider and J. F. Brennecke, "Chemically tunable ionic liquids with aprotic heterocyclic anion (AHA) for CO2 capture", *J. Phys. Chem. B*, 2014, **118**, 5740–5751.

[248] C. Wang, H. Luo, D.-e. Jiang, H. Li and S. Dai, "Carbon Dioxide Capture by Superbase-Derived Protic Ionic Liquids", *Angew. Chem.*, 2010, **122**, 6114–6117.

[249] C. Wang, X. Luo, H. Luo, D. E. Jiang, H. Li and S. Dai, "Tuning the basicity of ionic liquids for equimolar CO2 capture", *Angew. Chem. Int. Ed.*, 2011, **50**, 4918–4922.

[250] J. Nowicki, M. Muszyński and J.-P. Mikkola, "Ionic liquids derived from organosuperbases: en route to superionic liquids", *RSC Adv.*, 2016, **6**, 9194–9208.

[251] Y. Shang, H. Li, S. Zhang, H. Xu, Z. Wang, L. Zhang and J. Zhang, "Guanidinium-based ionic liquids for sulfur dioxide sorption", *Chem. Eng. J.*, 2011, **175**, 324–329.

[252] X. Lei, Y. Xu, L. Zhu and X. Wang, "Highly efficient and reversible CO2 capture through 1,1,3,3-tetramethylguanidinium imidazole ionic liquid", *RSC Adv.*, 2014, **4**, 7052–7057.

[253] F. Li, Y. Bai, S. Zeng, X. Liang, H. Wang, F. Huo and X. Zhang, "Protic ionic liquids with low viscosity for efficient and reversible capture of carbon dioxide", *Int. J. Greenhouse Gas Control*, 2019, **90**, 102801.

[254] D. J. Heldebrant, C. R. Yonker, P. G. Jessop and L. Phan, "Organic liquid CO2 capture agents with high gravimetric CO2 capacity", *Energy Environ. Sci.*, 2008, **1**, 487–493.

[255] K. Chen, G. Shi, W. Zhang, H. Li and C. Wang, "Computer-Assisted Design of Ionic Liquids for Efficient Synthesis of 3(2H)-Furanones: A Domino Reaction Triggered by CO2", *J. Am. Chem. Soc.*, 2016, **138**, 14198–14201.

[256] X. Zhu, M. Song and Y. Xu, "DBU-Based Protic Ionic Liquids for CO2 Capture", *ACS Sustainable Chem. Eng.*, 2017, **5**, 8192–8198.

[257] X. Zhu, M. Song, B. Ling, S. Wang and X. Luo, “The Highly Efficient Absorption of CO2 by a Novel DBU Based Ionic Liquid”, *J. Solution Chem.*, 2020, **49**, 257–271.

[258] F. Gao, Z. Wang, P. Ji and J.-P. Cheng, “CO2 Absorption by DBU-Based Protic Ionic Liquids: Basicity of Anion Dictates the Absorption Capacity and Mechanism”, *Front. Chem.*, 2019, **6**, 658.

[259] R. Vijayraghavan, S. J. Pas, E. I. Izgorodina and D. R. MacFarlane, “Diamino protic ionic liquids for CO2 capture”, *Phys. Chem. Chem. Phys.*, 2013, **15**, 19994–19999.

[260] T. Oncsik, R. Vijayaraghavan and D. R. Macfarlane, “High CO2 absorption by diamino protic ionic liquids using azolide anions”, *Chem. Commun.*, 2018, **54**, 2106–2109.

[261] T. Zhao, X. Zhang, Z. Tu, Y. Wu and X. Hu, “Low-viscous diamino protic ionic liquids with fluorine-substituted phenolic anions for improving CO2 reversible capture”, *J. Mol. Liq.*, 2018, **268**, 617–624.

[262] J. Clayden, N. Greeves, S. G. Warren and J. Clayden, *Organic chemistry*, Oxford University Press, Oxford, Second edition., 2012, ch. 22, pp. 514–527.

[263] T. R. Gohndrone, T. Bum Lee, M. A. Desilva, M. Quiroz-Guzman, W. F. Schneider and J. F. Brennecke, “Competing reactions of CO2 with cations and anions in azolide ionic liquids”, *ChemSusChem*, 2014, **7**, 19701975.

[264] C. Wang, H. Luo, H. Li, X. Zhu, B. Yu and S. Dai, “Tuning the physicochemical properties of diverse phenolic ionic liquids for equimolar CO 2 capture by the substituent on the anion”, *Chem. Eur. J.*, 2012, **18**, 2153–2160.

[265] K. Huang, X. M. Zhang, L. S. Zhou, D. J. Tao and J. P. Fan, “Highly efficient and selective absorption of H2S in phenolic ionic liquids: A cooperative result of anionic strong basicity and cationic hydrogen-bond donation”, *Chem. Eng. Sci.*, 2017, **173**, 253–263.

[266] X.-M. Zhang, K. Huang, S. Xia, Y.-L. Chen, Y.-T. Wu and X.-B. Hu, “Low-viscous fluorine-substituted phenolic ionic liquids with high performance for capture of CO2”, *Chem. Eng. J.*, 2015, **274**, 30–38.

[267] A. Stojanovic, D. Kogelnig, L. Fischer, S. Hann, M. Galanski, M. Groessl, R. Krachler and B. K. Keppler, “Phosphonium and Ammonium Ionic Liquids with Aromatic Anions: Synthesis, Properties, and Platinum Extraction”, *Aust. J. Chem.*, 2010, **63**, 511–524.

[268] A. Samanta, A. Zhao, G. K. H. Shimizu, P. Sarkar and R. Gupta, “Post-Combustion CO2 Capture Using Solid Sorbents: A Review”, *Ind. Eng. Chem. Res.*, 2012, **51**, 1438–1463.

[269] Y. Zheng, A. D. Jensen, C. Windelin and F. Jensen, “Review of technologies for mercury removal from flue gas from cement production processes”, *Prog. Energy Combust. Sci.*, 2012, **38**, 599–629.

[270] K. Yagihara, H. Ohno, A. Guzman-Urbina, J. Ni and Y. Fukushima, “Analyzing flue gas properties emitted from power and industrial sectors toward heat-integrated carbon capture”, *Energy*, 2022, **250**, 123775.

[271] D. G. Boer, J. Langerak and P. P. Pescarmona, “Zeolites as Selective Adsorbents for CO2 Separation”, *ACS Appl. Energy Mater.*, 2023, **6**, 2634–2656.

[272] S. B. Peh, S. Farooq and D. Zhao, “Techno-economic analysis of MOF-based adsorption cycles for postcombustion CO2 capture from wet flue gas”, *Chem. Eng. Sci.*, 2023, **268**, 118390.

[273] P. Panja, B. McPherson and M. Deo, “Techno-Economic Analysis of Amine-based CO2 Capture Technology: Hunter Plant Case Study”, *Carbon Capture Sci. Technol.*, 2022, **3**, 100041.

[274] M. G. Freire, C. M. S. S. Neves, P. J. Carvalho, R. L. Gardas, A. M. Fernandes, I. M. Marrucho, L. M. N. B. F. Santos and J. A. P. Coutinho, “Mutual Solubilities of Water and Hydrophobic Ionic Liquids”, *J. Phys. Chem. B*, 2007, **111**, 13082–13089.

[275] M. G. Freire, P. J. Carvalho, R. L. Gardas, I. M. Marrucho, L. M. N. B. F. Santos and J. A. P. Coutinho, “Mutual Solubilities of Water and the [Cnmim][Tf2N] Hydrophobic Ionic Liquids”, *J. Phys. Chem. B*, 2008, **112**, 1604–1610.

[276] M. G. Freire, P. J. Carvalho, A. M. S. Silva, L. M. N. B. F. Santos, L. P. N. Rebelo, I. M. Marrucho and J. A. P. Coutinho, “Ion Specific Effects on the Mutual Solubilities of Water and Hydrophobic Ionic Liquids”, *J. Phys. Chem. B*, 2009, **113**, 202–211.

[277] E. Rilo, A. Rosende-Pereiro, M. Domínguez-Pérez, O. Cabeza and L. Segade, “New Insights into the Hygroscopic Character of Ionic Liquids: Study of Fourteen Representatives of Five Cation and Four Anion Families”, *Int. J. Mol. Sci.*, 2024, **25**, 4429.

[278] H. Watanabe, T. Komura, R. Matsumoto, K. Ito, H. Nakayama, T. Nokami and T. Itoh, “Design of ionic liquids as liquid desiccant for an air conditioning system”, *Green Energy Environ.*, 2019, **4**, 139–145.

[279] J. L. McDonald, R. E. Sykora, P. Hixon, A. Mirjafari and J. H. Davis, “Impact of water on CO2 capture by amino acid ionic liquids”, *Environ. Chem. Lett.*, 2014, **12**, 201–208.

[280] G. M. Avelar Bonilla, O. Morales-Collazo and J. F. Brennecke, “Effect of Water on CO2 Capture by Aprotic Heterocyclic Anion (AHA) Ionic Liquids”, *ACS Sustainable Chem. Eng.*, 2019, **7**, 16858–16869.

[281] S. F. R. Taylor, C. McCrellis, C. McStay, J. Jacquemin, C. Hardacre, M. Mercy, R. G. Bell and N. H. de Leeuw, “CO2 capture in wet and dry superbase ionic liquids”, *J. Solution Chem.*, 2015, **44**, 511–527.

[282] Z. Henderson, A. G. Thomas, M. Wagstaffe, S. F. R. Taylor, C. Hardacre and K. L. Syres, “Reversible Reaction of CO2 with Superbasic Ionic Liquid [P66614][benzim] Studied with in Situ Photoelectron Spectroscopy”, *J. Phys. Chem. C*, 2019, **123**, 7134–7141.

[283] A. J. Greer, S. F. Taylor, H. Daly, M. Quesne, C. R. A. Catlow, J. Jacquemin and C. Hardacre, “Investigating the Effect of NO on the Capture of CO2 Using Superbase Ionic Liquids for Flue Gas Applications”, *ACS Sustainable Chem. Eng.*, 2019, **7**, 3567–3574.

[284] W. Wu, B. Han, H. Gao, Z. Liu, T. Jiang and J. Huang, “Desulfurization of Flue Gas: SO2 Absorption by an Ionic Liquid”, *Angew. Chem. Int. Ed.*, 2004, **43**, 2415–2417.

[285] S. Yan, F. Han, Q. Hou, S. Zhang and S. Ai, “Recent Advances in Ionic Liquid-Mediated SO2 Capture”, *Ind. Eng. Chem. Res.*, 2019, **58**, 13804–13818.

[286] S. Tian, Y. Hou, W. Wu, S. Ren and J. Qian, “Hydrophobic task-specific ionic liquids: Synthesis, properties and application for the capture of SO2”, *J. Hazard. Mater.*, 2014, **278**, 409–416.

[287] R. Vijayaraghavan, T. Oncsik, B. Mitschke and D. R. MacFarlane, “Base-rich diamino protic ionic liquid mixtures for enhanced CO2 capture”, *Sep. Purif. Technol.*, 2018, **196**, 27–31.

[288] S. H. McCalmont, I. C. M. Vaz, H. Oorts, Z. Gong, L. Moura and M. Costa Gomes, “Insights into the Absorption of Hydrocarbon Gases in Phosphorus-Containing Ionic Liquids”, *J. Phys. Chem. B*, 2023, **127**, 3402–3415.

[289] S. Liu, B. Lai and S. L. James, “Effects of Particle Size on the Gas Uptake Kinetics and Physical Properties of Type III Porous Liquids”, *ACS Appl. Mater. Interfaces*, 2024, **16**, 16436–16444.

[290] L. F. Lepre, J. Szala-Bilnik, L. Pison, M. Traïkia, A. A. H. Pádua, R. A. Ando and M. F. Costa Gomes, “Can the tricyanomethanide anion improve CO2 absorption by acetate-based ionic liquids?”, *Phys. Chem. Chem. Phys.*, 2017, **19**, 12431–12440.

[291] J. M. Young, S. H. McCalmont, S. Fourmentin, P. Manesiotis, J. D. Holbrey and L. Moura, “A High-Throughput Experimental Approach to Screening Gas Sorption by Liquids and Solids”, *ACS Sustainable Chem. Eng.*, 2023, **11**, 17787–17796.

[292] B. I. Lee and M. G. Kesler, “A generalized thermodynamic correlation based on three-parameter corresponding states”, *AIChE J.*, 1975, **21**, 510–527.

[293] M. Dilip, N. J. Bridges, H. Rodríguez, J. F. B. Pereira and R. D. Rogers, “Effect of Temperature on Salt-Salt Aqueous Biphasic Systems: Manifestations of Upper Critical Solution Temperature”, *J. Chem. Eng. Data*, 2015, **44**, 454–468.

[294] M. G. Freire, P. J. Carvalho, R. L. Gardas, L. M. N. B. F. Santos, I. M. Marrucho and J. A. P. Coutinho, “Solubility of water in tetradecyltrihexylphosphonium-based ionic liquids”, *J. Chem. Eng. Data*, 2008, **53**, 2378–2382.

[295] C. M. S. S. Neves, P. J. Carvalho, M. G. Freire and J. A. P. Coutinho, “Thermophysical properties of pure and water-saturated tetradecyltrihexylphosphonium-based ionic liquids”, *J. Chem. Thermodyn.*, 2011, **43**, 948–957.

[296] M. Matsumoto, A. Panigrahi, Y. Murakami and K. Kondo, “Effect of Ammonium- and Phosphonium-Based Ionic Liquids on the Separation of Lactic Acid by Supported Ionic Liquid Membranes (SILMs)”, *Membranes*, 2011, **1**, 98–108.

[297] K. Anderson, H. Rodríguez and K. R. Seddon, “Phase behaviour of trihexyl(tetradecyl)phosphonium chloride, nonane and water”, *Green Chem.*, 2009, **11**, 780–784.

[298] S. Lago, H. Rodríguez, M. K. Khoshkbarchi, A. Soto and A. Arce, “Enhanced oil recovery using the ionic liquid trihexyl(tetradecyl)phosphonium chloride: phase behaviour and properties”, *RSC Adv.*, 2012, **2**, 9392–9397.

[299] T. Koonsang, K. Aunnankat, K. Maneeintr, U. Pancharoen and T. Wongsawa, “The mutual solubility of organic-liquid membrane and aqueous phases at different water pH for the stability of SLM using Aliquat 336 as an ionic-liquid extractant”, *J. Mol. Liq.*, 2019, **292**, 111363.

[300] V. T. Nguyen, S. Riaño and K. Binnemans, “Separation of precious metals by split-anion extraction using water-saturated ionic liquids”, *Green Chem.*, 2020, **22**, 8375–8388.

[301] *Chemical book: Aliquat 336*, www.chemicalbook.com/ProductMSDSDetailCB4412612_EN.htm#2 (visited on 11/29/2022).

[302] T. Klein, S. Yan, J. Cui, J. W. Magee, K. Kroenlein, M. H. Rausch, T. M. Koller and A. P. Fröba, "Liquid Viscosity and Surface Tension of n-Hexane, n-Octane, n-Decane, and n-Hexadecane up to 573 K by Surface Light Scattering", *J. Chem. Eng. Data*, 2019, **64**, 4116–4131.

[303] M. L. Huber, R. A. Perkins, A. Laesecke, D. G. Friend, J. V. Sengers, M. J. Assael, I. N. Metaxa, E. Vogel, R. Mareš and K. Miyagawa, "New International Formulation for the Viscosity of H2O", *Journal of Physical and Chemical Reference Data*, 2009, **38**, 101–125.

[304] M. Tanaka, G. Girard, R. Davis, A. Peuto and N. Bignell, "Recommended table for the density of water between 0 °C and 40 °C based on recent experimental reports", *Metrologia*, 2001, **38**, 301.

[305] T. Vander Hoogerstraete, S. Wellens, K. Verachtert and K. Binnemans, "Removal of transition metals from rare earths by solvent extraction with an undiluted phosphonium ionic liquid: separations relevant to rare-earth magnet recycling", *Green Chem.*, 2013, **15**, 919–927.

[306] J. Jacquemin, P. Husson, A. A. H. Padua and V. Majer, "Density and viscosity of several pure and water-saturated ionic liquids", *Green Chem.*, 2006, **8**, 172–180.

[307] N. Rajapriya Inbaraj, S. Song, R. Chang, K. Fujita and T. Hayashi, "Investigation of Hydration States of Ionic Liquids by Fourier Transform Infrared Absorption Spectroscopy: Relevance to Stabilization of Protein Molecules", *Langmuir*, 2023, **39**, 2558–2568.

[308] G. Boari, L. Liberti, C. Merli and R. Passino, "Exchange equilibria on anion resins", *Desalination*, 1974, **15**, 145–166.

[309] I. Louati, F. Guesmi, A. Chaabouni, C. Hannachi and B. Hamrouni, "Effect of ionic strength on the ion exchange equilibrium between AMX membrane and electrolyte solutions", *Water Qual. Res. J.*, 2015, **51**, 60–68.

[310] Y. Marcus, "A simple empirical model describing the thermodynamics of hydration of ions of widely varying charges, sizes, and shapes", *Biophys. Chem.*, 1994, **51**, 111–127.

[311] M. Shi, L. F. F. Corrêa, K. Thomsen and P. L. Fosbøl, "Barium Sulfate Solubility in Aqueous Solutions Containing Chlorides or Nitrates", *Ind. Eng. Chem. Res.*, 2023, **62**, 13167–13180.

[312] M. Stewart and K. Arnold, Gulf Professional Publishing, 2009.

[313] C. C. Templeton, “Solubility of Barium Sulfate in Sodium Chloride Solutions from 25° to 95° C.”, *J. Chem. Eng. Data*, 1960, **5**, 514–516.

[314] P. Bajpai, *Management of Pulp and Paper Mill Waste*, Springer Cham, 2015.

[315] G. V. Hartland, “Statistical Analysis of Physical Chemistry Data: Errors Are Not Mistakes”, *J. Phys. Chem. C*, 2020, **124**, 5889–5892.

[316] M. Fabris, V. Lucchini, M. Noè, A. Perosa and M. Selva, “Ionic Liquids Made with Dimethyl Carbonate: Solvents as well as Boosted Basic Catalysts for the Michael Reaction”, *Chem. Eur. J.*, 2009, **15**, 12273–12282.

[317] D. Dupont, E. Renders and K. Binnemans, “Alkylsulfuric acid ionic liquids: a promising class of strongly acidic room-temperature ionic liquids”, *Chem. Commun.*, 2016, **52**, 4640–4643.

[318] A. J. Hall, P. Manesiotis, M. Emgenbroich, M. Quaglia, E. De Lorenzi and B. Sellergren, “Urea Host Monomers for Stoichiometric Molecular Imprinting of Oxyanions”, *J. Org. Chem.*, 2005, **70**, 1732–1736.

[319] A. A. Hassan, A.-F. E. Mourad, K. M. El-Shaieb, A. H. Abou-Zied and D. Döpp, “Thermolysis of symmetrical dithiobiurea and thioureidoethylthiourea derivatives”, *Heteroat. Chem*, 2003, **14**, 535–541.

[320] N. Busschaert, P. A. Gale, C. J. E. Haynes, M. E. Light, S. J. Moore, C. C. Tong, J. T. Davis and W. A. Harrell, Jr., “Tripodal transmembrane transporters for bicarbonate”, *Chem. Commun.*, 2010, **46**, 6252–6254.

[321] B. P. Hay, T. K. Firman and B. A. Moyer, “Structural design criteria for anion hosts: Strategies for achieving anion shape recognition through the complementary placement of urea donor groups”, *J. Am. Chem. Soc.*, 2005, **127**, 1810–1819.

[322] H.-J. Schneider and A. K. Yatsimirsky, “Selectivity in supramolecular host-guest complexes”, *Chem. Soc. Rev.*, 2008, **37**, 263–277.

[323] C. Godoy-Alcántar, I. L. Rivera and A. K. Yatsimirsky, “Anion recognition by Thiostrepton”, *Bioorg. Med. Chem. Lett.*, 2001, **11**, 651–654.

[324] D. H. Burns, K. Calderon-Kawasaki and S. Kularatne, “Buried Solvent Determines Both Anion-Binding Selectivity and Binding Stoichiometry with Hydrogen-Bonding Receptors”, *J. Org. Chem.*, 2005, **70**, 2803–2807.

[325] G. Tumcharern, T. Tuntulani, S. J. Coles, M. B. Hursthouse and J. D. Kilburn, “A Novel Ditopic Receptor and Reversal of Anion Binding Selectivity in the Presence and Absence of Bound Cation”, *Org. Lett.*, 2003, **5**, 4971–4974.

[326] P. D. Beer and S. W. Dent, “Potassium cation induced switch in anion selectivity exhibited by heteroditopic ruthenium(II) and rhenium(I) bipyridyl bis(benzo-15-crown-5) ion pair receptors”, *Chem. Commun.*, 1998, 825–826.

[327] O. Hoegh-Guldberg, D. Jacob, M. Taylor, M. Bindi, S. Brown, I. Camilloni, A. Diedhiou, R. Djalante, K. L. Ebi, F. Engelbrecht, J. Guiot, Y. Hijioka, S. Mehrotra, A. Payne, S. I. Seneviratne, A. Thomas, R. Warren and G. Zho, in *Global Warming of 1.5 ℃*, IPCC, 2018, ch. 3.

[328] H. S. Baker, R. J. Millar, D. J. Karoly, U. Beyerle, B. P. Guillod, D. Mitchell, H. Shiogama, S. Sparrow, T. Woollings and M. R. Allen, “Higher CO2 concentrations increase extreme event risk in a 1.5 ℃ world”, *Nat. Clim. Change*, 2018, **8**, 604–608.

[329] X. An, P. Wang, X. Ma, X. Du, X. Hao, Z. Yang and G. Guan, “Application of ionic liquids in CO2 capture and electrochemical reduction: A review”, *Carbon Resour. Convers.*, 2023, **6**, 85–97.

[330] L. Zheng, G. Yang, X. Hu and Z. Zhang, “CO2 capturing and in situ conversion at mild condition: Efficient synthesis of methyl phenyl carbonate”, *J. Environ. Chem. Eng.*, 2021, **9**, 105862.

[331] J. Stoimenovski, E. I. Izgorodina and D. R. MacFarlane, “Ionicity and proton transfer in protic ionic liquids”, *Phys. Chem. Chem. Phys.*, 2010, **12**, 10341–10347.

[332] H. Walba and R. W. Isensee, “Acidity Constants of Some Arylimidazoles and Their Cations”, *J. Org. Chem.*, 1961, **26**, 2789–2791.

[333] J. Clayden, N. Greeves, S. G. Warren and J. Clayden, *Organic chemistry*, Oxford University Press, Oxford, Second edition., 2012, ch. 8, pp. 163–181.

[334] S. Seo, L. D. Simoni, M. Ma, M. A. DeSilva, Y. Huang, M. A. Stadtherr and J. F. Brennecke, “Phase-Change Ionic Liquids for Postcombustion CO2 Capture”, *Energy Fuels*, 2014, **28**, 5968–5977.

[335] Y. U. Paulechka, A. G. Kabo, A. V. Blokhin, G. J. Kabo and M. P. Shevelyova, “Heat Capacity of Ionic Liquids: Experimental Determination and Correlations with Molar Volume”, *J. Chem. Eng. Data*, 2010, **55**, 2719–2724.

[336] L. E. Ficke, H. Rodríguez and J. F. Brennecke, “Heat Capacities and Excess Enthalpies of 1-Ethyl-3-methylimidazolium-Based Ionic Liquids and Water”, *J. Chem. Eng. Data*, 2008, **53**, 2112–2119.

[337] M. Yoo, S.-J. Han and J.-H. Wee, “Carbon dioxide capture capacity of sodium hydroxide aqueous solution”, *J. Environ. Manage.*, 2013, **114**, 512–519.

[338] N. Caeiro, M. K. Wojtczuk, H. Rodríguez, E. Rodil and A. Soto, “Recovery of dialkylimidazolium-based ionic liquids from their mixtures with acetone or water by flash distillation”, *J. Mol. Liq.*, 2022, **346**, 118292.

[339] A. Hoerning, F. R. Ribeiro, L. C. Filho, L. M. Lião, M. L. Corazza and F. A. Voll, “Boiling point elevation of aqueous solutions of ionic liquids derived from diethanolamine base and carboxylic acids”, *J. Chem. Thermodyn.*, 2016, **98**, 1–8.

[340] D. J. Heldebrant, P. G. Jessop, C. A. Thomas, C. A. Eckert and C. L. Liotta, “The Reaction of 1,8-Diazabicyclo[5.4.0]undec-7-ene (DBU) with Carbon Dioxide”, *J. Org. Chem.*, 2005, **70**, 5335–5338.

[341] S. Basel, K. Bhardwaj, S. Pradhan, A. Pariyar and S. Tamang, “DBU-Catalyzed One-Pot Synthesis of Nearly Any Metal Salt of Fatty Acid (M-FA): A Library of Metal Precursors to Semiconductor Nanocrystal Synthesis”, *ACS Omega*, 2020, **5**, 6666–6675.

[342] M. S. Miran, H. Kinoshita, T. Yasuda, M. A. B. H. Susan and M. Watanabe, “Hydrogen bonds in protic ionic liquids and their correlation with physicochemical properties”, *Chem. Commun.*, 2011, **47**, 12676–12678.

[343] W.-L. Yuan, G.-H. Tao, L. Zhang, Z. Zhang, Y. Xue, L. He, J. Huang and W. Yu, “Super impact stable TATB explosives recrystallized by bicarbonate ionic liquids with a record solubility”, *Sci. Rep.*, 2020, **10**, 4477–4484.

[344] E. Garand, T. Wende, D. J. Goebbert, R. Bergmann, G. Meijer, D. M. Neumark and K. R. Asmis, “Infrared Spectroscopy of Hydrated Bicarbonate Anion Clusters: HCO3-(H2O)1-10”, *J. Am. Chem. Soc.*, 2010, **132**, 849–856.

[345] P. G. Jessop, S. M. Mercer and D. J. Heldebrant, “CO2-triggered switchable solvents, surfactants, and other materials”, *Energy Environ. Sci.*, 2012, **5**, 7240–7253.

[346] D. Bernin and N. Hedin, “Perspectives on NMR studies of CO2 adsorption”, *Curr. Opin. Colloid Interface Sci.*, 2018, **33**, 53–62.

[347] M. C. Ball, C. M. Snelling, A. N. Strachan and R. M. Strachan, “Thermal decomposition of solid sodium bicarbonate”, *J. Chem. Soc., Faraday Trans.*, 1986, **82**, 3709–3715.

[348] E. Medina-Martos, J.-L. Gálvez-Martos, J. Almarza, C. Lirio, D. Iribarren, A. Valente and J. Dufour, “Environmental and economic performance of carbon capture with sodium hydroxide”, *J. CO2 Util.*, 2022, **60**, 101991.

[349] L. K. G. Bhatta, S. Subramanyam, M. D. Chengala, S. Olivera and K. Venkatesh, “Progress in hydrotalcite like compounds and metal-based oxides for CO2 capture: a review”, *J. Cleaner Prod.*, 2015, **103**, 171–196.

[350] Y. Shen, “Molten salt-mediated carbon capture and conversion”, *Fuel*, 2023, **339**, 127473.

[351] Y. L. Kobzar and K. Fatyeyeva, “Ionic liquids as green and sustainable steel corrosion inhibitors: Recent developments”, *Chem. Eng. J.*, 2021, **425**, 131480.

[352] M. Ouakki, M. Galai and M. Cherkaoui, “Imidazole derivatives as efficient and potential class of corrosion inhibitors for metals and alloys in aqueous electrolytes: A review”, *J. Mol. Liq.*, 2022, **345**, 117815.

[353] S. Shi, S. Li and X. Liu, “Mechanism Study of Imidazole-Type Deep Eutectic Solvents for Efficient Absorption of CO2”, *ACS Omega*, 2022, **7**, 48272–48281.

[354] W. Chen, Z. Huang, X. Liang, G. M. Kontogeorgis, B. Liu and G. Chen, “Experimental data and modeling of the CO2 solubility in 2-methylimidazole aqueous solution”, *Fuel*, 2023, **331**, 125694.

[355] N. J. Bridges, C. C. Hines, M. Smiglak and R. D. Rogers, “An Intermediate for the Clean Synthesis of Ionic Liquids: Isolation and Crystal Structure of 1,3-Dimethylimidazolium Hydrogen Carbonate Monohydrate”, *Chem. Eur. J.*, 2007, **13**, 5207–5212.

[356] M. Smiglak, C. C. Hines and R. D. Rogers, “New hydrogen carbonate precursors for efficient and byproduct-free syntheses of ionic liquids based on 1,2,3-trimethylimidazolium and N,N-dimethylpyrrolidinium cores”, *Green Chem.*, 2010, **12**, 491–501.

[357] J. Liu, G. Yang, Y. Liu, D. Wu, X. Hu and Z. Zhang, “Metal-free imidazolium hydrogen carbonate ionic liquids as bifunctional catalysts for the one-pot synthesis of cyclic carbonates from olefins and CO2”, *Green Chem.*, 2019, **21**, 3834–3838.

[358] T. Zhao, X. Hu, D. Wu, R. Li, G. Yang and Y. Wu, “Direct Synthesis of Dimethyl Carbonate from Carbon Dioxide and Methanol at Room Temperature Using Imidazolium Hydrogen Carbonate Ionic Liquid as a Recyclable Catalyst and Dehydrant”, *ChemSusChem*, 2017, **10**, 2046–2052.